



Universidade do Minho

Escola de Engenharia

Nuno Miguel Ferrete Ribeiro

IMUs – Validation, Gait Analysis and System’s Implementation

Dissertação de Mestrado

Mestrado Integrado em Engenharia Biomédica

Ramo Eletrónica Médica

Trabalho efetuado sob orientação de:

Doutora Cristina P. Santos

Universidade do Minho

DECLARAÇÃO

Nome: Nuno Miguel Ferrete Ribeiro

Endereço eletrónico: nuno_ribeiro07@hotmail.com

Número do cartão de cidadão: 14516699

Título da Dissertação: IMUs – Validation, Gait Analysis and System's Implementation

Orientador:

Doutora Cristina Manuela Peixoto dos Santos

Ano de conclusão: 2017

Designação do Mestrado: Mestrado Integrado em Engenharia Biomédica

Área de Especialização: Ramo Eletrónica Médica

É AUTORIZADA A REPRODUÇÃO INTEGRAL DESTA DISSERTAÇÃO APENAS PARA EFEITOS DE INVESTIGAÇÃO, MEDIANTE DECLARAÇÃO ESCRITA DO INTERESSADO, QUE A TAL SE COMPROMETE.

Universidade do Minho, ___ / ___ / _____

Assinatura: _____

“I’m free to be the greatest.

I’m alive.”

Sia

Acknowledgments

First of all, I would like to mention an immense gratitude to Professor Cristina Santos, who was crucial, not only at the level of scientific guidance, but also at the level of support, advice, encouragement and suggestions, being always present throughout this year. Beyond doubt, you have allowed, through a methodical and organized orientation, the concretization of this project. Consequently, I would like to offer you all my thanks.

In particular, I could not fail to thank Joana Figueiredo and César Ferreira for the collaboration, availability, patience and good disposition. Thank you for the support and knowledge you provide me with, which were fundamental.

To my laboratory colleagues, thank you for all the encouragement, and for your knowledge-sharing and advices you gave me throughout this year.

I would also like to express my gratitude to my friends, who have been unconditionally by my side during this phase as always.

I thank Ana Silva for all the sensitivity, affection, patience, support and love she has shown over the last few years, being always ready to help me and give me the strength to continue. I am very proud of you. By your presence, a huge thank you.

Finally, I want to thank my family for the unconditional support they have shown throughout my life, for being always present in all important moments, for always believing in my abilities and for never letting me give up or discourage by the difficulties or obstacles that have crossed my path. In particular, I should also thank my parents for providing me with the best conditions for my academic training, for always indicating to me the best way forward and for having given me the opportunity to join the Biomedical Engineering integrated master's degree. My family represents the great pillar on which I stand and in which I am very proud.

To all of you, my most sincere and humble thank you!

Nuno Ferrete Ribeiro

Agradecimentos

Primeiramente, gostaria de mencionar uma imensa gratidão para com a professora Cristina Santos, que foi crucial, não apenas ao nível da orientação científica, mas também ao nível de apoio, conselhos, encorajamento e sugestões, estando sempre presente ao longo deste ano. Sem margem para dúvidas, você permitiu, através de uma orientação metódica e organizada, a concretização deste projeto. Como tal, gostaria de lhe dirigir um enorme obrigado.

Não podia deixar de agradecer a colaboração, disponibilidade, paciência e boa disposição, em particular, da Joana Figueiredo e do César Ferreira. Um obrigado pelo apoio e pelos conhecimentos que me disponibilizaram, os quais foram fundamentais.

Aos meus colegas de laboratório, obrigado por todo o incentivo e pela partilha de conhecimentos e conselhos que me deram ao longo deste ano.

Queria deixar também uma palavra de agradecimento aos meus amigos, que estiveram incondicionalmente ao meu lado durante esta fase como sempre.

Agradeço à Ana Silva por toda a sensibilidade, carinho, paciência, apoio e amor que tem demonstrado ao longo destes últimos anos, estando sempre disposta a me ajudar e a me dar forças para continuar. Tenho muito orgulho em ti. Pela tua presença, um enorme obrigado.

Por fim, quero agradecer à minha família pelo apoio incondicional demonstrado ao longo de toda a minha vida, por estarem sempre presentes em todos os momentos importantes, por acreditarem sempre nas minhas capacidades e por nunca me deixarem desistir ou desanimar perante as dificuldades ou obstáculos que se atravessaram no meu caminho. Em particular, devo agradecer ainda aos meus pais por me fornecerem as melhores condições para a minha formação académica, por me indicarem sempre o melhor caminho a seguir e por me terem proporcionado a oportunidade de ingressar no Mestrado Integrado em Engenharia Biomédica. A minha família representa o grande pilar em que me sustento e no qual tenho muito orgulho.

A todos vós, o meu mais sincero e humilde Obrigado!

Nuno Ferrete Ribeiro

Abstract

Falls are a prevalent problem in actual society. The number of falls has been increasing greatly in the last fifteen years. Some falls result in injuries and the cost associated with their treatment is high. However, this is a complex problem that requires several steps in order to be tackled. Namely, it is crucial to develop strategies that recognize the mode of locomotion, indicating the state of the subject in various situations, namely normal gait, step before fall (pre-fall) and fall situation. Thus, this thesis aims to develop a strategy capable of identifying these situations based on a wearable system that collects information and analyses the human gait.

The strategy consists, essentially, in the construction and use of Associative Skill Memories (ASMs) as tools for recognizing the locomotion modes. Consequently, at an early stage, the capabilities of the ASMs for the different modes of locomotion were studied. Then, a classifier was developed based on a set of ASMs. Posteriorly, a neural network classifier based on deep learning was used to classify, in a similar way, the same modes of locomotion. Deep learning is a technique actually widely used in data classification. These classifiers were implemented and compared, providing for a tool with a good accuracy in recognizing the modes of locomotion.

In order to implement this strategy, it was previously necessary to carry out extremely important support work. An inertial measurement units' (IMUs) system was chosen due to its extreme potential to monitor outpatient activities in the home environment. This system, which combines inertial and magnetic sensors and is able to perform the monitoring of gait parameters in real time, was validated and calibrated. Posteriorly, this system was used to collect data from healthy subjects that mimicked Fs.

Results have shown that the accuracy of the classifiers was quite acceptable, and the neural networks based classifier presented the best results with 92.71% of accuracy. As future work, it is proposed to apply these strategies in real time in order to avoid the occurrence of falls.

Keywords: falls; gait parameters; inertial measurement units (IMUs); sensory fusion's algorithms; calibration; Principal Component Analysis (PCA); ASMs; deep learning.

Resumo

As quedas são um problema predominante na sociedade atual. O número de quedas tem aumentado bastante nos últimos quinze anos. Algumas quedas resultam em lesões e o custo associado ao seu tratamento é alto. No entanto, trata-se de um problema complexo que requer várias etapas a serem abordadas. Ou seja, é crucial desenvolver estratégias que reconheçam o modo de locomoção, indicando o estado do sujeito em várias situações, nomeadamente, marcha normal, passo antes da queda (pré-queda) e situação de queda. Assim, esta tese tem como objetivo desenvolver uma estratégia capaz de identificar essas situações com base num sistema *wearable* que colete informações e analise a marcha humana.

A estratégia consiste, essencialmente, na construção e utilização de *Associative Skill Memories* (ASMs) como ferramenta para reconhecimento dos modos de locomoção. Consequentemente, numa fase inicial, foram estudadas as capacidades das ASMs para os diferentes modos de locomoção. Depois, foi desenvolvido um classificador baseado em ASMs. Posteriormente, um classificador de redes neuronais baseado em *deep learning* foi utilizado para classificar, de forma semelhante, os mesmos modos de locomoção. *Deep learning* é uma técnica bastante utilizada em classificação de dados. Estes classificadores foram implementados e comparados, fornecendo a uma ferramenta com uma boa precisão no reconhecimento dos modos de locomoção.

Para implementar esta estratégia, era necessário realizar previamente um trabalho de suporte extremamente importante. Um sistema de unidades de medição inercial (IMUs), foi escolhido devido ao seu potencial extremo para monitorizar as atividades ambulatoriais no ambiente domiciliar. Este sistema que combina sensores inerciais e magnéticos e é capaz de efetuar a monitorização de parâmetros da marcha em tempo real, foi validado e calibrado. Posteriormente, este Sistema foi usado para adquirir dados da marcha de indivíduos saudáveis que imitaram quedas.

Os resultados mostraram que a precisão dos classificadores foi bastante aceitável e o classificador baseado em redes neuronais apresentou os melhores resultados com 92.71% de precisão. Como trabalho futuro, propõe-se a aplicação destas estratégias em tempo real de forma a evitar a ocorrência de quedas.

Palavras-chave: quedas; parâmetros da marcha; Unidades de medição inercial (IMUs); algoritmos de fusão sensorial; calibração; *Principal Component Analysis*; ASMs; *deep learning*.

Contents

Acknowledgments.....	VII
Agradecimentos.....	IX
Abstract.....	XI
Resumo.....	XIII
Contents.....	XV
List of Figures.....	XIX
List of Tables.....	XXV
Acronyms and Abbreviations.....	XXVIII
Chapter 1 - Introduction.....	1
1.1. Motivation.....	1
1.2. Problem Statement and scope.....	3
1.3. Goals and research questions.....	3
1.4. Contribution to knowledge.....	6
1.5. Publications.....	7
1.6. Thesis outline.....	7
Chapter 2 – Inertial Measurement Units: State-of-the-art.....	11
2.1. Introduction.....	11
2.2. Applications and Commercial IMUs.....	15
2.3. Advantages and Disadvantages.....	21
2.4. Methods and Problems.....	22
2.5. Calibration.....	25
2.6. Challenges.....	26
Chapter 3 – Falls Prevention and Risk Identification: state-of-the-art.....	29
3.1. Introduction.....	29
3.2. Classification of the Falls.....	30
3.3. Methods.....	32
3.3.1. Fall Detection Systems.....	32
3.3.2. Fall Prevention Systems/Fall Forecasting Systems.....	36
3.4. Gait Parameters, Sensors and Experimental Setup Information.....	40

3.4.1.	Gait Parameters.....	40
3.4.2.	Sensors and Experimental Setup Information	42
3.5.	Challenges, Issues and Trends.....	49
3.5.1.	Challenges	49
3.5.2.	Issues	49
3.5.3.	Trends.....	50
Chapter 4 –	Human Gait Monitoring System Overview.....	51
4.1.	Introduction.....	51
4.2.	Magnetic/Inertial Measurement System	51
4.3.	eLPRT protocol.....	52
4.4.	Algorithmic State Machine	53
4.5.	System Requirements and MATLAB Interface.....	54
4.5.1.	System Requirements.....	54
4.5.2.	MATLAB Interface.....	56
4.5.2.1.	Quality Assessment.....	59
4.5.2.2.	Results and Discussion	59
Chapter 5 –	IMUs based System Validation.....	61
5.1.	Validation of the communication protocol.....	61
5.1.1.	Trials.....	62
5.1.2.	Results.....	63
5.1.3.	Discussion.....	66
5.2.	Validation of the signals of the sensors.....	67
5.2.1.	Results and Discussion	68
5.2.1.1.	Foot.....	68
5.2.1.2.	Thigh.....	70
5.2.1.3.	Lower Back.....	72
5.3.	Validation of the estimation of joint angles.....	73
5.3.1.	Reference Measurement System - DARwIn OP.....	74
5.3.2.	Knee Joint Angle Measurement.....	75
5.3.3.	Results.....	75
5.3.4.	Discussion.....	77
Chapter 6 –	IMUs based System Calibration	79

6.1. Calibration procedures - Introduction.....	79
6.2. Methods.....	81
6.2.1. Process of the orientation estimation of the IMUs based system	81
6.2.2. Calibration Procedures.....	81
6.2.2.1. Method A.....	82
6.2.2.2. Method B.....	82
6.2.2.3. Method C.....	83
6.2.2.4. Proposed Method.....	84
6.2.3. Tracker Software.....	85
6.2.4. Experimental Protocol	85
6.3. Results.....	87
6.3.1. Stage 1	87
6.3.2. Stage 2	88
6.3.2.1. Stationary position	88
6.3.2.2. Walking trial.....	91
6.3.3. Stage 3	93
6.3.4. Stage 4	95
6.4. Discussion.....	96
Chapter 7 – Pre-Fall Detection System	99
7.1. Stage 1	99
7.1.1. Trials.....	100
7.1.2. PCA.....	101
7.1.3. ASMs	103
7.1.4. Evaluation of classification performance	107
7.1.5. Results.....	108
7.1.5.1. PCA.....	108
7.1.5.2. ASMs.....	114
7.2. Stage 2	133
7.2.1. Results.....	134
7.3. Stage 3	135
7.3.1. Convolutional Neural Networks.....	135

7.3.2. Results	137
7.4. Stage 4	138
7.5. Discussion.....	140
Chapter 8 – Conclusions	143
8.1. Future work.....	148
References	151
Appendices.....	169
Appendix 1	169

List of Figures

Figure 2.1 - Example of a RLVBIMU04 IMU from VBOX Automotive with wire connection [194].	13
Figure 2.2 - a) A mechanical Acc; b) A surface acoustic wave Acc [194], [29].	14
Figure 2.3 - A conventional mechanical Gyro [29].	14
Figure 2.4 - Image of a micro Mag structure [195].	15
Figure 2.5 - Xsens MVN products [38]. MVN Awinda is on the left side. MVN Link is on the right side.	17
Figure 2.6 - InterSense 3-DOF trackers [39]: a) InertiaCube4TM; b) InertiaCube BTM.	18
Figure 2.7 - InterSense 6-DOF trackers [39]: a) IS-900 system; b) IS-1200+ system.	18
Figure 2.8 - Technaid products [40]: a) IMU CV4; b) IMU V4	19
Figure 2.9 - Technaid Motion Capture System [40].	19
Figure 2.10 - IMeasureU IMU sensor [41].	20
Figure 2.11 - Noraxon myoMOTION device [42].	20
Figure 3.1 - Balance performance model [83].	30
Figure 3.2 - Possible Fs along the horizontal/lateral and vertical directions [88]: a) F forward; b) F laterally; c) F backward; d) F along vertical direction – slipping of foot; e) F along vertical direction – weak legs.	31
Figure 3.3 - Classification of F detection methods according to [89].	33
Figure 3.4 - Distribution of research studies on wearable sensors: Application vs Wearable Sensors [82].	34
Figure 3.5 - Typical output of a chest 3D Acc before and after a F event. Acceleration peaks are cause by floor impact [86]. It is possible to observe that acceleration suffers perturbations about 1 second before actual impact.	35
Figure 3.6 - STEADI F Risk Assessment algorithm [135].	38
Figure 3.7 - Representation of the stability in a vertical position.	41
Figure 3.8 - Different axis/planes. The frontal plane is referred to as Antero-posterior (AP), the lateral plane as Medio-lateral (ML) and the vertical simply as Vertical (VT).	43
Figure 4.1 - Magnetic/Inertial Measurement System Elements.	52
Figure 4.2 - a) Constitution of the frame; b) Constitution of the payload (S-sample/reading, T1 & T2-temperature byte 1 and 2, Bat1 & Bat2-battery byte 1 and 2).	52

Figure 4.3 - Data acquisition process flowchart.....	55
Figure 4.4 - Matlab GUI when initialized (Ang – Angles; GED – Gait Events Detection).	56
Figure 4.5 - Matlab GUI when the system is in the operational state.....	58
Figure 4.6 - Matlab GUI when the system was stopped.....	58
Figure 4.7 - Inquiry results in percentage per question number.....	60
Figure 5.1 – Phases of the validation process.....	61
Figure 5.2 - Spatial arrangement of the sensory modules in the body with their physical addresses: a) 5 sensory modules on trunk (3), foot (13-right, 6-left), and shank (7-right, 14-left); b) 4 sensory modules on foot (13-right, 6-left), and shank (7-right, 14-left); c) 3 sensory modules on right leg: foot (13), shank (7), and thigh (14); d) 2 sensory modules on the upper foot (13-right, 6-left); e) 1 sensory module on the upper foot (13-right); f) 2 sensory modules on the heel (13-right, 6-left); and g) 1 sensory module on the heel (13-right).	62
Figure 5.3 - Average percentage of loss for each spatial arrangement in laboratory (N-Normal pace; F- Fast pace).....	65
Figure 5.4 - Average percentage of loss for each spatial arrangement in the corridor (N-Normal pace; F- Fast pace).	66
Figure 5.5 - Average percentage of loss for each spatial arrangement in an outdoor environment (N-Normal pace; F- Fast pace).....	66
Figure 5.6 - Attachment location of the sensing devices used for the trials (Dark sensing devices are in the back of the body).	68
Figure 5.7 – a) Orientation of the Cartesian axes of the sensing device. b) Xsens’ IMU attached to the right foot.....	68
Figure 5.8 – Norm of the acceleration during a walking trial obtained from: a) a Jiménez’s trial (black line) [163]. b) IMUs based system (data not filtered).	69
Figure 5.9 - Gyro data during a walking trial obtained from: a) a Jiménez’s trial [163]. b) IMUs based system (data not filtered).	69
Figure 5.10 - Mag data during a walking trial obtained from: a) a Jiménez’s trial [163]. b) IMUs based system (data not filtered).	70
Figure 5.11 - Attachment location of the IMUs [51]. a) Elevation view. b) Side view. c) Real photo of the proposed capturing system.	71

Figure 5.12 – Gyro data (mediolateral axis) when an IMU is attached in the right thigh. a) Hamdi's typical signal (blue signal) [51]. b) IMUs system (data filtered: Butterworth lowpass filter – $F_c=3\text{Hz}$).
..... 71

Figure 5.13 - Acc data (vertical axis) when an IMU is attached in the right thigh. a) Hamdi's typical signal (blue signal) [51]. b) One gait cycle measured by the IMUs based system (data filtered: Butterworth lowpass filter – $F_c=3\text{Hz}$).
..... 72

Figure 5.14 - Gyro data (vertical axis) when an IMU is attached in the lower back. a) Hamdi's typical signal [51]. b) One gait cycle measured by the IMU's system (data filtered: Butterworth lowpass filter – $F_c=3\text{Hz}$).
..... 73

Figure 5.15 - a) DARwIn robot with two sensory modules attached to left thigh and shank (for both modules, the positive Z axis is perpendicular to the housing cover, Y axis – up, X axis – to the left of the robot). b) DARwIn robot performs an angle of -30° with the left leg (sagittal plane). In this situation, knee angles from the robot are represented as α , and the knee angles from the model implemented are represented as γ .
..... 74

Figure 5.16 - Typical knee angles ($^\circ$) during the trial where the DARwIn OP was walking (ANG Dar - robot real angles measured through encoders; ANG IMUs - calculated knee angles from sensory modules data; x-axis: time (s); y-axis: angles).
..... 76

Figure 5.17 - Typical knee angles ($^\circ$) during the trial where the DARwIn OP kept the leg stretched (ANG Dar - robot real angles measured through encoders; ANG IMUs - calculated knee angles from IMUs' data; x-axis: time (s); y-axis: angles).
..... 76

Figure 5.18 - Typical knee angles ($^\circ$) during the trial where the DARwIn OP performed an angle of -30° (ANG Dar - robot real angles measured through encoders; ANG IMUs - calculated knee angles from IMUs' data; x-axis: time (s); y-axis: angles).
..... 77

Figure 6.1 – Several steps of the calibration procedures from the raw measurements x to measurements v^a resolved in the anatomical frame [170].
..... 80

Figure 6.2 - Block diagram of the calibration process.
..... 81

Figure 6.3 - Basic Principle of Method A: Extraction of Acc Maximum and Minimum values for each axis through 6 different positions.
..... 82

Figure 6.4 - Sensors' attachment location to measure Gyro's offsets.
..... 86

Figure 6.5 - Walking trial angles of the thigh: a) roll; b) pitch; and c) yaw.
..... 93

Figure 6.6 - Tracker software environment working with a rotation trial.
..... 94

Figure 6.7 - Rotation angles of stage 3 experiment: a) Roll; b) Pitch; and c) Yaw.....	94
Figure 6.8 - Yaw angles obtained through a CF, Madgwick filter (w/ and w/o Mag), and Mahony filter (w/ and w/o Mag).....	96
Figure 7.1 - Block diagram of the first stage.	99
Figure 7.2 – Trial i) in the gymnasium – Subject (blue point) walks forward (Top – w/o F; Down – w/ F where the F's location is represented by the red X).....	100
Figure 7.3 – Trial ii) in the gymnasium – Subject (blue point) walks in circles (Top – w/o F – right and left; Down – w/ F where the F's location is represented by the red X).	100
Figure 7.4 – Trial iii) in the gymnasium – Subject (blue point) walks 10m forward bypassing an obstacle (Top – w/o F – right and left; Down – w/ F where the F's location is represented by the red X).....	100
Figure 7.5 - Sensing devices attachment location used for the trials (Dark sensing devices are in the back of the body; Red numbers represent the physical addresses of the sensing devices).	101
Figure 7.6 - Set of steps to obtain the most relevant variables (Case I).	102
Figure 7.7 - Set of steps to obtain the most relevant variables (Case II).	103
Figure 7.8 – Test data set of the left gripper right finger force cell. Example presented in [185]. The weighted standard deviation (blue line) was computed from the training set. The failure condition for all unsuccessful trials was detected correctly after an average of 2.4 seconds (shaded area).	104
Figure 7.9 - Scree Plot of the PCA procedure I when using the global walking locomotion mode.	108
Figure 7.10 - Scree Plot of the PCA procedure II when using the global data.	109
Figure 7.11 - Scree Plot of the PCA procedure II when using the Walking Forward (WF) data..	110
Figure 7.12 – Scree Plot of the PCA procedure II when using the PF data.....	111
Figure 7.13 - Scree Plot of the PCA procedure II when using the F data.	112
Figure 7.14 – Non-repeated and relevant metrics identified through PCA procedure and the indication to which group they belong.....	113
Figure 7.15 – Examples of ASMs. a) Gyr_X_6 from WF set of ASMs; b) SVM_6 from Global set of ASMs; c) Mag_Z_13 from PF set of ASMs; d) Mag_Y_3 from F set of ASMs.	114
Figure 7.16 – ROC curve of the first ROC analysis – ASM WF**.....	116
Figure 7.17 – Histogram of the number of failures per metric – ASM WF**.....	116

Figure 7.18 – Examples of ASMs. a) Gyr_X_6; b) Acc_Z_13; c) WD_Mag_Z_13; d) Mag_Z_13 (Green – Successful motion periods; Red – Unsuccessful motion periods; Blue – Weighted STD).	117
Figure 7.19 - ROC curve of the second ROC analysis – ASM WF*.....	118
Figure 7.20 - Histogram of the number of failures per metric – ASM WF*.....	119
Figure 7.21 - Examples of ASMs. a) Mag_Z_3; b) Mag_Z_13 (Green – Successful motion periods; Red – Unsuccessful motion periods; Blue – Weighted STD).	119
Figure 7.22 - ROC curve of the third ROC analysis – ASM WF.....	120
Figure 7.23 - Histogram of the number of failures per metric – ASM WF.....	121
Figure 7.24 – Examples of ASMs. a) Acc_Z_13; b) Mag_Z_13 (Green – Successful motion periods; Red – Unsuccessful motion periods; Blue – Weighted STD).	121
Figure 7.25 – ROC curve of the fourth ROC analysis – ASM Global*.....	122
Figure 7.26 – Histogram of the number of failures per metric – ASM Global*.....	123
Figure 7.27 – Examples of ASMs. a) Mag_Y_7; b) WD_Mag_Z_13 (Green – Successful motion periods; Red – Unsuccessful motion periods; Blue – Weighted STD).	123
Figure 7.28 – ROC curve of the fifth ROC analysis – ASM Global.....	124
Figure 7.29 - Histogram of the number of failures per metric – ASM Global.....	125
Figure 7.30 – Examples of ASMs. a) Mag_Z_13; b) WD_Mag_Z_13 (Green – Successful motion periods; Red – Unsuccessful motion periods; Blue – Weighted STD).	125
Figure 7.31 – ROC curve of the sixth ROC analysis – ASM F.....	126
Figure 7.32 – Histogram of the number of failures per metric – ASM F.....	127
Figure 7.33 – Examples of ASMs. a) ApEn_Acc_X_7; b) Mag_Z_3 (Green – Successful motion periods; Red – Unsuccessful motion periods; Blue – Weighted STD).	127
Figure 7.34 – ROC curve of the seventh ROC analysis – ASM PFΔ.....	128
Figure 7.35 – Histogram of the number of failures per metric – ASM PFΔ.....	129
Figure 7.36 – Examples of ASMs. a) ASMA_6; b) SVd_13 (Green – Successful motion periods; Red – Unsuccessful motion periods; Blue – Weighted STD).	129
Figure 7.37 – ROC curve of the eighth ROC analysis – ASM PF.....	130
Figure 7.38 – Histogram of the number of failures per metric – ASM PF.....	131
Figure 7.39 – Examples of ASMs. a) ApEn_Acc_Z_3; b) Mag_Z_6 (Green – Successful motion periods; Red – Unsuccessful motion periods; Blue – Weighted STD).	131

Figure 7.40 – Decision cascade to classify collected motion periods. 133

Figure 7.41 - Layers that constitute a neural network, which consist of a set of interconnected nodes [190]..... 136

Figure 7.42 – Processes of resampling and resizing to use data as input in the CNN. 137

Figure 7.43 – Top view of the walking trial performed in stage 4..... 138

List of Tables

Table 3.1 - Commercial wearable F detection products.....	36
Table 3.2 - Potentially relevant metrics for the prevention of gait, and the sensors, the location of the sensors, subjects' age, and the procedure used to obtain them (K – Kinematic; F – Frequency; ST – Spatiotemporal; Ph – Physiological; Ki – Kinetic; y – young; o – old; h – healthy; fp – fall prone; *-already mentioned)	43
Table 5.1 - Direction of the positive axis for each sensory module in each spatial arrangement.	63
Table 5.2 - Number of lost frames and total frames for each environment.....	64
Table 5.3 - Average percentage of loss of the five tests for each spatial arrangement (L-Lab; C-Corridor; O-Outdoor; N-Normal pace; F- Fast pace)	64
Table 6.1 - Error Percentage of the Maximum and Minimum values when compared to the homologous values of the Method A – Acc case	87
Table 6.2 - Error Percentage of the Maximum and Minimum values when compared to the homologous values of the Method A – Mag case	87
Table 6.3 - Error Percentage of the Gyro's Offsets in three body segments when compared to the homologous values when IMU was at Position 1	88
Table 6.4 - Mean of the RMSEs between methods for normalized data – Acc x-axis.....	88
Table 6.5 - Mean of the RMSEs between methods for normalized data – Acc y-axis.....	89
Table 6.6 - Mean of the RMSEs between methods for normalized data – Acc z-axis.....	89
Table 6.7 - Mean of the RMSEs between methods for normalized data – Mag x-axis.....	89
Table 6.8 - Mean of the RMSEs between methods for normalized data – Mag y-axis.....	89
Table 6.9 - Mean of the RMSEs between methods for normalized data – Mag z-axis.....	90
Table 6.10 - Mean of the RMSEs between methods for orientation angles – Roll (SI: degrees) ..	90
Table 6.11 - Mean of the RMSEs between methods for orientation angles – Pitch (SI: degrees)	90
Table 6.12 - Mean of the RMSEs between methods for orientation angles – Yaw (SI: degrees)..	90
Table 6.13 - Mean of the RMSEs between methods for normalized data – Acc x-axis.....	91
Table 6.14 - Mean of the RMSEs between methods for normalized data – Acc y-axis.....	91
Table 6.15 - Mean of the RMSEs between methods for normalized data – Acc z-axis.....	91
Table 6.16 - Mean of the RMSEs between methods for normalized data – Mag x-axis.....	91
Table 6.17 - Mean of the RMSEs between methods for normalized data – Mag y-axis.....	92

Table 6.18 - Mean of the RMSEs between methods for normalized data – Mag z-axis.....	92
Table 6.19 - Mean of the RMSEs between methods for orientation angles – Roll (SI: degrees) ..	92
Table 6.20 - Mean of the RMSEs between methods for orientation angles – Pitch (SI: degrees)	92
Table 6.21 - Mean of the RMSEs between methods for orientation angles – Yaw (SI: degrees)..	92
Table 6.22 - RMSEs between calibration methods and the optical reference.....	95
Table 6.23 - RMSEs between different sensor fusion algorithms and the optical reference	95
Table 7.1 – Classification of collected data.....	103
Table 7.2 – Relevant metrics identified from both PCA procedures (Global Data).....	109
Table 7.3 – Relevant metrics identified from PCA procedure II (WF Data).....	111
Table 7.4 – Relevant metrics identified from PCA procedure II (PF Data).....	112
Table 7.5 – Relevant metrics identified from PCA procedure II (F's Data)	113
Table 7.6 – Different ROC analyses and their considerations	115
Table 7.7 – Predicted conditions - ASM WF** (FP–False Positive; TN–True Negative; TP–True Positive; FN–False Negative)	115
Table 7.8 – Predicted conditions-ASM WF* (FP–False Positive; TN–True Negative; TP–True Positive; FN–False Negative)	118
Table 7.9 - Predicted conditions-ASM WF (FP–False Positive; TN–True Negative; TP–True Positive; FN–False Negative).....	120
Table 7.10 - Predicted conditions-ASM Global* (FP–False Positive; TN–True Negative; TP–True Positive; FN–False Negative)	122
Table 7.11 – Predicted conditions-ASM Global (FP–False Positive; TN–True Negative; TP–True Positive; FN–False Negative)	124
Table 7.12 – Predicted conditions-ASM F (FP–False Positive; TN–True Negative; TP–True Positive; FN–False Negative).....	126
Table 7.13 – Predicted conditions-ASM PF Δ (FP–False Positive; TN–True Negative; TP–True Positive; FN–False Negative)	128
Table 7.14 – Predicted conditions-ASM PF (FP–False Positive; TN–True Negative; TP–True Positive; FN–False Negative)	130
Table 7.15 – Best combinations of parameters and the minimal Euclidean distance for each ROC analysis.....	132
Table 7.16 – Metrics of each ROC analysis (TPR – True Positive Rate).....	132

Table 7.17 – Results of the decision cascade when PF’s data were considered as different from the other types of data	134
Table 7.18 – Results of the decision cascade when PF’s data were considered like WF and Global’s data	135
Table 7.19 – Results of the Case 2 of the stage 3 (Input image: 28x28)	137
Table 7.20 – Results of the Case 2 of the stage 3 (Input image: 100x41)	138
Table 7.21 – Results of the Case 1 of the stage 4 (ASMs based classifier)	139
Table 7.22 – Results of the Case 2 of the stage 4 (ASMs based classifier)	139
Table 7.23 – Results of the Case 1 of the stage 4 (CNN)	139
Table 7.24 – Results of the Case 2 of the stage 4 (CNN)	140
Table I - Acc’s main characteristics	169
Table II – Mag’s main characteristics	169
Table III – Gyro’s main characteristics.....	169
Table IV – Temperature sensor’s main characteristics	170

Acronyms and Abbreviations

2D	Two-Dimensional
3D	Three-Dimensional
AAL	Ambient Assisted Living
Acc	Accelerometer
ADC	Analogue-to-Digital Conversion
ALSM	Algorithmic State Machine
ASM	Associative Skill Memory
ASMA	Activity Signal Magnitude Area
BOS	Base of Support
CAN	Controller Area Network
CF	Complementary Filter
CMEMS	Center for MicroElectroMechanical Systems
CNN	Convolutional Neural Network
COM	Centre of Mass
COP	Centre of Pressure
CRC	Cyclic Redundancy Check
DOF	Degree of Freedom
EA	Euler Angle
EE	Energy Expenditure
EMG	Electromyography
F	Fall
FF	Foot-Flat
FFT	Fast Fourier Transform
GDA	Gradient Descent Algorithm

GS	Gram-Schmidt Method
GUI	Graphical User Interface
Gyro	Gyroscope
HR	Harmonic Ratio
HS	Heel-Strike
IEEE	Institute of Electrical and Electronic Engineers
IMU	Inertial Measurement Unit
KF	Kalman Filter
LDS	Local Dynamic Stability
LL	Lower Limb
MARG	Magnetic Angular Rate and Gravity
maxLE	Maximum Lyapunov Exponent
MCS	Motion Capture System
MEMS	Micro-Electro-Mechanical System
MIMU	Magnetic/Inertial Measurement Unit
PC	Principal Component
PCA	Principal Component Analysis
PF	Pre-Fall
PPv	Peak-to-Peak Angular Velocity
Q	Quaternion
RF	Radio Frequency
RM	Rotation Matrix
RMSE	Root Mean Square Error
ROC	Receiver Operating Characteristic
ROM	Range Of Motion

RQ	Research Question
RSSI	Received Signal Strength Indicator
SMA	Signal Magnitude Area
STD	Standard Deviation
SVd	Dynamic Sum Vector
SVM	Signal Vector Magnitude
SW	Swing Phase
T	Trunk
TO	Toe-Off
USB	Universal Serial Bus
WD	Wavelet Decomposition

Chapter 1 - Introduction

With the intention to conclude the fifth year of the Biomedical Engineering course, branch of Medical Electronics, this thesis clings on work developed throughout 2016/2017 year. From the Center for MicroElectroMechanical Systems (CMEMS) of Minho University, it was possible to carry out all idealized work for this thesis. The Inertial Measurement Units (IMUs) based system from CMEMS has been validated, and calibration methods were implemented in order to improve detected limitations. Besides that, a fall (F) and pre-fall (PF) detection system based on a classifier was also implemented, and delineated experiments were run and data was used to gait analysis.

In the scope of the assistance and rehabilitation field, the proposed work aims to detect situations with high probability of F with some advance in time. This type of gait analysis through orientation calculation of the lower limbs (LL) and trunk (T) is, effectively, the main goal of this work. In this context, it is needed firstly to validate the IMUs based system used, in order to inspect the reliability of the system. After, a calibration strategy would be integrated in the system to improve system's results. Finally, a F and PF detection system through IMUs based system's data was tested in order to achieve an offline scenario of walking assisted in clinical environments. All the procedures, analysis and conclusions are detailed in this dissertation.

1.1. Motivation

Human walking, which is one of many types of human gait, can be considered as complex and a common human physical activity that can be performed in a variety of ways and directions, and that requires muscular strength, joint's mobility and coordination of the central nervous system [1]. According to [2], the normal gait can be affected by a number of neurological injuries that have been investigated in order to improve the early diagnose techniques and to develop and/or to assess the treatments. Specially, from gait pathologies are highlighted: stroke; poliomyelitis (polio); spinal cord injury (SCI); Parkinson disease (PD); cerebral palsy (CP); multiple sclerosis; hip and knee osteoarthritis; muscular dystrophy; gait degeneration in elderly subjects; rheumatoid arthritis; degenerative joint disease; and myelomeningocele. Consequently, the main symptoms used to diagnose and to assess the progress of the gait impairments are disorders and abnormalities of the gait caused by walking diseases.

Thus, a detailed knowledge about gait's characteristics at a given time, and monitoring and evaluating over time, will allow early diagnosis of diseases and their complications, which contributes to the decision of the treatment that should be chosen [3] or to prevent the occurrence of Fs, which is one of the most common health concerns especially in elderly people [4], [5]. Even medications or normal physiological changes have the same trend than the above mentioned diseases and may result in alterations of balance, being as well risks of F.

In fact, Fs are the leading cause of fatal and non-fatal injuries among the elderly and represent a relevant economic burden to society [6]. Only in the United States of America, \$19 billion were spent on the direct medical costs of F related injuries in 2000. Only hip fractures, which are commonly associated with Fs, cost \$8.7 billion/ year [4]. Because the U.S. population is aging, both the number of Fs and the costs to treat F related injuries are likely to rise. In 2015, costs for Fs to Medicare alone totalled over \$31 billion [7], which is a far higher number than that registered 15 years earlier. The costs of treating F related injuries goes up with age and the F incidence is higher among women [7]. Fs, with or without injury, also carry a heavy quality of life impact. Fear of falling is common among the elderly and, as a result, it limits their activities and social engagements. Obviously, this tends to further physical decline, depression, social isolation, and feelings of helplessness [4].

In order to decrease the incidence of F and healthcare costs associated with F related injuries, it is necessary to widely implement F prevention methods. Currently, there are procedures to assess the patient's risk of F, where some parameters are assessed and then prevent measures such as medication or diet are implemented according to the determined level of risk. These procedures are also accompanied by methods to attempt to improve gait performance like: training assisted by therapists; the passive devices (as canes and wheeled walkers); the treadmill with partial body weight support; functional electrical stimulation; and the active lower limb devices (as orthoses and exoskeletons) [8], [9].

Aware of the existence of the presented type of procedures, there are also real-time monitoring devices capable of detecting Fs [10], [11]. Some of them are also able to act in order to avoid the subject's impact on the floor [12]. Nevertheless, the accuracy's values of these devices or even the time to detect Fs before impact are still not optimal. Additionally, the commercial designs should be improved in order to ensure an assistance according to patient's disability, assist therapists with early alerts of warning, and perform an efficient management of human-robot interaction without clinical assistance.

1.2. Problem Statement and scope

The field of Fs prevention is a very interesting area with a direct impact on the prevention of injuries due to Fs and the reduction of health costs. However, to get closer to the optimal idea of a real-time monitoring device capable of detecting and preventing Fs, it is necessary to do a preliminary work in order to determine what sensors will be used and where to place them, what gait parameters are relevant and should be calculated, and what technique will be used to classify gait's data. Thus, it is crucial to make a deep research in the scientific literature about several themes and only then start the practical part.

Firstly, it was decided to use an existing IMUs based system [13], which is wearable and capable of collecting data from human gait. In order to use well the IMUs based system it was necessary to validate and calibrate the system. The validation process involves the communication protocol, the typical gait signals of the sensors, and a system of knee angle measurement. Sensors also needed to be calibrated and several methods tested to get better and more reliable results. The comprehension of the system can be helped with a graphical user interface (GUI), and data can be well separated with an efficient algorithmic state machine (ALSM). Then, combining this knowledge with the important and related gait parameters or metrics, it was possible to have a system with the ability to give information about human gait. Through a statistical analysis, Principal Component Analysis (PCA), it was possible to restrict the number of metrics. Finally, by means of statistical methods or deep learning approaches it was possible to classify human gait's data.

All aspects previously expressed reveal a serious and important relevance of this field, presenting an innovative character, covering several areas of knowledge and contributing to the scientific community with advancements able to help answer some important questions.

1.3. Goals and research questions

The ultimate goal of this thesis is the development of an offline classifier capable of distinguish normal gait from F and PF's situations, from the integration of relevant gait's parameters by means of an IMUs based system during some daily living activities. In order to achieve this ultimate goal, it is required the knowledge of basic concepts of human walking, as well as the knowledge of sensors' characteristics, sensors' attachment location, specification of the walking trials, and the most relevant gait parameters to this particular situation. Additionally, it is

important to understand the evolution of the gait's parameters during the gait cycle and the way the F and PF's situations influence these gait parameters.

Thereby, with this thesis it is necessary to achieve the following goals:

- **Goal 1:** the first goal consists in a survey and critical analysis of relevant information about IMUs, namely the state of the art and methods used in the literature to overcome the problems in this technology, to calculate joints' angles and to validate the use of the system. It is also important to understand which sensors are most used in the literature to monitor human gait. This goal will make it possible to conclude on the potentials and the lacks of the current state of the art for these topics.
- **Goal 2:** this goal aims to understand how Fs are classified in the literature, as well as the existing types of systems, methods and devices concerning this field. In this goal it is also important to understand which are the typical gait parameters, sensors, attachment location of the sensors, age, and experimental setups. Since this field has potential to grow, challenges, issues, and trends are also important to understand the near future of this area.
- **Goal 3:** the third goal consists in improving on existent IMUs based system by developing real-time Matlab® GUI to get and process IMUs' data. This includes the development of an ALSM to process the data, and make the communication system more reliable. This goal is to improve the IMUs system from a previous work [13] and will made possible a more practical use of the current system.
- **Goal 4:** as fourth goal it is proposed the validation of the IMUs based system. This process should cover an important series of topics that allow the use of the system during everyday activities, namely: i) the communication protocol; ii) the typical sensors' signals of human gait; and iii) the joint's angles estimation. This goal is very important to verify the reliability of the IMUs based system, and is essential for the next goals.
- **Goal 5:** this fifth goal consists in a survey for calibration procedures in the scientific literature and its implementation in the IMUs based system. In this goal, several tests should be performed, as well as a comparative analysis, considering the recent works in the literature. An optical system should also be used as a ground truth system. Once

again, this goal is very important to make the IMUs system more accurate to the next goal.

- **Goal 6:** the last goal aims to develop a strategy able to recognize normal gait, F and PF's modes of locomotion from data of the gait cycles. Thus, it will be possible to combine in one system a F detection system and a PF detection system. In order to get good results, this goal need to have in consideration the extracted conclusions from previous goals, as well as a previous treatment of the data obtained from the IMUs based system. A statistical analysis (PCA) should be also performed to reduce the number of metrics, which reduces the computational weight. Then, two strategies were applied. Firstly, the concept of ASMs was innovatively used to build a classifier. Secondly, a Convolution Neural Network (CNN) was used to make the aforementioned classification. The overall work has been described throughout this master's thesis.

The following research questions (RQ) are expected to be answered in the present work:

- **RQ1:** What are the most used sensors to perform gait monitoring? Can the drift be compensated in the IMUs based system? And under what conditions? This RQ is addressed in Chapter 2.
- **RQ2:** What are the most commonly used sensors in F or PF detection systems? This RQ is addressed in Chapter 3.
- **RQ3:** To what extent does the GUI help to improve the user-system relationship? What is the reliability of the proposed ALSM? This RQ is addressed in Chapter 4.
- **RQ4:** Considering the used wireless IMUs based system, how many IMUs can be connected to the base station without problems? What can be done to increase the number of connected modules? This RQ is addressed in Chapter 5.
- **RQ5:** Given the sampling frequency of the system, is it possible to get the data of the human gait correctly? This RQ is addressed in Chapter 5.
- **RQ6:** Is it possible to perform an on-body calibration without major errors? This RQ is addressed in Chapter 6.

- **RQ7:** Which are the metrics with greater potential to detect F and PF's situations in the implemented classifiers? This RQ is addressed in Chapter 7.
- **RQ8:** Which is the best classifier to be used in the recognition of normal gait, F and PF's modes of locomotion? This RQ is addressed in Chapter 7.

1.4. Contribution to knowledge

The main contributions of this work are:

- The improvement of the wireless IMUs based system from the CMEMS, creating a real-time GUI to help monitor the human gait in real time that enables to better understand the information from the IMUs. The interface not only improved the speed of data processing, but also facilitated the interaction between the user and the system, providing a clearer information exchange.
- An ALSM that was implemented in order to ensure a clearer and more reliable data processing. Data from sensors can be used to estimate the orientation of each module through the use of a complementary filter (representation achieved in Quaternions and/or Euler angles) and other functionalities, based on previous work [13].
- The validation of the IMUs based system on several domains, e.g. the communication protocol or the estimation of orientation or joints' angles. This step proved to be very useful in the collection of human gait's data.
- A simple proposed method for initial calibration of the sensors. Several tests were performed to determine the accuracy of this quick method that does not take longer than 5 seconds.
- A tool that accurately implements of the locomotion mode recognition, *i.e.*, discriminate between different types of data, namely: normal gait, F's situation and PF's situation (step before a fall). This tool is fundamental to be integrated in the IMUs based system in order to apply adaptive assistance based on human gait during daily living activities. This tool and its major concepts were demonstrated offline and detailed comparisons were evaluated. Two different methods/tools presented in the literature were implemented: i) ASMs based classifier, and ii) a CNN which is an essential tool for deep learning. The ASMs concept was innovatively used within the context of human fall prediction.

1.5. Publications

From the work developed during this academic year, it was possible to publish four conference papers and the submission of one journal article. One conference paper was also selected for possible publication in a journal.

Journal article

- N. F. Ribeiro and C. P. Santos, "Orientation Estimation Using IMUs for Human Gait Analysis: A Systematic Review," *Journal of Medical Systems*, 2017. (*under revision*)

Conference papers

- N. F. Ribeiro and C. P. Santos, "Inertial measurement units: A brief state of the art on gait analysis," 2017 IEEE 5th Portuguese Meeting on Bioengineering (ENBENG), Coimbra, Portugal, 16-18 February, 2017.
- N. F. Ribeiro, J. Figueiredo and C. P. Santos, "Validation of a wireless communication protocol to monitor human gait using IMUs," 2017 IEEE 5th Portuguese Meeting on Bioengineering (ENBENG), Coimbra, Portugal, 16-18 February, 2017.
- N. F. Ribeiro and C. P. Santos, "An intuitive visual interface for a real-time monitoring system for human gait using IMUs," 2017 IEEE International Conference on Autonomous Robot Systems and Competitions (ICARSC), Coimbra, Portugal, 26-27 April, 2017, pp. 153-158. (***Selected for possible publication - Robotics and Autonomous Journal (Elsevier)***)
- N. F. Ribeiro, C. Ferreira, L. P. Reis, H. Silva, P. Macedo, L. Rocha and C. P. Santos, "Validation of a Knee Angle Measurement System Based on IMUs," in CLAWAR 2017 - The 20th International Conference on Climbing and Walking Robots and the Support Technologies for Mobile Machines, Porto, Portugal, 11-13 September, 2017.

1.6. Thesis outline

The reminder of this master's thesis is organized as follows. In Chapter 2 is presented a general overview of the IMUs, introducing the place of the IMUs in the gait analysis systems, the

group of sensors that can constitute an IMU, and relevant characteristics and applications of these sensors. Also, are highlighted commercial IMUs available on the market and their respective brands, the problems that IMUs can suffer from, methods to represent and estimate angles from this technology, the importance of calibration procedures, and challenges to overcome in the near future.

An introduction about Fs, the problems they constitute among the elderly, and how to classify them is available in Chapter 3. Herein, are also presented the methods used to prevent and detect Fs, and the most used gait parameters or metrics, sensors and respective attachment location in the scientific literature. Besides, this chapter end with the current challenges, issues and trend about this important theme.

Chapter 4 contains a complete overview about the IMUs based system used throughout the current master's thesis. The Magnetic/Inertial Measurement System is initially described by focusing in its constitution and in sensors' details. The communication protocol is also addressed, as well as the created GUI, and the ALSM.

Chapter 5 describes the implemented validation processes and their respective results. Firstly, the communication protocol was tested and validated through physical tests. Signals of the IMUs' sensors were compared to typical signals presented in the scientific literature in trials with similar conditions. DARwin OP was also used as a ground truth system to validate a knee angle measurement system based on IMUs.

Calibration procedures are truly important in the IMUs' domain to prevent errors. So, several calibration methods presented in the literature were implemented and tested in four different stages throughout Chapter 6. These stages involve comparisons between methods at the level of the raw data and estimated angles, comparisons of estimated angles with different calibration methods with an optical reference system, and the use of multiple filters to estimate orientation. Respective results and discussion are also presented.

An offline F and PF detection system is described in Chapter 7. In this chapter, the IMUs system is used to collect gait's data from several subjects and from some types of trials. This information was, initially, filtered, separated by gait cycles and used to estimate some gait parameters. Then, through PCA procedures, relevant data were extracted and used to build sets of ASMs for each type of locomotion mode. Best combination of parameters for each set of ASMs was determined using Receiver operating characteristic (ROC) analyses. These sets of ASMs were

also used to construct an ASMs based classifier. A CNN was also used as classifier. The results are also discussed.

The conclusions of this work are made in Chapter 8. Finally, the proposals to continue this work in the future are written in this chapter too.

Chapter 2 – Inertial Measurement Units: State-of-the-art

2.1. Introduction

Gait analysis systems are no exception in the set of monitoring systems that establish a symbiosis relationship with the Ambient Assisted Living (AAL) environments. Not only in individuals in need of treatment or rehabilitation, but also in healthy and elderly people, analysis of the human locomotion has a very important role always aiming at improving the quality of life. In fact, a deep and detailed knowledge about gait characteristics at a given time, and not least, monitoring and evaluating over time, will allow early diagnosis of diseases and their complications, and contribute to the decision of the treatment that should be chosen [3].

Gait analysis involves measurement, description and assessment of gait parameters that characterize human locomotion [14], [15]. In order to quantify these gait parameters, there is a set of several techniques [3] used for gait measuring:

- Image Processing: which is a collection of techniques used to calculate and obtain a map of distances from a viewpoint. They are able to obtain important elements of the image with a better and faster real-time process. For this purpose there are some technologies such as Stereoscopic Vision (camera triangulation), Time-of-Flight Systems (ToF), Structures Light, Infrared Thermography (IRT) and Laser Range Scanner;

- Floor Sensors: where sensors are placed along the floor on the force platforms. In this instrumented walkways gait is measured by pressure or force sensors and moment transducers when the subject walks on them. There are two types of floor sensors: force platforms and pressure measurement systems;

- Wearable Sensors: which includes, e.g., pressure and force sensors, accelerometers (Accs), gyroscopes (Gyros), active markers, extensometers, inclinometers, goniometers, ultrasonic sensors, IMUs, and electromyography (EMG). These are placed on various parts of the patient's body to measure different characteristics of the gait.

Among all the techniques mentioned, wearable sensors units reveal an extreme potential to monitor ambulatory activities in the home environment, and their reliability has since been demonstrated in various studies. So, the connection between this technique for measuring gait and

AAL is truly promising [16],[17],[18]. This way of analysing human motion is considered as continuous and ambulatory and has an outstanding importance in:

- i. The detection of risk situations such as F detection in elderly patients [18];
- ii. The process of rehabilitation in injured patients, generating input for health interventions (real-time personalized feedback), design of treatment plans and follow-up monitoring [19];
- iii. The diagnosis and treatment of patients with neurological diseases [20].

As already mentioned, wearable sensors have an important role in human gait analysis. The achievements of human gait analysis can be divided in three main areas, namely, kinematics, kinetics and EMG. Kinematics of human gait describes the movements of the major joints and components of the lower extremity, collecting gait's data through the use of multiple sensors. With this collected information, this type of analysis is able to recognize the gait phases, obtain the most important gait parameters and movement information on the body segments [14],[21],[22]. Gait kinetics studies forces and moments that result in the movement of body segments in a human gait, including the kinetic analysis, and has been an important part of healthcare evaluation and the clinical diagnosis. Forces between the foot and the ground are the focus of the kinetic measurement and allow the application of adaptive force sensors [14],[21],[22]. In turn, EMG is mostly used to detect and measure the small electric current produced by muscles during contraction and is now an important method in clinical gait analysis. With the development of wireless technology and its application on sensors, EMG has become a very reliable and wearable tool for gait analysis. EMG is obtained from the subject by a non-invasive intervention with surface electrodes [3],[14].

According to Liu et al. [16], recent research on wearable sensor systems for biomedical applications can be divided into two major parts. In one hand, state recognition on daily physical activities including walking feature assessment, walking condition classification and gait phase detection, in which the kinematic data obtained from inertial sensors such as Acc or Gyro are immediately used as inputs of some inference techniques. On the other hand, there is the accurate measurement of human motion such as joint angle, body segment 3D position and orientation, in which measurement calibration and data fusing of different inertial sensors are important to minimize errors of the quantitative human motion analysis.

Given its importance in gait analysis, it is then necessary to define what an IMU is. Thus, an IMU can be described as an electronic device that can combine multiple sensors such as Accs, Gyros, and magnetometers (Mags) (Fig. 2.1). This electronic device may be equipped with an antenna (wireless technology), or a secure digital (SD) card or even an output pin logged by wire to a base station. IMU is the most commonly designation for this electronic device [13], [23], [24]. However, when a Mag is present, some authors used other designations: magnetic/inertial measurement unit (MIMU) sensor [25] or even magnetic angular rate and gravity (MARG) sensor [26]–[28]. Thus, throughout this thesis the term IMU is the general designation to mention IMU, MIMU or MARG sensors.

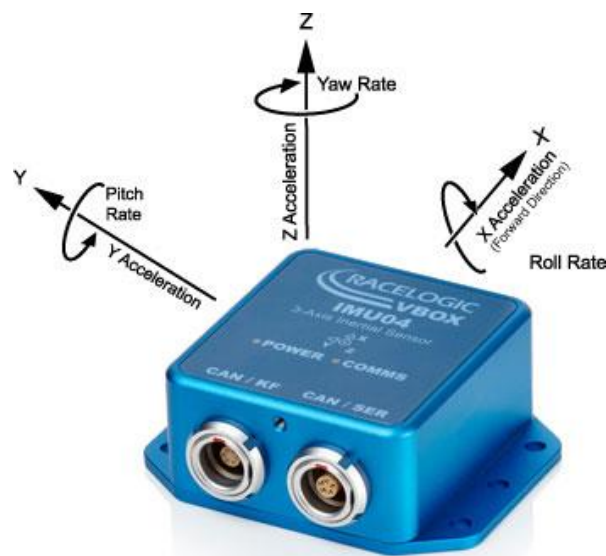


Figure 2.1 - Example of a RLVBIMU04 IMU from VBOX Automotive with wire connection [194].

Basically, the three sensors mentioned above are the commonly used in IMUs for gait analysis. This happens because they are important sensors for obtaining relevant data to this type of analysis. In particular, an Acc is a type of inertial sensor that can measure acceleration along its sensitive axis and can also be classified as either a mechanical or solid state device [14],[29]. A mechanical Acc, Fig. 2.2.a, consists of a mass suspended by springs. The displacement of the mass is measured using a displacement pick-off, giving a signal that is proportional to the force acting on the mass in the direction of the input axis. The mass proof can be forced to deflect by the inertial force because of acceleration or gravity according to Newton's Second Law [14], [29], [30]. Solid state Accs, Fig. 2.2.b, establish a set of various sub-groups that includes surface acoustic wave, vibratory, silicon and quartz devices. They are characterized as small, reliable and rugged [29]. Technically, they are often used to obtain physical activity levels, accelerations during

walking, gait cycle time and number of walking steps can be determined using several Accs affixed to the subject. Motion activated functions, free-fall detection, pedometer, display orientation and vibration monitoring and compensation are a few applications this device can perform [13], [30].

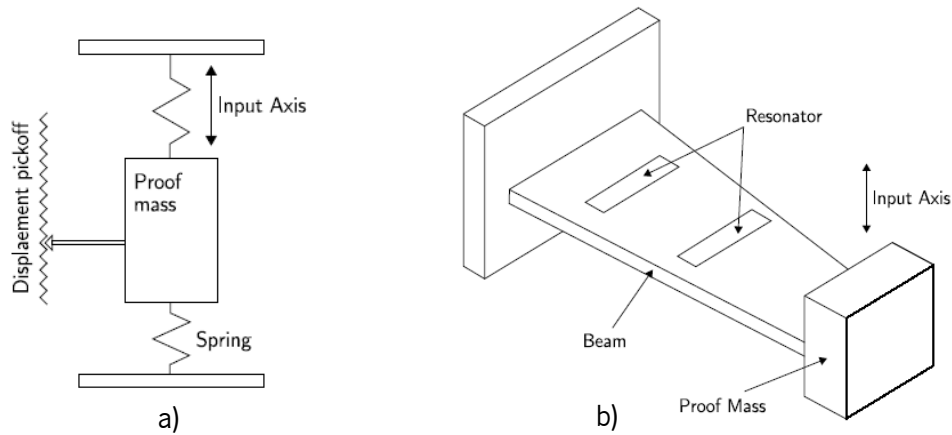


Figure 2.2 - a) A mechanical Acc; b) A surface acoustic wave Acc [194], [29].

In turn, a Gyro is a spinning wheel or disc in which the axis of rotation is free to assume any orientation by itself as depicted in Fig. 2.3. When rotating, the orientation of this axis is unaffected by tilting or rotation of the mounting, according to the conservation of angular momentum. For this, Gyro are useful for measuring or maintaining orientation and can be considered as an angular velocity sensor. It can be applied for the measurement of the motion and posture of the human segment in gait analysis by measuring the angular rate, angle of various joints and the flexion angle (integration of the angular rate) [13], [14], [16].

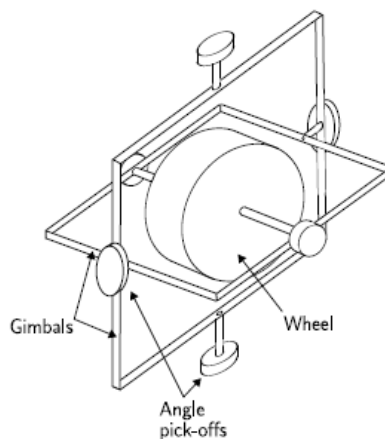


Figure 2.3 - A conventional mechanical Gyro [29].

IMUs can also be equipped with magnetic field sensors. This is a device capable to detect and measure magnetic fields. Its operating principle is based on detecting effects of the Lorentz force which may be measured electronically with a change in voltage or resonant frequency or

measured optically with a mechanical displacement [31]. Figure 2.4 depicts a micro Mag where white arrows indicate the current flow through the flexures while the location of the lower sensing electrode is indicated in yellow. Although the necessary concern with the compensation for temperature effects, advanced electronics are used to improve the sensitivity. So, these instruments have medical and biomedical applications, and implemented in an IMU it is mostly used to assist calibration against orientation drift. This allows better performance for dynamic orientation calculation and can be used in multiple applications such as reference measure for body orientation or earth gravity field, linear/rotary position, speed measurement and current sensing [31].

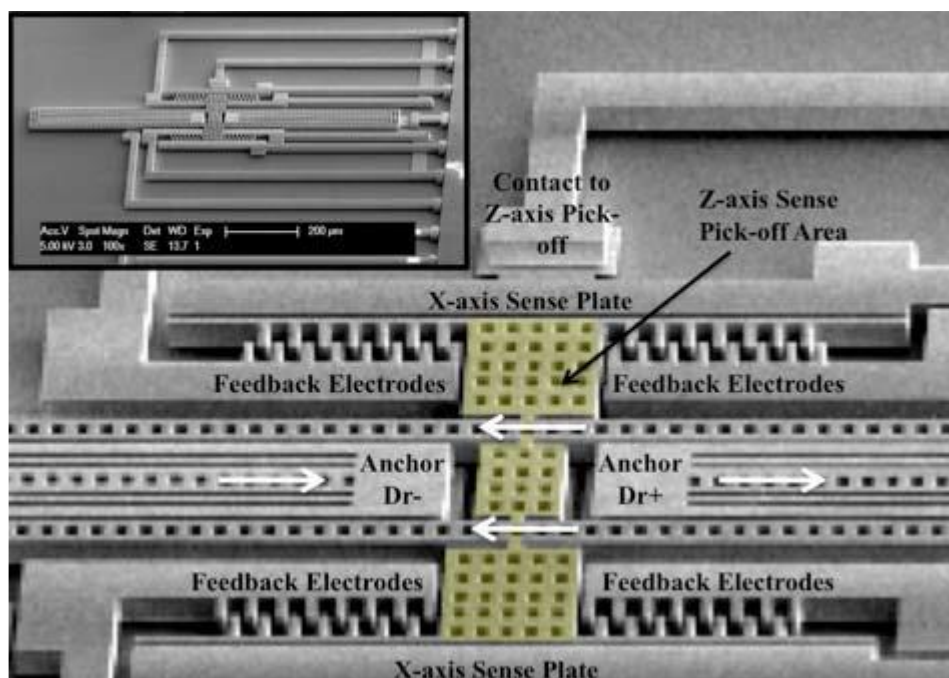


Figure 2.4 - Image of a micro Mag structure [195].

2.2. Applications and Commercial IMUs

In areas like mobile robots, IMUs are frequently used to improve odometry or for flight stabilization or autonomous hovering of helicopters or quadrotors. Moreover, this type of sensors is widely used for localization of airplanes and miniature indoor blimps. However, with regards the monitoring of the human being, IMUs can be integrated into clothes, shoes or even used with Velcro straps [13], [23]. Thus, IMUs enable full 3D location/orientation information and full-body motion capture [23]. In fact, IMUs show a vast number of applications in this kind of monitoring, allowing, for example [3], [32]: Gait symmetry and gait normality measurements [33]; Creation of

F-risk prediction models; Study of motion of each joint and the body orientations based on portable force plates and motion sensors; Prediction of gait initiation and termination [34]; Estimation of walking speed [35]; Estimation of movements of thighs from movements of shanks to reduce the number of sensing units; Long-term monitoring of human movements; Assessment of energy expenditure; Study physical activity, postural sway, postural orientation [36], activity classification and estimation of temporal gait parameters; 3D joint or lower limb angle measurement or orientation estimation of LLs or joints [37].

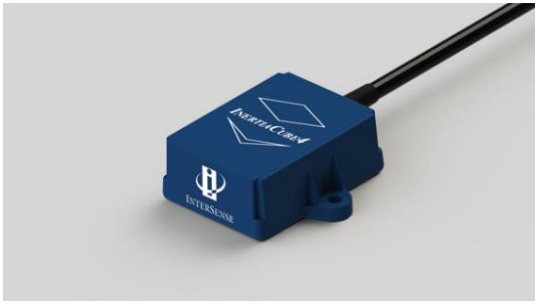
Obviously, the main focus is portable applications, in which small dimensions are essential and existing research prototypes are usually smaller and lighter than commercial products. Nevertheless, in dynamic applications, high raw data rates are required for precise data processing and state estimation, which affects the development of IMUs designs. Currently, the IMUs' performance can be accessed through the bandwidth, drift, linearity and sample rate of their sensors [23].

Today, at a commercial level, there are many companies interested in the production and improvement of IMUs. Obviously, at this level of competition, there is a constant race by companies to improve products' characteristics at competitive prices. Companies like Xsens, InterSense, Technaid, IMeasureU or Noraxon offer a wide range of products related to IMUs with own distinctive characteristics. For example, Xsens has products like isolated IMUs (MTi1-series, MTi10-series and MTi100-series) and two hardware versions of a full-body human measurement system based on inertial sensors that require the use of suit with trackers (MVN Awinda and MVN Link are shown in Fig. 2.5). MVN Awinda has 17 wireless trackers and a station per actor which requires 17 batteries with 6 hours of life. In terms of accessibility, it is characterized by wearable straps and one-size-fits-all. In turn, MVN Link has 17 wired trackers and one access point for multiple actors which requires only one battery with 9.5 hours of life. It is described by a Lycra suit with 5 sizes. This company also offers a software for motion capturing called MVN Studio. This software is able to exhibit, for example, real-time 3D visualization and data integration, and playback and editing of motion capture data [38].



Figure 2.5 - Xsens MVN products [38]. MVN Awinda is on the left side. MVN Link is on the right side.

InterSense motion tracking products are industry solutions, being integrated into the next generation position, navigation and stabilization systems. This company produces three degrees of freedom (DOF) and 6-DOF trackers. 3-DOF trackers belong to InertiaCube line of orientation sensors. From this line there are two products known as: 1) InertiaCube4TM (Fig. 2.6.a) that offers superior performance over its predecessors while minimizing size and price, and is ideal for real-time applications in simulation and training, virtual and augmented reality, motion capture, and human movement analysis; and 2) InertiaCube BTTM (Fig. 2.6.b) that provides real-time orientation data via a standard Bluetooth interface to computer. It is a wireless sensor for human movement analysis. In turn, in 6-DOF trackers category there are also two products: IS-900 system (Fig. 2.7.a) and IS-1200+ system (Fig. 2.7.b). The first one is the system of choice for precise position and orientation (6-DOF) tracking in military and industrial simulators, immersive displays, virtual prototyping and film production. This system is immune to metallic interference, while offering real-time tracking in various environments. IS-1200+ system is a recent optical and inertial based 6-DOF tracking system. The system offers tracking data utilizing a fusion of inertial-optical technology [39].



a)



b)

Figure 2.6 - InterSense 3-DOF trackers [39]: a) InertiaCube4TM; b) InertiaCube BTM.



a)



b)

Figure 2.7 - InterSense 6-DOF trackers [39]: a) IS-900 system; b) IS-1200+ system.

Technaid is a company developing technology for several applications such as biomechanics, rehabilitation, motion analysis, virtual reality and robotics. In respect to motion analysis, this company developed recently the Tech IMU V4 series. IMU V4 series represents the last versions of inertial sensors developed by this company. Each Tech IMU integrates three different MEMS (Micro-electro-mechanical system) sensors, a 3D Acc, a 3D Gyro, and a 3D Mag. IMU CV4 (Fig. 2.8.a) and IMU V4 (Fig. 2.8.b) are the two examples of developed inertial sensors from V4 series, and three types of communication interfaces are available: CAN (Controller Area Network) Standard, tech MCS (Motion Capture System), and USB (Universal Serial Bus). The mentioned company also has a motion capture system Tech MCS (Fig. 2.9) which is a complete wireless motion analysis solution, based on one of the lighter and smaller inertial sensors of the market (Tech IMU). It's similar to MVN Link from Xsens because it also has wired trackers and one access point for multiple actors which requires only one battery. Although, it is important to refer that motion capture system from Technaid is not a Lycra suit but comes with textile and plastic adapters. The company also developed a software that accompanies each Tech MCS package. It is able to record and show whole human performance in real-time on Personal Computer [40],[42].



Figure 2.8 - Technaid products [40]: a) IMU CV4; b) IMU V4



Figure 2.9 - Technaid Motion Capture System [40].

IMeasureU is a wearable technology company from New Zealand that build solutions capable to provide high fidelity athlete movement and workload data used to characterise fatigue, enabling optimal recovery, training and performance. Concerning to their product, they have a small, lightweight sensor that contains a 9-axis IMU (Fig. 2.10), where data sampling up to 1 kHz can be stored on the device or transmitted via Bluetooth Smart to a computer or phone. This way, IMU measures and quantifies an athlete's motion in their natural environment. The system accurately measures sports-specific movement and quantifies biomechanical workload used to identify athlete fatigue and up to 8 sensors can be synchronised simultaneously through IMU software [41].



Figure 2.10 - IMeasureU IMU sensor [41].

Noraxon is an American company that has been a leader in manufacturing and distributing high-end measurement and training devices, such as EMG, gait analysis, biofeedback, and 2D/3D motion analysis that enables a unique approach to a fully equipped analysis and therapy concept for evidence-based clinical and research applications. As products they have myoMOTION (Fig. 2.11) that enables the capture of human motion in 3-DOF, wirelessly. Translational data via double integration is simple and accurate with our built-in math tool kit. The entire process is portable by using IMUs placed on any segment of the body that precisely tracks the 3D angular orientation of that body section. This concept is easily expandable from a single joint of interest to a simultaneous full body measurement across all major articulations. The software provides orientation data and/or linear acceleration data [42].



Figure 2.11 - Noraxon myoMOTION device [42].

SparkFun is an online retail store that sells components and widgets, and offers classes and online tutorials designed to help educate individuals in the world of embedded electronics. This company also sells IMUs with six and nine DOFs [43]. Other companies such as Arduino, InvenSense, and x-io Technologies Limited also sell products like those mentioned above constituting a group of alternatives.

However, trademarks are not the only entities focused on IMUs. Research groups are also engaged in efforts to improve this technology. According to some research groups, efforts are being made to extol certain characteristics like the miniaturization of the device to apply this technology to the gait analysis [23]. Benocci et al. [44] used the IMU ADIS16350 which integrates a digital 3-axes Acc and a digital 3-axes Gyro in 22x22x22 mm with high resolution, bandwidth and sensitivity to communicate via Bluetooth with a base station to monitor gait. With the same type of sensors, IMU used by Macedo et al. [13] was the MPU-6000 with a Honeywell 3-axis Digital Compass IC HMC5883L connected to a CC2530EM module to allow a Radio Frequency transmission. Höflinger et al. [23] presented a wireless Micro-IMU based on MEMS sensors with large scale integration which can be integrated into clothes or shoes for accurate position estimation in mobile applications and location-based services. Barton et al. [45] also presented a cubic IMU design and wireless technology. Tsai et al. [46] showed 1 cm³ wireless IMU without Gyros and Lim et al. [47] made a combination of ordinary Accs and Gyros with a line encoder with a small size. Besides, it is important to refer that funding for research nowadays comes from projects that include both universities and companies. Therefore, the development is joined.

2.3. Advantages and Disadvantages

Taking into account all that has been mentioned about IMUs, multiple parameters like precision, conformability, usability or transportability demonstrate that the portable systems based on body sensors are promising methods for gait analysis [3]. As advantages, it is clear that inertial sensors compared to other systems are lighter, smaller, cheaper, portable, wearable, non-invasive and do not alter natural movement patterns [16], [48]. Nevertheless they have the advantage of identifying human motion in a wide variety of environments [49]. Even the gait analysis when using wearable sensors becomes cheaper, more convenient and provides an indication of the intensity level of physical activity [17]. In this type of analysis, the use of 3D-sensors allows the recording of motion in three planes and provides more information [17].

Despite all this, there are some characteristics with negative connotation that should be taken into account. Acc and Gyro's data cause computational problems for determining the angles [32]. Concerning to the magnetic sensor, the presence of magnetic disturbances (as induced, e.g., by ferromagnetic material) may limit the accuracy of the orientation estimates by means integration [50]. Like any machine, a wearable sensor system has imperfections. Some of these imperfections are sensor attachment errors, regular calibration maintenance, external signal noise, signal filtering errors and integration drift, and is computationally complex [3],[51]. Therefore, inertial sensors are less accurate than laboratory systems [48]. A further disadvantage is the need to place devices on the subject's body, which may be uncomfortable [14]. Lastly, the size of power consumption of the IMUs is an important limitation of the current gait analysis systems, which affects directly the measurement capacity of the system and monitor the gait parameters over long time period [3].

2.4. Methods and Problems

As for the methods, Quaternions or Euler parameters (Q), Rotation matrices (RM) or Euler angles (EA) are examples of methods used to represent orientation of segments or joints. Usually, these three methods are applied in 3D orientation [51]. Gram-Schmidt method (GS) is an optimization method used to find the best orientation [52]. Kalman filters and their derivatives (KF) [53], the gradient descent algorithm (GDA) , and the complementary filter (CF) [54] are the most used sensor fusion algorithms among the studies. Usually tools like the GS method [52].

IMUs also have problems that must be solved in order to allow more precise and accurate measurements especially in gait analysis field. One of the biggest problems is integration. Blumrosen et al. [55] indicated that small errors in the measurements can be accumulated and increase the tracking error over time in respect to the Acc and Gyro integration. When accumulated, integration errors can cause deviations of the calculated results from the true values. This situation is often referred to as a drift [16], [32], [49]. Although this problem occurs with some frequency, today there are solutions to integration problems that are used by research groups.

According to Blumrosen et al. [55] the repetition pattern of gait can be used to estimate the time intervals needed for carrying an efficient implementation of the strap-down integration, exclude the IMU bias and minimize the error to less than 10% of the stride length. The same authors state that anthropometric considerations or advanced filtering e.g. using extended Kalman filters can be used as well. The aggregation of other sensors can also reduce the error

accumulation. This group of researchers used the Received Signal Strength Indicator (RSSI), which is a measurement of the signal power on a radio link, to estimate mobile nodes location. They focus on three main techniques to exploit the RSSI measurements: track body part based on RSSI measurements only; extract kinematic features; and aggregation of RSSI measurements and other sensor modalities like IMU (RSSI data was aggregated with only one IMU data using a KF). According to their results was demonstrated that the accumulation of error was minimized using the RSSI measurements and the tracking accuracy compared with the one based only on RSSI measurements, can be improved by around 50 percent.

Djurić-Jovičić et al. [32] argue that the use of KF in the integration procedure decreases the drift and provides for real-time applications, however it requires calibration and data from other sensors (Accs, Gyros, and magnetic sensors in most cases) for error minimization, as well as noise statistics and good probabilistic models. These group of researchers presented a new method for estimating angles of leg segments and joints, which uses Acc's arrays attached to body segments. The absolute angle of each body segment was determined by band pass filtering of the differences between signals from parallel axes from two Accs mounted on the same rod. Joint's angles were evaluated by subtracting absolute angles of the neighbouring segments. This method eliminates the need for double integration as well as the drift typical for double integration. Another way to reduce the error accumulation is by aggregation of other sensors (Acc and Mag's data), through sensor fusion algorithms [48], [50], [55].

In turn, Ambrozic et al. [48] implemented a kinematic model of the human body into their sensory fusion algorithm with the purpose to greatly reduce the drift without the need for standstill. With a wearable sensory system that comprises sensorized insoles, pressure-sensitive pads to measure human-robot interaction, IMUs, vibrotactile modules for afferent feedback and sensors for detection of amputee psychophysiological stress status, they perform a tracking of motion parameters and an estimation of kinematic data of the wearer for use in controlling active lower-limb ortho-prostheses. At an algorithmic level, this group of authors combined data collected from IMUs that is used to produce estimates of segment orientations and from sensorized insoles worn inside sneaker shoes that provide information on vertical ground reaction force amplitude and distribution, in order to extract information about the subject's kinematics, movement type and phase, and track selected biomechanical stability descriptors. In order to assess kinematic parameters, these researchers made a common approach for determining orientations that

consists in the use of a KF from collected data of seven IMUs. They are based on individual segment's angular velocity integration during motion and orientation correction in relation to gravity. They used the Acc as an inclinometer to determine the intermediate angle of inclination. A Mag was also used and was assumed that magnetic field in space is locally constant and non-parallel to gravity. It was concluded that the approach often results in a drift during long-term dynamical movement due to Gyro's drift, errors introduced by separations of gravity and dynamic acceleration, and changes of the magnetic field. This way, to solve the problem or try to mitigate it, these researchers introduced the resetting during standstill in a first attempt. However, the introduction of a kinematic model of the human body into the sensory fusion algorithm was able to reduce the drift without need for standstill.

Errors introduced by separation of gravity and dynamic acceleration, changes of the magnetic field and temperature dependency, and the orientation error tends to grow with time owing to the drift of integrated Gyro output [16], [48]. Gyro is sensitive to a temperature change or small changes in the structure (mechanical wear), which leads to fluctuating offsets from sensor output in applications of human motion measurements [16]. Even skin motion artefacts cause errors to all body-fixed sensors. Sensors placed on thighs are more susceptible to skin and soft tissue related motion, because the majority of femur is concealed by a substantial amount of soft tissue [32]. Boerema et al. [17] have shown the existence of an interaction effect between sensor position and type of activity. According to their results the most lateral position on a waist belt favors all other positions, and if a person may touch the sensor with the motion the best alternative is to position the sensor slightly more forward on the belt to a more central position (In legs that is not so important or relevant). They also conclude that sensors should be fitted to the body as tightly as possible. This can be possible with mounting material that ensures this tight fit, like an elastic waist belt, Velcro or clips that create a firm connection to a waistband. Novak et al. [56] found that some pathologies such as Parkinson's disease exhibit simultaneous T, head, and pelvis reorientation, this nonetheless suggests that IMUs placed on the head or T may allow faster detection of turns during gait and would be preferable to IMUs on the pelvis or foot. So, they perform some turning strategies in an experimental test with subjects. Their results showed that the best results can be obtained using an IMU placed on the upper or lower back, while IMUs on the legs consistently produce worse onset detection results. This group of researchers believe that happens because of two reasons. First, the top-down turning strategy, where the upper body generally turns earlier than the lower body. The second reason is that the trunk begins turning

immediately regardless of the leg used to make the turn while the two legs do not turn simultaneously.

Summing up, from studies, corrected errors were also identified, namely: (1) drift in [28], [49], [57]–[65]; (2) noise in [51], [54], [57], [60]–[62], [64], [66]–[68]; (3) skin movement artifacts in [49], [69]–[71]; (4) bias, offsets, scale factor or systematic errors in [51], [52], [59], [64], [66], [67], [72], [73]; (5) effect of vibration on sensors in [74]; (6) orientation of sensing device on the installation location on the human body in [25]–[28], [37], [49], [51]–[54], [60], [61], [66], [68]–[70], [72], [73], [75]–[78]; (7) steady state error in [58]; (8) temperature effects in [52]; and (9) ferromagnetic disturbances in [26], [28].

2.5. Calibration

Calibration is also a problem to be taken into account. Most guidelines recommend a systematic calibration to all users to establish the range, sensitivity, accuracy, precision, and inter-unit variability. Beyond this, an efficient calibration can allow a significant reduction of drift errors [16], [17]. There are two different distinguishable levels of calibration: (1) Unit calibration: The internal reliability of the accelerometer sensors across multiple units; and (2) Value calibration: The conversion of Acc's output into more meaningful information, such as time spent in moderate intensity physical activities which would give more clarity to patients or healthcare professionals [17]. In particular, the calibration of the Acc sensor is carried out during the static state as well as Gyro, which is advantageous [16], [32]. With regard to the magnetic sensors, from the datasheet of XEN-1210 it is possible to claim that this sensor has a very low offset and the device does not need calibration. It has no hysteresis and is indestructible by high magnetic fields [79].

Among studies, the calibration procedures can also be divided in four types: (1) Hardware Calibration (HC), where the goal of the calibration procedure focused only on the sensing device sensors. This type of calibration can be found in [52], [64], [65], [67], [73], [74], [80]; (2) Output Data Calibration (ODC), where data from sensing device sensors were used in order to adjust the orientation or angles parameters [25], [28], [49], [51], [54], [57]–[59], [62], [63], [66], [69], [70], [72], [75], [76], [26], [68], [71], [78]; (3) Calibration with help of a Camera-based System (CHCS), where an alternative system in addition to the sensing devices helps calibrating frames or synchronization between the two systems [27], [37], [77]; and (4) Monitoring Software Calibration

(MSC), where calibration procedure followed the instructions from a commercial brand software [53], [60], [61], [81].

Blumrosen et al. [55] suggested a new calibration scheme for small indoor environment, using *a priori* information about the medium. The calibration process for the inertial sensor included extraction of acceleration biases, and calculation of initial values of angular velocity biases.

Liu et al. [16] proposed an intelligent calibration for quantitative gait analysis including gait phase detection and leg segment orientation estimation. The present proposal is based on the precision measurement of Acc during static situation and a linear regression method for simplified assessment of drift error. In respect to the calibration of sensor units the authors calibrate the Acc during a static stage. This sensor is subjected to different gravity vectors by rotating a based axis. In turn, Gyro is calibrated in a dynamic calibration that is completed when the Acc is tested in a moving condition. In both cases calibration matrixes are computed using the least squares method. Regarding the intelligent calibration for reducing drift, authors explain that the mid stance phase can be detected just using Gyro signals and raw integration results of Gyro signals from the three sensor units. They also find that the rotational angular velocities of the shank and thigh are very small in later interval of this phase, and the Acc can be used for inclination measurement with respect to gravity acceleration. In each mid stance phase of the four strides, the angle signals from Acc were used as initial value of integral calculation instead of the value from integral signal of the Gyro. According to their experimental results was proved the validity of the intelligent calibration method for decreasing drift errors.

2.6. Challenges

There are many challenges in the field of gait analysis. To be in accordance with research groups a list of future challenges was prepared. Thereby, according to some research groups the list's topics are presented. In this thesis, the challenges 1, 2, 7, and 8 will be discussed.

1. It is necessary develop an algorithm to estimate joint angles from IMUs independent on speed of the subject's gait [32];
2. An intelligent and online calibration that utilizes instantaneous location estimations would be very important, since it would avoid the use of manual calibration with a number of movements to compute joint angles, could mitigate for part of the dynamic changes caused by changes in the environment and in sensor orientation, would improve the overall tracking estimation accuracy, and would decrease drift

errors [16],[52],[55]. A fundamental problem in IMU-based human motion analysis is that the IMUs' local coordinate axes are not aligned with any physiologically meaningful axis. The solution is to do this via calibration postures and/or calibration movements [50];

3. Equally innovative would be the development of a wearable sensor system for estimating muscular tensions instead of EMG [16]. Analysis of human walking pattern by the eight gait phases more directly identifies the functional significance (muscular tensions) of the different motions accruing at the individual joints and segments;
4. Application to longer distance gait trials is still unknown and this underlying limitation will have to be investigated to better assess the accuracy and repeatability [49]. So, it is important to check the evolution of the drift with the time;
5. One of the ideas is to evaluate the potential of the method in clinical applications with a large number of volunteers. The environment where the methods are tested is also very important, once the proposed methods aim people in need of treatment or rehabilitation and elderly people. So, it is important that the proposed methods work in this type of environment;
6. Tao et al. [14] claim that technical matters still need to be improved, like the stability of sensor signals, the reliability of analytical algorithms for kinematics and kinetics in gait analysis, development of low cost and small volume integrated wearable sensor systems;
7. One of the most promising areas is the improvement of signal processing and analysis algorithms. The current movement tracking algorithms based on the application of KFs using Direction Cosine Matrix (DCM) to data acquired from Gyros and Accs should be improved [3].
8. Still, many physical phenomena like shadowing, absorption by the human tissue, creeping of the electromagnetic wave along the body, affect the accuracy of the tracking information, as it is based on statistical models that cannot fully mitigate over instantaneous dynamic changes [55].

:

Chapter 3 – Falls Prevention and Risk Identification: state-of-the-art

3.1. Introduction

Health care has been increasingly required due to the increase in average life expectancy in developed countries. It is also a well-known fact that the majority of health problems affect the elderly [82]. In this context, Fs are one of the most common health concerns especially in elderly people, being a marker of frailty, and acute and chronic health impairment [4], [5]. Frequently, Fs result in injury, disability, and institutionalization [4]. According to [4], the majority of Fs result in no injury, however 31% of the cases result in an injury requiring medical attention or restriction of activities for at least one day. Normally, those injuries or restrictions are minor soft tissue injuries, but 10-15% of Fs result in fracture, and 5% of Fs in more serious problems such head trauma. Fear of falling usually happens to elderly fallers, and almost half of fallers have a great probability to have a repeated F within the next year.

Actually, Fs are associated with greater functional decline, social withdraw, anxiety and depression, and an increased use of medical services. Even fear of falling has been associated with impaired mobility and decreased functional status. Thus, older adults who have fallen have a greater risk of F regardless if they had an injurious F. Death related to Fs increases with advancing age and greater number of co-morbidities. Accidental Fs are the leading cause of unintentional injury deaths in people aged over 65 years old [4]. Hip fractures are correlated with F related injuries, and they are greatly associated with a high mortality within the first six months, particularly in men [4], [5].

Concerning the pathophysiology of Fs, the majority of Fs occur due to more than one single cause. In fact, multiple interactions between a subject with great risk of F and acute mediating factors are responsible for the Fs. For example, neurological and muscular diseases such as Parkinson, Stroke, Dementia or Osteoarthritis can increase the risk of F. Normal physiological changes have the same trend than the above mentioned diseases and may result in alterations of balance. Even medications such as antidepressants, sedative hypnotics or neuroleptics are potential reversible risk factors for Fs in the elderly. Hypoglycemic agents have been implicated as a risk factor for Fs in a few retrospective studies, and footwear or environment hazards, including

wet floors, poor lighting or improper bed height, may also be a predisposing risk factors for Fs [4], [5].

The risk of F can be described according to a scale model (Fig. 3.1) that illustrates the interaction between balance capacity and balance demands of the task (in the case of locomotion: terrain type, distance to travel or velocity requirements for example). From this interaction it is possible to obtain an outcome which is measured on a given scale. In this particular situation, the heavier the first, the closer walking performance is to optimal [83].

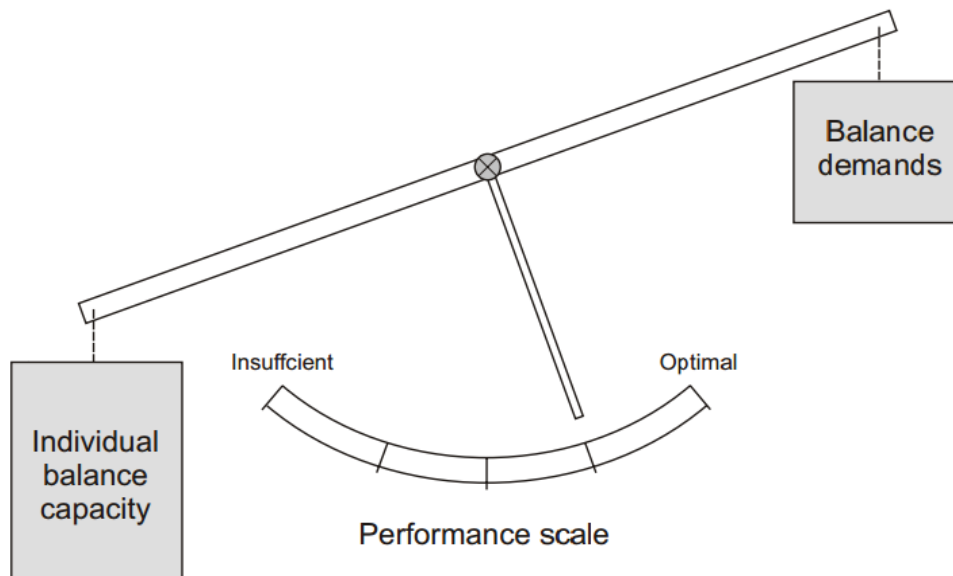


Figure 3.1 - Balance performance model [83].

In general, there are two ways to prevent a F in elderly people: i) with physical activity; or ii) a F forecasting system. In the first case, as already mentioned above, skeletal muscle strength and mass decline with age and immobility. So, exercise might prevent Fs and injury by strengthening muscles and increasing endurance; maintaining and improving posture, joint motion, and postural reflexes; stimulating cardiorespiratory function; and improving alertness [5]. In relation to the F forecasting system, capable of warning a F in advance, it would allow a technician to prevent a subject from falling or a system to act in order to avoid falling. Nowadays, there are some studies that focus in machine learning techniques in order to detect a F before happening. So, with this technology, a system would be capable of prevent a subject's F.

3.2. Classification of the Falls

Concerning the literature, there are several works that propose division and classification of Fs. In [84], six types of Fs are listed: i) syncope/fainting; ii) tripping; iii) sitting on an empty chair;

iv) slipping; v) lateral F; vi) rolling out of bed. In turn, [85] identifies seven distinct F's situations: i) slips; ii) trips; iii) extrinsic (collisions, obstacles); iv) intrinsic; v) from stairs; vi) from an upper level; vi) non-defined. And [86] enumerates up to 9 F scenarios (grouped in forward, backward and vertical Fs). Looking only within the context of biped locomotion, and from a purely motion-based analysis, Fs can be roughly grouped in two main categories: i) Fs along the horizontal/lateral direction; and ii) Fs along the vertical direction.

The first are usually caused by stumbling (loss of balance in gait generation, or obstacles in locomotion's path), and can therefore be subdivided in forwards, backwards and lateral Fs, while the second are mainly related to weak legs or foot slipping [87], [88]. Figure 3.2 depicts a simplified sketch of these types of Fs. These Fs are obviously from a scenario where an individual is in locomotion, which is ultimately the point of this section.

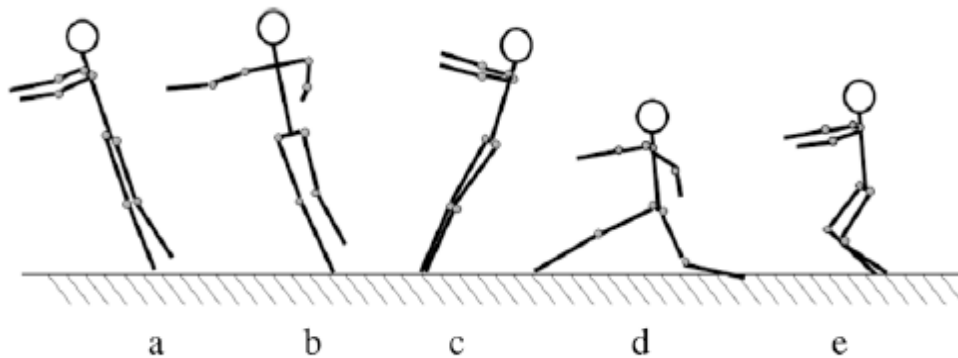


Figure 3.2 - Possible Fs along the horizontal/lateral and vertical directions [88]: a) F forward; b) F laterally; c) F backward; d) F along vertical direction – slipping of foot; e) F along vertical direction – weak legs.

However it is also possible to identify Fs from other situations, such as stationary positions (standing, sitting or on a ladder) and there are voluntary, deliberate and risk-free motions that can be misinterpreted as Fs (e.g. crouching) [89].

Finally, there are two main events associated with a F: a change in trunk's orientation to a horizontal lying position, and a negative peak in acceleration/sudden decelerations due to impact with the floor. From normal behaviour/locomotion to the motionless stance (where acceleration values are equal to the gravitational acceleration) after the F can go up to a 1 second interval [90]. The final posture however can stabilize only 2 seconds after the impact with the floor [91]. This information, while helpful in identifying if a F has occurred, can do little to prevent it [12], [86], [92], [93]. Thus, it is crucial to understand or find solutions to detect a F before it happens.

3.3. Methods

As already mentioned, Fs are a major health problem among the elderly. Consequently, the number of systems that detect Fs has increased significantly in recent years [94]. At this point it is very important to make a distinction between F detection systems/algorithms and F prevention or F forecasting systems/algorithms. According to [94], a F detection system can be described as an assistive device capable of alerting technicians/surrounding people when a subject Fs. In one hand, these systems can mitigate some of the adverse consequences of a F, namely on the reduction in the fear of falling and the rapid provision of assistance after a F. Note that depending on the severity of the F, the subject may be unable to move for an extended period of time after falling. Critical complications during this time such as hypothermia, dehydration, broncho-pneumonia and pressure sores can actually happen to older fallers if they live alone or lose consciousness. On the other hand, it is unable to prevent or avoid a F.

In turn, a F prevention system/algorithm can actually avoid the F of the subject, contributing more to reduce the fear of falling and the need of assistance after a F. However, nowadays there are few F prevention systems and the majority of the studies focus on determining or assess the risk of F.

3.3.1. Fall Detection Systems

F detection systems are often based on impact detection [84], [86]. However, according to the literature, these systems can be differentiated or classified, and there are many attempts to structure F detection systems. Some authors perform a two-class division in motion sensors and image processing approaches [12]. Lai et al. [95] classifies these system according to the historical evolution from passive alarms to audio/video external systems and to wearable motion-sensing devices that detect risk situations. Mubashir et al. [89] proposes a three-class division of existing F detection algorithms: wearable sensor based, ambience sensor based, and camera based as depicted in Fig. 3.3. According to them, wearable sensors can be divided into two categories: posture based and motion based devices. Ambience devices can be classified into presence and posture based sensors. And the camera (vision) based systems can be further categorised into three classes as shape change, inactivity and 3D head motion. In relation to the existing approaches, they usually share the same general framework, although data acquisition varies according to the number of sensors or cameras.

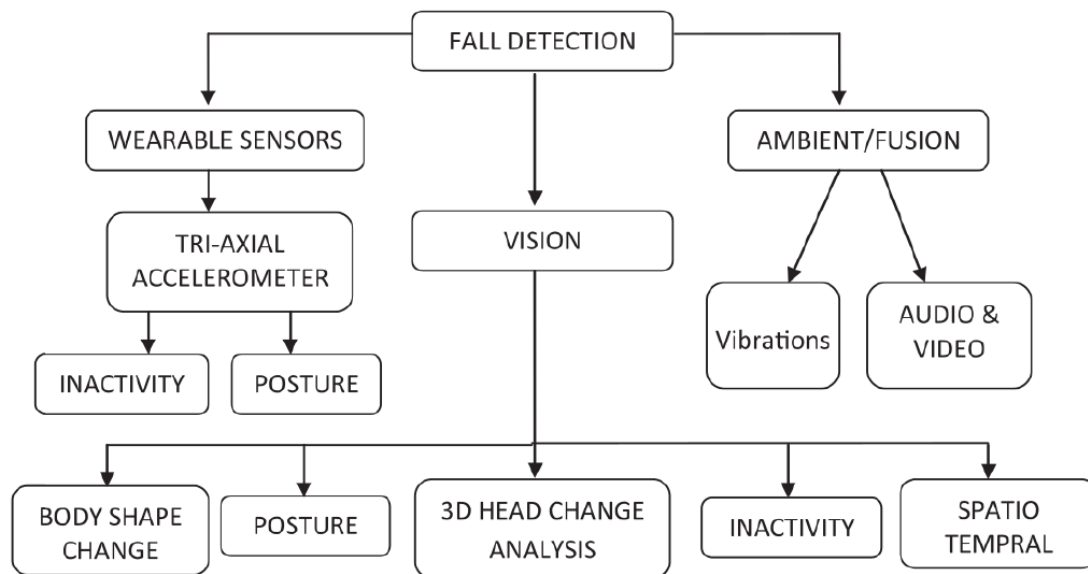


Figure 3.3 - Classification of F detection methods according to [89].

Perry et al. [96] also divided these system into three categories: methods that measure acceleration, methods that measure acceleration combined with other methods, and methods that do not measure acceleration. And finally, through a review of the literature, Igual et al. [94] realized that F detectors can be categorized in two types: context-aware systems and wearable devices. However, since all this project is about IMUs and related sensing devices, the aim of this part of the study will be F detection systems/algorithms based on wearable sensors that are typically used in body segments due to their advantages.

According to [94] the majority of wearable F detectors are in the form of Acc devices, and some of them also incorporate other sensors such as Gyros to obtain the patient's position. Even today's smartphones come with a rich set of embedded sensors, such as Acc, Mag, Gyro, GPS, microphone, and camera [97]. Figure 3.4 also illustrates the last sentence [82]. As can be seen, Acc are widely used by F detection systems. In [82] research attention has focused on the different application areas with varying intensities. So, IMUs or sensing devices can be considered a wearable solution to detect Fs. The only relevant exception to this are force platforms [92], [98]–[100], and, less commonly, goniometers on the legs [92], [93], and air pressure barometers [101].

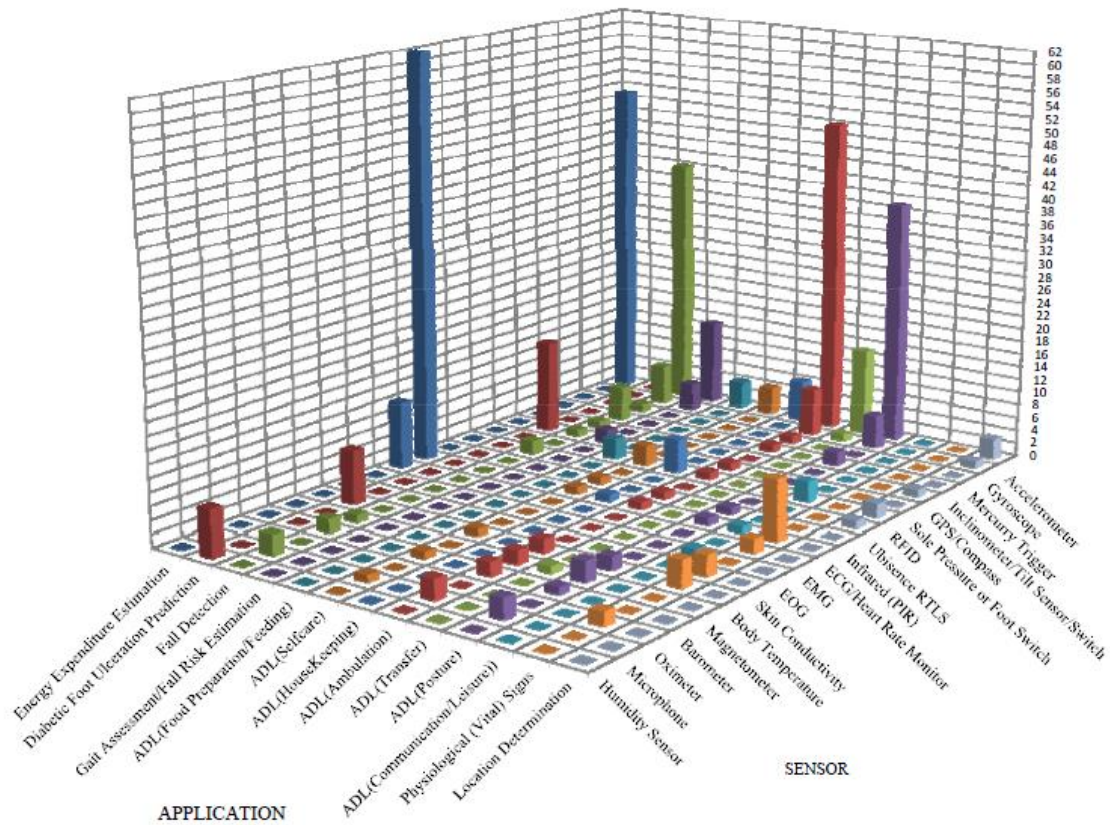


Figure 3.4 - Distribution of research studies on wearable sensors: Application vs Wearable Sensors [82].

Fs can be identified through the output of Accs based on great signal amplitudes and within a specific set of frequencies. These signals can be used to differentiate Fs from other daily life activities [86]. Figure 3.5 is a truly example of the variation of the Acc's signal before, during, and after a F. Studies like [12], [86], [92], [93] are examples of approaches that have proposed F detection systems based on Acc's output, and on the identification of these kinematic traits.

Concerning the systems' specifications, during locomotion the Acc's output is only relevant between 0.25 to 20Hz (lower frequency components can be discarded) [84], [102]–[104]. Mathie et al. [92] claim that most human movements occur between 0.3 and 3.5Hz, and 90% of the signal power is under 10Hz. In fact, acceleration is mostly in the vertical direction, and running is known to produce greatest values of vertical acceleration (around 8.1 to 12 g at the ankle, 5g at the lower back, and up to 4g at the head), while at walking leads to acceleration values in the range of 2.9 to 3.7g [92].

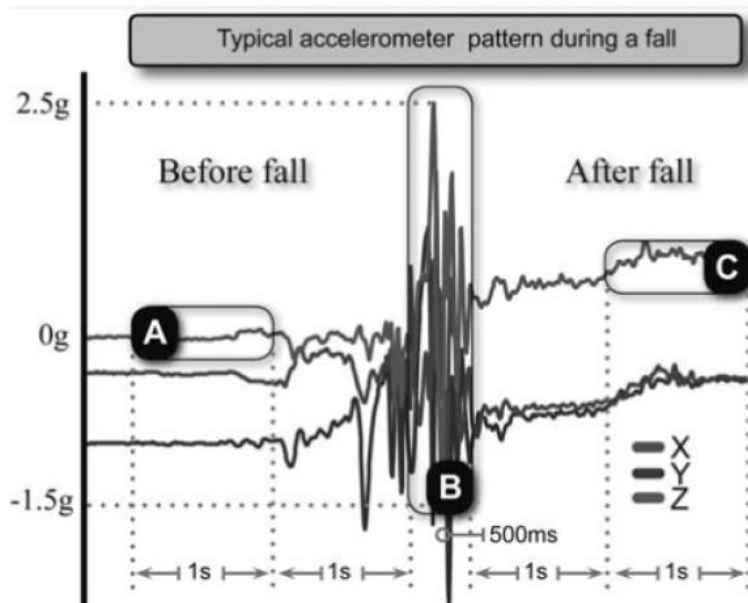


Figure 3.5 - Typical output of a chest 3D Acc before and after a F event. Acceleration peaks are caused by floor impact [86]. It is possible to observe that acceleration suffers perturbations about 1 second before actual impact.

Establishing acceleration thresholds is the most common approach in F detection systems based on accelerometry [84], [86], [89], [105]–[108], and some studies implemented adaptive thresholds [95], [109]. But according to Kangas et al. [84] these are not the optimal approaches in terms of accuracy, since they never present values greater than 95%.

Thus, the scientific literature enumerates other solutions under the F detection systems theme which have better results namely: decision tree classifiers [92], [101], [106], fuzzy logic [86], and uses of machine learning algorithms such as Support Vector Machine, Non-Negative Matrix Factorization (NNMF) and k-Nearest Neighbour (k-NN) [90], [110], [111], which have achieved up to 97% success rates and are also used in gait classification and walking pattern recognition [102], [103]. Nowadays, there are also several products available on the market. The majority of them are wearable devices in order to be usable at home environments, and normally the usual attachment location of the sensors is the waist. These wearable devices are usually equipped with an alarm button to call for emergency when a F is not automatically detected, and their battery has a maximum lifetime of up to two years. Table 3.1 contains some examples of commercial F detection systems and some relevant details such as sensor type, attachment position, battery life, and some features.

Table 3.1 - Commercial wearable F detection products

Name	Sensor Type	Attachment Location	Battery Life	Features
SENSO [10]	N/A	Waist	Up to 2 years	-Emergency button; -Send emergency text to emergency contacts.
Tunstall iVi Pendant [11]	N/A	Neck/Waist/Chest	12 months	-Replaceable battery; -Water resistant.
MySOS Mandown [112]	3D Acc	Neck/Waist	25h	-Two-way audio; -Dual band: 900/1800 MHz
SensorBand [113]	3D Acc	Waist	1 year	-Connect to internet; -Speech communication.
Badge-iT Fall Detector [114]	N/A	Waist	N/A	-Detect potential hypothermia; -Detect wandering using radio signal strength.
Fall detector MCT-241MD PERS [115]	N/A	N/A	N/A	-Full waterproof; -Anti-collision algorithm;
VitalBase [116]	N/A	Wrist	2 years	-Waterproof; -Emergency call.
Climax Fall Sensor [117]	N/A	Neck	2 years	-Waterproof; -Pendant style.
Tynetec Fall Detector [118]	2D Acc	Neck/Waist	1 year	-5 user-selectable levels of sensitivity; -3 event logs; impacts, pre-alarms & alarms.
Blue Alert Fall Detection Sensor [119]	N/A	Waist	N/A	-Automatically call for help when falling.
CSEM Wrist Fall Detection [120]	3D Acc	Wrist	15 days to one month	-LCD display; -Re-chargeable battery.
Tynetec Wrist Worn Fall Detector [121]	2D Acc	Neck	2-3 years	-5 user-selectable levels of sensitivity; -Daily battery self-test.

3.3.2. Fall Prevention Systems/Fall Forecasting Systems

F prevention systems or F forecasting systems have the potential to act in order to prevent a F. These systems require understanding F risk factors, assessing these risk factors, and developing F prevention mechanisms. Otherwise, F detection systems, mentioned before, are only able to confirm a F. However, both systems can use gait parameters, Acc's output, decision tree classifiers or machine learning algorithms [122]. These inputs or algorithms are truly important and their study is the first step of F prevention. Many authors dedicated their time to study changes in human behaviour before, during and after a F. Brauer et al. [123] focused on postural balance and its influence in predicting Fs by testing in one hundred elderly. They made a large set of tests including: Berg Balance Scale [124], the Functional Reach Test [125], the Lateral Reach Test

[126], and the Step-Up Test [127]. Boissy et al. [86] used a two-stage F detection algorithm based on fuzzy logic using as inputs typical accelerations patterns during a F. They were able to check differences in Acc's signal before, during and after a F. Nyan et al. [128], for example, obtained a threshold of $\pm 10^\circ$ of body's inclination (torso and thigh) by analysing the variation of angles before, during and after a F.

At this point is very important to distinguish two different F prevention related systems: i) F risk assessment system (FRAS) – where some parameters are assessed and then prevent measures such as medication or diet are implemented; and ii) PF detection systems (PFDS) – where systems are capable of detecting a F before it happens in real-time. These systems can predict a F at least 300ms-1s before [12], [86], and they are the future trend in this investigation area.

Concerning the first type, it is important to retain some examples of popular measures, tools or scales used to assess the risk of F [129]: i) the Morse F Scale (MFS); ii) St Thomas Risk Assessment Tool in Falling Elderly Impatients (STRATIFY) [130]; iii) Heindrich II F Risk Model (HFRM); iv) TUG (Time up & go) [131]; v) Barthel Index [132]; vi) TGBA (Tinetti Gait and Balance Assessment) [133]; vii) WSFRAT (WilsonSims F Risk Assessment Tool – Psychiatric Patients) [134]; and viii) EPFRAT (The Edmonson Psychiatric F Risk Assessment Tool – Psychiatric Patients) [134].

However, these are not the only tools available. Stopping Elderly Accidents, Deaths & Injuries (STEADI), which is an organization capable of provide training, tools, and resources exclusive to prevent F in the elderly population and identify the risks of F [135], has a F risk assessment algorithm that can classify F risk in three categories: i) low; ii) moderate; and iii) high. The algorithm consists in assessing gait, balance, and strength through three tests: i) TUG (recommended); ii) a 30 seconds chair stand test (optional); and iii) a 4 Balance test (optional). The historic of the patient is also important to determine the F risk, namely for example the number of Fs. Thus, concerning the risk of F obtained, an effective intervention can be made, although not in real time. The entire algorithm is depicted in the following Fig. 3.6.

In fact TUG score is the easiest and most commonly used measure. In this test, the elderly perform a sequence of activities (stand up from a chair, walk with normal speed for 3 meters, turn around, walk back to the chair and sit down on the chair) for movement evaluation. For each activity, the time is recorded and if an activity takes longer than 14 s, the risk of falling is considered high [131]. This measures can also be obtained with wearable sensors, and Fig. 3.4 also show

that the IMU's sensors are widely used in gait assessment or F risk estimation. For example, Najafi et al. [136] tracked activity patterns using a single tri-axial Acc attached to the chest through validation of timed up and go and standard measures of balance and gait. The implemented algorithm was accurate in identifying the number of steps taken and walking duration, which are important parameters in F risk estimation.

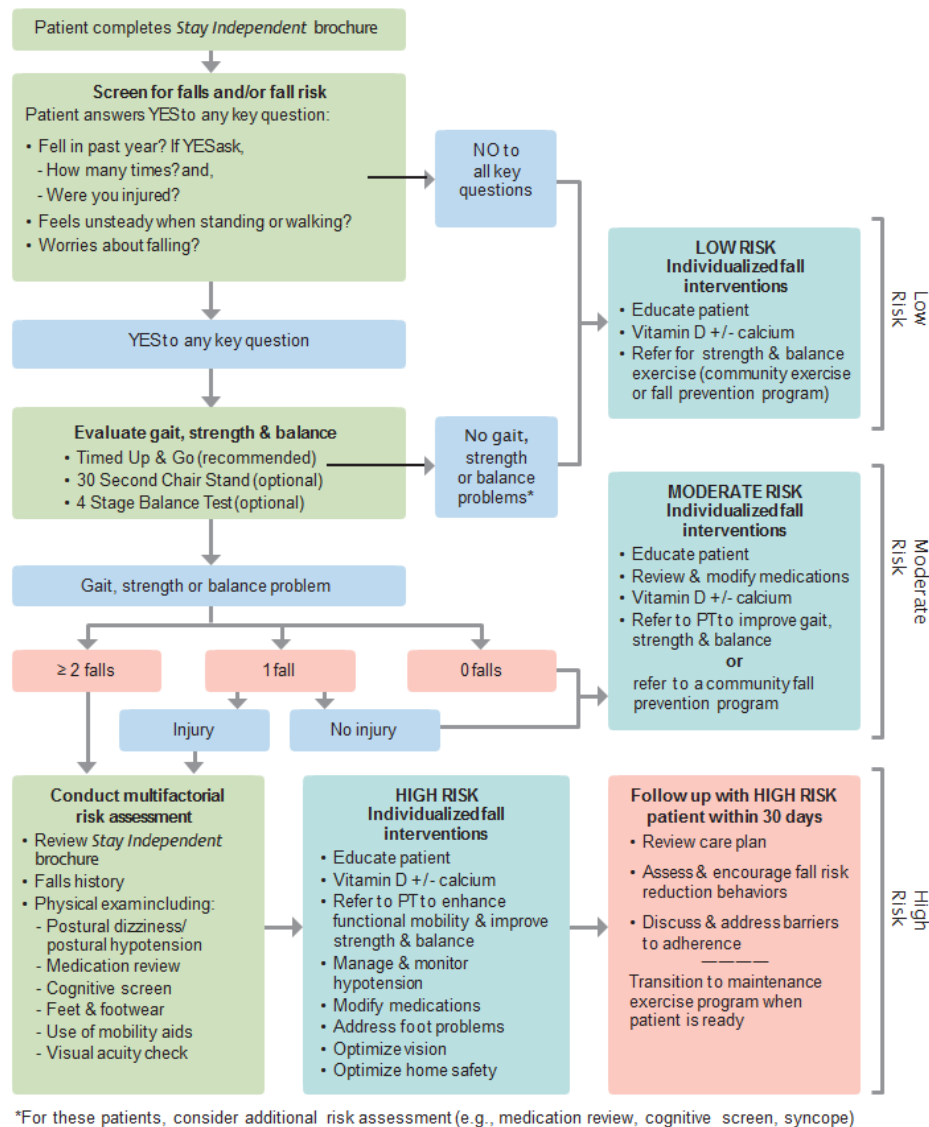


Figure 3.6 - STEADI F Risk Assessment algorithm [135].

Recently, several studies have focused on PFDS. Tamura et al. [12] created a wearable airbag incorporated with a PFDS based on Acc and Gyros's signals to trigger inflation of the airbag. In this study, the main assumption in the algorithm is that the subject is in free F, and before the impact the airbag is triggered and the patient's head, neck, hip, and thigh are protected. Concerning their results, they claim a change in the pitch signal 0.5 s before the change in the acceleration signal. According to their algorithm, a F occurred when the acceleration was less than

$\pm 3 \text{ m/s}^2$ and the angular velocity exceeded 0.52 rad/s . The free-F conditions were detected at an average of $193.4 \pm 57 \text{ ms}$ in forward Fs and $197.4 \pm 54.7 \text{ ms}$ in backward Fs. The mean F time was $0.249 \pm 0.094 \text{ ms}$, the inflation time was $0.121 \pm 0.019 \text{ ms}$, and the accuracy of the system was 93% in all experiments. The prototype system was tested by 16 young, healthy subjects (mean age $22.2 \pm 5.1 \text{ years}$) who mimicked Fs to the front, back, and sides while wearing the device without airbags.

Leone et al. [137] developed a wireless and minimal invasive surface Electromyography-based system (EMG) that is capable of detecting people instability through muscle activity. The algorithm uses a threshold based approach that allows the detection of a typical imbalance condition about 200ms after the stimulus perturbation in simulated and controlled F conditions. They test several thresholds and the best result for the sensitivity was 87.3%. Again subjects mimicked Fs.

Nyan et al. [138] presented an implementation and clinical trial's results of a wearable PFDS prototype. They used inertial sensors to detect faint Fs in its incipience. The approach is based on the characteristics of angular movements of the thigh and torso segments in Fs. Basically, if one of two dimensional angular signals intersects the threshold level of $\pm 10^\circ$, then a F is confirmed using their algorithm. A F is confirmed when the correlation coefficient of thigh angular data and torso angular data, and the correlation coefficient between the band-pass filtered Gyro segment are bigger than 0.8. The system's accuracy is high with a lead-time of 700ms before impact occurs to the vulnerable areas of the body. No false alarms were found in the experiment (100% specificity). All Fs, except for two front Fs, could be detected; thus, a sensitivity of 95.2% (40/42) was achieved. Fs were simulated by the subjects.

Lopez-Yunez et al. [139] implemented a Freescale ZSTAR3 system with wireless tri-axial Accs and ZigBee network (2.4GHZ) capability. They used the tilt angle and phase shift between the pulse wave (prior to F event) and the pulse magnitude which were analysed to obtain the characteristics of the F. Even the direction of the F can be determined. The sensors were placed on the back neck, the abdomen area, and on waist left side. Ninety percent (90%) overall efficiency for the system was achieved when considering all four types of Fs (back F, front F, F from a chair, and side F). All falls were simulated.

3.4. Gait Parameters, Sensors and Experimental Setup Information

Above mentioned systems can rely either on the recording of specific data from the hardware (e.g. absolute acceleration values already explained), or alternatively, in computed metrics from sensor's raw data. These computed metrics give more information about subject's gait, making it possible to draw relevant conclusions or informations. Due to the great amount and diversity of these metrics, it becomes necessary to identify which of them can be more helpful when considering reliable F prevention and detection, as well as the used sensors and their attachment location. This is the aim of this subsection.

3.4.1. Gait Parameters

In order to not use only the raw data of the sensing device in the current F forecasting study, a study was carried out to determine gait parameters which may be relevant in predicting of Fs. Firstly, there are several needed concepts to be introduced prior to discussing gait metrics. Concerning scientific literature [83], [92], [104], [140]–[143], it was found that gait analysis attempts to classify or quantify three main traits of human bipedal locomotion: i) Stability; ii) Variability; and iii) Harmony. Each one is related to different aspects of locomotion.

The first mentioned trait of human bipedal locomotion has been associated with F risk in elderly population [141]. Gait stability can be divided into postural and dynamic. Postural stability quantifies the amount of postural sway, which is measured through the mean velocity of the centre of the pressure (COPv), and is managed by the musculoskeletal and sensory systems [140]. The stability in the vertical position is obtained when the projection of the Centre of Mass (COM) is on the base of support (BOS), and the higher the stability, the less the distance to the COP – Figure 3.7. An external or internal disturbance changes the projection of the COM to the limits of the BOS resulting in postural imbalance. The distance from the position of the COM to the closest boundary of the BOS (COM - BOS) represents static equilibrium control [144].

On the other hand, dynamic stability happens when body segments are moved in a coordinated fashion way and the upper body oscillations are minimal [140]. As mentioned before, several pathological conditions have been linked to a certain degree of instability during locomotion. The Local Dynamic Stability (LDS) value, which is the most relevant dynamical stability parameter, and is defined as the sensitivity of a locomotor body to infinitesimal perturbations [142], [143], complement variability measures. LDS measures the robustness of a locomotor body against interference from either control errors or environmental noise, and is characterized by the

maximum Lyapunov exponent (maxLE) [140]. However, there are other gait parameters related to gait stability: i) root mean square of the acceleration (Acc_{RMS}); ii) maximum and minimum acceleration peak (a_{max} , a_{min}); and iii) peak-to-peak angular velocity (PPV). Moreover, [140] concluded that a combination of postural and dynamical stability measures can achieve better results in identifying Fs than individual metrics.

Laessoe et al. [83] have shown that greater variability increases F risk. Additionally, [142], [143] claim that gait stability should not be confused with gait variability - there are reports showing that pathological gait, characterized by lower speeds, can exhibit higher local stability but a greater kinematic variability [141], [142], though not always the case ([104] found that cerebral palsy greatly decreases stability, while maintaining similar walking velocities to healthy counterparts). It has also been widely suggested that individuals with pathological gait tend to decrease walking velocity in order to gain stability, which leads to a lower variability between strides [145]. Particularly, variability measures are unable to take into account infinitesimal small perturbations that local stability metrics are based upon - even so, they can add important information about the neuromuscular processes behind gait generation [102], [142], and it has been shown that greater gait variability increases F risk [83]. Metrics that quantify gait variability usually compare acceleration data in subsequent steps/strides and compute the standard deviation (STD) [143]. Other metrics require averaging over several steps, which has been suggested to decrease the impact variability has on the values [143].

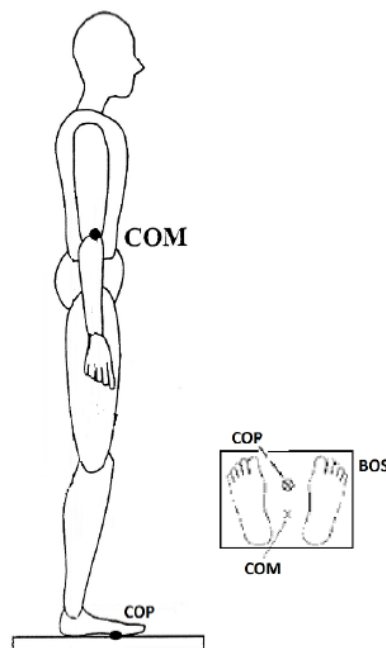


Figure 3.7 - Representation of the stability in a vertical position.

Iosa et al. [104] described gait harmony by how alternate, synchronized, symmetric and rhythmic is body motion with regards to inter-limb, intra-limb, and lower-upper body coordination. Basically, it quantifies how smooth gait is, and can be mainly (but not restricted to) quantified by the Harmonic Ratio (HR), the computation of which involves an analysis of the frequency spectrum of the acceleration data - regarding the ratio of odd and even harmonics. In addition to this parameter, there are two more: the ratio index of the minimum acceleration peak ($a_{min}RI$), and the ratio index of the peak-to-peak angular velocity (PPv RI).

Basic gait parameters were also found such as: step length, step duration, gait symmetry, cadence, walking velocity, sum vector magnitude (SVM), postural orientation, step length, and step duration. Gait symmetry refers to the similarity between the movements of the right and left sides, and it is compared step by step [98], [101]. In turn, SVM quantifies the movement's intensity [106] and it is used to detect the impact [91]. Basically, when a F occurs, a great acceleration is produced, but when the body touches the ground, the acceleration is suddenly reduced. At this point, the SVM of the Acc generates a significant peak, this being produced by the F, much larger than the periodic peak produced by the walk [95]. As for the postural orientation, it refers to the relative inclination of the body in space [106]. Another important metrics found were: i) Signal magnitude area (SMA); ii) roll, pitch and yaw angles; iii) Dynamic sum vector (SVd); iv) Energy expenditure (EE); and v) the Fast Fourier Transform (FFT). All F and gait related metrics are explored in Table 3.2. This table also contains other metrics, different from those mentioned earlier.

3.4.2. Sensors and Experimental Setup Information

Before discussing this subsection, it is crucial to properly establish measurement directions and adopt a proper nomenclature regarding the axis. So, for now on, the nomenclature used is presented in Fig. 3.8, which is the most common in the scientific literature under this investigation area.

To obtain all mentioned metrics it is necessary the use of sensors attached to the body. Concerning the articles found, wearable sensors such as IMUs [140], [146], [147], Accs [12], [83], [84], [88], [90], [91], [95], [101]–[104], [106], [141]–[143], [148]–[152], Gyros [12], [104], [141], and force plates [98]–[100], [102], [140], [143], [148], [153]–[155] were used to detect, predict and assess F risk. These sensors were attached in general to all body segments: trunk, shanks, thighs, feet, and head. However, lower trunk or waist are the most common attachment location. Subjects involved in these articles were healthy young adults, although a large amount of studies included details and clinical results of elderly people. Few studies included middle-aged

participants. Participants performed, in general, walking trials involving walking strides, and simulated Fs (horizontal/lateral and vertical). Table 3.2 contains all these informations for each metric in detail.

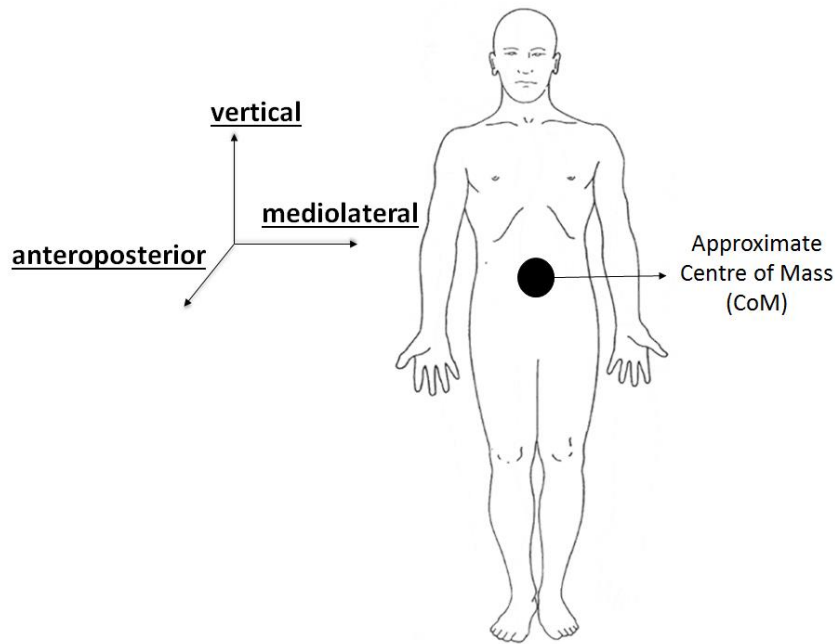


Figure 3.8 - Different axis/planes. The frontal plane is referred to as Antero-posterior (AP), the lateral plane as Medio-lateral (ML) and the vertical simply as Vertical (VT).

Table 3.2 - Potentially relevant metrics for the prevention of gait, and the sensors, the location of the sensors, subjects' age, and the procedure used to obtain them (K – Kinematic; F – Frequency; ST – Spatiotemporal; Ph – Physiological; Ki – Kinetic; y – young; o – old; h – healthy; fp – fall prone; *-already mentioned)

Metric	Type	Sensors	Attachment Location	Exp. Setup	Age	Refs
COPv	K	Force plates	(not attached)	1 st – Standing tasks; 2 nd – Treadmill-walking test.	12 subj. (4h.y+8o) h.y - 21.75±0.96 h.o. - 73.25±7.09 fp.o. - 74.50±2.65	[140]
		2 adjacent force platforms	(not attached)	Data acquired in a double-leg stance with feet at pelvis width.	7 subj. h.o. - 67.9±4.3	[155]
maxLE	F	IMU	Lower back (L5/S1)	*	*	[140]
		Acc/Gyro; Piezo sensor	Knee, Ankle, and Heel	Walk on the treadmill at a controlled	13 subj. (5h.y+4h.o+4fp.o) h.y - 26.4±2.3 h.o. - 71.3±6.5	[141]

Metric	Type	Sensors	Attachment Location	Exp. Setup	Age	Refs
				speed (3 speed levels).	fp.o. - 71.0±3.0	
		Acc	Head, Trunk, Foot, Tibia and Thigh	*	*	[102]
		Acc; electrogoniometers	Chest; right leg	Walked around a rectangular (7m wide and 200m long) (self-selected comfortable speed).	36 subj. (10h.y+12h.o+14fp.o) h.y - 27.10±3.25 h.o. - 57.6±7.7 fp.o. - 61.0±6.6	[142]
		Camera	Sacrum, iliac spine, thigh, anterior shin, lateral malleolus of the fibula, dorsum of the foot, 5th metatarsal, calcaneous and hallux.	4 repeated collections of 30 walking strides per velocity condition per subject.	19 subj. h.y - 22.5±2.8	[145]
		Acc; camera	Right anterior superior iliac spine; heels.	Walk without requiring the use of the handrails on the treadmill (1 min. at a self-selected comfortable speed).	13 subj. (5h.y+4h.o+4fp.o) h.y - 26.40±2.3 h.o. - 71.3±6.5 fp.o. - 71.0±3.0	[143]
		Camera	Trunk	Walked on a level treadmill for 3 trials of 5 min each (self-selected comfortable speed).	20 h. subj. 18-73 (mean age: 40)	[154]
Step/Stride distance	ST	Acc	*	*	*	[143]
d_{step} $/d_{stride}$		piezo-resistant Accs	Head, pelvis	Walk 20m (2 trials for two different walkways).	20 subj. h.y. - 29.0±4.3	[148]
		GaitMat system	(not attached)	Walk barefoot at a self-selected speed (4 trials).	97 subj. (44fp.y+53con.) fp.y. - 36.7±15.0 control-36.6±13.3	[99]
		GaitMatTMII system	(not attached)	Walk 4 times on the mat from one end to the other at	2911 f.p. subj. male - 70.0±21.8 female-60.5±16.5	[100]

Metric	Type	Sensors	Attachment Location	Exp. Setup	Age	Refs
				a self-selected speed.		
BOS	ST	IMU/Acc; Force plates	*	*	*	[99],[100], [143], [154]
Cadence	ST	IMU; Acc; Gyro; Force plates	*	*	*	[99],[100], [143], [148]
		Acc	Lower back (L3)	9 specific tests	94 h. subj. (14 fallers; 80 non-fallers) fallers-73.0±2.9 non-fallers-73.8±2.9	[83]
Walking Velocity	K	IMU/Acc/Gyro; Force plates	Soles; Chest, Thighs, Shanks; Head and Waist	*	*	[98]–[100], [148]
Swing / Stance / SS / DS duration	ST	IMU,Acc,Gyro; Force plates	Soles; Chest, Thighs, Shanks	*	*	[98]–[100]
Stride / Cycle duration	ST	IMU,Acc,Gyro; Force plates	Soles; Chest, Thighs, Shanks.	*	*	[98], [100], [102]
$d_{COP,sf}$ (sf – supporting foot); COG (Center of gravity)	ST	Acc	Trunk, Thigh, Shanks	2 types of Fs. Walk several steps and suddenly pretend to F.	2 y. subj. (1 male & 1 female)	[88]
Wavelet decomposition	F	*	*	*	*	[98], [102]
		IMU	Sternum	Daily activities– walking, standing upright/sitting down and laying down on a bed	5 subj. (2 females; 3 males) Mean age: 28	[146]
		Acc	Waist	5 walking patterns. 10 min each.	52 subj. (39 males & 13 females) 21-64 years	[103]
$\sigma_{acc_{x,y,z}}$ (variance)	K	*	*	*	*	[103], [148]
acc_{RMS}	K	*	*	*	*	[102], [103], [148]
		Acc and Gyro	Lower trunk	10m walking test (self-	34 y. subj. (17fp.y.+17h.y)	[104]

Metric	Type	Sensors	Attachment Location	Exp. Setup	Age	Refs
				selected speed)	h.y.-5.7±2.5 fp.y.-5.0±2.3	
		Acc	Waist	30 runs of training data and 30 runs of testing data for eight activity states.	1 subj.	[149]
SVM	K	Acc and Gyro	-	Subjects mimicked Fs (front, back and sides).	16 h.y. subj. 22.2±5.1	[12]
		Acc	Waist, Wrist, Head	Intentional Fs during trials	2 subj. (22 and 38)	[84]
		Acc	Waist	System test contains five kinds of activities of daily living. 20 repeats.	3 subj. 23-60	[150]
		Acc	Waist in front of the anterior superior iliac spine.	6 different Fs in a lab.	41 subj. (20 m.a. and 21 fp.o) 20 m.a.-48.4±6.8 21 fp.o.-82.8±9.4	[91]
		Acc	Chest	Daily living activities and 4 types of Fs.	18 h.y. subj. 19-28	[151]
		IMU	Sternum and Shank.	All walking trials were conducted on a linear walkway.	17 h.y. subj. 29.0±11.0	[147]
		Acc	Left hand, right hand, waist, neck, left foot, and right foot	240 tests to measure system accuracy.	16 subj.	[95]
		Acc	Belt	3 protocols to investigate the implemented Fs.	20 h.y. subj. 23.7±3.0	[101]
		Acc	Belt	12 different directed tasks per subject.	6 h. subj. 22-60	[106]
		Mobile phone	Chest, waist, thigh.	Fs with different directions and in different environments.	15 h. subj. 20-30	[108]
a_y vertical acceleration	K	*	*	*	*	[84], [91], [108]
		Acc	Belt	6 categories	-	[90]
a_y transversal acceleration	K	*	*	*	*	[90]

Metric	Type	Sensors	Attachment Location	Exp. Setup	Age	Refs
SV_D Dynamic Sum Vector	K	*	*	*	*	[84], [91]
a_{min} & a_{max}	K	*	*	*	*	[102], [104], [147]
PPv	K	*	*	*	*	[104]
Angular velocity	K	*	*	*	*	[12]
HR – Harmonic Ratio	F	*	*	*	*	[102], [104], [148]
$a_{min}RI$	K	*	*	*	*	[104]
PPvRI	K	*	*	*	*	[104]
Gait events	ST	*	*	*	*	[98], [100], [102]
$SMA_{acc_{x,y,z}}$	K	*	*	*	*	[95], [101], [106]
d(SMA)/dt	K	*	*	*	*	[95]
Postural Orientation	K	*	*	*	*	[95], [101], [102], [106]
Roll, Pitch, and Yaw	K	*	*	*	*	[95], [98], [102], [150]
Energy Expenditure ΔP	Ph	*	*	*	*	[106], [147]
(Differential pressure)	Ki	*	*	*	*	[101]
Frequency Analysis	F	*	*	*	*	[102], [103], [147]
		Acc	Waist	Device used each day for a period of 2-3 months.	6 h.o. subj. 80-86	[152]
ApEn (Approximate entropy)	F	*	*	*	*	[102]
acc_{trunk} auto-correlation	K	*	*	*	*	[83]
WR (Walk Ratio); t_{step} variability	ST	*	*	*	*	[148]
COM	K	Camera; Force Plates	-	Subjects walked barefoot on a level surface at a self-selected pace.	12 o. subj. 76.9±5.8	[153]

Metric	Type	Sensors	Attachment Location	Exp. Setup	Age	Refs
ASMA (Activity Signal Magnitude Area)	K	*	*	*	*	[95]
Foot Clearance	K	IMU	Ankle	Subjects walked under three walking conditions (10m).	10 h. subj. Mean age: 27.3	[156]
		IMU	Ankles	Subjects walked on a pre-designed loop including one vertical obstacle.	11 subj. (7h.y+4o) h.y - 32.6±7.5 fp.o. - 58.3±23.4	[157]

From all available metrics presented in Table 3.2, only the following metrics were selected to be part of the offline F and PF detection system, namely: i) Roll, Pitch and Yaw angles; ii) Gait events (GE or gait phases); iii) Hip joint angles (Joint_Ang – Left or Right); iv) ApEn from all sensors; v) ASMA (from all Acc axes); vi) SVM (from all Acc axes); vii) dSVM/dt; viii) SVd; ix) Vertical acceleration (Z2_Vert_Acc); x) SMA (from all Acc axes); xi) FFT from all sensors' axes; and xii) Wavelet decomposition (WD) also from all sensors' axes. Besides, raw data from the sensors was also included. Thus, a total of 228 signals can be calculated per trial or gait cycle if the IMUs based system has 5 modules. From now on the term metric or variable will be used to mention these signals. The way of calculating the metrics can be found in the articles mentioned in Table 3.2.

The aforementioned metrics were selected because most of them can be calculated in real-time or are quick to calculate and are described throughout the gait cycle, which means they have more information. Other metrics like walking velocity only have one value per gait cycle, and we decided to only use instantaneous metrics. Foot clearance is a very important metric in the field of Fs. However, metrics that allow the calculation of the foot clearance are already included. Thus, foot clearance was not included in the selected metrics, and the computational weight can be also reduced.

Finally, due to the great amount of variables, it is necessary the use of a nomenclature to better understand what metrics are being used or treated in the context. Concerning the raw data from the sensors, the nomenclature used is "Sensor_Axis_PhysicalAddress". For example, Mag_X_3 means "Mag X-axis from the sensory module number 3". On the other hand, metrics derived from more than one sensor need a different nomenclature:

“DerivedMetric_Sensor_Axis_PhysicalAddress”. For example, ApEn_Mag_X_3 means “Approximate Entropy from the Mag X-axis of the sensory module number 3”.

3.5. Challenges, Issues and Trends

3.5.1. Challenges

Under this area, there are three main challenges to take into account [94]: i) Performance under real-life conditions; ii) Usability; and iii) Acceptance. Obviously, all of them should be carefully treated in order to bring F detection and/or prevention systems to AAL.

Concerning the first mentioned challenge, as first step, F detectors shall be provided with a strong set of characteristics to do not decrease the detection rate. They should be reliable, accurate, robust, and should exhibit both high sensitivity and specificity. Another concern is the fact that these systems are designed and tested under controlled conditions or situations. Even Fs are simulated which does not correspond to daily life situation. Usually, authors also use data from Fs or activities of daily living of young people when the main focus of these systems are the elderly population. Finally, experimental time is also a problem in the majority of the studies. Usually these studies collect data for a few minutes or hours, which is not acceptable or enough to assess the system performance in a real situation. Longer monitoring periods like months should help to improve the system’s performance.

Usability is an important challenge for producers or developers. Smartphone-based F detectors are attractive because it is a well-known technology, equipped with a rich set of sensors. However, they are limited to a specific position of the body, and it also depends on the way people carry their smartphones every day.

Elderly population does not use electronic devices and this is a challenge to overcome in the future. Obviously, the way the system operates is crucial for elderly’s acceptance. For example, the system should activate and operate automatically, without user intervention. Even smartphones could help in this challenge since they are already a well-known technology, though they demand some cognitive capabilities.

3.5.2. Issues

Obviously, all engineering systems have issues, and F detection/prevention systems are no exception. Concerning what was found, there are three crucial issues related to wearable

sensors [94]: i) Smartphone limitations; ii) Comparison among different techniques: public data bases; and iii) Real-life Fs.

The first one was also discussed previously, however it is understandable that smartphones are not devices initially intended for F detection or any other safety critical application. There are some examples of problems related to real-time operations, the sensing architecture or the specific features of the operating system. Another problem is related to the battery. It is important to manage the sleep cycle of the components in order to regulate the consumption of battery, since smartphone's battery life is always low. Thirdly, it is important that these system can be implemented in easy-to-use smartphones and this only depends on the manufacturers. This point is crucial since elderly, which have low technical skills, are the target audience.

Another issue is related to public data bases. Obviously, different authors collect data in a different ways, varying the types of Fs, position of the sensor, sampling frequency or extracted features. So, a public database could be an important help to compare different methods of detection or risk assessment. Thirdly, the evaluation of the system is severely limited because it is inconceivable ask older people to simulate Fs. The number of trials and their duration are still low.

3.5.3. Trends

In the future, this technology is expected to evolve in terms of robustness and detection/prevention efficiency. Smartphones have built-in communication protocols that allow simple data logging to the device and wireless transmission. Price is also significantly reduced due to high production volume. IMUs also have the same trend than smartphones so they can also be used as an alternative tool to optical methods [122].

In addition to these sensors, there is also the machine learning approach. This approach is considered as sophisticated and leads to better detection rates. Deep learning is also a type of machine learning approach, and it can bring better results. However, it necessitates a large amount of data for training [122].

Chapter 4 – Human Gait Monitoring System Overview

4.1. Introduction

As already mentioned, for this project it is intended a IMUs based system for real time human gait monitoring. As such, there is a lot of information to be processed and displayed instantly. The GUI will provide for an intuitive visual interface and real-time data visualization and recording. So, this chapter intends to demonstrate the extension of previous work [13], the developed Matlab GUI, and the quality assessments of several users about it. The remainder of this chapter is organized as follows. In Sections 4.2, 4.3, and 4.4 the system used, the communication protocol established between system elements, and the explanation of the implement ASM are presented, respectively, Section 4.5 presents a list of needs identified from the system to build an interface, and explains in detail the built GUI. This section also provides methods for assessing the quality of the GUI and to validate the communication protocol, and the results and discussion of the quality assessment and the validation of the communication protocol's methods.

4.2. Magnetic/Inertial Measurement System

The overall system, able to monitor human gait, is shown in Fig. 4.1. A personal computer, a SmartRF05EB (base station), and sensory modules are the three main elements of the system used [13]. A MPU-6000 [158] from InvenSense, which contains a three-axis MEMS Acc, a Gyro, and a temperature sensor, allowed an integration with a Honeywell three-axis Digital Compass IC HMC5883L [159]. This sensor board is connected to the CC2530EM module (Evaluation Module) from Texas Instruments which is a System-on-chip solution to IEEE 802.15.4 applications (IEEE Std 802.15.4, 2006) through two 20-pin header connectors. Thus each sensory module is formed. Sensors' specifications are available on Tables I, II, III, and IV. Throughout the project, MPU6000 was programmed to have a Full-Scale Range of $\pm 4g$ for Acc, $\pm 1000^\circ/s$ for Gyro, and ± 0.88 Gauss for digital Mag.

The CC2530EM module is used to establish communication between sensory modules and base station SmartRF05EB (Evaluation board) via wireless. Data received by the base station is routed to the Personal Computer via serial port (RS-232). Subsequently, the data are properly processed. Each sensory module can be firmly attached to one body segment to be monitored.

Sensors from each sensory module were calibrated as mentioned in [13] before a gait monitoring. Thus, there is a system capable of monitoring human gait. The entire system is controlled by the developed GUI. In the following it is presented the use of the communication protocol, the proposed ALSM, and a brief explanation of the human gait. The sampling frequency is at least 0.63Hz, and 160Hz is the maximum value. However, 30Hz is the minimum value used to monitor gait in this project.

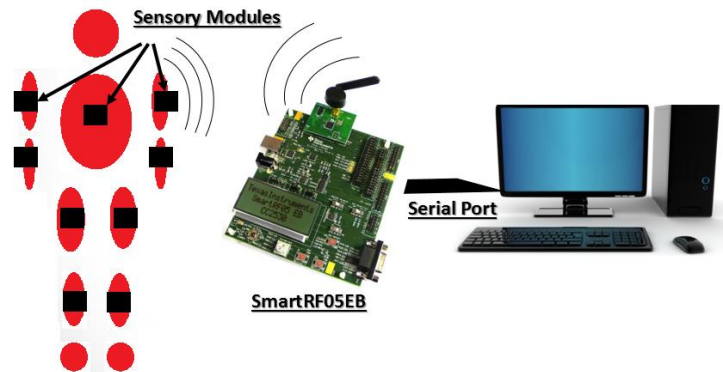


Figure 4.1 - Magnetic/Inertial Measurement System Elements.

4.3. eLPRT protocol

The Enhanced Low Power Real Time (eLPRT) protocol controls the communication through the wireless medium, and was designed to optimize the quality of service (QoS) support and the bandwidth utilization efficiency [160]. In order to transmit the multiple sensor readings between the sensory modules and the base station, a multi-byte message is formed after the sensors readings have been collected. This message, depicted in Fig. 4.2, will be designated from now on as frame. The frame can be described as follows: i) Start byte and stop byte have the same value (122 in decimal), and they are responsible, respectively, for the beginning and end of reading the bytes by the part of the processing code. ii) Two bytes identify the sensory module where the

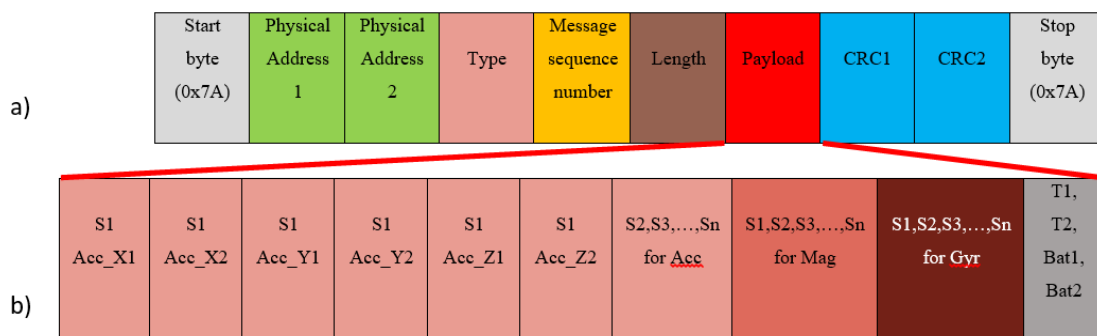


Figure 4.2 - a) Constitution of the frame; b) Constitution of the payload (S-sample/reading, T1 & T2-temperature byte 1 and 2, Bat1 & Bat2-battery byte 1 and 2).

message came from (Physical Address 1 and 2). iii) The “Type” byte indicates if the message is a command message or a sensors’ data message. iv) Every message has a sequence number. Because it is only one byte, the sequence number goes from 0 to 255. After 255 it returns to 0. v) The “Length” byte gives information about the size of the payload. vi) Payload is where the sensor’s data is. Each reading is expressed in two bytes for each axis of each used sensor. In Fig. 4.2, “S1 Acc_X1” represents the first byte from the first Acc reading/sample, and “S1 Acc_X2” the second byte from the same reading. This strategy is also applied to the remaining axes and other samples. And vii) The CRC (cyclic redundancy check) values (CRC1 and CRC2) are used to detect accidental changes to raw data. If they do not match, then the block contains a data error. Otherwise, message is ready to be used.

Once frames reach the base station, they are processed to obtain relevant information from the sensory modules correctly. This process must be fast and efficient. For instance, two equal frames, i.e., two equal sequence numbers, should not be processed. Thus, an ALSM was implemented to improve the reliability of the data processing where the frame's constitution is considered. This ALSM showed an efficiency of 100% for a use of 500 times. The ALSM is described next.

4.4. Algorithmic State Machine

As the data is received by the base station, it is necessary to process the bytes in order to obtain the relevant information from the sensory modules. To this end, it must be ensured that the frame is received correctly, and two equal frames are not processed. Thus, an ALSM was made in order to improve the reliability of the data processing (Fig. 4.3).

As soon as the user clicks the “Start” button, a start command is sent through the selected serial port to all activated sensory modules to start sending data. At the same time, frame size (blocksize) is set. Then, the serial port starts to be read. In order to start information processing at least one frame has to be constituted. From Fig. 4.2, it is possible to retain that the start byte and the stop byte have the same value. Thus, the byte position corresponding to the decimal value 122 is collected to the array “str_byte_pos”. So, a “for” loop sweeps this array through a count variable “i”. While “i” is less than the number of possible start bytes, the CRC bytes will be checked, and if “CRC state” variable is one, it means that the frame is valid for processing.

When “i” is one, the frame is immediately checked. Otherwise, the frame is checked if there are as many or more bytes between possible start bytes than the size of the “blocksize”, or even if there are fewer bytes between possible start bytes than the “blocksize”, the “CRC state” variable must be 0 in this particular case. If “CRC state” variable is one, the stop byte corresponding to the checked frame is eliminated from the array “str_byte_pos” except for the first position of this array. Thus, it is possible to shorten the number of iterations of the “for” loop.

Sequence number of the frame is compared to the last received. If the frame is equal to the last one, the last frame received is not processed. So, two consecutive processed messages are necessarily different. Taking into account the payload structure shown in Fig. 4.2, the data is then separated, processed, displayed, and saved in real-time. When the “for” cycle ends (Stop states), the whole process will repeat itself again when the number of bytes received by the serial port is enough to constitute a new frame. This process occurs while the selected modules are activated. After several uses of this ALSM, its operation is considered exemplary, since it never had problems of operation. With the aid of a CF to estimate the orientation, it is possible to obtain the angles of each sensory module represented in Qs and/or EAs. Another feature is the detection of human gait events, namely foot flat, toe off, swing phase (SW), and heel strike (HS) by using sensory modules on the upper foot or on the heel.

4.5. System Requirements and MATLAB Interface

Data acquisition can be facilitated by the development of a GUI. A logical and intuitive man-machine interaction can be achieved as long as all the necessary variables and requirements of the system are known. Moreover, the GUI can display relevant information in a simple and easy-to-understand way, which would be more difficult if only the command line was used to display the information.

4.5.1. System Requirements

In order to properly develop the GUI, it is necessary to establish a list of requirements based on the user and system needs, as follows: a) an easy way to select the serial port; b) an interactive way to choose which sensory modules to use and where to place them; c) from the selected modules choose a module of interest; d) provide information about the battery status of the selected sensory modules; e) display the temperature from the temperature sensor of the sensory module of interest; f) count the time from start to finish; g) allow real time data visualization

of the sensors data and the calculated angles of the module of interest; h) allow recording the data to files; and i) count total frames, lost frames and their percentage over real-time monitoring.

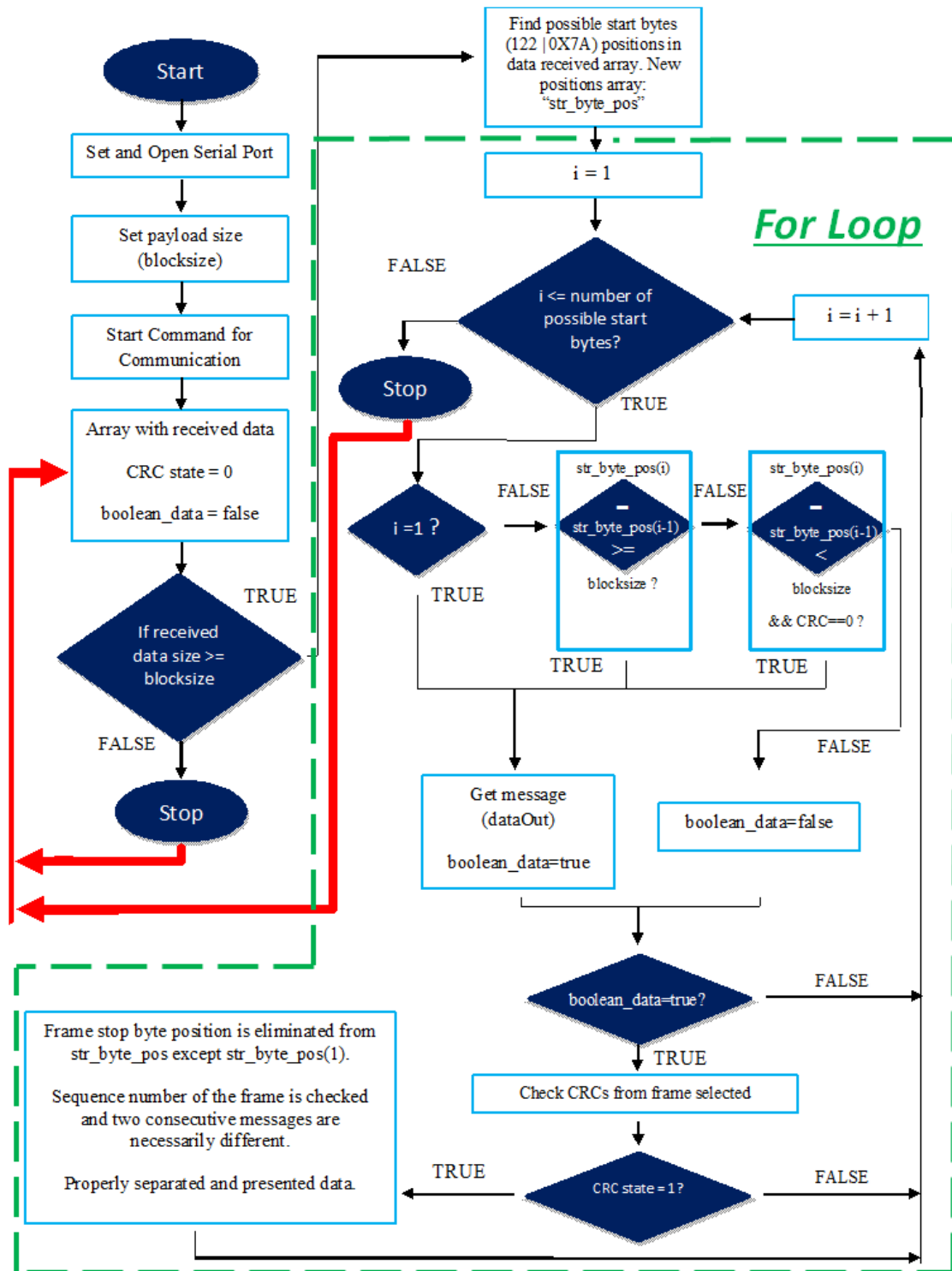


Figure 4.3 - Data acquisition process flowchart.

4.5.2. MATLAB Interface

Once the system requirements were defined, a Matlab GUI that fulfilled the previously mentioned requirements was developed. Thus, each requirement has been evaluated and structured in such a way to be represented in the Matlab GUI with simplicity, so that the user can interact with the interface intuitively and easily.

The interface acts as follows. When the interface is initialized (Fig. 4.4), it is displayed: i) a representation of the **human body** appears displaying the body segments where the respective sensors can be allocated (only body segments are considered); ii) a **control panel** where there is a "Start" button (disabled at the beginning), a time display, a panel that assesses the communications quality by displaying the lost frames/packets and the total packets received, and two displays (battery and temperature) of the module of interest; and iii) a **settings panel**, where it is possible to select the serial port, the module of interest, which information to visualize in graphs from a dropdown list (e.g. Acc, Gyro, Mag, sensory module angles and the gait event detectors) and the state of the batteries of all sensory modules.

As a first step, the user must start by indicating the location of the sensory modules in the body segments shown in the representation of the human body in the interface, inserting the

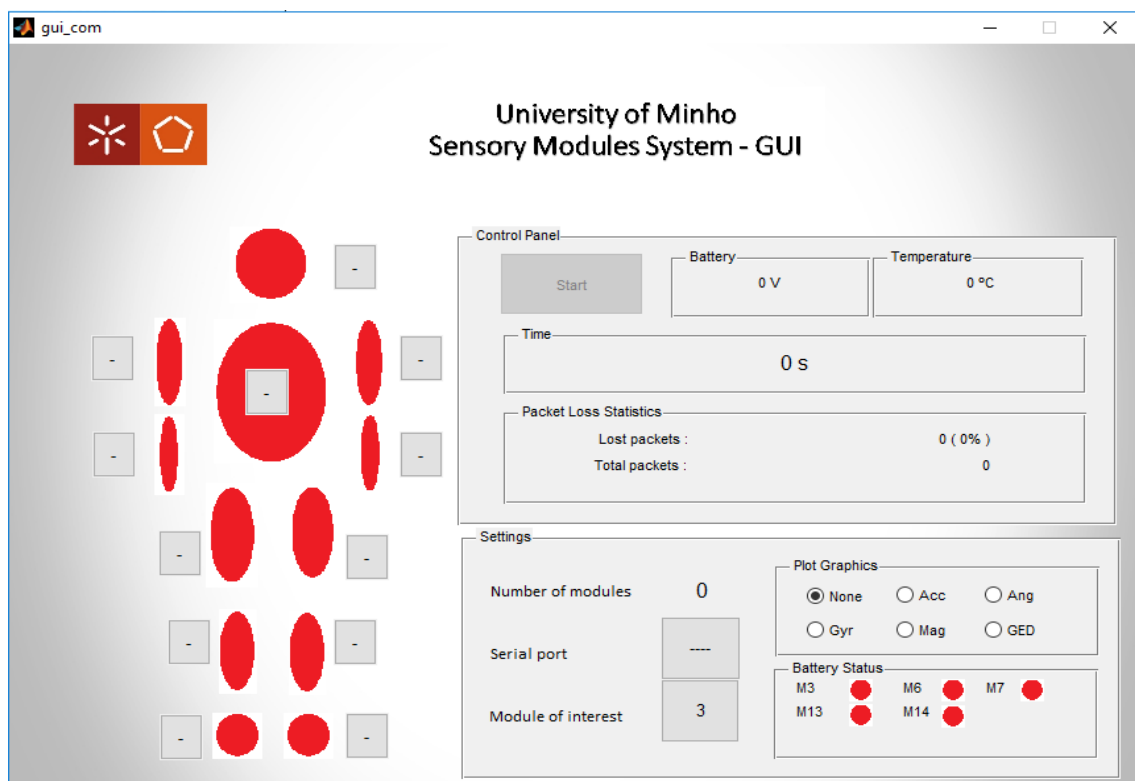


Figure 4.4 - Matlab GUI when initialized (Ang – Angles; GED – Gait Events Detection).

physical address of the sensory module in the textbox of the respective segment. Each module has its number recorded and in view of the user.

The representation of the human body in the interface contemplates the following segments and parts of the body: i) head; ii) trunk; iii) (right and left) upper arm and forearm; iv) (right and left) upper and lower leg; and v) (right and left) foot. When a segment or body part is selected, the red colour is replaced by green. Figure 4.6 shows an example when the trunk segment was selected and the physical address was the number 7.

Subsequently, the user must select the serial port by clicking on the button to the right of the respective text, and must select the module of interest that is where the temperature, battery and graphics information comes from. In order to achieve real time data visualization, the user may also select which graphics to display. Only when all these steps are done, the "Start" button becomes enabled and changes its colour to green. Once the base station and sensory modules are activated, a click on the "Start" button starts the monitoring process. Figure 4.5 provides an example of system operation with only one sensory module. In this particular situation, only the graphs of the three axes of the Acc were selected. All the mentioned information is available and is displayed in real time. Special highlight for battery states panel, where the green colour means that the sensory module has a battery value higher than 3.40 Volts in a total of 3.60 Volts; the orange colour means that the battery has a value less than 3.40 Volts but the sensory module is connected; and the red colour indicates that the sensory module is not active.

While the sensory modules are activated and the monitoring process has been initiated, the gait monitoring process is taking place. When the modules are switched off, the data acquisition process is interrupted and consequently all the information is saved and available in text files. To safeguard the occurrence of possible errors the data coming from the IMUs are constantly stored in text files. Only at the end of the process is the information separated by sensory modules, and the statistics of losses are also saved. This provides for recording which is essential in any system aiming for real time gait monitoring. Figure 4.5 is an example of the situation mentioned above. When the user disconnects the sensory modules, the process will be interrupted and a message will appear in the Matlab GUI saying «Communication finished and data saved!» (Fig. 4.6). In the end of the process, there is no reset in the information displayed in the interface, however as soon as the user starts the process again by clicking on the start button, the interface itself resets the available information and returns everything to the beginning.

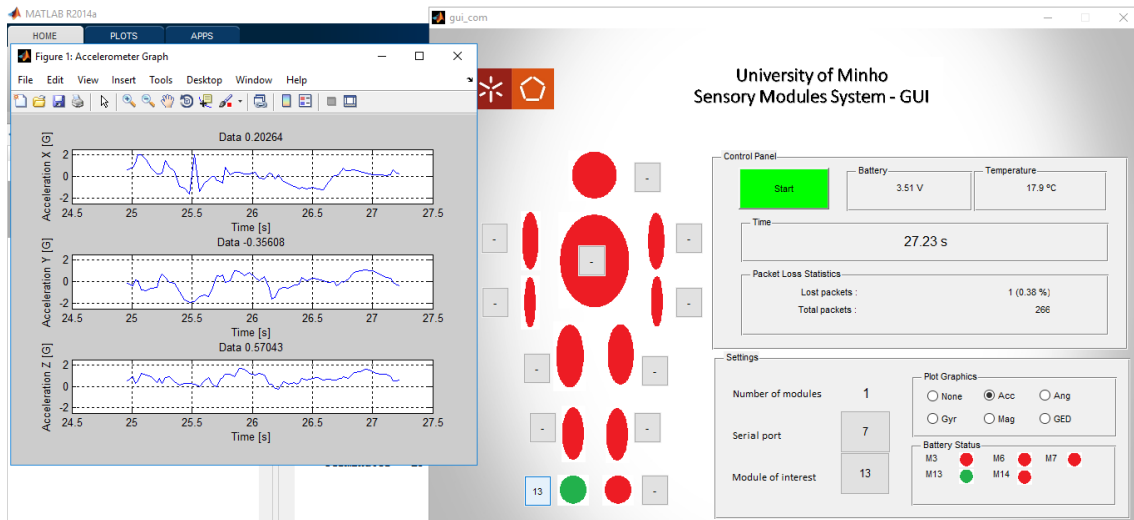


Figure 4.5 - Matlab GUI when the system is in the operational state.

Finally, just note that when the user wishes to visualize the graphs of the sensors, angles, and/or even the gait event detection, only the graphs corresponding to the module of interest are displayed. Moreover, the gait event detection graphic only gives one of four stages at a given time with a predefined value (Foot-Flat (FF) – 0; Toe-Off (TO) – 1; SW– 2; HS– 3). In order to visualize in real time other locations, the user just has to select a different module of interest.

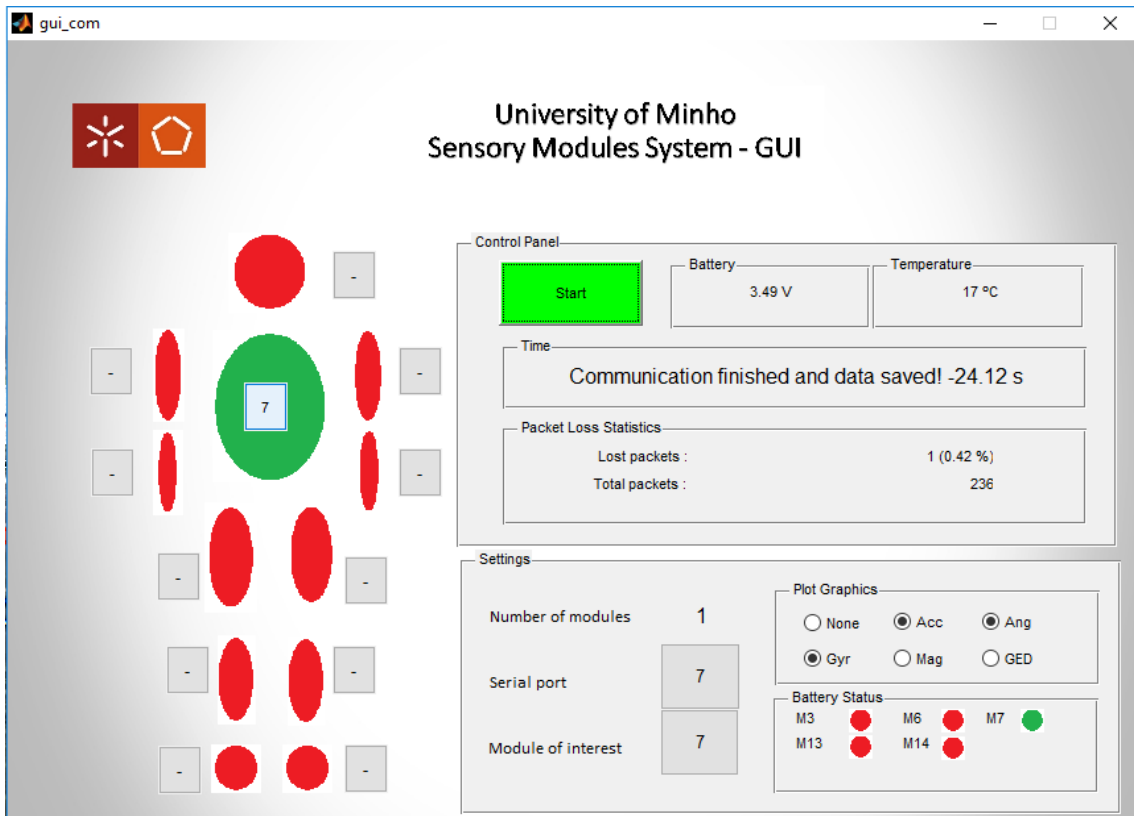


Figure 4.6 - Matlab GUI when the system was stopped.

4.5.2.1. Quality Assessment

During the development of the GUI, some potential end-users were contacted in order to collect their feedback and include it in the development. After the interface was completed, the human-machine interaction was evaluated based on an inquiry made in a group with thirty-six participants (25 males, 11 females; mean age of 27.4 ± 4.9 years old, range from 22 to 35 years old; 7 health technicians, 29 with engineering knowledge). The idea was to perform some usability tests that would indicate the easy-to use and intuitiveness of the developed GUI.

Previous to any contact with the developed Matlab GUI, the system was explained to these users as well as the aim of the overall system. They interacted alone with the GUI for five minutes. In addition, users were informed where the modules and the base station are activated, that the connection between the base station and the Personal Computer is established via serial port, and that each sensory module has a physical address.

When users finished working with the GUI, they answered five questions that are as follows: 1 - Do you think the background is simple and enjoyable? ; 2 - Do you consider that the sequence of steps is intuitive? ; 3 - Do you find it easy to choose and allocate the sensory modules in the virtual respective segment? ; 4 - Do you consider that the information obtained from the graphics, battery status from sensory modules and lost data is sufficient? ; 5 - Did you need help during the process?

In order to evaluate the overall methodological quality of the Matlab GUI, any criteria or question on the quality assessment were assigned a score of zero point if the criterion was not met. As there are five questions, it was considered that one point corresponds to twenty percent, and thus, it is possible to have a percentage scale. The Matlab GUI is considered "Good" if it has 60% or more of the criteria. "Fair" is the second classification, and the percentage of criteria is between 40% and 60% ($\geq 40\%$; and $< 60\%$). Finally, "Poor" is the last classification with less than 40%.

4.5.2.2. Results and Discussion

Twenty-five people described the background as simple and enjoyable ($\approx 69.4\%$). Fifty-six percent, approximately, (20 people) defined the process as intuitive. Only two people ($\approx 6\%$) did not describe as easy to choose and allocate the sensory modules in the virtual respective segment. Thirty-two people ($\approx 88.9\%$) considered the displayed information sufficient. Eleven subjects needed help during the process. Information is resumed in Fig. 4.7. In general, the majority of the people

considered the Matlab GUI as “Good”. In a total of 180 answers, 136 were positive (75.6%) which means that the quality assessment reveals that the Matlab GUI is able to be used by a common person. Main comments from the respondents are: a) the inclusion of a “Stop” button; and b) an explanation of how it works through images or video before using the interface. As an immediately outcome of this quality assessment, these two last suggestions were already implemented.

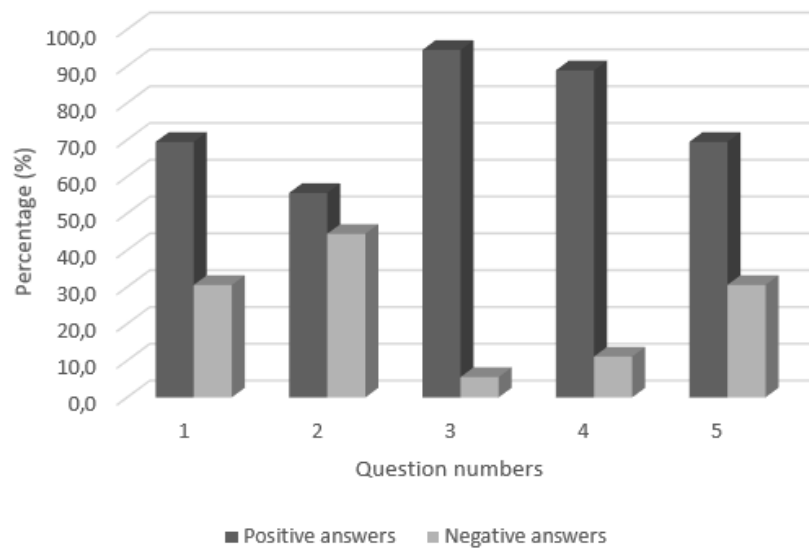


Figure 4.7 - Inquiry results in percentage per question number.

Chapter 5 – IMUs based System Validation

Once the IMUs based system is implemented, it is necessary to validate its operation. In other words, it is crucial to understand if the IMUs based system is reliable, and if not, find ways to overcome the problems. This point is of the utmost importance, as it will influence all the work that follows. It will serve also as a basis to know how close it is to the ideal functioning, and on the other hand to overcome any difficulties in a more decisive, consistent and founded manner.

The validation process can be subdivided into 4 different phases as represented in Fig. 5.1, namely: i) Communication protocol; ii) Signals of the sensors; iii) Calibration; and iv) Estimation of joint angles (Knee). From these, only the calibration process is not explored in this chapter, since its description can be found in Chapter 6.

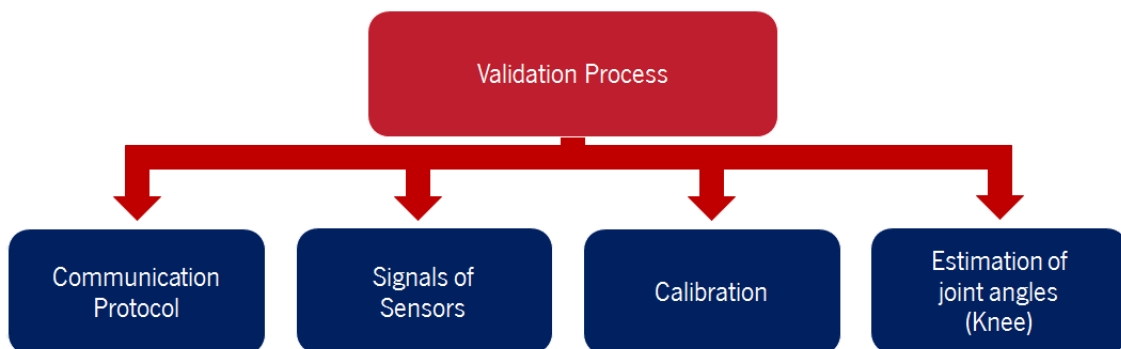


Figure 5.1 – Phases of the validation process.

5.1. Validation of the communication protocol

The presented IMUs based system establishes a wireless communication between a base station and IMUs by means of Radio Frequency (RF). Without considering interferences from other sources or wireless communications, four basic phenomena occur in the wireless medium [161]: i) Path-loss; ii) Reflection; iii) Diffraction; and iv) Scattering. These effects have a negative impact on the signal propagation and are responsible for path-loss and the distortion of the received signal. In an indoor environment, the probability of having more reflections is higher which significantly affects the propagation of the RF signal frequency. In this scenario, the wave partially reflects and partially absorbs if the propagation radio waves reach a surface that is larger than the radio waves wavelength [161]. On the other hand, the presence of more wireless communications at the same

place can also affect the performance of the wireless communication [162]. Concerning the literature [162], to prevent or mitigate the risk of interference, these wireless systems can use: i) Narrow beam adaptive antennas; ii) Power Control; iii) Physical Diversity; and iv) a Monitoring Program.

The first step was to evaluate the communication protocol, quantifying the loss of frames, and if there are losses, try to understand the reasons why these losses happen. Thus, the primary goal of this validation test is to check for differences in wireless data transmission between sensory modules and the base station in different environments. In order to fulfil the proposed objective, the losses of data packets were accounted for during specific trials.

5.1.1. Trials

A healthy subject with 22 years old performed two different trials in three different environments: i) inside a laboratory; ii) in a corridor; and iii) in an outdoor environment free of any ferromagnetic influence or other wireless communication. The trials can be described as follows: i) stand upright for 20 seconds at one meter from base station; and ii) stand upright for 5 seconds and then walk forward 5 meters (inside a laboratory) and 10 meters (in the other two environments) at two different paces (normal and fast). In both scenarios, after the test was completed, the subject turned off the sensory modules. The losses in this period of time were also accounted for until all sensory modules were off.

The first mentioned trial was performed only with five sensory modules as depicted in Fig. 5.2. The other trial was performed for all spatial arrangements (Fig. 5.2). In each of the environments, these two trials were repeated five times for each spatial arrangement of the sensory modules in the body.

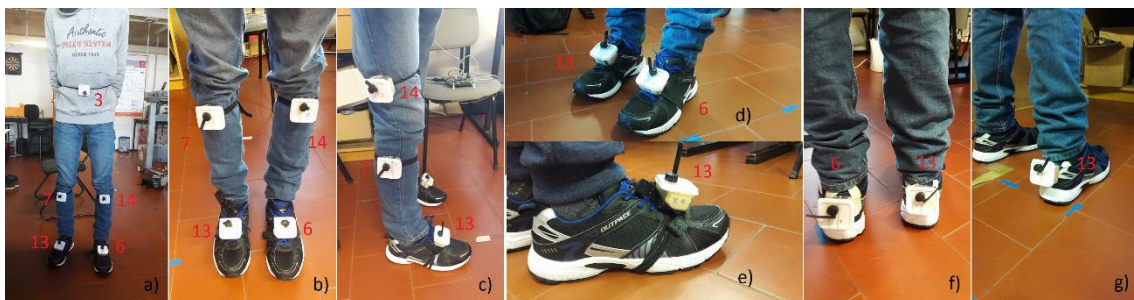


Figure 5.2 - Spatial arrangement of the sensory modules in the body with their physical addresses: a) 5 sensory modules on trunk (3), foot (13-right, 6-left), and shank (7-right, 14-left); b) 4 sensory modules on foot (13-right, 6-left), and shank (7-right, 14-left); c) 3 sensory modules on right leg: foot (13), shank (7), and thigh (14); d) 2 sensory modules on the upper foot (13-right, 6-left); e) 1 sensory module on the upper foot (13-right); f) 2 sensory modules on the heel (13-right, 6-left); and g) 1 sensory module on the heel (13-right).

The information of the direction of the axes is shown in the following table, where this information is available for each spatial arrangement of the sensory modules, and for each sensory module.

Table 5.1 - Direction of the positive axis for each sensory module in each spatial arrangement

Spatial arrangement of the sensory modules	Physical addresses				
	<u>3</u>	<u>6</u>	<u>7</u>	<u>13</u>	<u>14</u>
5	x - to the right	x - to the right	x - to the right	x - to the right	x - to the right
	y - down	y - forward	y - down	y - forward	y - down
	z - front	z - up	z - front	z - up	z - front
4		x - to the right	x - to the right	x - to the right	x - to the right
		y - forward	y - down	y - forward	y - down
		z - up	z - front	z - up	z - front
3			x - back	x - to the right	x - back
			y - down	y - forward	y - down
			z - to the right	z - up	z - to the right
2 - on the upper foot		x - to the right		x - to the right	
		y - forward		y - forward	
		z - up		z - up	
2 - on the heel		x - to the left		x - to the left	
		y - down		y - down	
		z - back		z - back	
1 - on the upper foot				x - to the right	
				y - forward	
				z - up	
1 - on the heel				x - to the left	
				y - down	
				z - back	

5.1.2. Results

Concerning the results of the first trial, the average percentage of loss of the five tests was $3.40 \pm 2.59\%$ inside the laboratory, $2.03 \pm 0.97\%$ in the corridor, and $0.28 \pm 0.07\%$ in the outdoor environment. Table 5.2 details the number of losses verified by each test, as well as the total number of frames received during the trial. In this trial, the number of lost frames is always less than 5 in an outdoor environment. On the other hand, the number of lost frames is greater than 10 in every experiment carried out inside of the laboratory and in the corridor.

Table 5.2 - Number of lost frames and total frames for each environment

Test Number	Number of Lost frames			Number of Total frames		
	Lab	Corridor	Outdoor	Lab	Corridor	Outdoor
1	57	10	3	1167	1157	1157
2	19	37	4	1234	1174	1176
3	26	32	4	1194	1175	1147
4	85	14	3	1174	1158	1145
5	14	26	2	1200	1190	1130

The second trial was performed seven times repeated five times each, since this was done for all forms of spatial arrangement of the sensory modules described above in Fig. 5.2. Table 5.3 summarizes the values of the average percentage of loss of the five tests for each spatial arrangement in the three mentioned environments at different paces (normal and fast pace). These values are also represented in Figure 5.3 (one figure per environment: Lab, Corridor, and Outdoor, respectively) to make a simple comparison between normal and fast pace for each spatial arrangement of the sensory modules. Moreover, as results, for self-comfortable gait speed the subject performed a mean velocity of 3.24 ± 0.17 km/h, and for fast pace the tests velocity was 6.04 ± 0.34 km/h.

Table 5.3 - Average percentage of loss of the five tests for each spatial arrangement (L-Lab; C-Corridor; O-Outdoor; N-Normal pace; F-Fast pace)

Spatial arrangement of the sensory modules	Percentage of loss for Environment and Type of Pace (%)					
	N			F		
	L	C	O	L	C	O
1 on the upper foot	0.78±0.25	3.57±2.09	1.07±0.41	1.68±0.87	3.06±1.58	1.19±0.60
2 on the upper foot	0.59±0.19	1.15±0.86	1.36±1.49	0.52±0.15	1.32±0.81	1.87±0.61
1 on the heel	1.31±0.11	1.37±0.72	0.90±0.35	1.64±1.27	2.52±1.58	0.90±0.35
2 on the heel	0.74±0.71	3.46±2.17	1.18±0.64	0.87±0.49	1.72±0.37	1.36±0.42
3	9.86±3.46	4.28±2.33	0.90±0.60	8.24±5.35	5.43±2.89	1.32±0.58
4	5.82±3.87	6.72±4.94	3.14±1.84	12.64±5.87	3.84±1.87	4.85±2.81
5	15.21±4.04	8.93±5.41	5.40±2.04	9.74±2.82	5.80±3.27	7.51±2.07
Mean	4.90±1.81	4.21±2.65	1.99±1.05	5.05±2.40	3.38±1.77	2.71±1.06

In Fig. 5.3, the average percentage of loss inside the laboratory for 2 or less sensory modules is relatively low. However, when the number of sensory modules is equal to or greater than three, the average percentage of loss is always bigger than 5%. In some cases, this percentage is bigger than 10% which can affect the gait monitoring process.

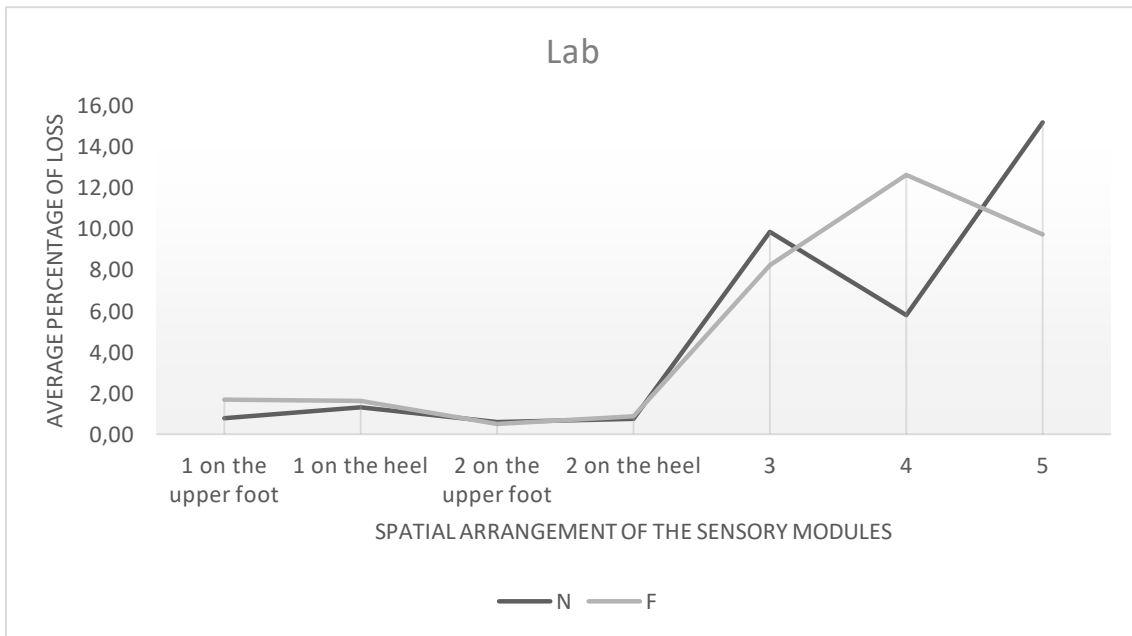


Figure 5.3 - Average percentage of loss for each spatial arrangement in laboratory (N-Normal pace; F- Fast pace).

In general, at the corridor, the average percentage of loss (Fig. 5.4) is lower than inside the laboratory, but still greater than 8%. In this case, when the number of sensory modules is 3, the average percentage of loss is lower than 6%, which is inferior to the value in the previous situation (8.24% at the fast pace, and 9.86% at the normal pace). A similar finding is observed when 4 or 5 sensory modules were used. However, in the situation where one sensory module was used, the result was higher in comparison to the result evidenced in Fig. 5.3. This also happens when 2 sensory modules were attached to the heel and on the upper foot.

In an outdoor environment, the average percentage of loss (Fig. 5.5) is lower than 2% when 3 or fewer sensory modules were used. When the subject wore 4 and 5 sensory modules, the average percentage of loss was lower than, 5% and 8%, respectively. In general, the developed protocol for the wireless communication of various sensory modules based on IMUs, was more efficient and robust in outdoor than inside the laboratory or in the corridor. In Table 5., in the “Mean” line, the average percentage values are accompanied by the mean of the standard deviations of the various sensory modules spatial arrangements (Fig. 5.2).

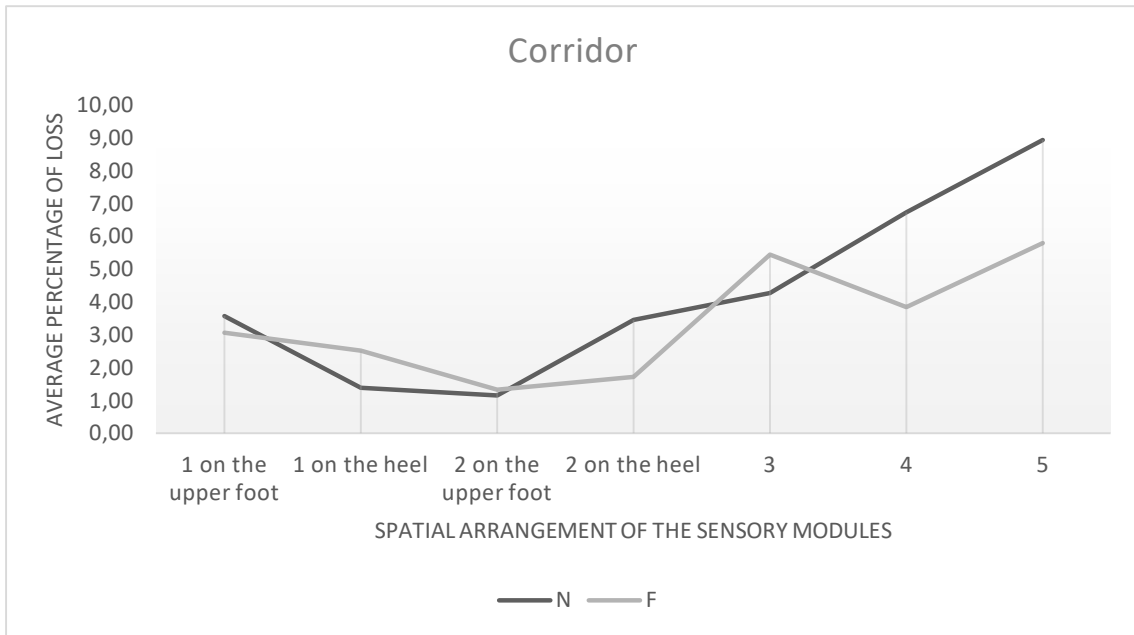


Figure 5.4 - Average percentage of loss for each spatial arrangement in the corridor (N-Normal pace; F- Fast pace).

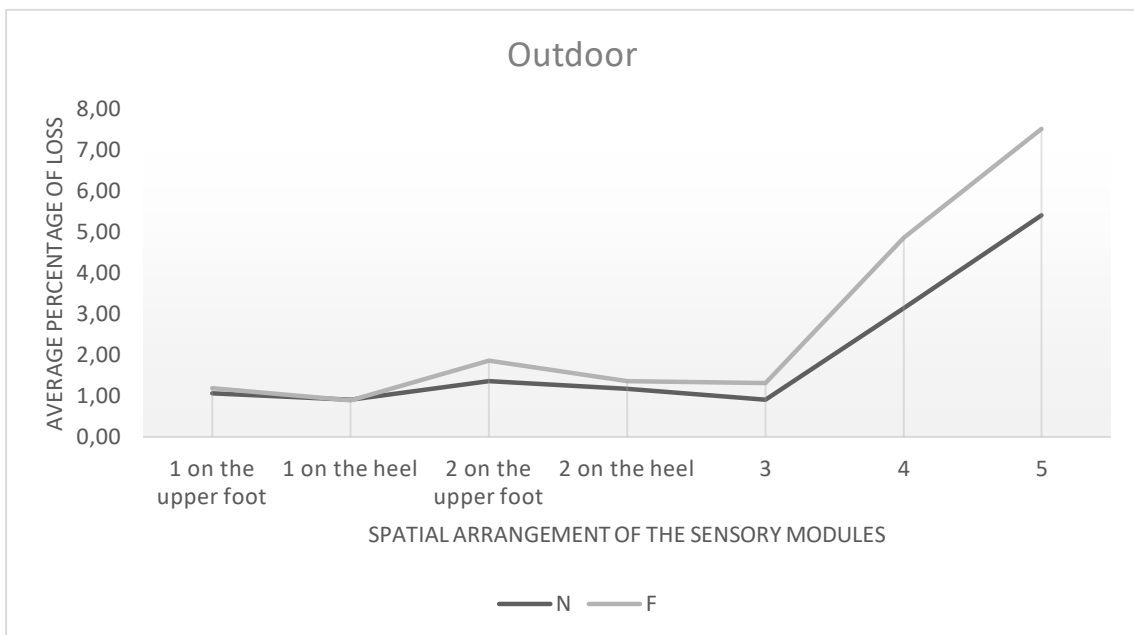


Figure 5.5 - Average percentage of loss for each spatial arrangement in an outdoor environment (N-Normal pace; F- Fast pace).

5.1.3. Discussion

Regarding the first trial, a better result was expected in the outdoor environment, since it is an environment free of any wireless communications like those existing in the laboratory and in the corridor. In fact, the average percentage of loss in the outdoor environment was lower than the one observed in the other environments (Outdoor- $0.28 \pm 0.07\%$; Lab- $3.40 \pm 2.59\%$; Corridor- $2.03 \pm 0.97\%$), as expected. In addition, in the corridor the losses are slightly lower than those found

in the laboratory, which means that any interferences in these two environments have greater influence inside the laboratory than in the corridor.

The results of the second trial reveal that as the number of modules increases, the percentage of loss also increases. However, once again and for the same reasons the average percentage of loss is smaller in an outdoor environment than in the corridor and inside the laboratory, and results in the corridor are better than inside the laboratory. Taking into account the graphs depicted in Fig. 5.3, it is possible to retain that the average percentage of loss when the subject performed normal and fast speed shows the same trend in both scenarios for every environment. In other words, the gait speed has almost no influence on the loss of frames. However, in the majority of the spatial arrangements of the sensory modules, it was found that there is a slightly higher average percentage of loss when the subject walked at a fast speed. Although not significant, this may be justified by the fact that during a more sudden movement, the connection between the sensor board and the CC2530 module may fail.

The first trial can be compared to the second trial when the subject used 5 sensory modules (Fig. 5.2). Thus, it is possible to verify that when the subject walked, independently of the gait speed, the average percentage of loss was higher than the homologous value recorded when the subject was standing upright at one meter from the base station. This increase is explained by the gradual increase in the distance between the sensory modules and the base station. When the distance increases, the risk of interferences, reflections, diffractions, and scattering also increases.

5.2. Validation of the signals of the sensors

A comparison study between the typical signals of the sensing devices and those measured by the IMUs based system during human gait was performed. Basically, a research in the scientific literature was made to identify the typical signals of the sensing devices attached in various parts of the human body, namely on the foot, thigh and lower back (Fig. 5.6). Later, with the help of the sensing devices of the IMUs system, in the mentioned locations, human gait's data were collected from a healthy subject through walk forward trials. Finally, the signals were compared, and due discussions were reached.

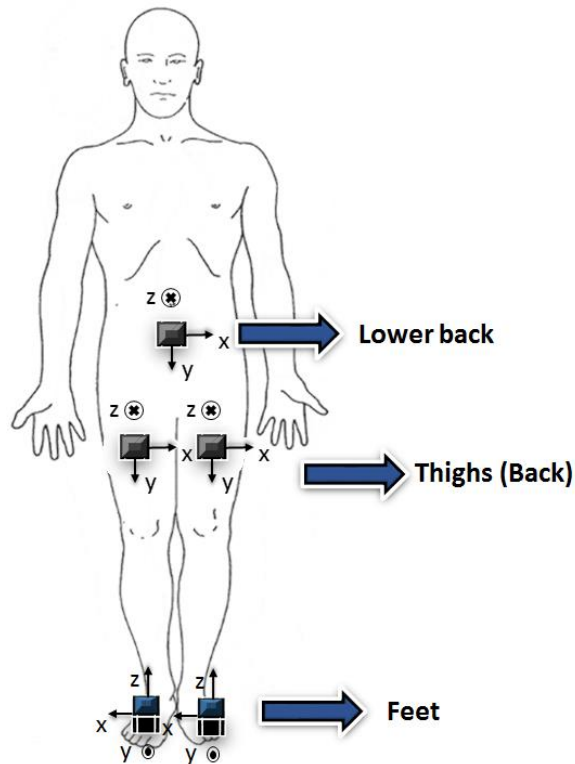


Figure 5.6 - Attachment location of the sensing devices used for the trials (Dark sensing devices are in the back of the body).

5.2.1. Results and Discussion

5.2.1.1. Foot

Jiménez et al [163], which used a Xsens' IMU attached to the right foot using the shoe's laces (Fig. 5.7), demonstrated the typical signals of the IMU's three axes during a walking trial. Raw sensor's readings were collected from a subject that walked 30m in one direction and returned back after a 180 degrees turn.

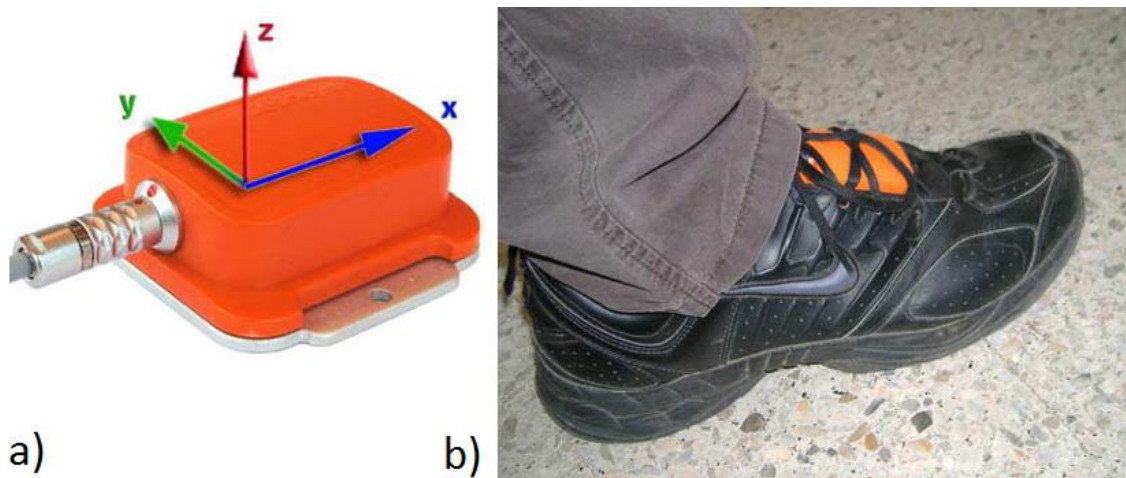


Figure 5.7 – a) Orientation of the Cartesian axes of the sensing device. b) Xsens' IMU attached to the right foot.

Typical signals (Acc, Gyr, and Mag) measured by Jiménez's IMU attached on the foot are depicted in Fig. 5.8.a, as well as the signals obtained by the IMUs based system (Fig. 5.8.b). The orientation of the sensing device is different in both situations. Compared to the Fig. 5.7, only the z-axis coincides with that used in the IMUs based system (Fig. 5.6 – right foot). The x and y axes are changed, and the positive sense of the mediolateral axis of the IMUs based system is to the right.

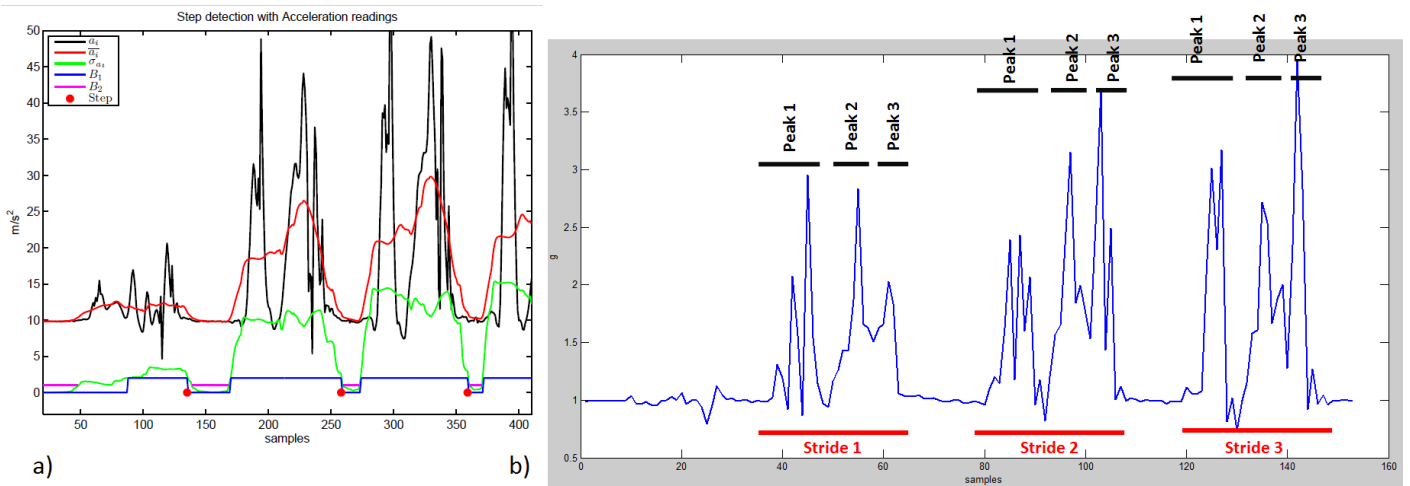


Figure 5.8 – Norm of the acceleration during a walking trial obtained from: a) a Jiménez's trial (black line) [163].
b) IMUs based system (data not filtered).

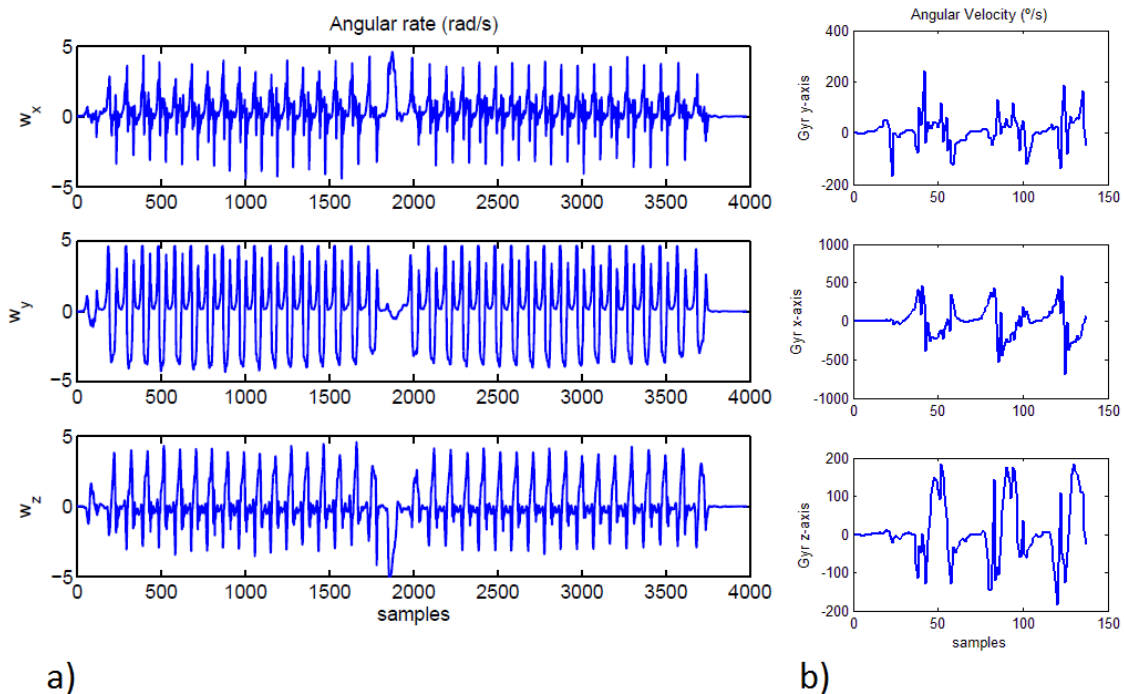


Figure 5.9 - Gyro data during a walking trial obtained from: a) a Jiménez's trial [163]. b) IMUs based system (data not filtered).

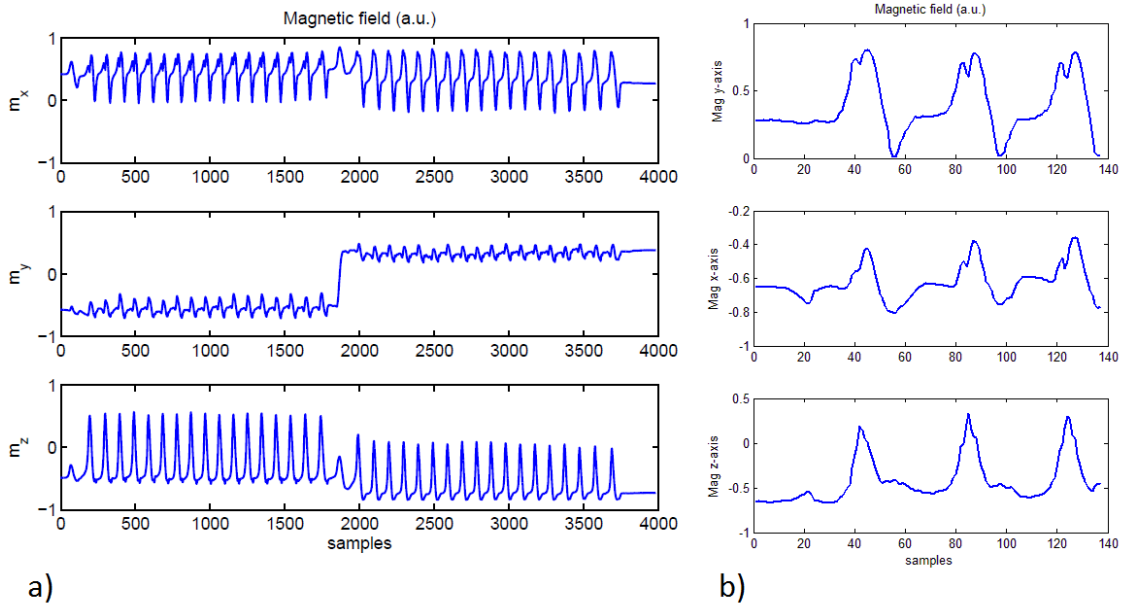


Figure 5.10 - Mag data during a walking trial obtained from: a) a Jiménez's trial [163]. b) IMUs based system (data not filtered).

From Fig. 5.8, it is possible to observe a similarity between the two depicted signals, i.e. the typical one (Fig. 5.8.a) and that measured by our system (Fig. 5.8.b). In fact, the norm of the acceleration in one stride is represented by three main peaks [163], [164]. In both signals this characteristic is present which indicates the validity of our system.

In Fig. 5.9, the comparison between the typical signal of the Gyro and the one measured by our system is made by axis. Once again, similarities can be found, particularly in the middle graph of Fig. 5.9. Essentially, this axis measures the slope of the foot. It is characterized by a set of positive peaks, followed by negative peaks, whose connection to the next positive peak is made from a loop with the concavity facing upwards [51], [163]. The data measured by the Gyro are in agreement with the scientific literature.

Mag's data depicted in Fig. 5.10 are also in agreement with the scientific literature [163], [164]. Once again, the comparison between the typical signal and the one measured by the IMUs based system is made by axis, and it is possible to observe a huge similarity between signals due to the low noise of the sensor.

5.2.1.2. Thigh

Hamdi et al [51] constructed a MCS with 7 IMUs to monitor the LL's segments. Their sensing devices were used to measure direct biomechanical variables such as angular velocity and linear acceleration. The local frame assignment of the sensors attached to each lower limb segment is depicted in Fig. 5.6. All sensors are 3D-axis which allows 3D orientation.

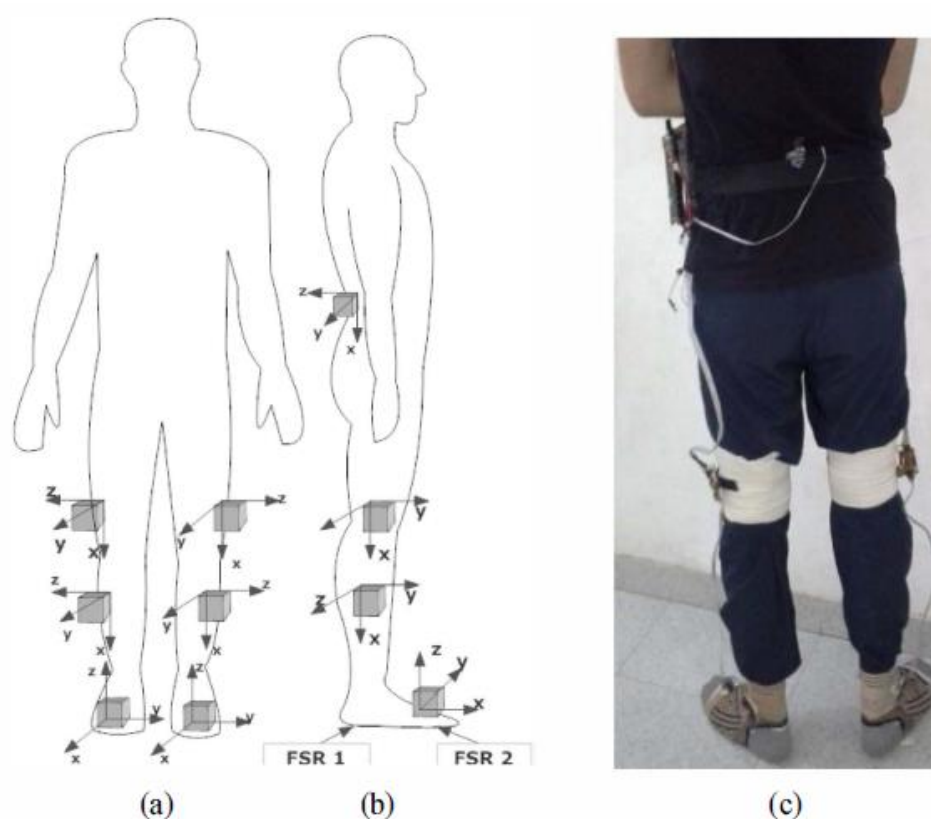


Figure 5.11 - Attachment location of the IMUs [51]. a) Elevation view. b) Side view. c) Real photo of the proposed capturing system.

Comparing to Fig. 5.6, the orientation of the sensing devices is different. Even the attachment location is not the same. In Figure 5.6 the sensing device is in the back of the leg, and in Fig. 5.11 the sensing device is in the exterior part of the leg. However, this will not influence the thigh's data.

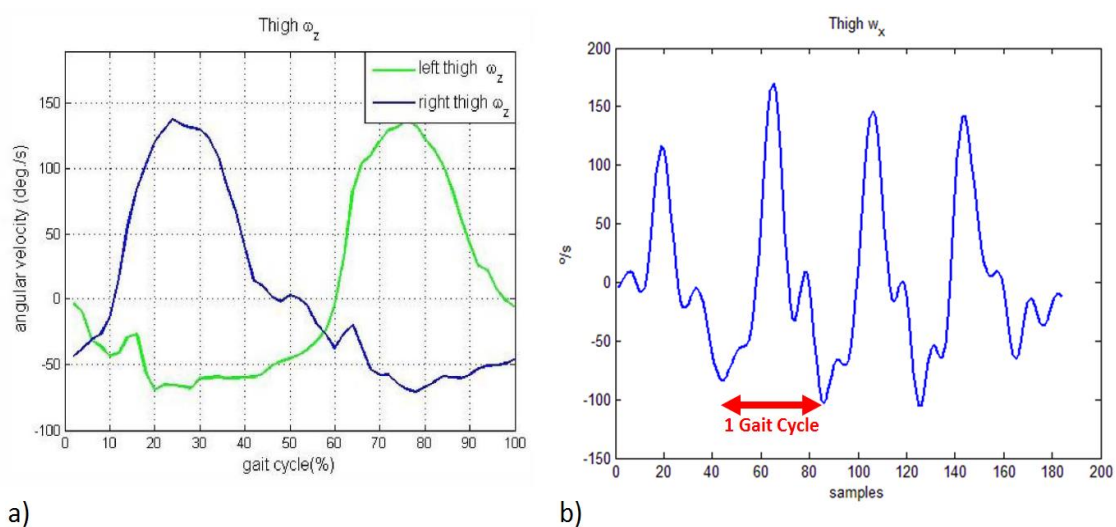


Figure 5.12 – Gyro data (mediolateral axis) when an IMU is attached in the right thigh. a) Hamdi's typical signal (blue signal) [51]. b) IMUs system (data filtered: Butterworth lowpass filter – $F_c=3\text{Hz}$).

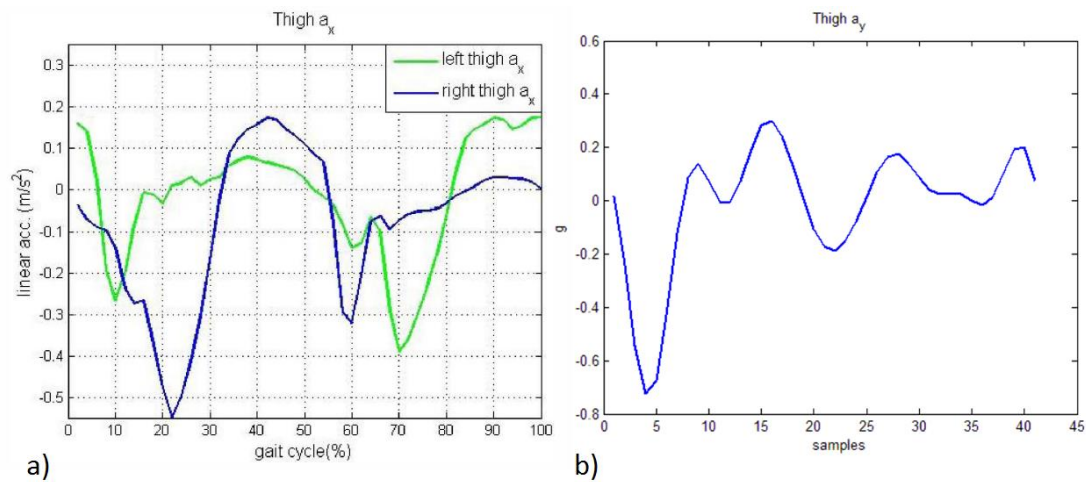


Figure 5.13 - Acc data (vertical axis) when an IMU is attached in the right thigh. a) Hamdi's typical signal (blue signal) [51]. b) One gait cycle measured by the IMUs based system (data filtered: Butterworth lowpass filter– $F_c=3Hz$).

Typical signals (Gyro and Acc) measured by Hamdi's IMU attached on the thigh are depicted in Figs. 5.12 and 5.13, as well as the signals obtained by the IMUs based system.

According to the signals present in [51] about human gait, there are similarities between those typical signals and the ones measured by our system (Figs. 5.12 and 5.13). In Fig. 5.12, it is possible to observe the occurrence of a peak in a gait cycle in both signals, which means the IMUs system is in agreement with the scientific literature.

Concerning the Acc's data (Fig. 5.13), it is possible to claim that there are similarities between signals, although the noise of the Acc affects slightly. In both signals, the gait cycle is described as initially having a negative peak, followed by a positive peak, a negative peak of smaller amplitude, and stabilizing again before the next gait cycle. Once again it is possible to claim validity of the IMUs system.

5.2.1.3. Lower Back

In [51] there is also information about the typical signal measured in the lower back using a Gyro. This typical signal is depicted in Fig. 5.14 (only one axis), as well as the signal measured by the IMUs system during walk forward trials in the same axis.

Once again there are similarities in the presented peaks. However there is no time period between the two peaks where the value of the sensor is around zero.

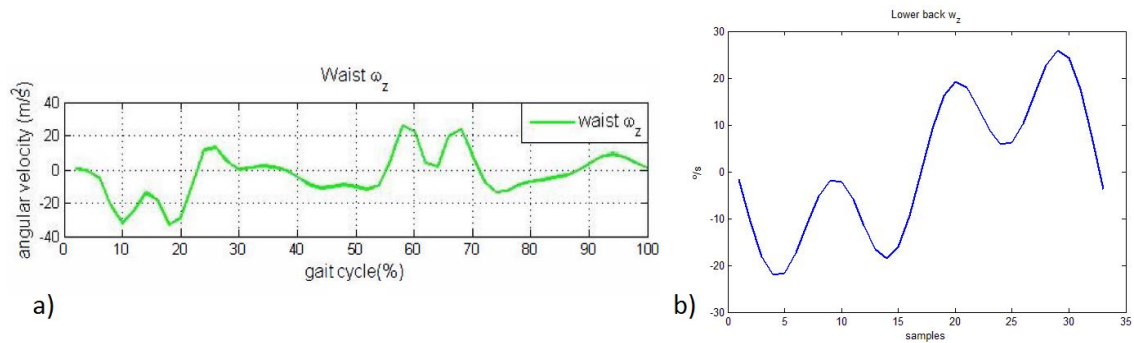


Figure 5.14 - Gyro data (vertical axis) when an IMU is attached in the lower back. a) Hamdi's typical signal [51]. b) One gait cycle measured by the IMU's system (data filtered: Butterworth lowpass filter – $F_c=3\text{Hz}$).

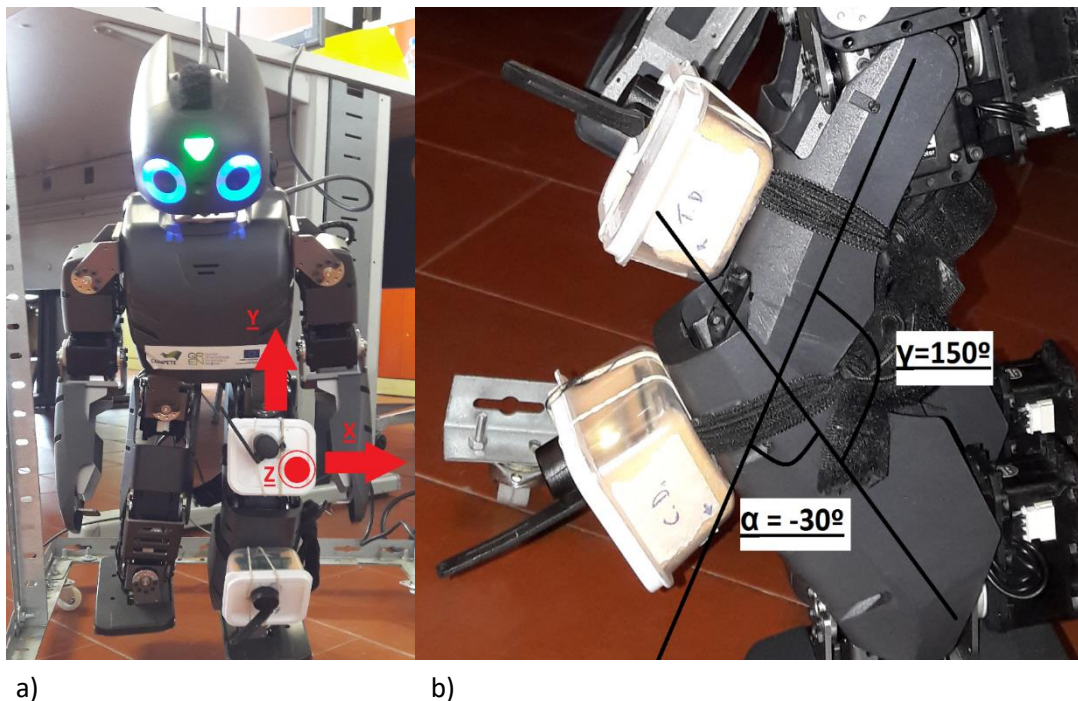
5.3. Validation of the estimation of joint angles

In general, sensing devices present some small errors compared to other more reliable systems. For example, Leardini et al. [53] validated their inertial-measurement-unit based rehabilitation system by using an 8-TV-camera stereophotogrammetric system (Vicon motion systems, UK) as ground truth system, and their root mean square error (RMSE) was less than 5° . Takeda et al. [68] presented a method for gait analysis using wearable sensors (Acc and Gyro), and they tested it in healthy subjects. As ground truth system they used a camera MCS, and their RMSE values were on average 6.79° for knee flexion-extension (F-E). Normal range of motion (ROM) at the knee is considered to be 0° of extension (stretched leg) to 135° of flexion [165]. Feldhege et al. [54] also validated their knee angle measurement sensor system with an electro-mechanical goniometer. The calculated F-E angle of the knee joint showed a RMSE lower than 5° .

In this section, knee joint angles were calculated from IMUs' data and they were compared with DARwIn OP (ground truth system) knee joint angles. Two sensing devices were attached to the DARwIn OP left shank and thigh to acquire data (Fig. 5.15). Initially, as first trial, the robot started a walking process after being programmed to do so. Each trial was repeated five times for ninety seconds at one gait cycle per 2.5 seconds. Later, the robot was programmed to keep the left leg stretched on a static position (knee joint angle= 0°) for thirty-five seconds. The previous procedure was performed again at an angle of -30° as depicted in Fig. 5.15. These tests were repeated five times each. Data from the two systems were acquired simultaneously by the same Personal Computer and both are synchronized.

5.3.1. Reference Measurement System - DARwIn OP

DARwIn OP (Fig. 5.15) was developed by RoMeLa at Virginia Tech [166] together with Robotics Co [167], and it is a humanoid-robot platform with sophisticated sensors, advance computational power, and dynamic motion ability that enable research, education, and outreach activities [168]. Users are encouraged to modify not only the hardware but also the software. On the one hand, the mechanical structure of DARwIn OP is divided into several sub-assemblies, namely: head; chest; arms; pelvis; and legs. It has 20 actuator modules with durable metallic gears, embedded sensors (3-axis Gyro and Acc, and a webcam), a hardware platform to control the robot, and a battery [167]. On the other hand, the robot is compatible with various programming languages, including C++, LabView® or Matlab®, which allows for better interaction. It is also considered a miniature humanoid robot since its height is 454.5 mm [167], and has 6 DOFs on each leg, 3 DOFs on each arm, and 2 DOFs on the neck. The robot also allows controlling the angle of the joints, as well as knowing the real value of the angles along the gait or any other process [168]. The real values of the joints angles recorded by the robot have a low offset with respect to the theoretical value programmed in the robot. The registration of the knee joint angles in each trial will serve as ground truth to validate the IMUs based system. The data were recorded with a sampling frequency of 62.5 Hz.



a) b)
Figure 5.15 - a) DARwIn robot with two sensory modules attached to left thigh and shank (for both modules, the positive Z axis is perpendicular to the housing cover, Y axis – up, X axis – to the left of the robot). b) DARwIn robot performs an angle of -30° with the left leg (sagittal plane). In this situation, knee angles from the robot are represented as α , and the knee angles from the model implemented are represented as γ .

5.3.2. Knee Joint Angle Measurement

Collected data were used to estimate roll, pitch, and yaw orientation for each attached sensory module by using a CF that works with normalized values from calibration procedure [13]. The orientation representation can be done by EAs. At this point a precise calibration is crucial, since it has a lot of influence in obtaining these estimates. Due to ferromagnetic influence from DARwIn OP structures, Mag was not considered in the orientation estimation. Thus, this estimation can suffer from the occurrence of drift, since the presence of this sensor would serve to correct the Gyro measures [61].

The next step is to estimate the angle of the DARwIn OP left knee joint. Continuing the previous step, it is essential to use roll, pitch, and yaw (radian) from each module to achieve the angle between two planes, which are XY planes in this particular case (sensory modules axes are represented in Fig. 5.15). In order to do so, the normal vectors ($T_{upper-robot\ thigh}$, and $T_{lower-robot\ shank}$) to each plane are rotated as follows by the following rotation matrix [169]:

$$R = R_x(roll)R_y(pitch)R_z(yaw) \quad (5.1)$$

Thus, from each initial normal vector ($[x\ y\ z]=[0\ 0\ 1]$) is obtained a new and rotated vector based on each roll, pitch, and yaw angles (in radians) estimated in the previous step. The initial vectors are rotated by the order of presentation of the rotation matrices in Eq. (5.1). Later, the calculation of the knee angles is performed by using these two rotated vectors

$$\gamma = \arcsin\left(\frac{\overrightarrow{T_{upper}} \cdot \overrightarrow{T_{lower}}}{\|\overrightarrow{T_{upper}}\| \|\overrightarrow{T_{lower}}\|}\right). \quad (5.2)$$

Where γ is the knee angle in radians. This value is then converted to degrees, and changed to the DARwIn OP reference (e.g., to α in Fig. 5.15). Finally, it is only necessary to perform a resampling process so data from the robot encoders and from this estimation can be compared by calculating the RMSE. Although knee F-E is the only movement evaluated, this method can calculate 3D joint angles.

5.3.3. Results

Concerning the first set of trials when the robot was walking, typical knee joint angles obtained with the encoder and the inertial-based system are displayed in Fig. 5.16. In this situation the RMSE value was $5.68^\circ \pm 0.34^\circ$. Typical results obtained for knee joint angles with both systems

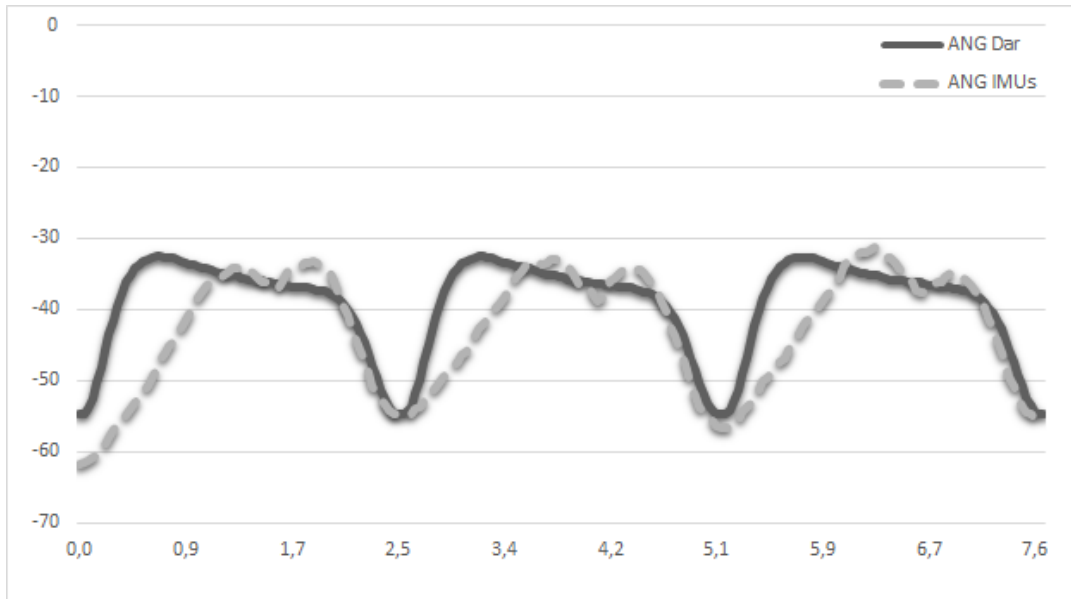


Figure 5.16 - Typical knee angles (°) during the trial where the DARwIn OP was walking (ANG Dar - robot real angles measured through encoders; ANG IMUs - calculated knee angles from sensory modules data; x-axis: time (s); y-axis: angles).

when the robot kept the left leg stretched are depicted in Fig. 5.17. The RMSE value was $4.29^{\circ} \pm 0.09^{\circ}$. When the robot performed a knee angle of -30° , the RMSE value was similar to the previous one with $4.30^{\circ} \pm 0.16^{\circ}$. Typical results from both systems in this last situation are represented in Fig. 5.18.

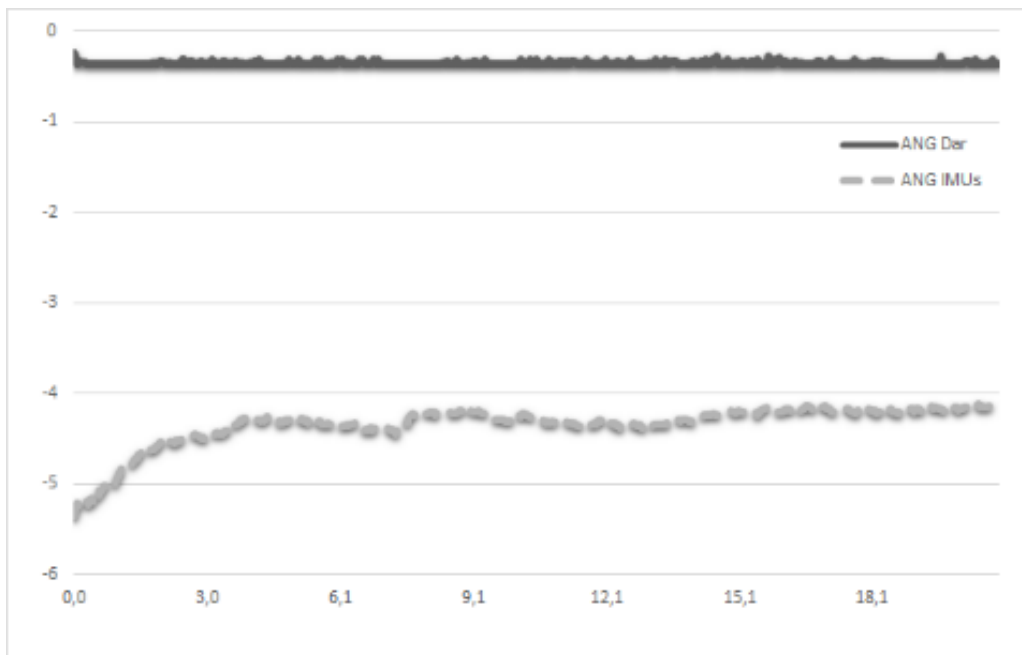


Figure 5.17 - Typical knee angles (°) during the trial where the DARwIn OP kept the leg stretched (ANG Dar - robot real angles measured through encoders; ANG IMUs - calculated knee angles from IMUs' data; x-axis: time (s); y-axis: angles).

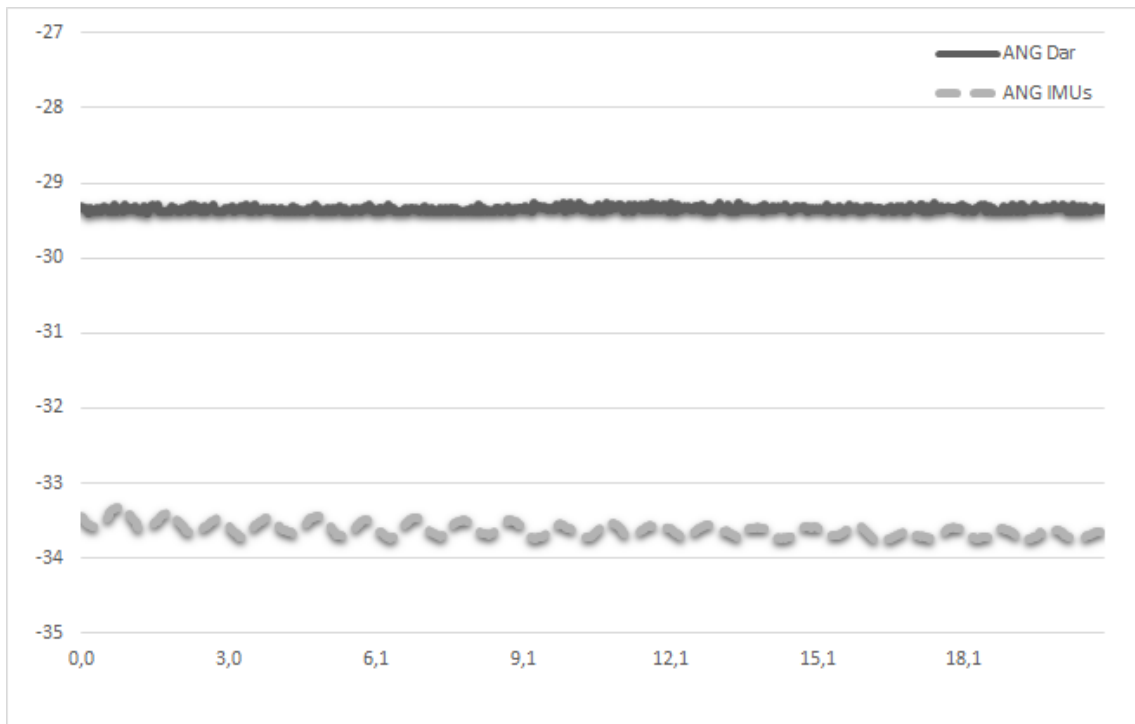


Figure 5.18 - Typical knee angles (°) during the trial where the DARwIn OP performed an angle of -30° (ANG Dar - robot real angles measured through encoders; ANG IMUs - calculated knee angles from IMUs' data; x-axis: time (s); y-axis: angles).

5.3.4. Discussion

Starting with the first trial, the RMSE value was $5.68^{\circ} \pm 0.34^{\circ}$, which is in accordance with the literature, despite being the highest value in the results. Analysing the graph of Fig. 5.16, it is possible to observe a slight delay in the ascent. This is essentially due to a rapid transition of the segments and the model cannot follow so quickly. However, it has a similar waveform.

In the other two situations, the result was lower than 5° , and the results are very similar to each other. Note that the real value of the angle of the robot knee joint is not exactly 0° and 30° in Figs. 5.17 and 5.18, respectively. There is an offset between the ideal value and the actual value measured by DARwIn OP. In summary, the results for knee F-E angles are in accordance with the literature. This error range is within the values found in the gait analysis literature when using IMUs.

Chapter 6 – IMUs based System Calibration

6.1. Calibration procedures - Introduction

Calibration procedures are present in a wide range of gait analysis systems. This procedures have a tremendous role in systems' reliability, dramatically reducing the existing error between what is measured and what really happened [170]. Thus, inertial/magnetic sensors also need to be calibrated to be used in gait analysis. Despite the fact that these sensors have advantages that attract their use in a home environment, in general, they present some small errors compared to other more reliable systems even when the calibration procedures are implemented [53], [54], [68]. For example, Leardini et al. [53] present a maximum mean error of 3.1 ± 1.8 degrees and 1.9 ± 0.8 degrees respectively in the medio-lateral malposition and frontal-plane misalignment tests. However, calibration stage is considered a critical point in the use of inertial/magnetic motion-sensing. So, it is important to distinguish several aspects, as depicted in Fig. 6.1, in the calibration process [170]:

1. **Sensor frame calibration procedure:** Pretends to compensate for gain variations, offsets and alignment errors between the mechanical sensor's axes for each sensor in the sensory module. Focus, essentially, on allowing the conversion of voltage measurements into physical units. It can be performed only once or can also be repeated when it is needed, for instance for magnetic sensor measurements since sensitivities and offsets (electronic calibration parameters) may vary with temperature. However, some parameters like Gyro's bias should always be measured before using the system or even more frequently.
2. **Mounting frame calibration procedure:** Uses the precise knowledge of the geometrical relations between the different sensor frames to improve the system's accuracy. This mechanical calibration, considering a practical viewpoint, has to find the RM between the housing case frame and the sensor frame.
3. **Anatomical frame calibration procedure:** Determines the relations between the mounting frame and the frame of the object/body segment on which the sensor is attached on. When the sensor is attached on the object/body segment, it can be misaligned with respect to the anatomical directions. In this case, this procedure estimates the RM

concerning the anatomical frame. Note that this procedure should be repeated for each application.

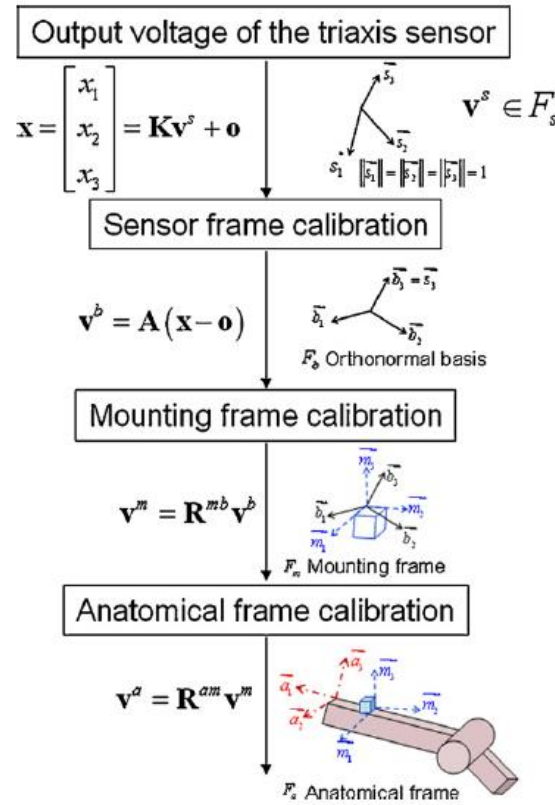


Figure 6.1 – Several steps of the calibration procedures from the raw measurements \mathbf{x} to measurements \mathbf{v}^a resolved in the anatomical frame [170].

Many calibration procedures of the sensors have been proposed in the literature [171]. However, in this section it will be presented the implementation of three in-field and one on-body calibration procedures related to the output data from the Analog-to-Digital-Converter (ADC) of the sensory modules. The on-body procedure is proposed in this thesis. The difference between in-field and on-body methods is the place where the calibration of the sensory modules is done. In-field methods are performed with the sensory module in a horizontal surface or with specific movements [172]. On the other hand, on-body methods are performed with the sensory module attached to the object/body's segment, although in some studies it requires specific movements of the subject before the start of the system's use [25]. Obviously, the ideal would be a fast method with the sensory modules already attached to the body's segments. Thus, the aim of this chapter is to implement the above mentioned four methods and compare them to assess their accuracy. The remainder of this chapter is organized as follows: in 6.2 the methods used in this experiment such as the process of the system, the calibration procedures, the experimental protocol, and the optical

reference are presented; in 6.3 the results are demonstrated; 6.4 presents the discussion and conclusion. The goal of this chapter is to determine the best calibration method and the one closest to the considered reference method or evaluation system.

6.2. Methods

6.2.1. Process of the orientation estimation of the IMUs based system

The all process is depicted in Fig. 6.2 as a block diagram. In a first moment (group 1 of the block diagram), the calibration procedures are performed, and as results the maximum and minimum values of each axis of the Acc and the Mag, and the Gyro's offsets were obtained. These values are the parameters used to normalize the sensors' raw data.

The group 3 represents the process to obtain the orientation angles with the data obtained from normal trials (group 2). In group 3, the data is normalized, and with the help of a CF, the angles are finally estimated.

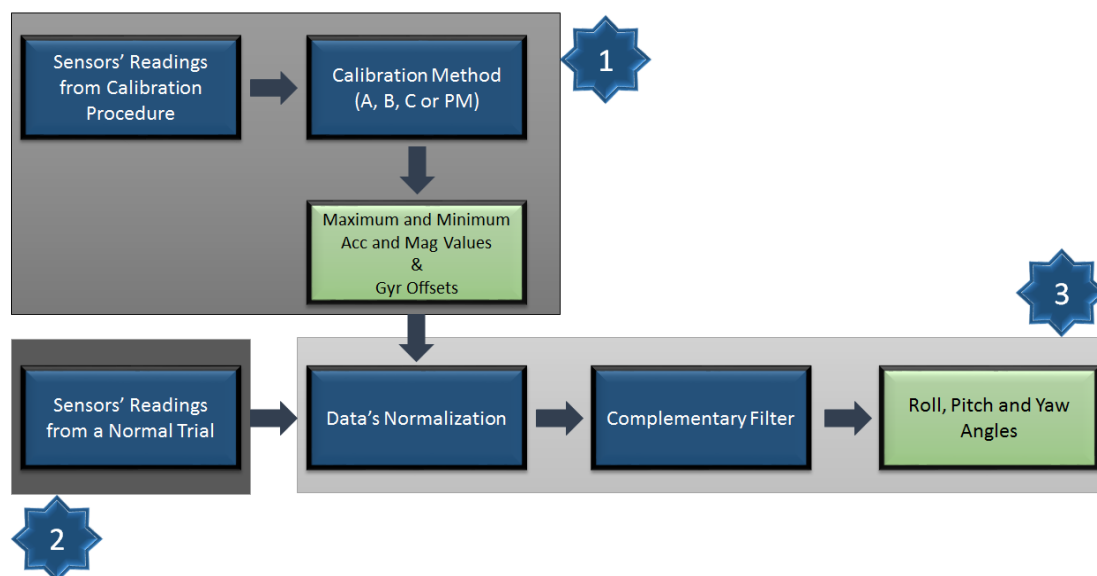


Figure 6.2 - Block diagram of the calibration process.

6.2.2. Calibration Procedures

Four calibration procedures were implemented before proceeding to using the sensory modules in order to obtain calibrated roll, pitch and yaw angles by using a CF. Concerning the goal of this chapter, four different techniques, namely, Methods A, B, and C, and the Proposed Method

(PM) will be compared. The three sensors presented in the sensory modules were calibrated with these methods.

6.2.2.1. Method A

The first in-field method consists in three types of movements (one for each type of sensor – Acc, Gyro, and Mag respectively): i) the sensory module is placed on a surface as horizontal as possible on its different faces as described in Fig. 6.3. At each position of the sensory module the gravity value from the Acc is stored, taking into account only the sensitive axis parallel to the gravitational force; ii) Gyro's offsets are obtained with the sensory module also placed in the position 1 (Fig. 6.3); iii) digital Mag axes (parallel and anti-parallel) are aligned with the north of the magnetic field and maximum and minimum values are obtained for each axis.

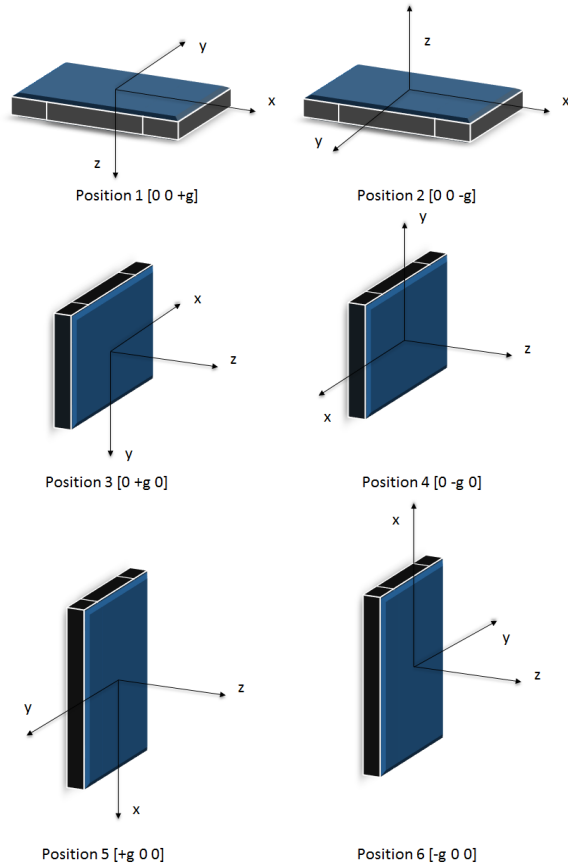


Figure 6.3 - Basic Principle of Method A: Extraction of Acc Maximum and Minimum values for each axis through 6 different positions.

6.2.2.2. Method B

The Method B is a standard in-field calibration method applied in the Acc's raw data [172]. Acc and digital Mag' maximum and minimum values, and Gyro's offsets are obtained as described in Method A. However, it consists this time in not neglecting the scale and misalignment factor by using a rotation matrix in the Acc's raw data. Computationally, this can be described as follows:

$$Y = w \cdot X \quad (6.1)$$

Or

$$[A_{x1} \quad A_{y1} \quad A_{z1}] = [A_x \quad A_y \quad A_z \quad 1] \cdot \begin{bmatrix} ACC_{11} & ACC_{21} & ACC_{31} \\ ACC_{21} & ACC_{22} & ACC_{32} \\ ACC_{31} & ACC_{32} & ACC_{33} \\ ACC_{10} & ACC_{20} & ACC_{30} \end{bmatrix} \quad (6.2)$$

Where

- Matrix X has the 12 calibration parameters that need to be determined. This matrix is used to rotate the Acc's raw data in further trials;
- Matrix w is Acc's raw data collected at 6 stationary positions (Fig. 6.3);
- Matrix Y is the known normalized earth gravity vector (eg. $Y_1 = [0 \ 0 \ 1]$ when IMU is at the Position 1 in Fig. 6.3).

In a first step, matrix w is obtained through data acquisition in the 6 stationary positions. For those positions matrix Y is known and it is possible to obtain matrix X through:

$$X = [w^T \cdot w] \cdot w^T \cdot Y \quad (6.3)$$

Then, during further trials, matrix X is used to obtain the real and calibrated values, which matrix Y represents.

6.2.2.3. Method C

The in-field Method C consists of slowly rotating the IMU on all directions, thus covering as many orientations as possible. Digital Mags can be calibrated through this method, since they suffer from local interferences of the magnetic field. This interferences are due to soft- and hard-iron effects [173]. However, Accs can also be calibrated using this method.

This method is based on least-mean squares to fit a regular geometric form between the points of the measurements. Ideally, on a 3D plot, this would be a centered sphere with the radius equivalent to the strength of the earth's magnetic field at the given location. However the present above mentioned effects will tilt, respectively shift the sphere. If there is no soft-iron distortion inside the device, or the soft-iron effect is very small and can be ignored, then the ellipsoid from 3D rotations is not tilted. Therefore, the least square fitting ellipsoid method can be used to discover the parameters of scale (M_SCi) and offsets (M_OSi), where $i = x, y, z$. Thus, applying these parameters to the collected 3D rotations data and three 2D full round rotations, the shifted tilted ellipsoid becomes a centered unit sphere. Offsets are subtracted to the data, and scale values are used to normalize data. Gyro's offsets are obtained as mentioned in Methods A and B.

Computationally, to calibrate the Acc and the Mag, this method can be translated as follows [172], where $a, b,$ and c are constants, and $x, y,$ and z are the measures of each axis of the sensor:

$$x^2 = [x \ y \ z \ -y^2 \ -z^2 \ 1] \cdot \begin{bmatrix} 2x_0 \\ \frac{a^2}{b^2} 2y_0 \\ \frac{a^2}{c^2} 2z_0 \\ \frac{a^2}{b^2} \\ \frac{a^2}{c^2} \\ \left[a^2 R^2 - x_0^2 - \frac{a^2}{b^2} y_0^2 - \frac{a^2}{c^2} z_0^2 \right] \end{bmatrix} \quad (6.4)$$

Or

$$w_{n \times 1} = [H]_{n \times 6} \cdot X_{6 \times 1} \quad (6.5)$$

The least square method can be applied to determine the parameters X vector as:

$$X = [H^T \cdot H] \cdot H^T \cdot w \quad (6.6)$$

Then Offset values are obtained for each axis:

$$M_{OS_x} = x_0 = X(1)/2 \quad (6.7)$$

$$M_{OS_y} = y_0 = X(2)/(2 \cdot X(4)) \quad (6.8)$$

$$M_{OS_z} = z_0 = X(3)/(2 \cdot X(5)) \quad (6.9)$$

And as well the Scale factors:

$$M_{SC_x} = \sqrt{A} = \sqrt{X(6) + x_0^2 + X(4) \cdot y_0^2 + X(5) \cdot z_0^2} \quad (6.10)$$

$$M_{SC_y} = \sqrt{B} = \sqrt{A/X(4)} \quad (6.11)$$

$$M_{SC_z} = \sqrt{C} = \sqrt{A/X(5)} \quad (6.12)$$

6.2.2.4. Proposed Method

The Proposed Method (PM) intends to be an on-body, fast, and with a low margin of error method. The concept of this method is based on obtaining the vector's norm of the acceleration and the magnetic field when the subject performs a stationary position before normal use. These values and their symmetric will be considered as the maximum and minimum values of the sensors in the subsequent normalization process. Eq. 6.13 demonstrates how to obtain the norm of a vector ($\|\vec{A}\|$). Gyro's offsets will also be determined on that stationary position, similarly to the above mentioned methods (A, B, and C). This calibration method was performed in a horizontal surface as in position 1 of Fig. 6.3. However, its purpose is to be made in a body's segment or joint when the subject performs a static position.

$$\|\vec{A}\| = \sqrt{A_x^2 + A_y^2 + A_z^2} \quad (6.13)$$

6.2.3. Tracker Software

Nowadays, optical softwares are considered precise and reliable reference systems among the others gait analysis systems. In fact, they are used as a ground truth in several studies to validate the gait parameters measured with sensing devices. For example, [26], [28], [51], [57], [59], [60], [72], [74], [77] used a Vicon/MoCap system to compare information related to gait from sensing devices; [37], [61], [67], [81] had Optotrack as reference system; Oqus Qualysis was the evaluation system of [62], [66]; [49], [68] used a DIPP Motion Pro system; Micron Tracker H40 was used in [49], [53]; and six other studies used a Selspot II in [65], a video system in [58], a BTS Bioengineering optoelectronic system in [52], a Bonita B10 in [73], a Lotus 3D MA-3000 in [63], and a Motion Analysis OWL Digital Real Time system in [64].

Although there are many optical systems available on the market, the all equipment and the software are too expensive. Thus, Tracker software [174] is an alternative, free, and modelling tool capable of video analysis built on Open Source Physics (OSP). In a brief explanation about the software, the user only needs a regular camera, and then he has to define the size of the calibration stick (calibration process in the video), define the position of the coordinate system, define the object's centre of mass, and select the video's time interval of interest. With this procedure, the user can obtain relevant information from an object's trajectory like distance, velocity, rotation angle, among other parameters. Further, this software will be used as a ground truth system. The sampling frequency used was 30Hz.

6.2.4. Experimental Protocol

The aim of this stage is to assess all methods and find the method that gives closest results to reality. The experimental protocol has four stages. 1) The calibration procedure takes 20 seconds for methods A, B and PM. Method C lasts 150 seconds. In this stage, raw data are stored, and information for normalization phase is obtained, namely, the maximum and minimum values of the axes of the Acc and the Mag, and the Gyro's offsets. This last information will be compared according to the implemented methods, and the errors between method A and the other methods will be calculated for the Acc and the Mag. Since Gyro's offsets were obtained similarly in the four methods, in this stage the difference of the offsets values between on-body positions and "on

horizontal surface” position will be determined instead. On-body positions are represented in Fig. 6.4. 2) Then, two trials are performed: i) IMU is at a stationary position different from those depicted in Fig. 6.3; and ii) a subject walked 4 meters front, turned around, and returned to the starting position with the IMU on the thigh as depicted in Fig. 6.4. Both trials are made for each sensory module of the system. In this stage, normalized data and obtained angles are compared according to the different methods by RMSE. In this experiment, Method A is considered the ground truth method, since this method is strongly used in the literature and normally accepted as the more reliable [173]. 3) A modified version of the PM will be performed in order to overcome some problems that PM method presented. So, in this stage, all methods and the modified PM will be compared with an optical reference system. This optical reference will determine rotation angles of the sensing device (roll, pitch and yaw), and the respective data will be used as ground truth. 4) Finally, Mahony [175] and Madgwick [176] filters used to obtain roll, pitch and yaw angles, were tested and compared with the results of the implemented CF. A simple trial was performed by rotating the sensing device 90° around z-axis to one side and return to the starting position. The yaw angles obtained from each filter were compared by RMSE.

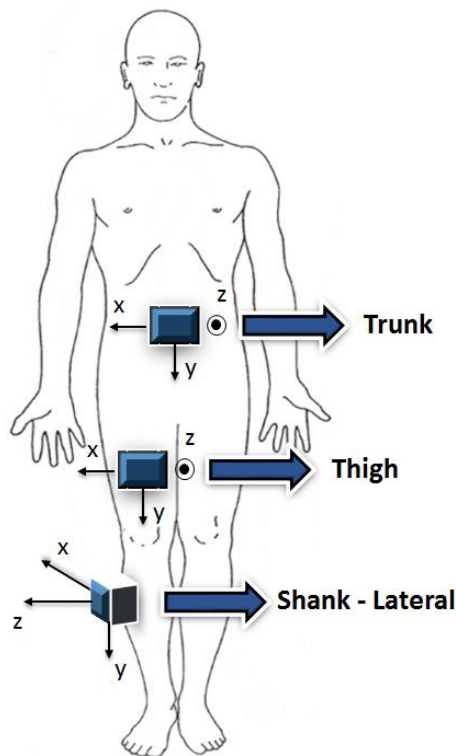


Figure 6.4 - Sensors' attachment location to measure Gyro's offsets.

6.3. Results

6.3.1. Stage 1

At the stage 1 of the experimental protocol, normalization parameters from each calibration method were obtained, and they will be compared in this sub-section. As mentioned before, all results were compared to the results of the method A because this method is considered the calibration's ground truth method. The first step was to determine the difference between maximum and minimum values of methods B, C and PM with the maximum and minimum values of the method A. This difference is called as error and the percentage of this error in the 4g scale, in the case of the Acc, and 0.88 Gauss, in the case of the Mag, was further determined for each module. The mean error percentage is available at Table 6.1 in the case of the Acc, and Table 6.2 in the case of the Mag.

Table 6.1 - Error Percentage of the Maximum and Minimum values when compared to the homologous values of the Method A – Acc case

Methods	MAX X (%)	MAX Y (%)	MAX Z (%)	MIN X (%)	MIN Y (%)	MIN Z (%)
B	0.344±0.357	0.362±0.113	2.618±2.071	0.353±0.460	0.316±0.235	2.123±1.685
C	2.688±2.025	1.052±0.397	1.762±1.285	2.132±2.298	1.370±0.611	3.087±2.440
PM	2.633±1.879	2.426±1.961	0.006±0.003	2.816±1.775	2.761±2.100	4.735±3.666

From Table 6.1, it is possible to observe that the lowest error percentage (0.006%±0.003%) occurs in the maximum value of z-axis when method PM was used. However, the biggest value (4.735%±3.666%) occurred in the same axis with the same method, although in other direction. In general, Method B is more close to the method A.

Table 6.2 - Error Percentage of the Maximum and Minimum values when compared to the homologous values of the Method A – Mag case

Methods	MAX X (%)	MAX Y (%)	MAX Z (%)	MIN X (%)	MIN Y (%)	MIN Z (%)
B	0.000±0.000	0.000±0.000	0.000±0.000	0.000±0.000	0.000±0.000	0.000±0.000
C	1.595±1.282	7.050±2.647	4.894±4.170	2.263±1.252	8.487±3.445	5.184±3.489
PM	5.275±6.366	7.706±5.067	8.230±8.185	3.966±3.265	10.796±4.387	5.499±3.394

Table 6.2 demonstrates that method B is equal to method A, since they use the same procedure to calibrate the Mag. However, when methods C and PM are compared to method A the difference is huge. Methods C and PM are very close to each other.

Gyro's offsets are also a concern in the calibration procedure. All methods use the same procedure to determine the Gyro's offsets, and there is no difference between them. Thus, each sensory module was attached to three different body segments (thigh, shank, and trunk), and the subject was static for 20 seconds. Finally, the offsets measured in these three positions were compared to the offsets obtained when each sensory module was at Position 1. The error percentage in the $1000^\circ/s$ scale was calculated and the mean is presented in Table 6.3.

Table 6.3 - Error Percentage of the Gyro's Offsets in three body segments when compared to the homologous values when IMU was at Position 1

Position	X (%)	Y (%)	Z (%)
Thigh	0.007±0.004	0.011±0.002	0.009±0.005
Shank-lateral	0.009±0.008	0.014±0.009	0.010±0.007
Trunk	0.020±0.009	0.013±0.009	0.009±0.004

As can be seen from Table 6.3, the influence of the human movement at a static position is very small. The highest error percentage was in the trunk ($0.020\% \pm 0.009\%$) in the x-axis.

6.3.2. Stage 2

In this second stage, the RMSEs between all methods for normalized data and angles were calculated. The RMSEs between methods for the normalized data were only obtained for the Acc and the Mag, because all methods used the same procedure to obtain Gyro's offsets. In this particular case, the RMSEs between methods were obtained for each axis of each sensory module. The RMSEs between methods for roll, pitch and yaw angles were also obtained for each sensory module. Finally, further results are the calculated mean of the RMSEs previously mentioned.

6.3.2.1. Stationary position

Concerning the situation when the sensory module was at a stationary position, the RMSEs between methods for the normalized data are available at Tables 6.4 to 6.9. In turn, the information of the obtained RMSEs between methods for the angles is presented in Tables 6.10 to 6.12.

Table 6.4 - Mean of the RMSEs between methods for normalized data – Acc x-axis

	A	B	C
A			
B	0.0119±0.0116		
C	0.0170±0.0205	0.0255±0.0184	
PM	0.0116±0.0149	0.0120±0.0073	0.0250±0.0199

Table 6.5 - Mean of the RMSEs between methods for normalized data – Acc y-axis

	A	B	C
A			
B	0.0190±0.0141		
C	0.0200±0.0148	0.0361±0.0087	
PM	0.0163±0.0124	0.0333±0.0090	0.0039±0.0028

Table 6.6 - Mean of the RMSEs between methods for normalized data – Acc z-axis

	A	B	C
A			
B	0.0023±0.0011		
C	0.0150±0.0123	0.0143±0.0145	
PM	0.0039±0.0036	0.0030±0.0037	0.0157±0.0137

As mentioned before, the normalized data has values between -1 and 1. So, the mean of the RMSEs can tell a percentage directly. In the case of the Acc, all methods are very close to each other with errors never exceeding 0.04. In this particular case, method C is the most distant method of all. On the other hand, in general, PM is the closest method to the method A.

Table 6.7 - Mean of the RMSEs between methods for normalized data – Mag x-axis

	A	B	C
A			
B	0±0		
C	0.0115±0.0072	0.0115±0.0072	
PM	0.0792±0.0613	0.0792±0.0613	0.0718±0.0649

Table 6.8 - Mean of the RMSEs between methods for normalized data – Mag y-axis

	A	B	C
A			
B	0±0		
C	0.0359±0.0287	0.0359±0.0287	
PM	0.2408±0.1481	0.2408±0.1481	0.2115±0.1191

Table 6.9 - Mean of the RMSEs between methods for normalized data – Mag z-axis

	A	B	C
A			
B	0±0		
C	0.0152±0.0204	0.0152±0.0204	
PM	0.1344±0.1203	0.1344±0.1203	0.1414±0.1427

Concerning the Mag normalized data, the PM is the method that presents the highest values. Method B is equal to the method A because used the same calibration procedure. In turn, method C is close to methods A and B.

Table 6.10 - Mean of the RMSEs between methods for orientation angles – Roll (SI: degrees)

	A	B	C
A			
B	1.0686±0.7963		
C	0.7500±0.5836	1.7089±0.7013	
PM	0.8170±0.5048	1.7617±0.7195	0.1230±0.0962

Table 6.11 - Mean of the RMSEs between methods for orientation angles – Pitch (SI: degrees)

	A	B	C
A			
B	0.6802±0.6701		
C	1.0310±1.2030	1.5184±1.0731	
PM	0.7019±0.8113	0.6992±0.4083	1.4850±1.1599

Table 6.12 - Mean of the RMSEs between methods for orientation angles – Yaw (SI: degrees)

	A	B	C
A			
B	2.3359±1.7141		
C	6.7515±6.6974	7.5287±9.4404	
PM	20.6554±9.3094	21.6129±11.4436	14.2054±6.6301

The results of the means of the RMSEs between methods for orientation angles reveal that methods B, C and PM have mean RMSE values less than 1.1° when compared to method A in roll and pitch angles. In fact these three methods are close to each other with values never exceeding 1.8°. However, for yaw angles in Table 6.12 the results get worse, and PM is the method with the highest values of RMSE. In this situation, only method B has the closest value to method A.

6.3.2.2. Walking trial

In a similar way to the previous section, the RMSEs between methods for the normalized were obtained for each sensory module and the mean of RMSEs is presented in Tables 6.13 to 6.18. The mean of the RMSEs between methods for the orientation angles is shown in Tables 6.19 to 6.21.

Table 6.13 - Mean of the RMSEs between methods for normalized data – Acc x-axis

	A	B	C
A			
B	0.0069±0.0030		
C	0.0244±0.0273	0.0243±0.0239	
PM	0.0599±0.0873	0.0246±0.0102	0.0417±0.0274

Table 6.14 - Mean of the RMSEs between methods for normalized data – Acc y-axis

	A	B	C
A			
B	0.0061±0.0037		
C	0.0484±0.0237	0.0489±0.0213	
PM	0.0833±0.0651	0.0836±0.0637	0.0445±0.0346

Table 6.15 - Mean of the RMSEs between methods for normalized data – Acc z-axis

	A	B	C
A			
B	0.0102±0.0062		
C	0.0232±0.0151	0.0260±0.0163	
PM	0.0849±0.0629	0.0844±0.0646	0.0700±0.0460

Contrary to the case of the stationary position, the PM was the method with the highest mean RMSE values. Method B remains the closest method to the method A on any axis.

Table 6.16 - Mean of the RMSEs between methods for normalized data – Mag x-axis

	A	B	C
A			
B	0±0		
C	0.0424±0.0611	0.0424±0.0611	
PM	0.0872±0.0667	0.0872±0.0667	0.0794±0.0727

Table 6.17 - Mean of the RMSEs between methods for normalized data – Mag y-axis

	A	B	C
A			
B	0±0		
C	0.0422±0.0336	0.0422±0.0336	
PM	0.2687±0.1366	0.2687±0.1366	0.2410±0.0949

Table 6.18 - Mean of the RMSEs between methods for normalized data – Mag z-axis

	A	B	C
A			
B	0±0		
C	0.0167±0.0101	0.0167±0.0101	
PM	0.1549±0.0976	0.1549±0.0976	0.1575±0.1165

Concerning the Mag’s normalized data, the PM is the method that presents the highest values again. Method C is close to methods A and B. However with values never lower than 0.0167.

Table 6.19 - Mean of the RMSEs between methods for orientation angles – Roll (SI: degrees)

	A	B	C
A			
B	0.4311±0.3388		
C	1.0742±0.5004	1.2228±0.8381	
PM	4.7248±3.3217	4.8330±3.4568	4.0545±2.6675

Table 6.20 - Mean of the RMSEs between methods for orientation angles – Pitch (SI: degrees)

	A	B	C
A			
B	0.3230±0.1096		
C	1.1558±1.2525	1.0958±1.0200	
PM	3.8709±3.5233	3.9537±3.3964	4.4018±3.2594

Table 6.21 - Mean of the RMSEs between methods for orientation angles – Yaw (SI: degrees)

	A	B	C
A			
B	0.5433±0.3999		
C	7.7405±7.5122	7.9362±7.4291	
PM	21.0741±14.4848	21.1964±14.3796	22.9910±12.8997

Once again, as well as in the case of the normalized data, PM mean RMSE values increased when compared to the case of the stationary position. In this case, in roll and pitch angles, the mean RMSE values are never lower than 3.8° when compared to methods A, B, and C. In Table 6.21, PM mean RMSE values are tremendously different when compared to other methods. Figure 6.5 depicts the typical graphs of the roll, pitch, and yaw angles obtained from different calibration methods.

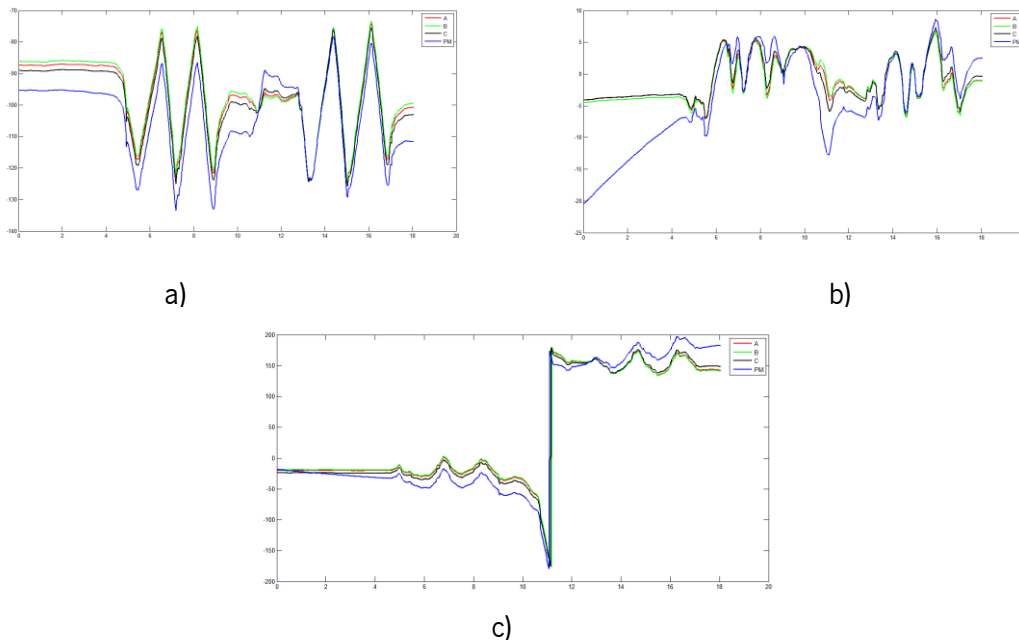


Figure 6.5 - Walking trial angles of the thigh: a) roll; b) pitch; and c) yaw.

6.3.3. Stage 3

In the third stage, the sensing device number 6, which was the one that had the best results in the last 2 stages, was attached to a cylindrical stick as depicted in Fig. 6.6. As procedure, the stick was rotated 90° degrees to the right, and then it was rotated 180° to the left. At the same time, data from the sensing device was collected, and a smartphone's camera recorded the movements from a viewpoint where was possible to record the rotation. The axis to rotate must be as perpendicular as possible to the plane of the camera. Through Tracker software, the roll, pitch and yaw rotation angles were obtained positioning the sensory module attached to the stick. So, performing the same rotation moves with the stick, it was possible to obtain each rotation angle in three different moments. Finally, due to Mag's high error calibration values obtained through the PM and described in the last two stages, a new modified version of the PM emerged (PM2), and will be presented in these results. The difference between this new method and the original PM is

that PM2 uses the Mag's calibration values from method A. Further, RMSEs between all calibration methods and the optical data were obtained, and Table 6.22 contains these results. Figure 6.7 depicts the typical evolution of the angles in the described rotation trial for roll, pitch and yaw.

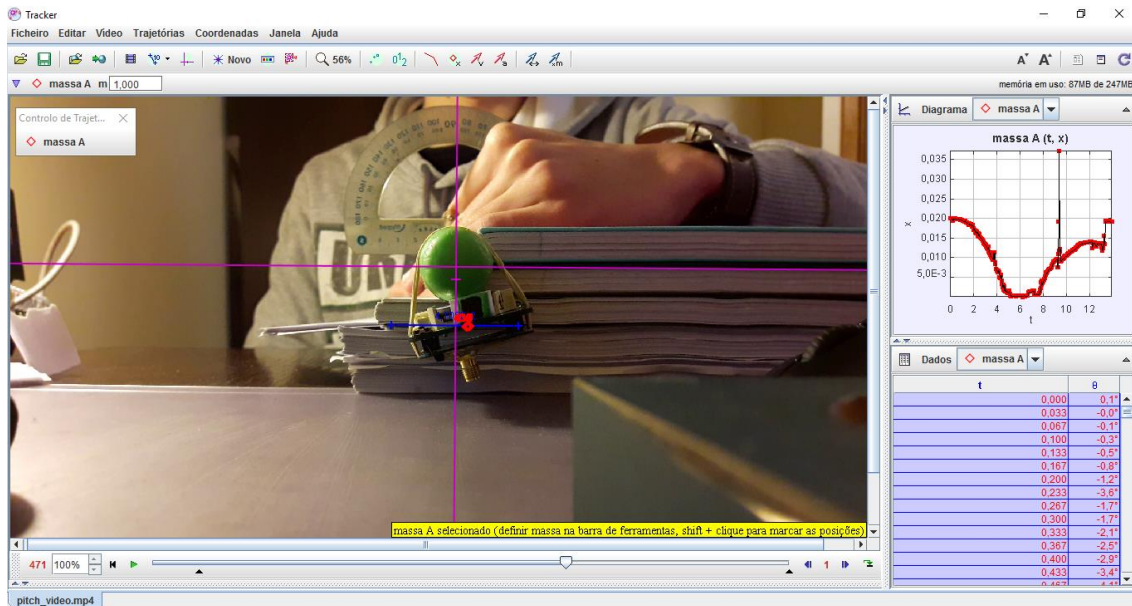


Figure 6.6 - Tracker software environment working with a rotation trial.

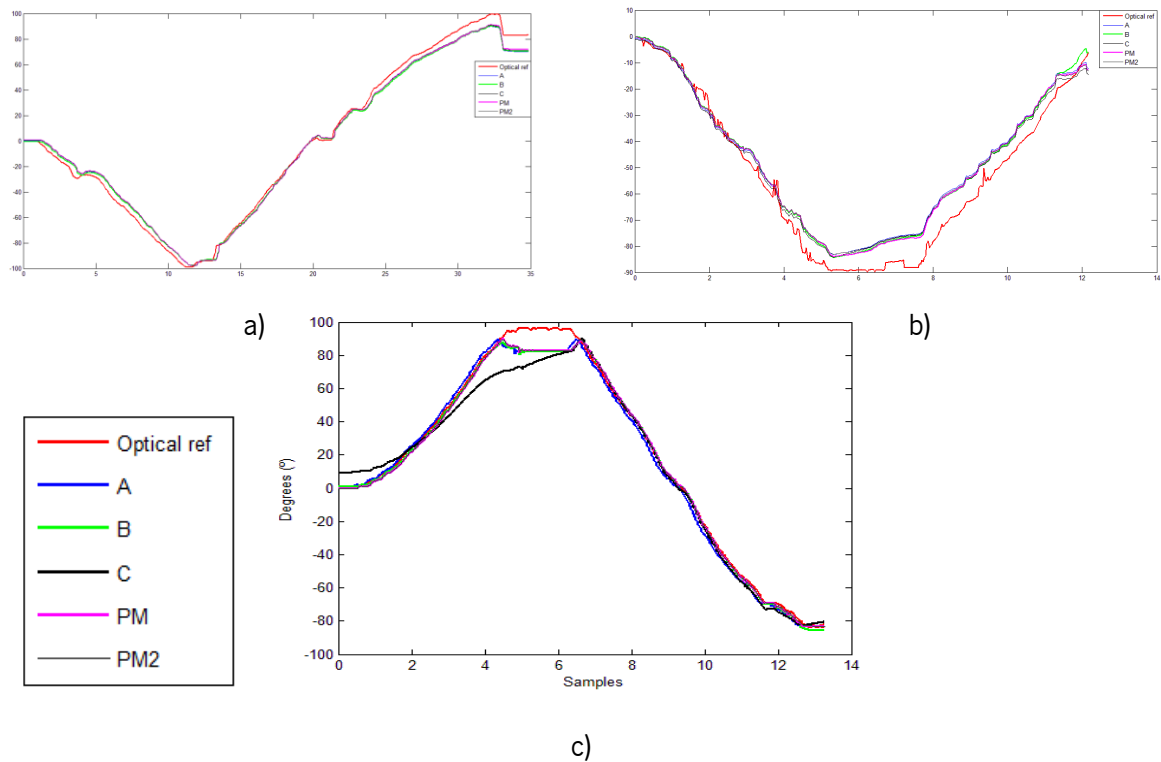


Figure 6.7 - Rotation angles of stage 3 experiment: a) Roll; b) Pitch; and c) Yaw.

Table 6.22 - RMSEs between calibration methods and the optical reference

Methods	Roll	Pitch	Yaw	Mean \pm STD
A	5.4652°	7.2370°	5.4990°	6.0671° \pm 1.0133°
B	5.3585°	6.6144°	5.0903°	5.6877° \pm 0.8136°
C	5.3144°	6.5354°	9.1881°	7.0126° \pm 1.9805°
PM	5.2083°	6.6624°	4.9055°	5.5921° \pm 0.9392°
PM2	5.2223°	7.0489°	4.8837°	5.7183° \pm 1.1647°

Considering Table 6.22, it is possible to retain that PM is, in general, the closest method to the optical reference. PM2 was also good, but PM was better. Method B also demonstrates better results when compared to methods A and C. Method C is clearly the method with worst results. RMSEs of the Roll, Pitch, and Yaw angles are considered as normal.

6.3.4. Stage 4

Different sensor fusion algorithms were applied to the normalized data in order to obtain rotation angles of the sensing device. Specifically, two filters were implemented: Madgwick which was applied with and without Mag, and the filter made by Mahony that was also applied with and without Mag. From the same trial, yaw angles were obtained and the RMSEs between the signals were calculated. This information is available in the Table 6.23. Figure 6.8 depicts the different results of the described trial.

Table 6.23 - RMSEs between different sensor fusion algorithms and the optical reference

	CF	Madgwick	Mahony	Madgwick w/o Mag	Mahony w/o Mag	Opt. Ref.
CF						5.499°
Madgwick	7.5103°					9.8444°
Mahony	7.9017°	13.1867°				3.9757°
Madgwick w/o Mag	8.5871°	1.6302°	14.4491°			11.044°
Mahony w/o Mag	6.8666°	12.0118°	1.6737°	13.2116°		2.849°

Through Table 6.23, it is possible to observe a clear approximation between the results of the Madgwick/Mahony filter with or without Mag. The difference in angles between each filter, using or not using Mag is less than 2°. Madgwick and Mahony results are very different when compared to the optical reference. The RMSE value of the Madgwick is higher than 9° with and

without Mag. When the Mag is not used in the Mahony filters, the result is closer to the CF with a RMSE of 6.8666° . The Mahony filter with or without using Mag reveals great results as can be seen in the Fig. 6.8. The RMSE of this filter when compared to the optical reference is less than 4° .

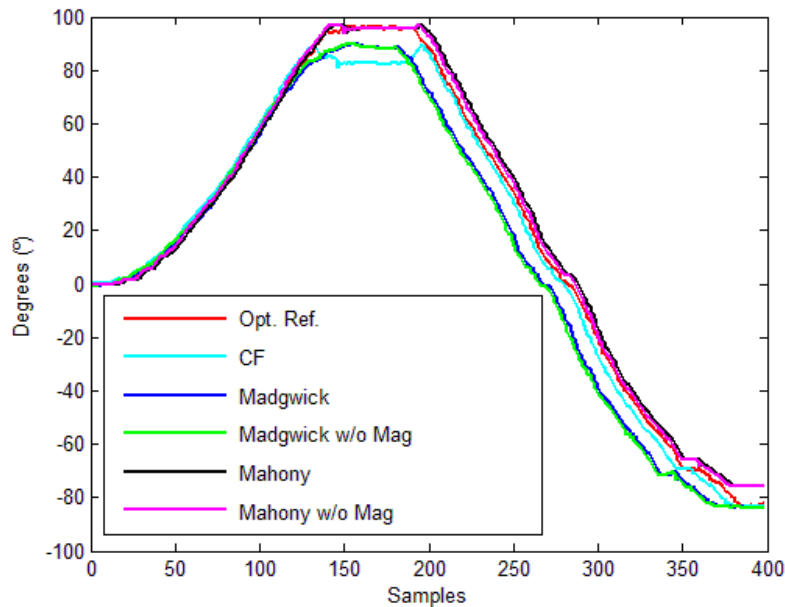


Figure 6.8 - Yaw angles obtained through a CF, Madgwick filter (w/ and w/o Mag), and Mahony filter (w/ and w/o Mag).

6.4. Discussion

With regard to phase 1, considering the Acc case, it is possible to retain that PM is the closest method to method A in the z-axis maximum value. This happens because the PM calibration procedure was performed at the position 1 of the Fig. 6.3. Theoretically, the sensor raw data for any axis should be 8192 for positive axis, and -8192 for negative axis in the positions described in Fig. 6.3. However, that is not what happens in real sensors, and those differences caused this errors in PM. Calibrating this way, the axes close to acceleration vector will be close to the real value, however in the opposite direction, the maximum/minimum values will not be as close as intended. In the case of the Mag these differences are higher and that is the reason why the error percentages are higher.

Gyro's offsets measured on-body were very close to those measured in a horizontal surface. That shows this gyro's static calibration can be done on-body. The highest value recorded occurred when the sensory module was at the trunk, mainly due to the natural breathing that causes movements in the abdomen.

In stage 2, considering the stationary position trial, the PM reveals closest results to method A, as well as the other methods. This happens, essentially, because the static position is similar to the calibration static position. When the subject performed the trials with the previous normalization parameters, the error increased in the normalized data and, consequently, in the orientation angles, which is expected. However, the waveform is very similar.

In the stage 3, in general, PM revealed that was the best method in the experiment, however the rest of the methods were also close. RMSEs of the Roll, Pitch, and Yaw angles were in accordance to the literature.

The procedure of stage 4 revealed, as expected, that Mahony and Madgwick filters can also be used as sensor fusion algorithms to obtain orientation angles. However, results obtained from the Mahony filter were closest to the optical reference with a RMSE less than 4° , which is a very interesting and good result.

Chapter 7 – Pre-Fall Detection System

The main goal of this thesis was to be able to estimate a fall. In order to achieve this prediction, and according to the literature, a F and PF states were considered relevant to be detected. In this chapter, an offline F and PF detection system will be implemented and tested by using data from sensing devices attached to body segments. This chapter will be divided in four major parts: i) implementation of all process, which includes collecting data from sensing devices through trials in health young people, calculation of metrics, selection of the most relevant metrics through PCA, construction of ASMs, and their test; ii) Construction of a decision cascade based on built ASMs. This second stage intends to distinguish and classify automatically normal gait and F and PF's situations (locomotion modes). iii) Use of a CNN also to classify different types of locomotion modes. In addition to classifying the different types of locomotion modes, the results of this stage will be used to compare ASMs and neural networks. And iv) Validation of both approaches proposed by comparing between the implemented classifiers in indoor trial.

7.1. Stage 1

Firstly, it is certainly of interest to understand the function of the first stage. As described in the Figure 7.1, sensors' raw data were collected from trials, and these data from five sensing devices were synchronized in time, interpolated in case of loss of frames, and normalized through a calibration process (Method A – Chapter 6). Subsequently, each normalized gait cycle was extracted from the data through a step detector algorithm present in [163], which uses a sensing device on the upper foot and it is capable of determining the stance and swing phases. This normalized version of sensor data is phase-indexed, which eliminates issues with the rhythmicity of locomotion. For each gait cycle, the above mentioned metrics were calculated (See Chapter 3). Gait metrics are truly important to characterize human locomotion. However, due to their quantity, a preliminary study based on PCA analysis will be important to determine which features are

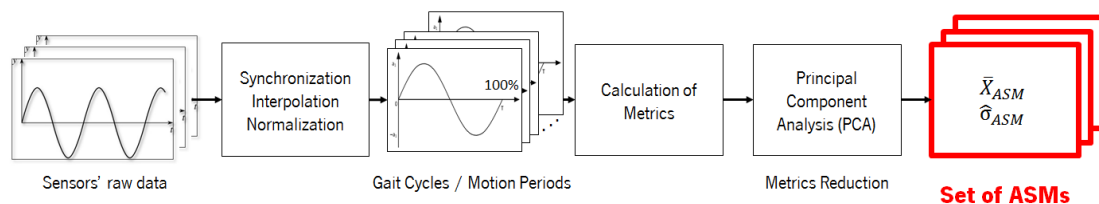


Figure 7.1 - Block diagram of the first stage.

relevant to characterize the human gait and to be used on the ASMs. Finally, ASMs will be constructed to be used in the next stage. To do so, 75% of collected data were used as train data, and the rest were used as test data. Best parameters of the ASMs were obtained through a receiver operating characteristic (ROC) analysis.

7.1.1. Trials

A total of 12 subjects (3 Females and 9 Males; 25.33 ± 6.33 years old; 66.92 ± 10.07 kg; 1.74 ± 0.11 m) performed three different trials, namely: i) Walk forward (WF) (Fig. 7.2); ii) walk in circle (both sides – right and left (CR and CL)) (Fig. 7.3); iii) walk forward bypassing an obstacle (both sides – OR and OL) (Fig. 7.4). All trials were performed at a gymnasium, and they were repeated three times without a simulated F and other three times with a simulated F, which is a F ordered by the responsible of the trials and does not occur in normal daily life situations. An amount of five sensing devices were used attached to the lower back, to both back thighs, and to both feet. Figure 7.5 depicts the attachment location of the sensing devices.

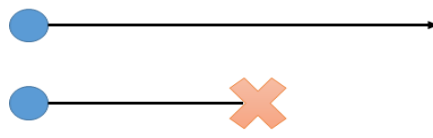


Figure 7.2 – Trial i) in the gymnasium – Subject (blue point) walks forward (Top – w/o F; Down – w/ F where the F's location is represented by the red X).

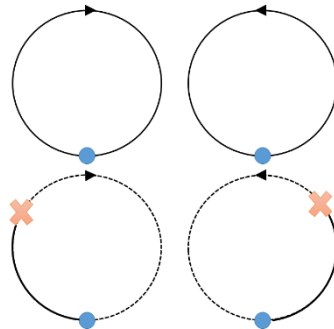


Figure 7.3 – Trial ii) in the gymnasium – Subject (blue point) walks in circles (Top – w/o F – right and left; Down – w/ F where the F's location is represented by the red X).

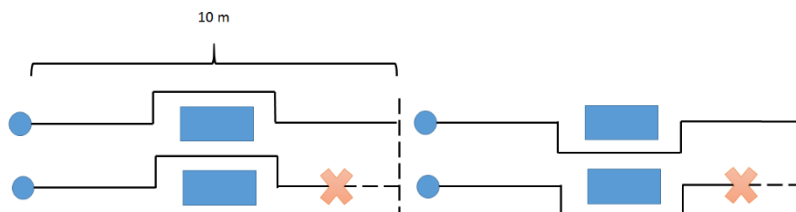


Figure 7.4 – Trial iii) in the gymnasium – Subject (blue point) walks 10m forward bypassing an obstacle (Top – w/o F – right and left; Down – w/ F where the F's location is represented by the red X).

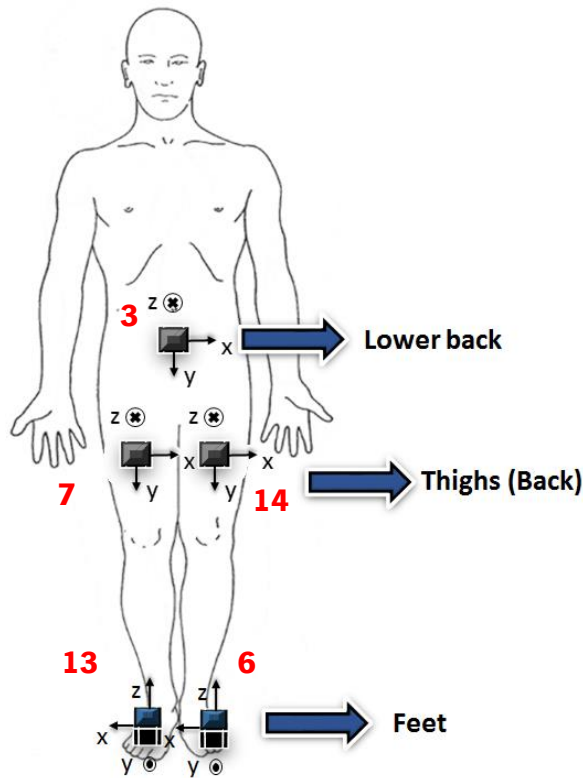


Figure 7.5 - Sensing devices attachment location used for the trials (Dark sensing devices are in the back of the body; Red numbers represent the physical addresses of the sensing devices).

7.1.2. PCA

The PCA is able to reduce the dimensionality of a data set consisting of a large number of interrelated variables [177]. Thus, PCA is a data analysis tool to identify patterns in a data set, and express their similarities and differences. Once these patterns have been found, the data can be reduced by obtaining a smaller set of points. Thus, given a set of correlated points, the PCA uses orthogonal transformations to transform them into fewer uncorrelated points (major components or principal components - PCs), and which are ordered so that the first few retain most of the variation present in all of the original variables [177]. These points are calculated in order to minimize the loss of information that the initial points contain. Each main component must have greater variance than the next element, and the first point must present the greatest variability. Within the scope of the applications of this method, the points with greater variation are chosen [178],[179].

In this thesis, in order to perform the PCA, data is separated in gait cycles and organized (Fig. 7.6) into a n -by- m matrix where each column (m) represents a variable (gait metric), and each row (n) represents an observation of that variable per gait cycle. Usually, it is necessary to calculate

the mean on each dimension of an array with a dataset (Case I). However, the PCA will be also performed for each sample of each variable as depicted in Fig. 7.7 (Case II). Usually in literature, Case I is implemented, however Case II brings more information to the feature selection. The output of the PCA is an m -by- m matrix where each column represents the principal components, and each row represents a variable. Concerning the PCs, the first column is the most significant one, and the last column is the less significant one. Since it is intended to extract the variables with greater variability, each element of the output matrix of PCA is squared (b elements). Then, the number of relevant PCs is obtained according to the Kaiser's rule/criterion [177], where only PCs whose variances exceed 1 are selected (or 10% in case of percentage). Then, a similar proportion of PCs is obtained for each variable, and variables are selected to be used in the next stage if their PC value is greater than $\frac{1}{\text{number of variables } (m)}$. This means that variables with great contributions to the variability of the data are selected. In this squared matrix, the sum of each column is one. In Case II (Fig. 7.7), there will be as many matrices (before PCA) as data samples (usually, 100 samples). So, in the end of the process, all squared matrices will be summed, and the proportion of each variable will be obtained (PC value). Once again, variables are selected to be used in the next stage if their PC value is greater than $\frac{1}{\text{number of variables } (m)}$.

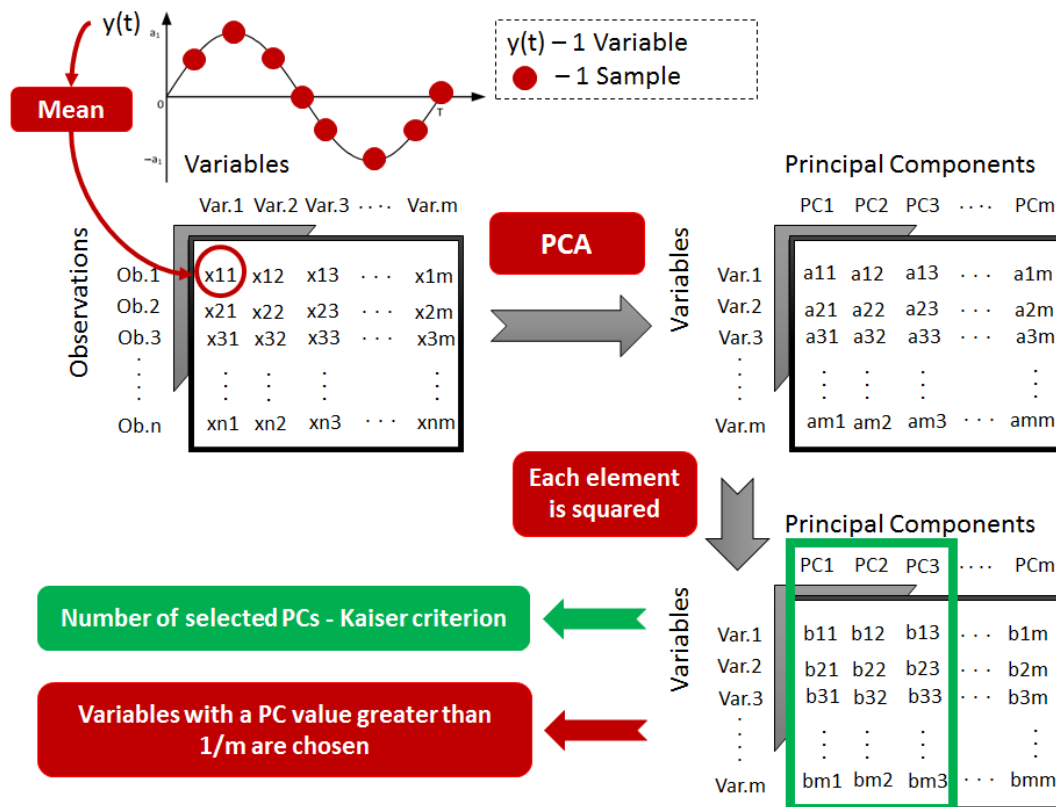


Figure 7.6 - Set of steps to obtain the most relevant variables (Case I).

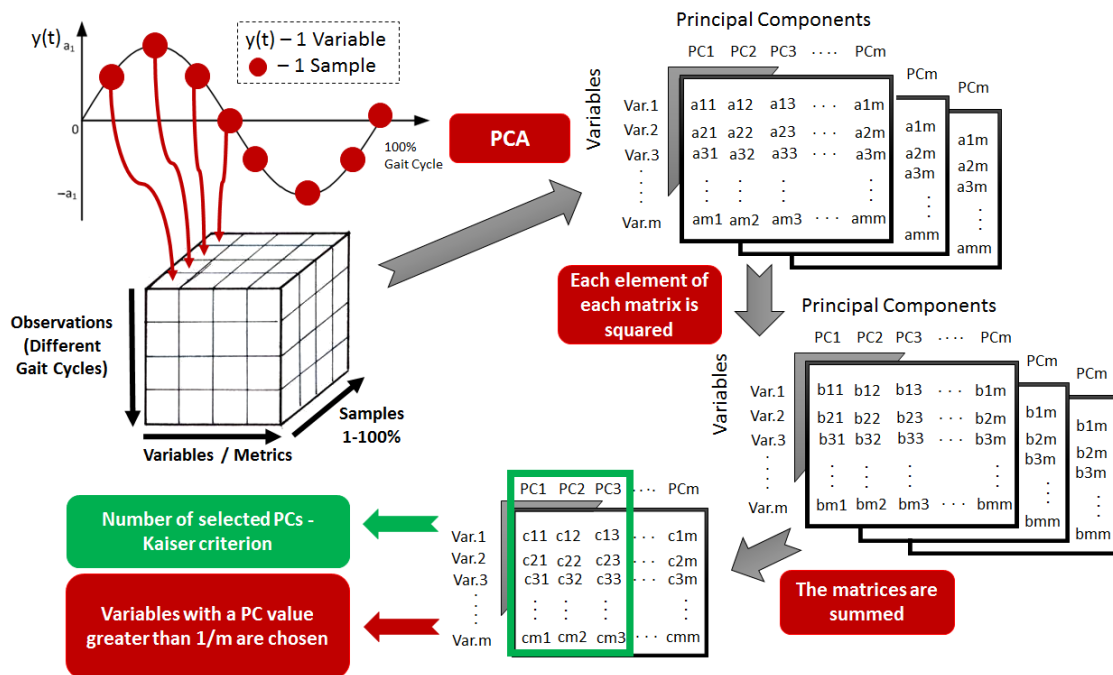


Figure 7.7 - Set of steps to obtain the most relevant variables (Case II).

The PCA procedure was performed four times. One for each type of locomotion mode collected during the explained trials. The designation of each type of locomotion mode is available on Table 7.1, accompanied by a description for each type. This discrimination was carried out with the purpose of classify different states of human activity, in particular in the F's domain.

Table 7.1 – Classification of collected data

Locomotion Mode	Description
Walk Forward - WF	Observations of normal gait from walk forward trials
Global	Observations of normal gait from WF, OR, OL, CR, and CL trials
PF	Observations of the gait cycle before the F's situation
F	Observations of the F's situation

7.1.3. ASMs

Several failure detection systems include particle filters [180] and neural-network based approaches [181], [182]. However these are highly focused in industrial and wheeled robots, and up to our knowledge there is still no such framework proposed regarding biped locomotion in humans using IMUs. Hence it is necessary to establish a structure or framework that stores relevant perceptual information in a consistent form so that it can be used in the future to monitor and

improve movement execution, a skill memory of sorts. Thus, the notion of ASM was proposed by Pastor et al. [183]. An ASM illustrates the most common values and variation of perceptual data when executing a certain task that is performed repeatedly in a similar way. It is called *associative* because the memory itself is not solely based on sensor information, but rather on the association of this specific repeatedly information (sensor footprint) with the corresponding movement, skill or end task [184]. In other words, manipulation tasks often decompose into a sequence of skills, where each skill can be seen as a stereotypical movement (movement primitives), with respect to its goal frame. Assuming that movement dictates sensory feedback, sensory traces can be associated with the movement primitive (e.g. encoded as Dynamical Motion Primitives - DMPs), forming ASMs [183]. Thus, if a certain task is repeated in a similar way as a typical task, which means the perceptual data is inside the variation of the common values, it is considered that this task corresponds to the typical one. Otherwise, it is considered an unsuccessful trial and a failure since the typical task was not recognized. Figure 7.8 depicts the test data set of a particular skill or variable. This test data set contains successful (green) and unsuccessful (red) trials, and the ASM is illustrated by the area inside the two blue lines (\pm weighted STD).

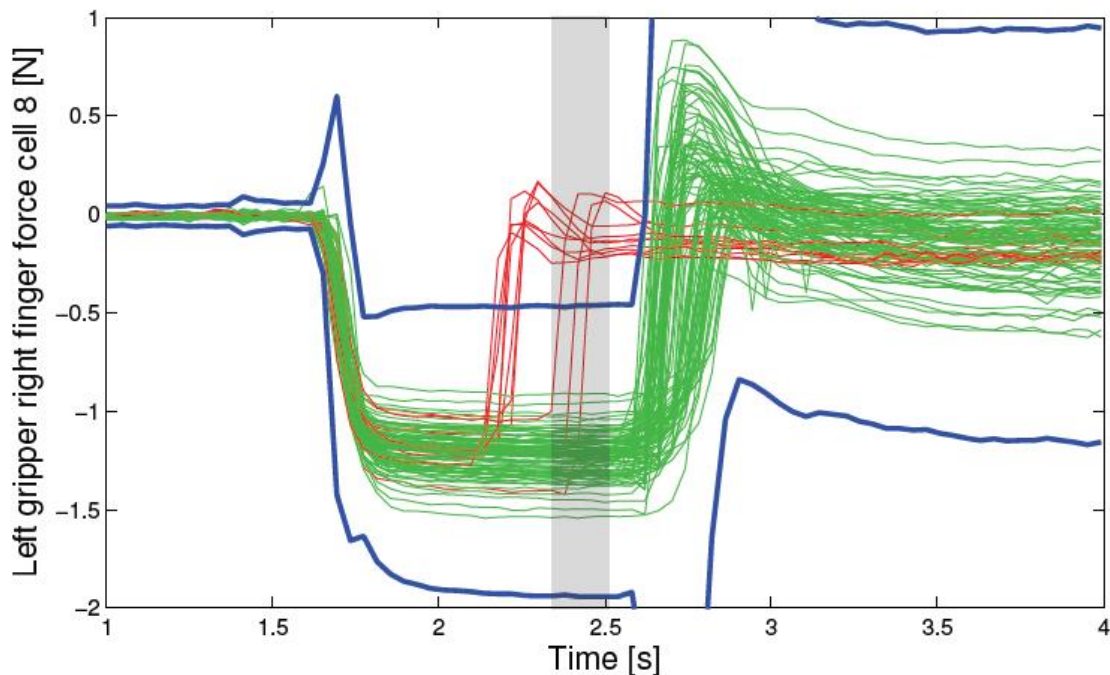


Figure 7.8 – Test data set of the left gripper right finger force cell. Example presented in [185]. The weighted standard deviation (blue line) was computed from the training set. The failure condition for all unsuccessful trials was detected correctly after an average of 2.4 seconds (shaded area).

Mathematically, the most common values of a skill or variable are represented in an ASM as the average of the several training trials \bar{X}_{ASM} , and the variation of perceptual data when

executing a certain task is represented by a weighted STD, $z\hat{\sigma}_{ASM}$, around the \bar{X}_{ASM} . These values are calculated for each instant n of the trial. Thus, a tolerance interval is established for each set of ASMs according to:

$$X_{trial}(n) > \bar{X}_{ASM}(n) - z\hat{\sigma}_{ASM}(n) \wedge X_{trial}(n) < \bar{X}_{ASM}(n) + z\hat{\sigma}_{ASM}(n) \quad (7.1)$$

Where X_{trial} is the variable's data of the current trial, and z represents the zscore which is very important to have a high confidence level (empirically determined). If the condition in Eq. 7.1 is satisfied, then the null hypothesis of being a successful trial is not rejected and the variable's data is assumed to be in conformity with the expected values - there are no signs of failure conditions. If, on the other hand, $X_{trial}(n)$ is out of the confidence bounds established in Eq. 7.1, then there is a high probability of failure occurring, or that movement objective is not achieved at the end of the trial. Whether or not the current trial is flagged as failure depends on the thresholds for failure detection: the minimum number of sensors (M) and the minimum number of consecutive instants failing (N). Simply put, if the system detects at least M sensors failing for N instants consecutively, then it is predicted that, based on the previous experiences stored into the ASM, task verification will fail. z , M , and N are all variables determined empirically.

Usually, in the literature, each trial is evaluated according to a cost threshold, C_x , characterizing all training data. This value, C_x , is used to obtain the weights of each trial, which will influence the calculation of the average, \bar{X}_{ASM} , and the STD, $\hat{\sigma}_{ASM}$. Although this is a common practice in the literature, in this work the costs will not be calculated, which means that each training trial will have the same weight as the rest trials. This can be done because only good trials were used from the entire data.

ASMs also allow to learn predictive models, which can be used to e.g. cope with uncertainty and noise in the perceptual system of the robots. ASMs have been successfully used to address several important issues towards an autonomous manipulation platform [183].

- Having a general skill library which allows to e.g. grasp an object robustly, the sequence of skills has to be determined based on the sensory feedback of the execution. For example, [183] showed how to incrementally determine a correct skill sequence despite perceptual errors using ASMs.

- Errors both in the perceptual and action system are inevitable. Predictive models learned from ASMs allow to predict failures in an online fashion [185].
- For robust manipulation errors have to be detected online and possible successor skills selected in real time. In [186] this problem is formulated as a data-driven online decision making problem, integrating visual, acoustic, and haptic sensors, as well as the system state to make real time decisions using the sensory information provided by the ASMs.

Besides, interesting open research questions related to ASMs and manipulations are: Automatic skill decomposition; Learning good representation from unsupervised sensory information; and better failure incorporation.

Overall, in this work, IMUs' data from human gait were used, and locomotion is a periodic task and this knowledge should be considered when building an ASM. The associative variable's traces should consider a gait cycle and not a time frame of the movement (the entire trial – all steps). Accordingly, perceived variable's signals during successful walking should match the predicted ones during a gait cycle. This provides a generalized representation of a rhythmic task that can be loaded at the beginning of each period, eliminating the issues associated with movement periodicity. Additionally, this structure adds time-invariance to the locomotion task - the skill memory does not depend on the time but rather on the period or phase of the gait cycle. So, from all trials mentioned before, gait cycles and F's situations (from beginning to end of a F) were extracted and resampled to 100 samples, where a sample represents a percentage point of human gait, for a more intuitive and generic representation. Note that this representation is invariant to movement duration and thus better suited for an ASM. Therefore, all these gait cycles, F and PF's situations will be designated from now on as motion periods.

In order to successfully complete stage 1 of this chapter, it was necessary to construct at least four sets of ASMs. One for each type of locomotion mode (Table 7.1), and each set of ASMs contains as many stereotypical variables as the relevant metrics selected by PCA procedure for each type of locomotion mode (Table 7.1). It was also necessary to perform a ROC analysis to determine empirically the z , M , and N values. For this purpose the results are cross-validated with separate train and test data subsets. 75% of all motion periods were used to construct the sets of ASMs, and the rest of the data was used to test the sets of ASMs and to determine z , M , and N values through a ROC analysis [177].

7.1.4. Evaluation of classification performance

In order to evaluate the performance of ASMs based classifier in locomotion mode recognition, three dimensions, accuracy, sensitivity and specificity are commonly used. These metrics are obtained based on a confusion matrix [187], being determined through function “classperf” of MATLAB®. Accuracy, as expressed in equation (7.2), is defined as the classifier’s ability to accurately recognize the gait patterns in the classification. TP, FP, TN and FN correspond to true positive, false positive, true negative and false negative values, respectively [147].

$$\text{Accuracy (\%)} = \frac{\text{TN} + \text{TP}}{\text{TP} + \text{TN} + \text{FP} + \text{FN}} \times 100\% \quad (7.2)$$

Sensitivity, or True Positive Rate (TPR), presented in equation (7.3), measures the proportion of actual positives which are correctly identified as such.

$$\text{Sensitivity (\%)} = \frac{\text{TP}}{\text{TP} + \text{FN}} \times 100\% \quad (7.3)$$

Specificity (SPC), showed in equation (7.4), measures the proportion of negatives which are correctly identified as such [147]. It is possible to determine the negative likelihood ratio (NLR), a ratio between false and true negatives, through a confusion matrix [188].

$$\text{Specificity (\%)} = \frac{\text{TN}}{\text{TN} + \text{FP}} \times 100\% \quad (7.4)$$

Besides, conclusions about the performance of the failure detection algorithm were based on a detection score computed from sensitivity and specificity values [189]:

$$\text{Detection score} = \sqrt{\text{sensitivity}^2 + \text{specificity}^2} \quad (7.5)$$

Which can be interpreted as inversely proportional to the distance to the optimal operation point of maximal (100%) sensitivity and specificity - a higher detection score implies better performance when detecting failure conditions.

7.1.5. Results

7.1.5.1. PCA

First, the PCA procedure was made for Global's locomotion mode. Due to the great amount of gait cycles (970), there are more observations than variables (228), which is the ideal situation when the PCA procedure is used to select the relevant metrics. So, statistically, the validity of this procedure can be claimed.

The first outcome of the PCA is the scree plot. Through this plot for each PCA procedure, and the application of a criterion (Criterion of Kaiser in this particular case), it is possible to select the number of relevant PCs, which will influence the selection of the relevant metrics. For this first step, the obtained scree plots for the two PCA procedures are represented in the Figs. 7.9 and 7.10.

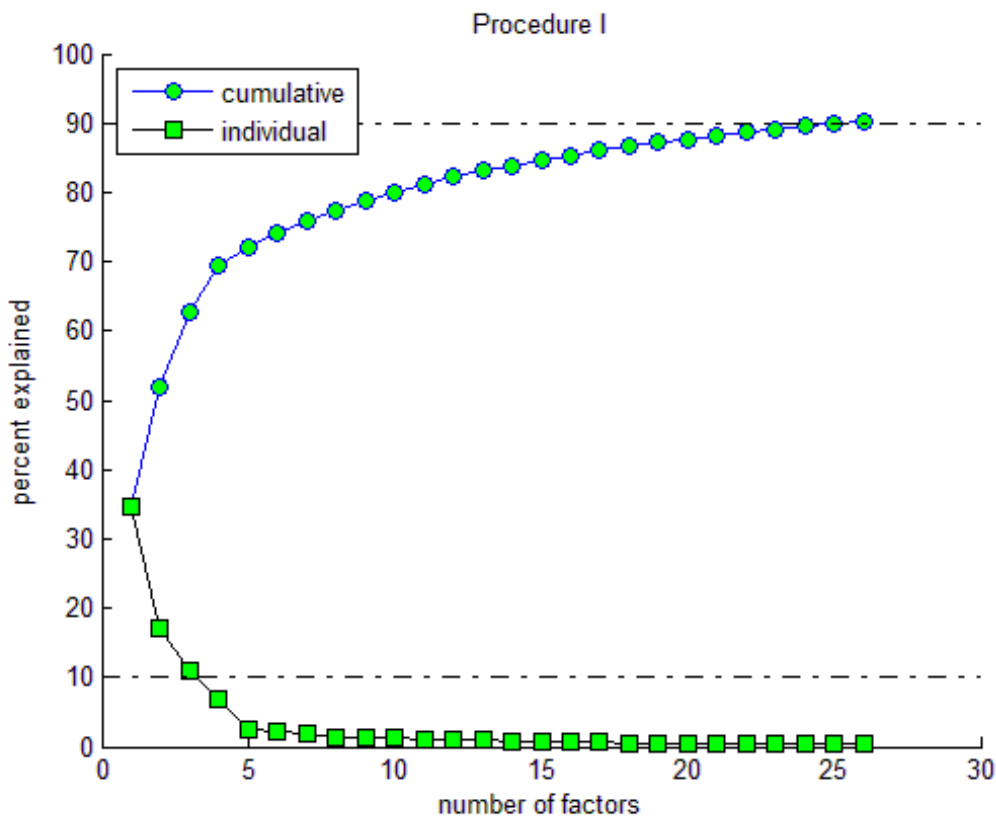


Figure 7.9 - Scree Plot of the PCA procedure I when using the global walking locomotion mode.

According to the criterion of Kaiser, in both procedures, the number of selected PCs is three. However, there is a difference in the percentage explained between procedures. In Figure 7.9, the cumulative percent explained of the three first PCs is higher than 60%, what it is not verified in procedure II (Fig. 7.10). Then, using the information contained in the three PCs in both

procedures, relevant metrics were extracted. From PCA procedure I, 27 metrics were selected, however, 41 metrics were identified as relevant from the PCA procedure II. Relevant metrics extracted from both procedures are represented in the following table.

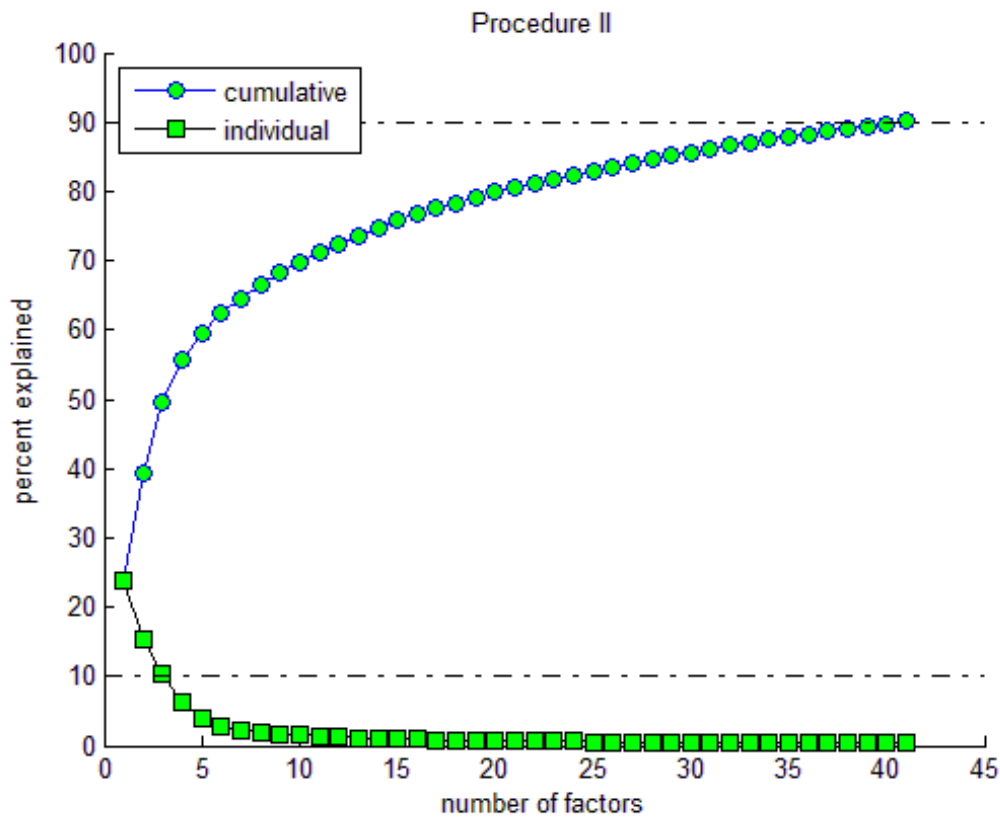


Figure 7.10 - Scree Plot of the PCA procedure II when using the global data.

Table 7.2 – Relevant metrics identified from both PCA procedures (Global Data)

PCA Procedure I		PCA Procedure II		PCA Procedure I & II	
42) Pitch_6	43) ApEn_Gyr_Z_13	7) Mag_Y_7	19) Gait_Events	1) Mag_X_3	2) Mag_Z_3
		20) ApEn_Acc_X_3	21) ApEn_Acc_Z_3	3) Mag_X_6	4) Mag_Y_6
		22) ApEn_Gyr_Y_3	23) ApEn_Gyr_Z_3	5) Mag_Z_6	6) Mag_X_7
		24) ApEn_Mag_X_3	25) ApEn_Mag_Y_3	8) Mag_Z_7	9) Mag_X_13
		26) ApEn_Mag_Z_3	27) ApEn_Gyr_Y_13	10) Mag_Y_13	11) Mag_Z_13
		28) ASMA_6	29) ASMA_13	12) Mag_X_14	13) Mag_Z_14
		30) SVM_6	34) WD_Mag_Y_6	14) Pitch_3	15) Yaw_6
		38) WD_Mag_Y_13	39) WD_Mag_Z_13	16) Pitch_7	17) Pitch_13
				18) Pitch_14	31) WD_Mag_X_3
				32) WD_Mag_Z_3	33) WD_Mag_X_6
				35) WD_Mag_X_7	36) WD_Mag_Z_7
				37) WD_Mag_X_13	40) WD_Mag_X_14
				41) WD_Mag_Z_14	

From Table 7.2, it is possible to retain that PCA procedure II identified more relevant metrics than PCA procedure I. Besides that, PCA procedure II identified metrics that are used in

the scientific community concerning the study of Fs such as ASMA and SVM. Thus, for now on, in the next steps, it will be used only the PCA procedure II to identify the relevant metrics.

The second step consists in performing the same process using data from WF. Note that this second step had fewer observations (129 gait cycles) than the number of variables (228). Figure 7.11 depicts the scree plot of PCA procedure II. This time the number of selected PCs decreases to two, and the cumulative percent explained was 47.14%, which is lower when compared to the results of the previous step.

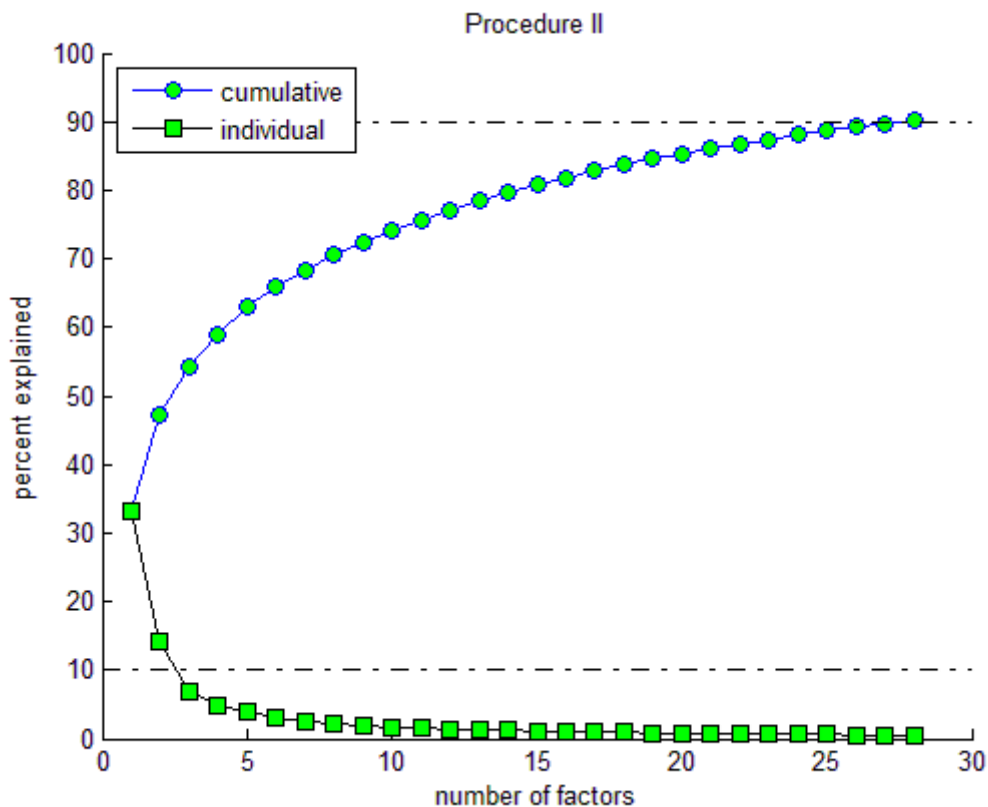


Figure 7.11 - Scree Plot of the PCA procedure II when using the Walking Forward (WF) data.

From PCA procedure II were extracted 44 relevant metrics, and their description is available on Table 7.3. Comparing to the results obtained in the previous step (Table 7.2), it is possible to claim that the number of relevant metrics is higher, and metrics like SVd or SMA appear.

The third step focused on the PF data, identifying the relevant metrics once again through the PCA procedure II. As in the previous step, the number of observations (135 gait cycles) is less than the number of variables (228). According to the scree plot depicted in Fig. 7.12, it is possible to observe that the number of PCs that respect the criterion of Kaiser is three.

Table 7.3 – Relevant metrics identified from PCA procedure II (WF Data)

PCA Procedure II – WF data					
1) Mag_X_3	2) Mag_Z_3	3) Acc_Y_6	4) Gyr_X_6	5) Mag_X_6	6) Mag_X_7
7) Mag_Z_7	8) Acc_Y_13	9) Acc_Z_13	10) Gyr_X_13	11) Mag_X_13	12) Mag_Y_13
13) Mag_Z_13	14) Mag_X_14	15) Mag_Z_14	16) Gait_Events	17) ApEn_Acc_X_3	18) ApEn_Acc_Y_3
19) ApEn_Acc_Z_3	20) ApEn_Gyr_Y_3	21) ApEn_Gyr_Z_3	22) ApEn_Mag_X_3	23) ApEn_Mag_Y_3	24) ApEn_Mag_Z_3
25) ApEn_Mag_Y_7	26) ApEn_Acc_Y_13	27) ApEn_Gyr_X_13	28) ApEn_Gyr_Y_13	29) ApEn_Mag_Y_14	30) ASMA_6
31) ASMA_13	32) SVM_6	33) SVM_13	34) SVd_13	35) Z2_Vert_Acc_13	36) SMA_6
37) SMA_13	38) WD_Mag_X_3	39) WD_Mag_X_6	40) WD_Mag_X_7	41) WD_Mag_X_13	42) WD_Mag_Y_13
43) WD_Mag_Z_13	44) WD_Mag_X_14				

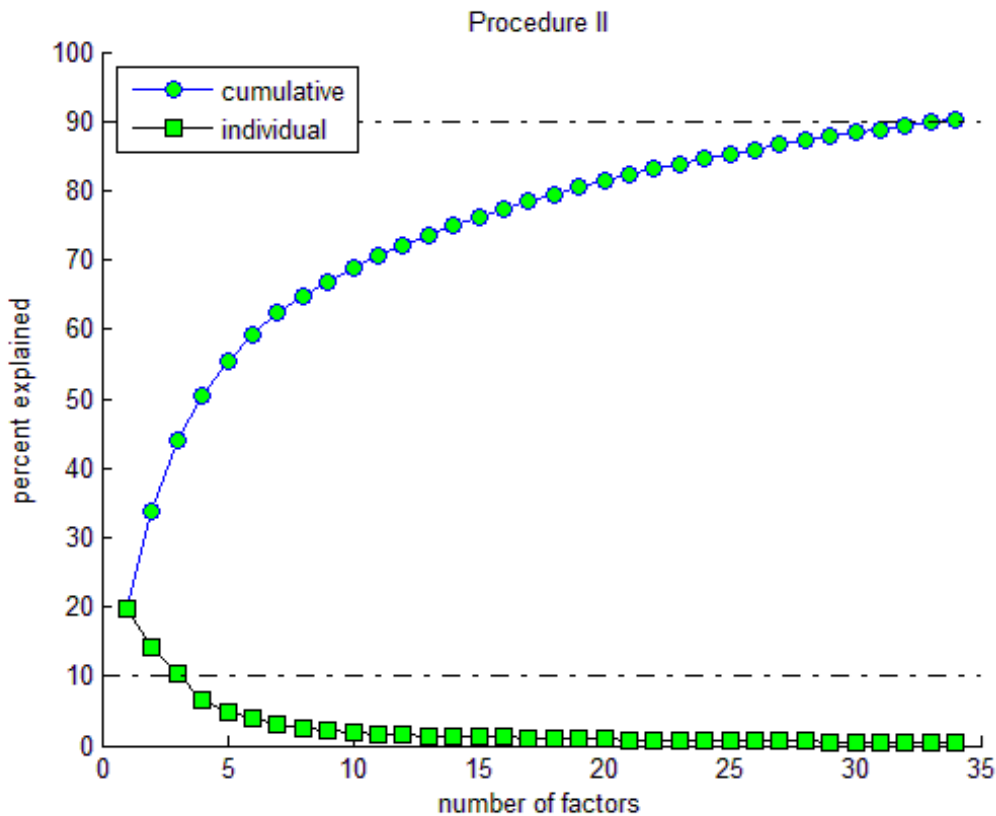


Figure 7.12 – Scree Plot of the PCA procedure II when using the PF data.

This time, 45 relevant metrics were selected through the PCA procedure II (Table 7.4), which is a very close number to that obtained in the previous step (44). However, there are quite differences in the selected metrics when compared to results of Table 7.3. Therefore, there is a clear predominance of the Mag and metrics derived from this sensor.

Table 7.4 – Relevant metrics identified from PCA procedure II (PF Data)

PCA Procedure II – PF data					
1) Mag_X_3	2) Mag_Z_3	3) Mag_X_6	4) Mag_Y_6	5) Mag_Z_6	6) Mag_X_7
7) Mag_Z_7	8) Mag_X_13	9) Mag_Y_13	10) Mag_Z_13	11) Mag_X_14	12) Mag_Z_14
13) Pitch_3	14) Pitch_6	15) Yaw_6	16) Pitch_7	17) Pitch_14	18) Gait_Events
19) Joint_Ang_L	20) ApEn_Acc_Y_3	21) ApEn_Acc_Z_3	22) ApEn_Gyr_X_3	23) ApEn_Gyr_Y_3	24) ApEn_Gyr_Z_3
25) ApEn_Mag_Y_3	26) ApEn_Mag_Z_3	27) ApEn_Gyr_Y_13	28) ApEn_Gyr_X_14	29) ApEn_Gyr_Z_14	30) ApEn_Mag_Y_14
31) ASMA_6	32) ASMA_13	33) SVM_6	34) SVd_13	35) WD_Mag_X_3	36) WD_Mag_Z_3
37) WD_Mag_X_6	38) WD_Mag_Y_6	39) WD_Mag_X_7	40) WD_Mag_Z_7	41) WD_Mag_X_13	42) WD_Mag_Y_13
43) WD_Mag_Z_13	44) WD_Mag_X_14	45) WD_Mag_Z_14			

Finally, as last step, relevant metrics from F data were extract once again from the same procedure previously used. Due to the criterion of Kaiser, the number of selected PCs is two like when was used WF data. Figure 7.13 depicts the scree plot created with the PCA procedure using F data. Once again, the number of observations (134) is less than the number of variables (228).

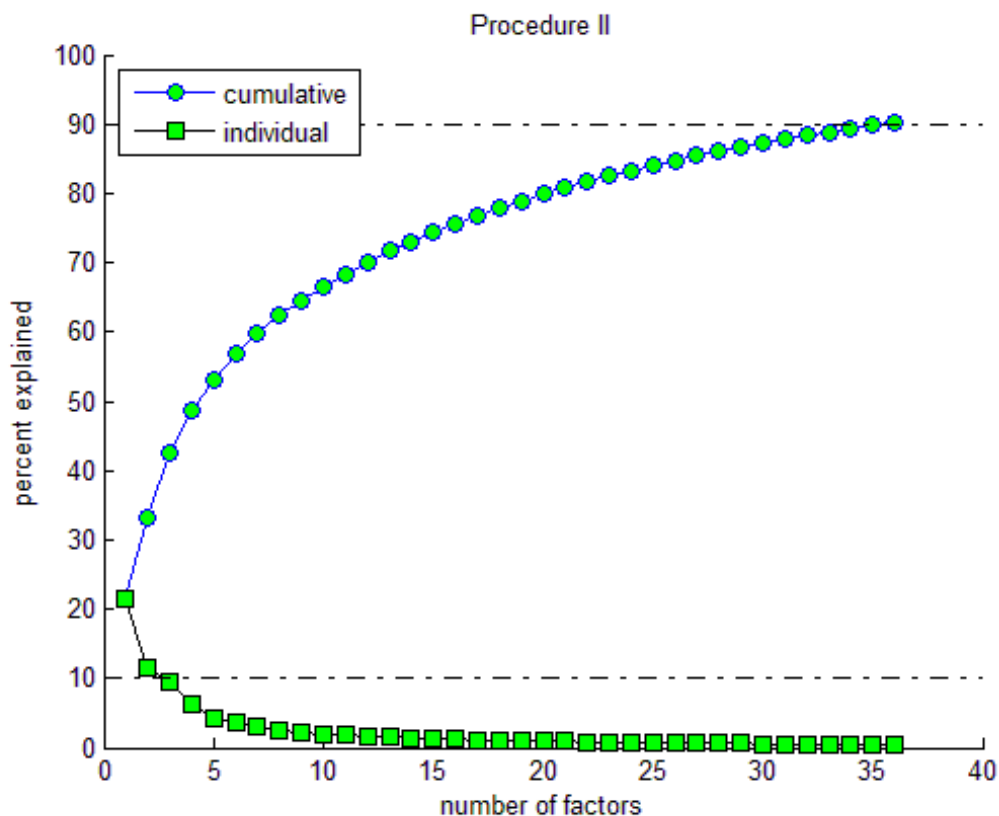


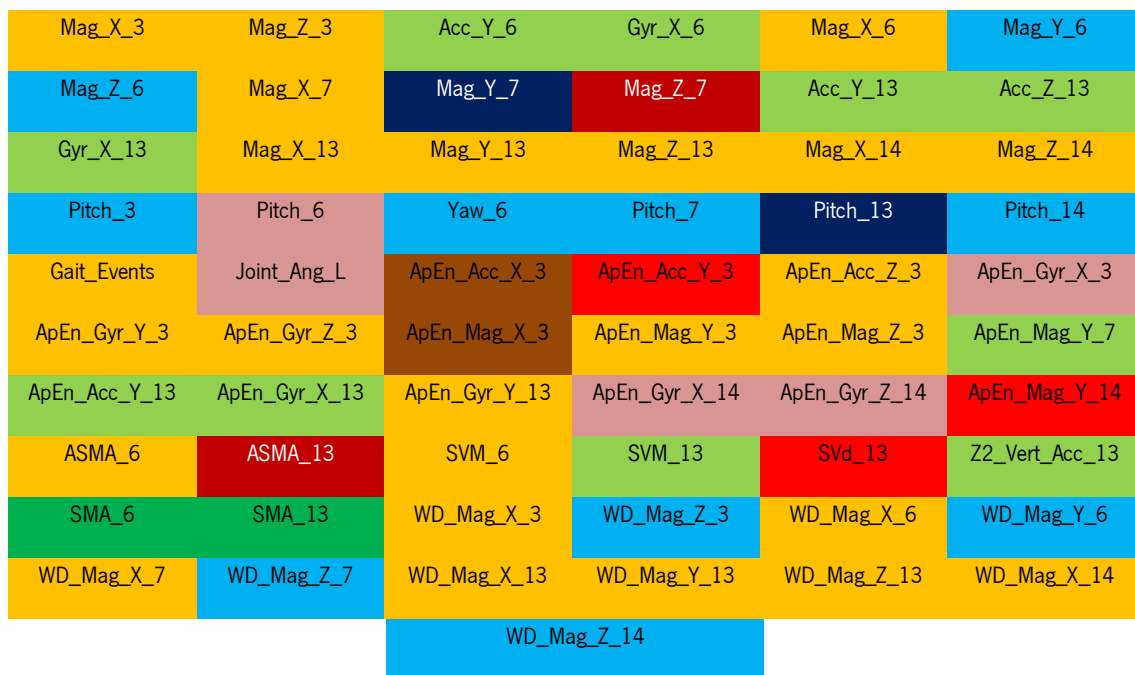
Figure 7.13 - Scree Plot of the PCA procedure II when using the F data.

In this step, the number of selected metrics through the PCA procedure II was 30, which is an inferior value when compared to the two previous steps. As observed previously in Table 7.4, it was verified once again a clear predominance of the Mag and metrics derived from this sensor

(Table 7.5). Overall, from this PCA procedure the number of variables (228) was reduced to 61 non-repeated and relevant variables distributed among the four locomotion modes. Figure 7.14 depicts all metrics and locomotion modes they belong.

Table 7.5 – Relevant metrics identified from PCA procedure II (F's Data)

PCA Procedure II – F data					
1) Mag_X_3	2) Mag_Y_3	3) Mag_Z_3	4) Mag_X_6	5) Mag_Y_6	6) Mag_Z_6
7) Mag_X_7	8) Mag_Y_7	9) Mag_Z_7	10) Mag_X_13	11) Mag_Y_13	12) Mag_Z_13
13) Mag_X_14	14) Mag_Y_14	15) Mag_Z_14	16) Gait_Events	17) ApEn_Mag_Z_3	18) ApEn_Acc_Y_6
19) ApEn_Acc_X_7	20) ApEn_Gyr_Y_7	21) ApEn_Acc_X_14	22) ApEn_Gyr_Y_14	23) WD_Mag_Y_3	24) WD_Mag_Z_6
25) WD_Mag_X_7	26) WD_Mag_Y_7	27) WD_Mag_Z_7	28) WD_Mag_Y_13	29) WD_Mag_Z_13	30) WD_Mag_Y_14



Legend:

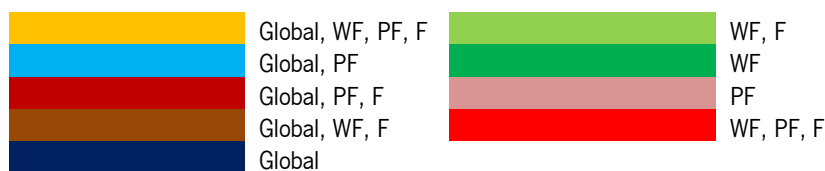


Figure 7.14 – Non-repeated and relevant metrics identified through PCA procedure and the indication to which group they belong.

7.1.5.2. ASMs

Concerning the construction of the sets of ASMs, 75% of each type of data were used as training data. So, from 129 WF gait cycles, 97 were used as training data. From 970 Global gait cycles, 727 were used. 101 PF motion periods were used in a total of 135, and 100 F motion periods were also used to train F's set of ASMs. Consequently, 4 sets of ASMs were constructed (one for each locomotion mode). Each set of ASMs contains as many stereotypical variables (ASMs) as the relevant variables selected by PCA procedure for each locomotion mode (Table 7.1). Figure 7.15 depicts four examples of stereotypical variables (only $\bar{X}_{ASM} \pm \hat{\sigma}_{ASM}$).

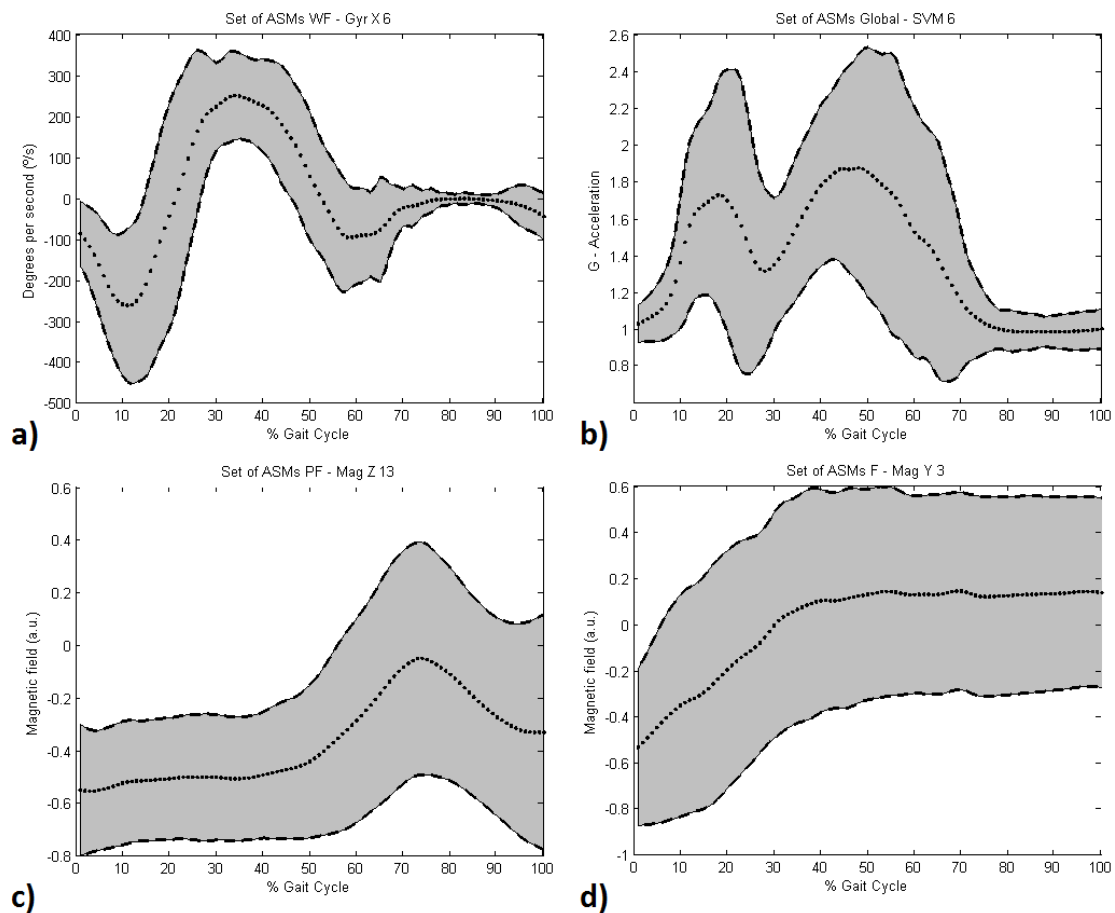


Figure 7.15 – Examples of ASMs. a) Gyr_X_6 from WF set of ASMs; b) SVM_6 from Global set of ASMs; c) Mag_Z_13 from PF set of ASMs; d) Mag_Y_3 from F set of ASMs.

One of the initial doubts about the type of data was whether PF data should be considered as normal gait or abnormal gait. Hence, after the sets of ASMs were constructed, a total of eight ROC analyses were performed. Table 7.6 contains the designation and the description of each ROC analysis. For each ROC analysis, z value ranged from 1 to 5, M ranged from 3 to 6, and N ranged from 1 to 6. The chosen criterion to select the best combination of parameters was the criterion of the minimal Euclidian distance.

Table 7.6 – Different ROC analyses and their considerations

Designation	Training Data	Description
1) ASM WF**	WF	PF data were not used in the tests
2) ASM WF*	WF	PF data as non-normal gait
3) ASM WF	WF	PF data as normal gait
4) ASM Global*	Global	PF data as non-normal gait
5) ASM Global	Global	PF data as normal gait
6) ASM Fall	F	PF data as normal gait (different from F data)
7) ASM PF Δ	PF	PF different from other types of data
8) ASM PF	PF	PF data as normal gait

The first ROC analysis did not count with the PF's data. Under these circumstances, the best combination of parameters was found: $z=3.2$, $M=5$, and $N=6$. Respective ROC curve is depicted in Fig. 7.16. Moreover, the results could not be better. All gait cycles from WF and Global's data were considered as non-failures. On the other hand, all motion periods from F's data were considered as failures. Table 7.7 contains the predicted conditions from the WF's set of ASMs.

Table 7.7 – Predicted conditions - ASM WF** (FP–False Positive; TN–True Negative; TP–True Positive; FN–False Negative)

Locomotion mode	FP	TN	TP	FN
WF	0	32		
Global	0	243		
F			34	0

In addition to this study, we also tried to understand, among the variables, those in which more failures or situations outside the range of the set were detected. It is expected that metrics measured in the axis perpendicular to the direction of movement (mediolateral axis) have less failures. Figure 7.17 shows a histogram for all 44 metrics counting the number of failures per variable or metric.

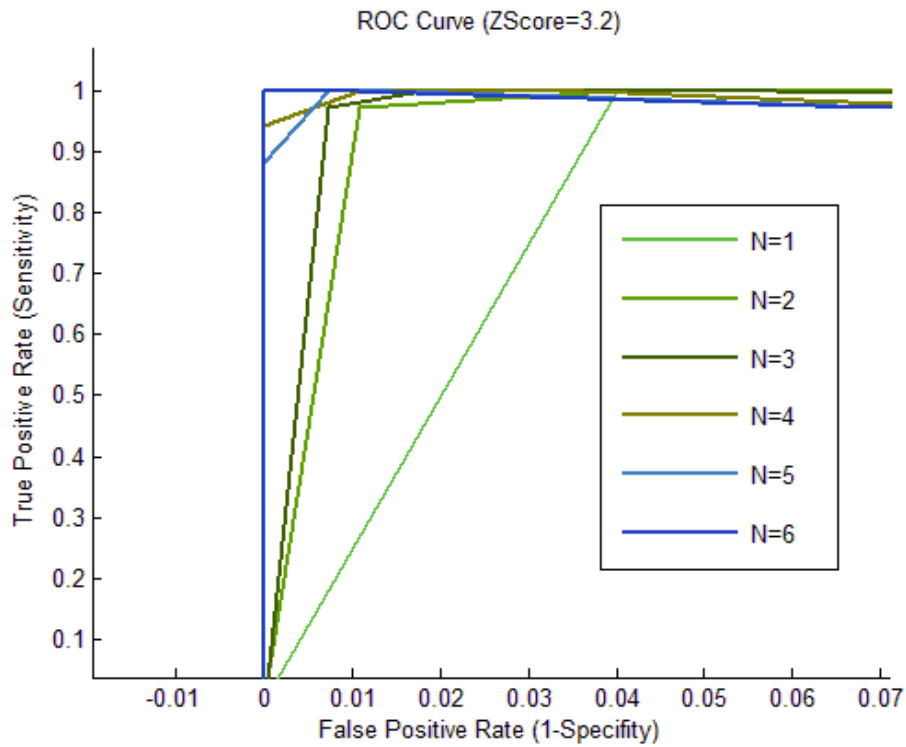


Figure 7.16 – ROC curve of the first ROC analysis – ASM WF**.

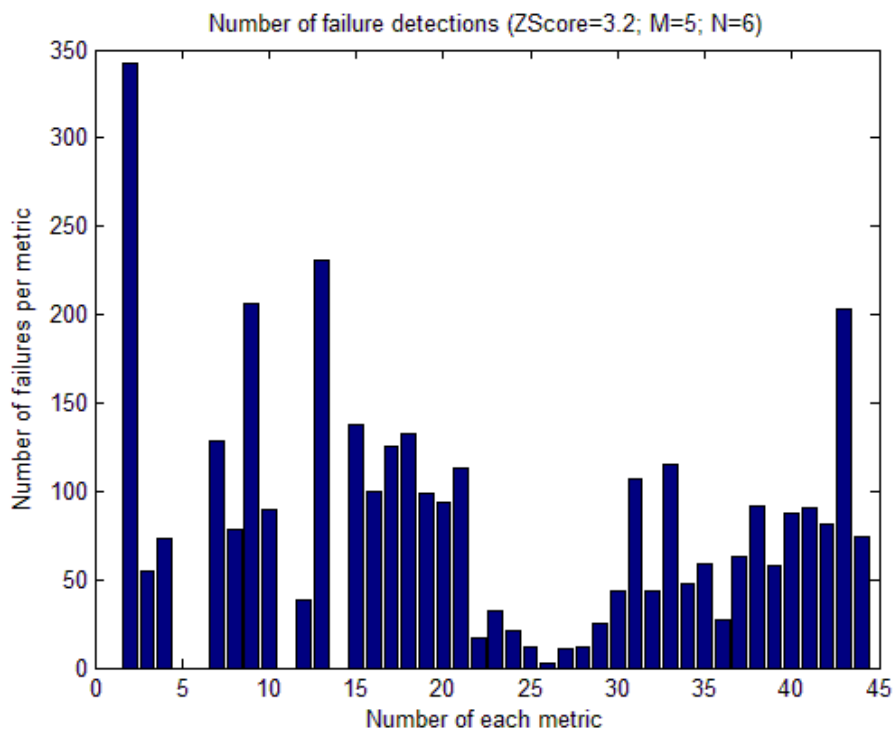


Figure 7.17 – Histogram of the number of failures per metric – ASM WF**.

Figure 7.17 reveals that in all failure's situations, variables 1, 5, 6, 11, and 14 (Mag X-axis from all sensing devices – Numbering in Table 7.3) have never been outside the normal range of the ASM values. This means that no change was registered in the direction perpendicular to the

movement. On the other hand, variables 2, 9, 13, and 43 (Mag_Z_3, Acc_Z_13, Mag_Z_13, and WD_Mag_Z_13, respectively – Numbering in Table 7.3) have been outside the normal range of the ASM values more than 200 times. All these variables have axes parallel to the sagittal plane of the subject. Once obtained the best parameters, it is possible to observe the ASMs of this WF's set, as well as the successful and unsuccessful trials. Figure 7.18 depicts some examples of ASMs of this WF's set of ASMs.

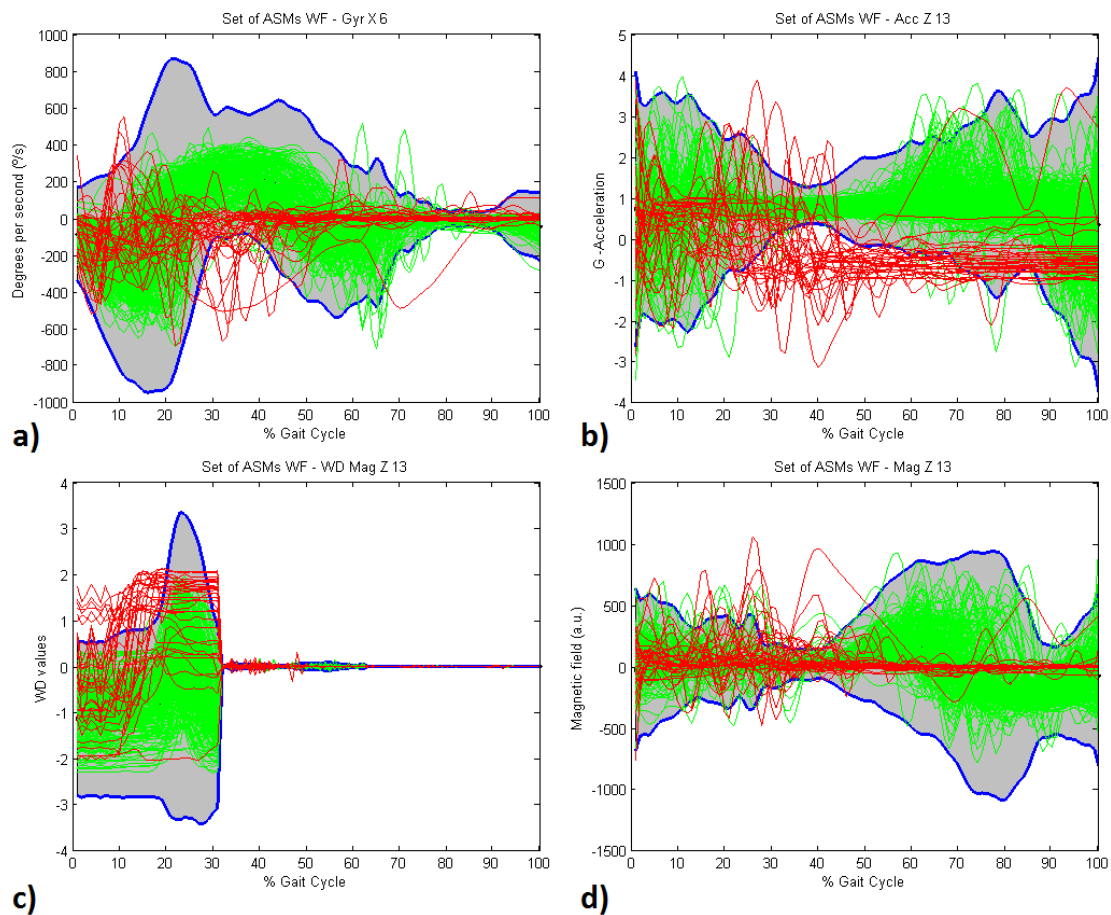


Figure 7.18 – Examples of ASMs. a) Gyr_X_6; b) Acc_Z_13; c) WD_Mag_Z_13; d) Mag_Z_13 (Green – Successful motion periods; Red – Unsuccessful motion periods; Blue – Weighted STD).

In the second ROC analysis, PF's data were considered as non-normal gait. So, F's situations or PF's data were considered as failures, while the remaining data (WF and Global) were considered as non-failure. The best combination of parameters was: $z=3.4$, $M=3$, and $N=2$. Respective ROC curve is depicted in Fig. 7.19. This time, not all WF's gait cycles (3) or Global's gait cycles (36) were considered as true negatives as they should. Even PF's data was not successfully identified as non-normal gait since 50% of the test's data were considered as false

negative. However F's data were successfully identified as failure, because 100% of the test's data were considered as true positive. Table 7.8 contains all this information.

Table 7.8 – Predicted conditions-ASM WF* (FP–False Positive; TN–True Negative; TP–True Positive; FN–False Negative)

Locomotion mode	FP	TN	TP	FN
WF	3	29		
Global	36	207		
F			34	0
PF			17	17

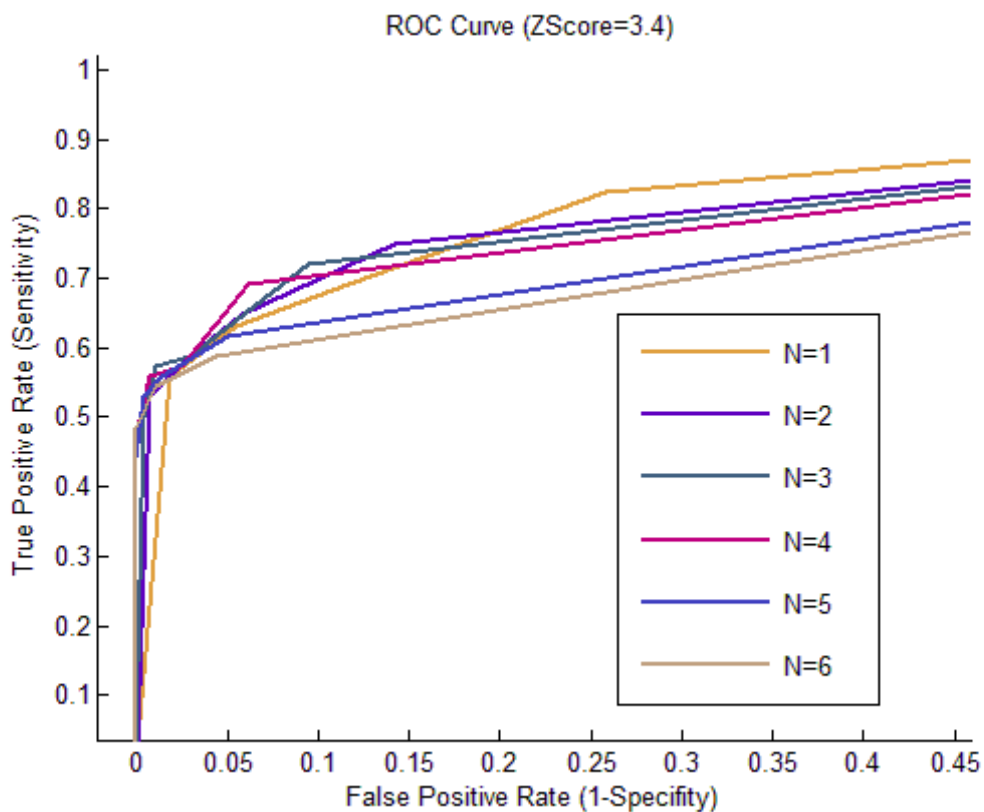


Figure 7.19 - ROC curve of the second ROC analysis – ASM WF*.

Furthermore, again a histogram for all 44 metrics counting the number of failures per variable or metric was made (Fig. 7.20). As in the previous analysis, variables 1, 5, 6, 11 and 14 (Mag X-axis from all sensing devices – Numbering in Table 7.3) have never been outside the normal range of the ASM values. However, this time, only variables 2 and 13 (Mag_Z_3 and Mag_Z_13, respectively – Numbering in Table 7.3) have been outside the normal range of the ASM values

more than 200 times. Under these circumstances, the successful and unsuccessful motion periods concerning these two variables are depicted in Fig. 7.21 as well as the weighted standard deviation of the respective ASMs.

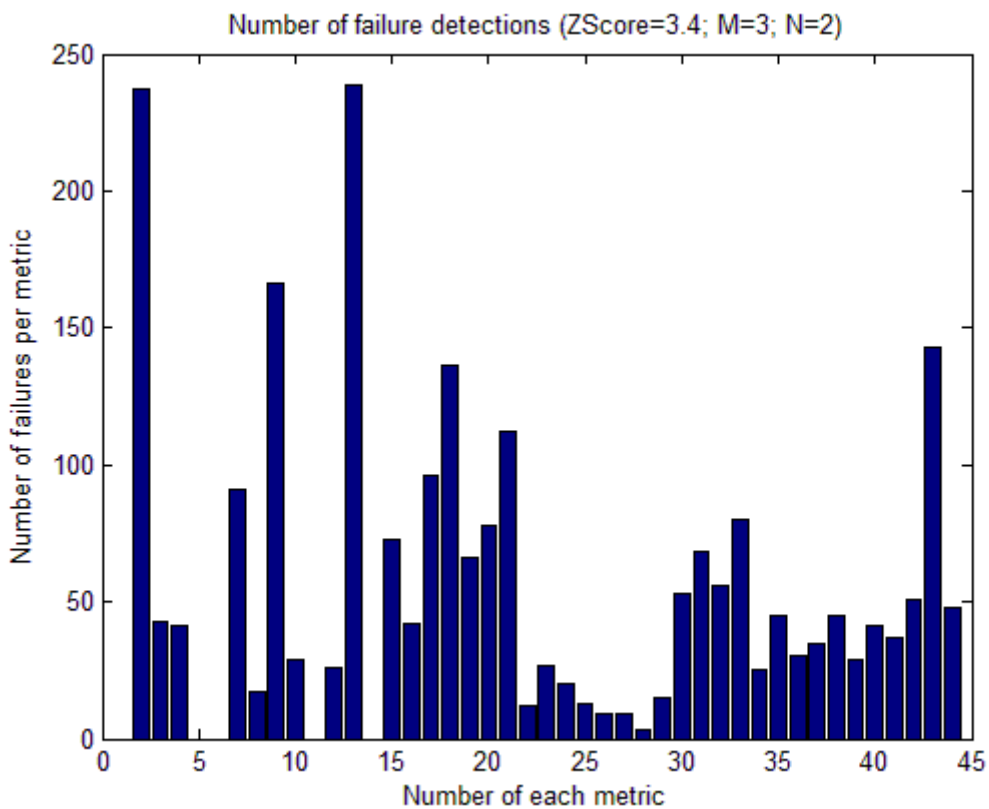


Figure 7.20 - Histogram of the number of failures per metric – ASM WF*.

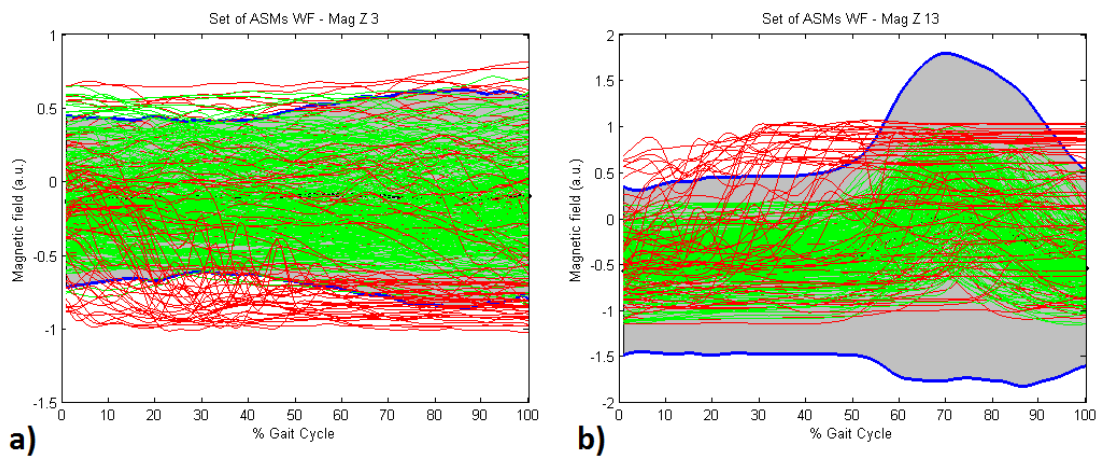


Figure 7.21 - Examples of ASMs. a) Mag_Z_3; b) Mag_Z_13 (Green – Successful motion periods; Red – Unsuccessful motion periods; Blue – Weighted STD).

The third ROC analysis was the last one that was made to the set of ASMs whose training data are WF. This time, PF's data were considered as normal gait like WF and Global's data. So,

only F's situations data were considered as failures. Thus, the best combination of parameters was $z=2.8$, $M=6$, and $N=6$. The ROC curve of this ROC analysis is depicted in Fig. 7.22. Contrary to the previous ROC analysis, the results (Table 7.9) were quite good since only one gait cycle was considered a false positive in a total of 275 (Global and WF). In 34 PF's motion periods, only two were considered as false positive, and none F's motion period was considered as false negative.

Table 7.9 - Predicted conditions-ASM WF (FP-False Positive; TN-True Negative; TP-True Positive; FN-False Negative)

Locomotion mode	FP	TN	TP	FN
WF	0	32		
Global	1	242		
F			34	0
PF	2	32		

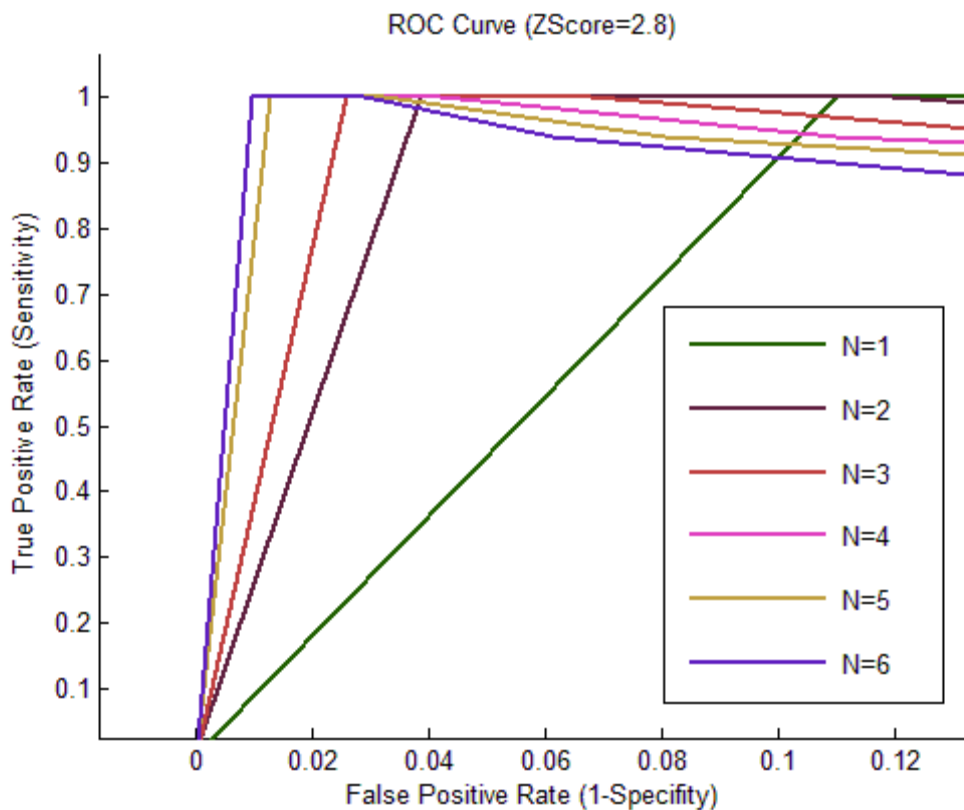


Figure 7.22 - ROC curve of the third ROC analysis – ASM WF.

From the histogram of the Fig.7.23, it is possible to observe that the same variables (1, 5, 6, 11 and 14 - Mag X-axis from all sensing devices – Numbering in Table 7.3) identified in the last two ROC analysis have never been outside the normal range of the ASM values. Variables 2, 9,

and 13 (Mag_Z_3, Acc_Z_13, and Mag_Z_13) appear again as the variables that have been outside the normal range of the ASM values more than 200 times. Examples of successful and unsuccessful motion periods can be found in Fig. 7.24.

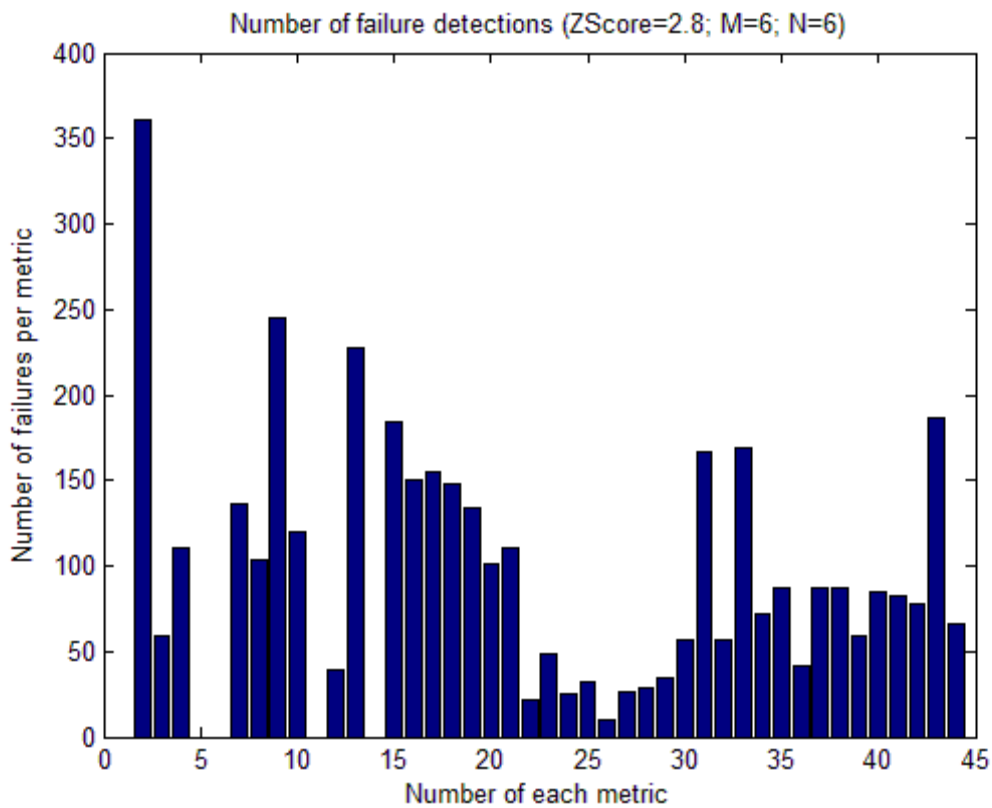


Figure 7.23 - Histogram of the number of failures per metric – ASM WF.

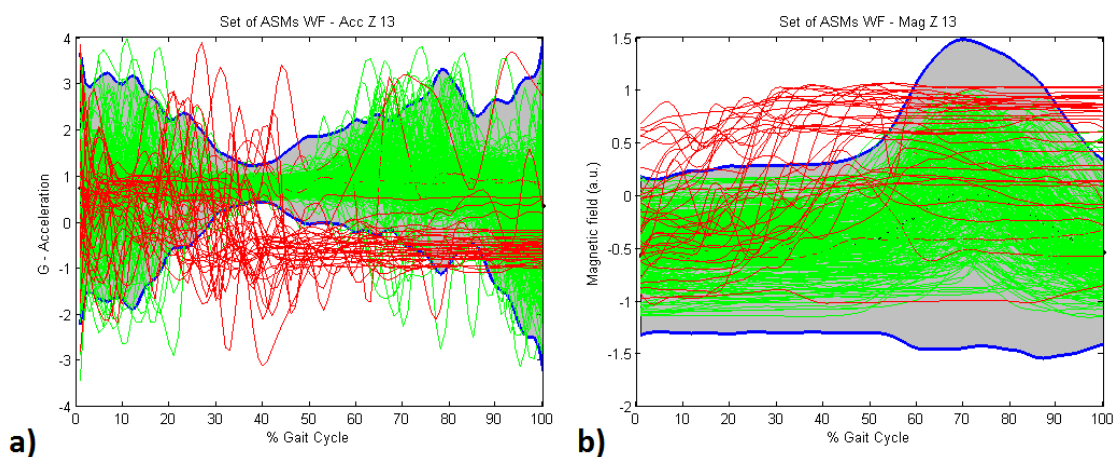


Figure 7.24 – Examples of ASMs. a) Acc_Z_13; b) Mag_Z_13 (Green – Successful motion periods; Red – Unsuccessful motion periods; Blue – Weighted STD).

The fourth ROC analysis had Global's motion periods as training data. In this ROC analysis, PF's data were considered as non-normal gait. So, F's situations and PF's data were considered

as failures, while the remaining data (WF and Global) were considered as non-failure. The best combination of parameters was: $z=3.2$, $M=3$, and $N=1$, and the respective ROC curve is depicted in Fig. 7.25. This time, not all WF's gait cycles (7) or Global's gait cycles (38) were considered as true negatives as they should. PF's data was not successfully identified even as non-normal gait since 16 motion periods of the test's data were considered as false negative. However F's data were successfully identified as failure, because only one in 34 of the test's data were considered as false negative. These results (Table 7.10) were not as good as the previous ones.

Table 7.10 - Predicted conditions-ASM Global* (FP-False Positive; TN-True Negative; TP-True Positive; FN-False Negative)

Locomotion mode	FP	TN	TP	FN
WF	7	25		
Global	38	205		
F			33	1
PF			18	16

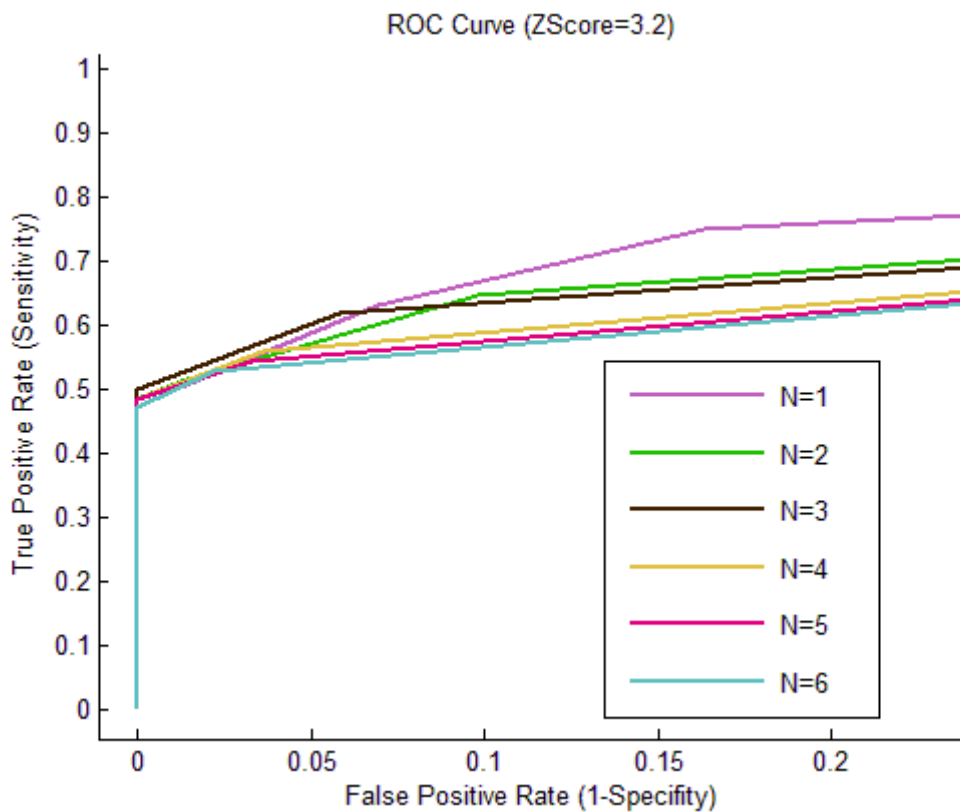


Figure 7.25 – ROC curve of the fourth ROC analysis – ASM Global*.

Taken into account the histogram of the Fig. 7.26, it is possible to retain that there are no variables that have been outside the normal range of the ASM values more than 200 times. Only three have more than 100 failures (7, 11, and 39 – Mag_Y_7, Mag_Z_13, and WD_Mag_Z_13 – Numbering in Table 7.2). On the other hand, there are more variables that had no failures, namely variables 1, 3, 9, and 12 (Mag X-axis from all sensing devices except number 7 – Numbering in Table 7.2). These findings do not differ so much from the previous ones. Examples of successful and unsuccessful motion periods, concerning this ROC analysis, can be found in Fig. 7.27.

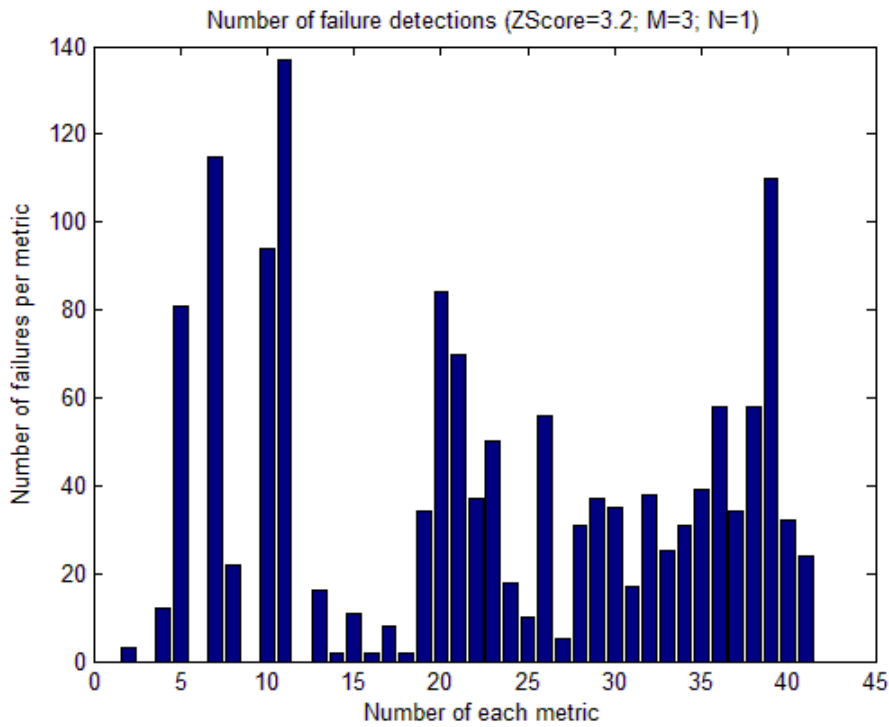
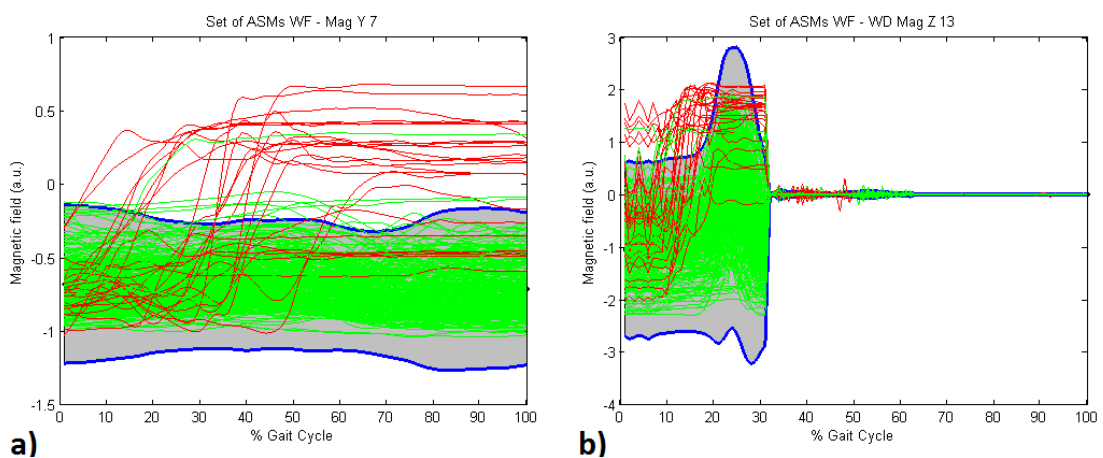


Figure 7.26 – Histogram of the number of failures per metric – ASM Global*.



a) b) Figure 7.27 – Examples of ASMs. a) Mag_Y_7; b) WD_Mag_Z_13 (Green – Successful motion periods; Red – Unsuccessful motion periods; Blue – Weighted STD).

Following the fourth ROC analysis, a new analysis was carried out considering the PF's data as normal gait like WF and Global's data. Only F's data were considered as potential failures. Hence the best combination of the parameters was achieved ($z=4.2$, $M=4$, and $N=1$) through the ROC curve (Fig. 7.28). Overall, the results (Table 7.11) were quite good because only 6 motion periods of normal gait were considered as false positive (WF – 1, Global – 3, and PF - 2), and all F's test data were identified as true positive (failure). However, the results of the third ROC analysis (WF's data as training data) were better.

Table 7.11 – Predicted conditions-ASM Global (FP–False Positive; TN–True Negative; TP–True Positive; FN–False Negative)

Locomotion mode	FP	TN	TP	FN
WF	1	31		
Global	3	240		
F			34	0
PF	2	32		

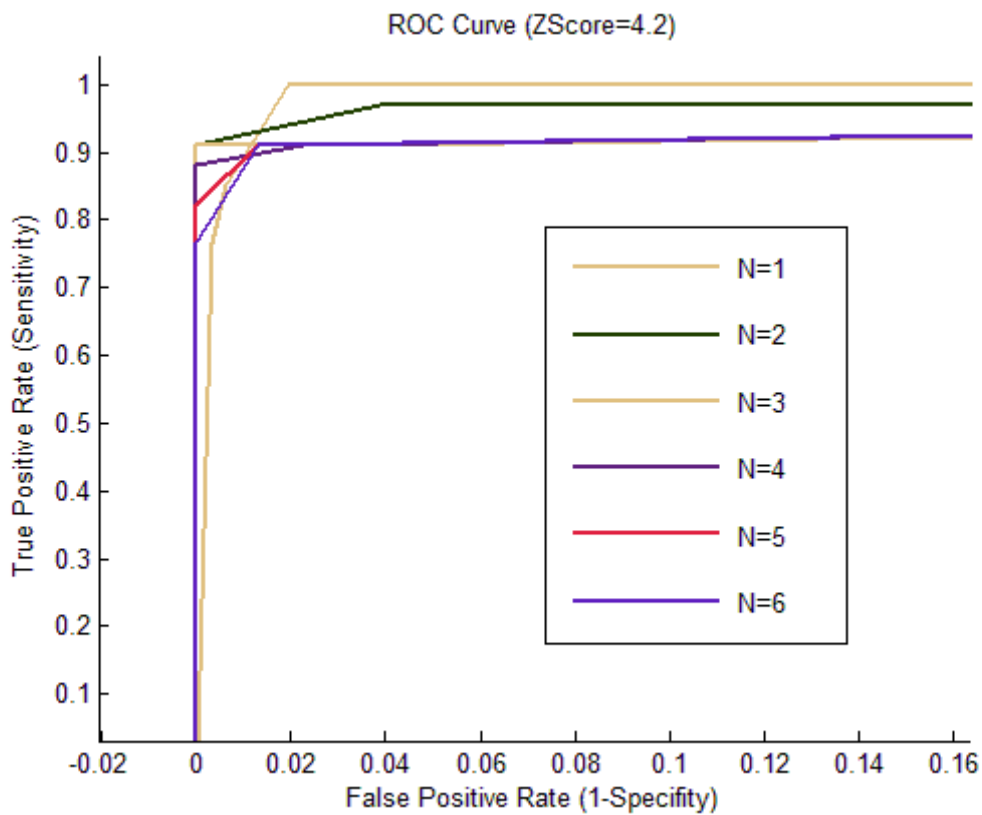


Figure 7.28 – ROC curve of the fifth ROC analysis – ASM Global.

Furthermore, again a histogram for all 41 metrics counting the number of failures per variable or metric was made (Fig. 7.29). This time, the number of variables without detected failures is higher (14). Those variables are 1, 2, 3, 4, 6, 8, 9, 10, 12, 13, 14, 16, 18, and 27 (Mag_X_3, Mag_Z_3, Mag_X_6, Mag_Y_6, Mag_X_7, Mag_Z_7, Mag_X_13, Mag_Y_13, Mag_X_14, Pitch_7, Pitch_14, and ApEn_Gyr_Y_13, respectively – Numbering in Table 7.2). On the other hand, the number of failures per metric is less when compared to other previous ROC analyses. Only, two metrics have more failures than 15, namely 11 and 39 (Mag_Z_13 and WD_Mag_Z_13). Examples of successful and unsuccessful motion periods, concerning these considerations, can be found in Fig. 7.30.

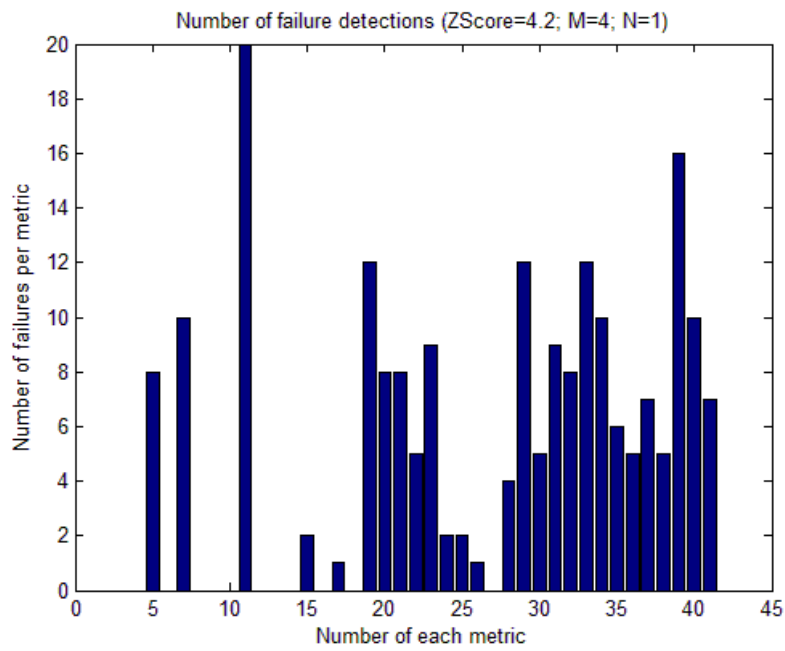


Figure 7.29 - Histogram of the number of failures per metric – ASM Global.

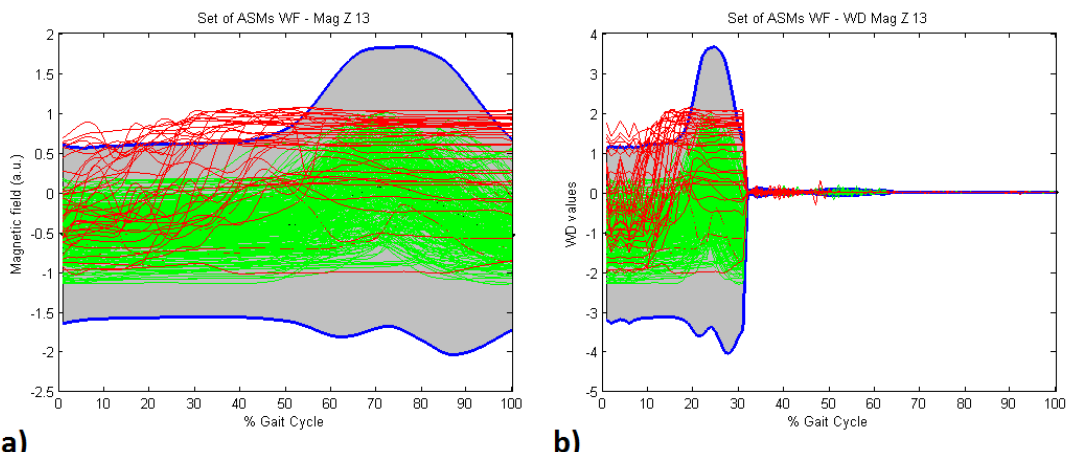


Figure 7.30 – Examples of ASMs. a) Mag_Z_13; b) WD_Mag_Z_13 (Green – Successful motion periods; Red – Unsuccessful motion periods; Blue – Weighted STD).

The sixth ROC analysis focuses on the set of ASMs for F's situations. In this particular case, the notion of failure or non-failure is totally different from the previous ROC analyses. This time, it was considered failure every motion periods different from F's situations. So, PF, Global and WF's data were considered failure, and F's data were considered non-failure instead. Therefore, the best combination of the parameters was achieved ($z=1.7$, $M=6$, and $N=4$) through the ROC curve (Fig. 7.31). The results (Table 12) were considered as fair because not all WF (11), Global (39), and PF's gait cycles (7) were considered as true positives as they should. Concerning the F's data, 6 in 34 were identified as false positive.

Table 7.12 – Predicted conditions-ASM F (FP–False Positive; TN–True Negative; TP–True Positive; FN–False Negative)

Locomotion mode	FP	TN	TP	FN
WF			21	11
Global			204	39
F	6	28		
PF			27	7

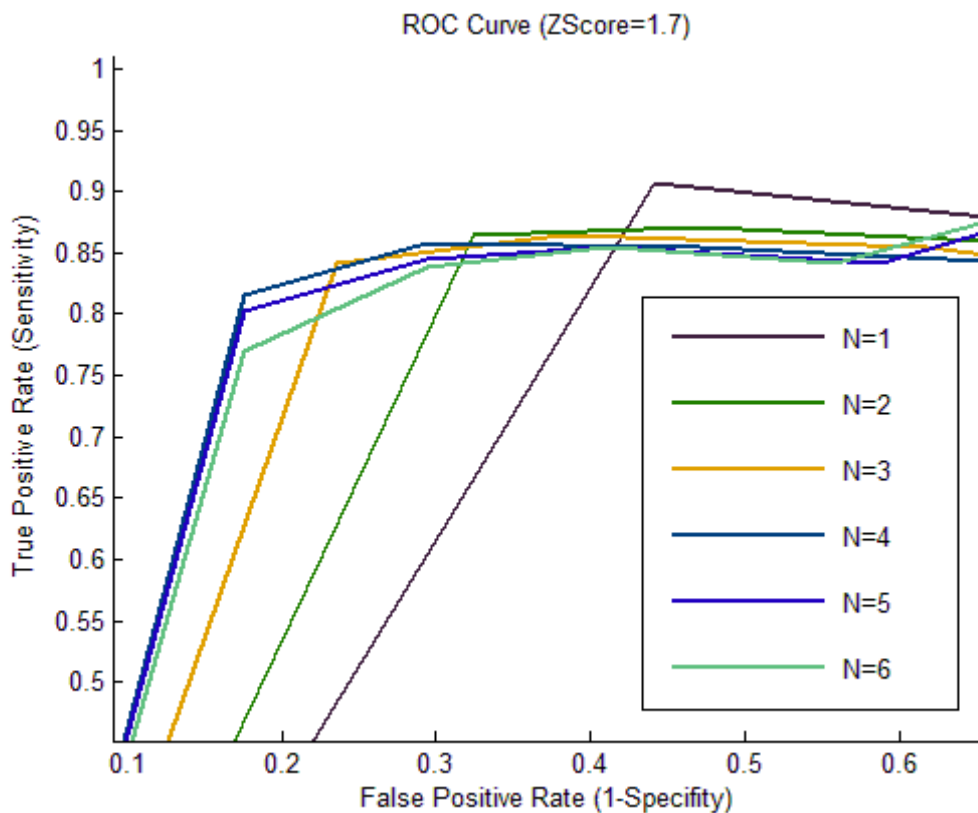


Figure 7.31 – ROC curve of the sixth ROC analysis – ASM F.

Taken into account the histogram of the Fig. 7.32, it is possible to observe that there are no variables that have no failures' situations. Since the number of failures is higher, because WF, Global and PF's data were considered as predictable failures, the number of failures per metric reach values higher than 100 to more than 2500. Five variables have more than 2500 failures (1, 3, 4, 7 and 13 – Mag_X_3, Mag_Z_3, Mag_X_6 and Mag_X_14 – Numbering in Table 7.5). Examples of successful and unsuccessful motion periods, concerning this ROC analysis, can be found in Fig. 7.33.

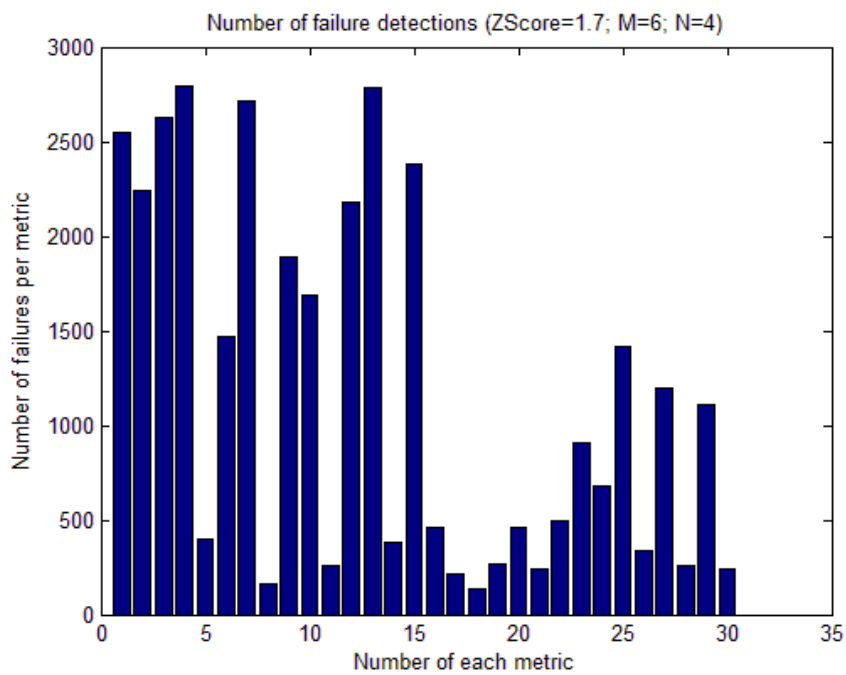
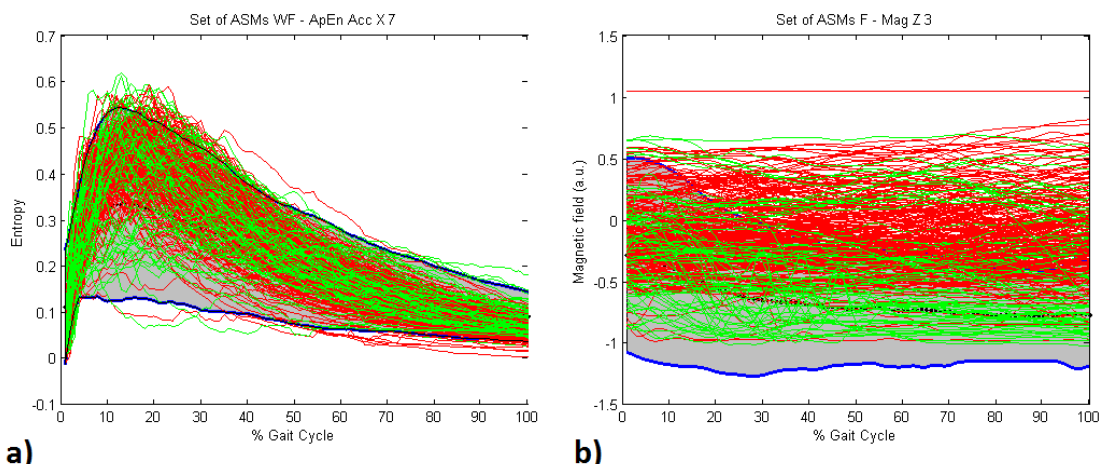


Figure 7.32 – Histogram of the number of failures per metric – ASM F.



a) ApEn_Acc_X_7; **b)** Mag_Z_3 (Green – Successful motion periods; Red – Unsuccessful motion periods; Blue – Weighted STD).

The last two ROC analyses considered the PF's data as training data of the set of ASMs. Firstly, PF's data were considered as different from WF, Global and F's data. In the last case, PF's data were considered as normal gait like WF and Global's data. Thus, this is a similar consideration to the third and fifth ROC analyses' considerations. In the seventh ROC analysis, the best combination of the parameters was $z=1.8$, $M=5$, and $N=4$. Respective ROC curve is depicted in Fig. 7.34. The results (Table 13) were considered as poor because, in general, concerning WF, Global and F's data, it had more false negatives than true positives. Concerning the PF's data, 9 in 34 were identified as false positive.

Table 7.13 – Predicted conditions-ASM PFD (FP–False Positive; TN–True Negative; TP–True Positive; FN–False Negative)

Locomotion mode	FP	TN	TP	FN
WF			12	20
Global			113	130
F			17	17
PF	9	25		

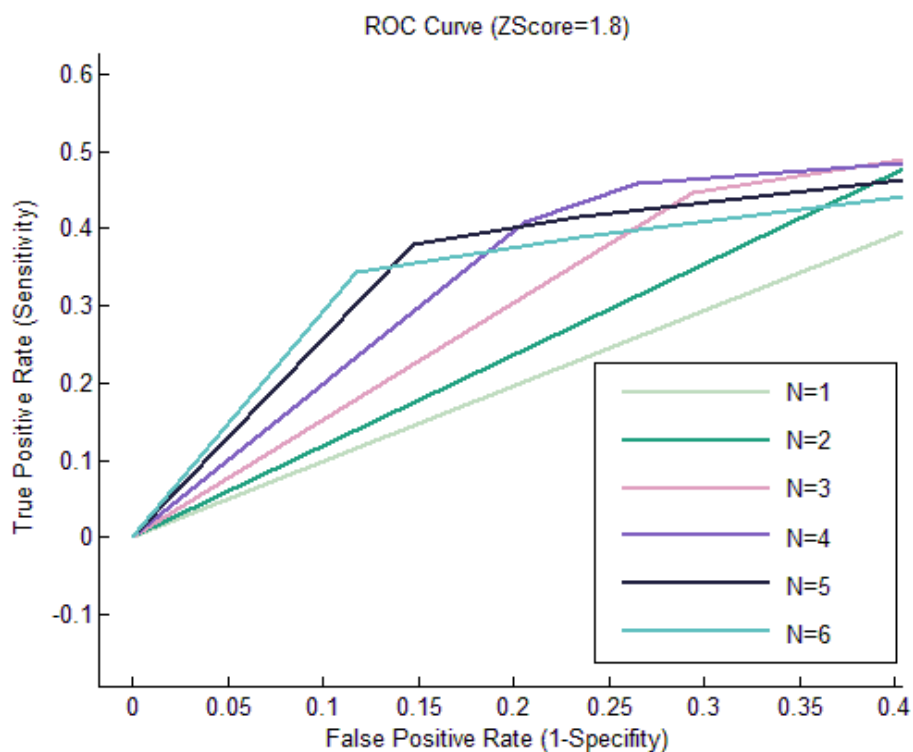


Figure 7.34 – ROC curve of the seventh ROC analysis – ASM PFD.

As verified in the last histogram, the number of times that a variable went out of the range of the respective ASM is high (Fig. 7.35). First, there are no variables that have no failures' situations. And second, there are five variables that have more than 2500 failures (1, 3, 6, 8 and 11 – Mag X-axis from all sensing devices – Numbering in Table 7.4). Given the considerations made for this particular situation, it is considered normal to have a huge number of failures. Examples of successful and unsuccessful motion periods, concerning this ROC analysis, can be found in Fig. 7.36.

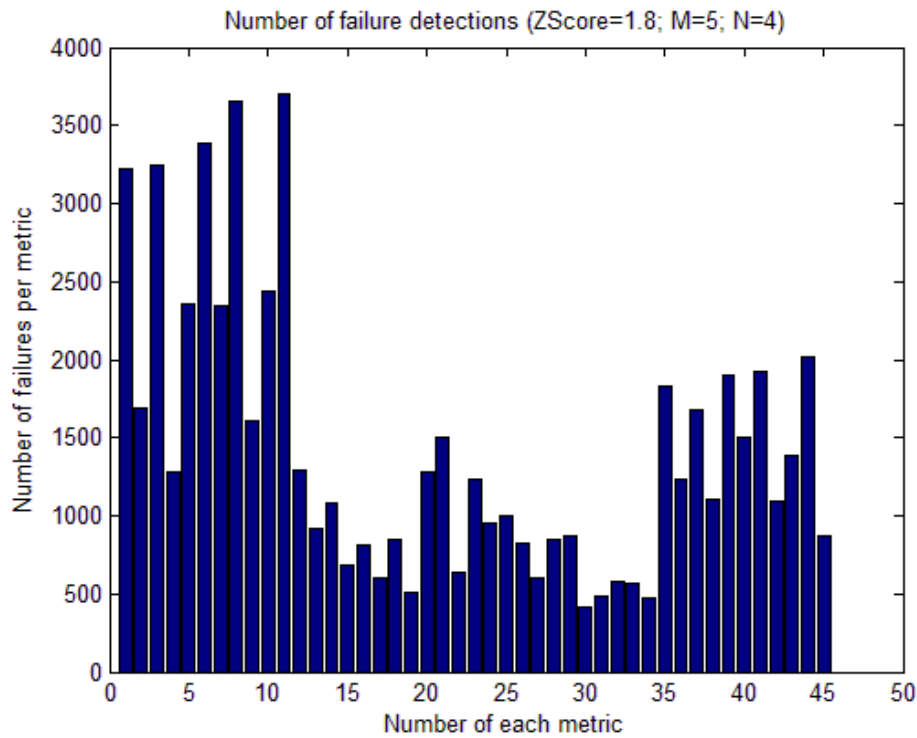


Figure 7.35 – Histogram of the number of failures per metric – ASM PFA.

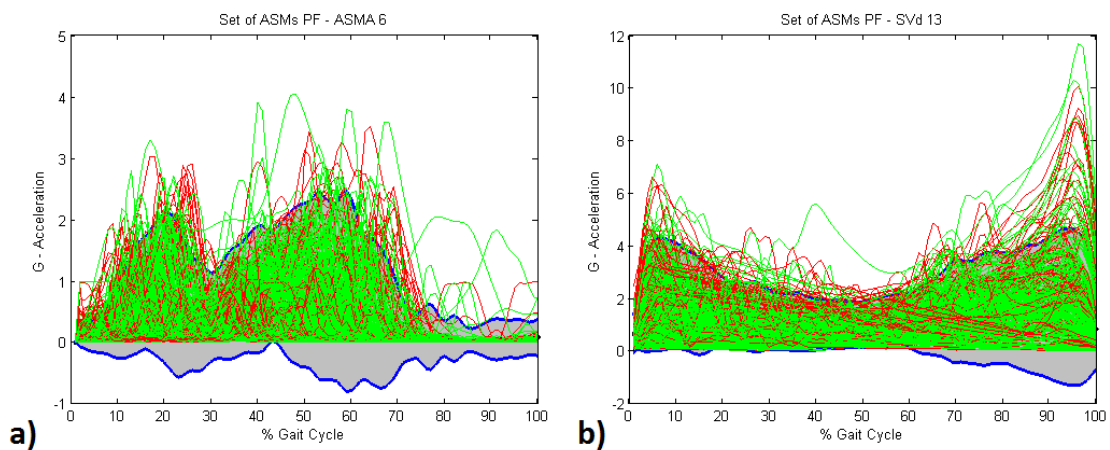


Figure 7.36 – Examples of ASMs. a) ASMA_6; b) SVd_13 (Green – Successful motion periods; Red – Unsuccessful motion periods; Blue – Weighted STD).

The best combination of the parameters in the last ROC analysis was $z=3.4$, $M=5$, and $N=1$. Respective ROC curve is depicted in Fig. 7.37. Once again, considering the PF's data as normal gait like WF and Global's data, the results (Table 14) were considered as good. In general, the number of false positives was low (6 in a total of 309 motion periods). On the other hand, all predictable failures (true positives) were confirmed as failures. This finding indicates that the PF's data, once again, are closer to the normal gait data.

Table 7.14 – Predicted conditions-ASM PF (FP–False Positive; TN–True Negative; TP–True Positive; FN–False Negative)

Locomotion mode	FP	TN	TP	FN
WF	1	31		
Global	4	239		
F			34	0
PF	1	33		

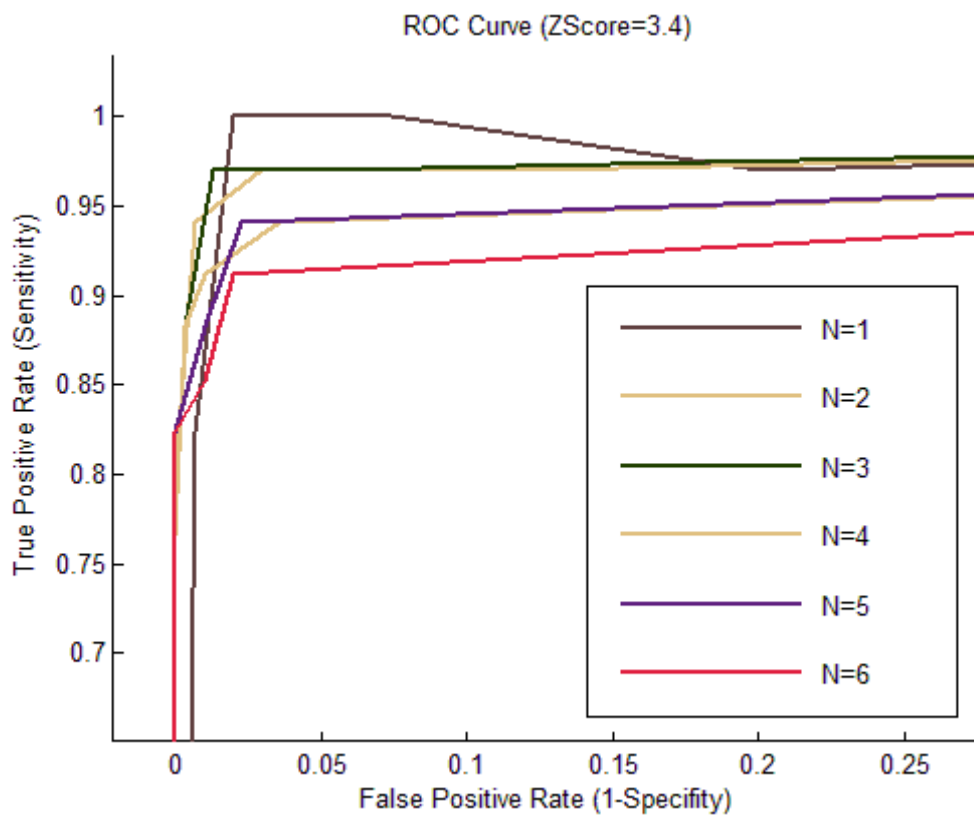


Figure 7.37 – ROC curve of the eighth ROC analysis – ASM PF.

Furthermore, the histogram depicted in the Fig. 7.38 reveals that there is a high number (9 in 45) of variables without detected failures. Those variables are 1, 2, 3, 6, 11, 12, 16, 17, and 27 (Mag_X_3, Mag_Z_3, Mag_X_6, Mag_X_7, Mag_X_14, Mag_Z_14, Pitch_7, Pitch_14, and ApEn_Gyr_Y_13, respectively – Numbering in Table 7.4). On the other hand, the number of failures per metric is less when compared to other previous ROC analyses. Only, three metrics have more failures than 25, namely 10, 21 and 43 (Mag_Z_13, ApEn_Acc_Z_3 and WD_Mag_Z_13). Examples of successful and unsuccessful motion periods, concerning these considerations, can be found in Fig. 7.39.

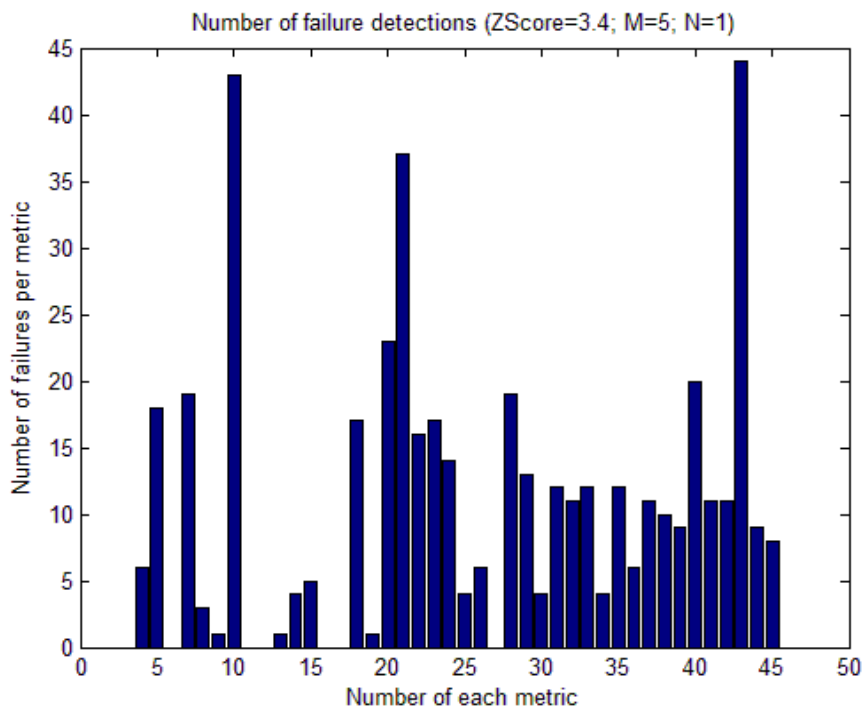
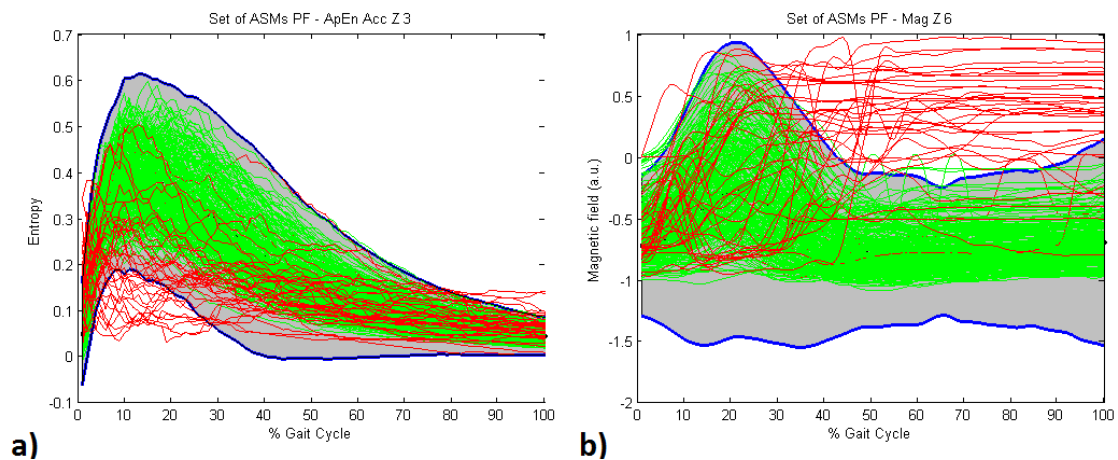


Figure 7.38 – Histogram of the number of failures per metric – ASM PF.



a) ApEn_Acc_Z_3; b) Mag_Z_6 (Green – Successful motion periods; Red – Unsuccessful motion periods; Blue – Weighted STD).

In order to summarize all relevant information in tables, Table 7.15 contains the best combination of parameters for each ROC analysis, as well as the value of the minimal Euclidian distance. On the other hand, Table 7.16 contains the values of the sensitivity, specificity, detection score, false positive rate, and false negative rate for each ROC analysis.

Table 7.15 – Best combinations of parameters and the minimal Euclidean distance for each ROC analysis

ASM set (ROC analysis)	z	M	N	Minimal Euclidean Distance
ASM WF**	3.2	5	6	0
ASM WF*	3.4	3	2	0.2874
ASM WF	2.8	6	6	0.0097
ASM Global*	3.2	3	1	0.2988
ASM Global	4.2	4	1	0.0194
ASM Fall	1.7	6	4	0.2553
ASM PFD	1.8	5	4	0.6018
ASM PF	3.4	5	1	0.0194

Table 7.16 – Metrics of each ROC analysis (TPR – True Positive Rate)

Metric	ASM WF**	ASM WF*	ASM WF	ASM Global*	ASM Global	ASM Fall	ASM PFD	ASM PF
Sensitivity (TPR)	100%	75%	100%	75%	100%	81.55%	45.95%	100%
Specificity (SPC)	100%	85.82%	99.03%	83.64%	98.06%	82.35%	73.53%	98.06%
Detection score	1.41	1.14	1.407	1.12	1.4006	1.159	0.8671	1.4006
False Positive Rate (1-SPC)	0%	14.18%	0.97%	16.36%	1.94%	17.65%	26.47%	1.94%
False Negative Rate (1-TPR)	0%	25%	0%	25%	0%	18.45%	54.05%	0%

7.2. Stage 2

The second stage focuses on the construction of a classifier of motion periods based on the constructed sets of ASMs, and this is therefore possible only with the results of the first stage. The first step was the construction of a decision cascade based on built sets of ASMs with the intention of classifying a motion period as one of four things, namely: 1) normal gait; 2) F; 3) PF step; and 4) other type. The decision cascade is shown in Fig. 7.40 and its explanation is given below.

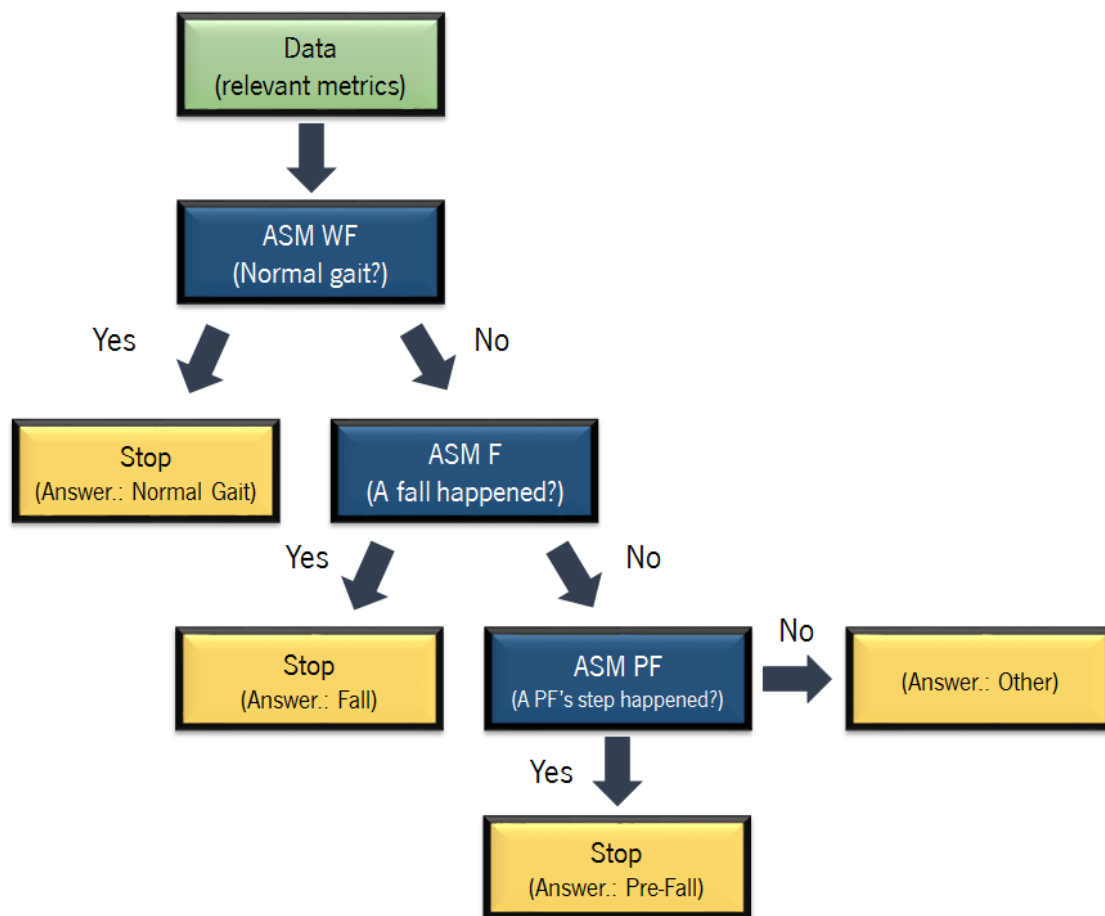


Figure 7.40 – Decision cascade to classify collected motion periods.

Decision cascade uses relevant metrics to classify motion periods. As first step, it was decided to check if the motion period is considered as normal set (Normal gait). If a non-failure happens then the all process is stopped and the motion period is labelled as “Normal gait”. Otherwise, it is necessary to verify other conditions. The first condition to be checked is the falling situation. In this situation, a F is detected if a non-failure situation is detected, which means that the motion period’s data should be inside the weighted STD of the respective set of ASMs. If a

failure is detected in the ASM_F, then the PF's condition is the last one to be verified. Once again, if a failure is detected, the final answer is "Other" which will label the motion period. Otherwise, a PF's motion period is detected.

The order to check or classify the motion period was decided based on the results of the first stage. Basically, the WF's set of ASMs obtained the best results, even when compared to the results of the Global's set of ASMs. Then, between F's set of ASMs and PF's set of ASMs, the first one had better results. So, in order to have better results in the classification process, the presented order in Fig. 7.40 was established. To test the decision cascade was used the test's data of the stage 1, and two considerations were made separately. The first consideration is to treat PF's data as different from F, WF and Global's data. The other consideration is to treat PF's data as normal gait like WF and Global's data.

7.2.1. Results

A total of 343 motion periods were used (WF – 32; Global – 243; F – 34; PF - 34) to test the decision cascade. The results of the first consideration are available on the Table 7.17. In this consideration, the parameters used for WF's set of ASMs were $z=3.4$, $M=3$, and $N=2$, and the parameters used for PF's set of ASMs were $z=1.8$, $M=5$, and $N=4$. On the other hand, Table 7.18 contains the results of the second consideration. This time, the parameters of the WF's set of ASMs were $z=2.8$, $M=6$, and $N=6$, and the parameters used for PF's set of ASMs were $z=3.4$, $M=5$, and $N=1$. The respective accuracies will be also presented.

Table 7.17 – Results of the decision cascade when PF's data were considered as different from the other types of data

Locomotion mode	Normal Gait	F	PF	Other	Well Classified	Percentage (%)
WF	29	1	0	2	29	90.63%
Global	207	2	3	31	207	85.19%
F	0	26	0	8	26	76.47%
PF	17	2	10	5	10	29.41%

The first result is not optimal due to the low percentages in the recognition of PF's gait cycles, but can be considered as good. Obviously, from the results of the first stage, it is possible

to retain that PF's data is more close to the WF and Global's data than F's data. However, from the 343 motion periods, 272 were well classified. Thus, under these circumstances, the accuracy of this decision cascade is 79.3%.

Table 7.18 – Results of the decision cascade when PF's data were considered like WF and Global's data

Locomotion mode	Normal Gait	F	PF	Other	Well Classified	Percentage (%)
WF	32	0	0	0	32	100%
Global	242	0	1	0	243	100%
F	0	26	0	8	26	76.47%
PF	32	0	1	1	34	97.06%

When PF's data were considered as normal gait or similar to WF and Global's motion periods, the results improved. 334 motion periods were well classified in a total of 343. PF's data were classified as normal gait mostly. Only 1 motion period was identified as PF. The accuracy of the decision cascade was 97.38%.

7.3. Stage 3

7.3.1. Convolutional Neural Networks

Deep learning is a machine learning technique that learns features and tasks directly from data, where data can be images, text, or sound. This key technology achieves recognition accuracy at higher levels than ever before. Due to recent advances, deep learning has been improved to the point where deep learning outperforms humans in some tasks classifying objects in images. Although deep learning was idealized in the 1980s, it only began to be useful recently due to two main reasons: Deep learning requires i) large amounts of labelled data; and ii) substantial computing power (high-performance GPUs have a parallel architecture that is efficient for deep learning) [190].

Neural network architectures are commonly used in most deep learning methods, and the term “deep” usually refers to the number of hidden layers in the neural network (Fig. 7.41). Traditional neural networks only have 2-3 hidden layers, while deep networks can have a high number e.g. 150 [190].

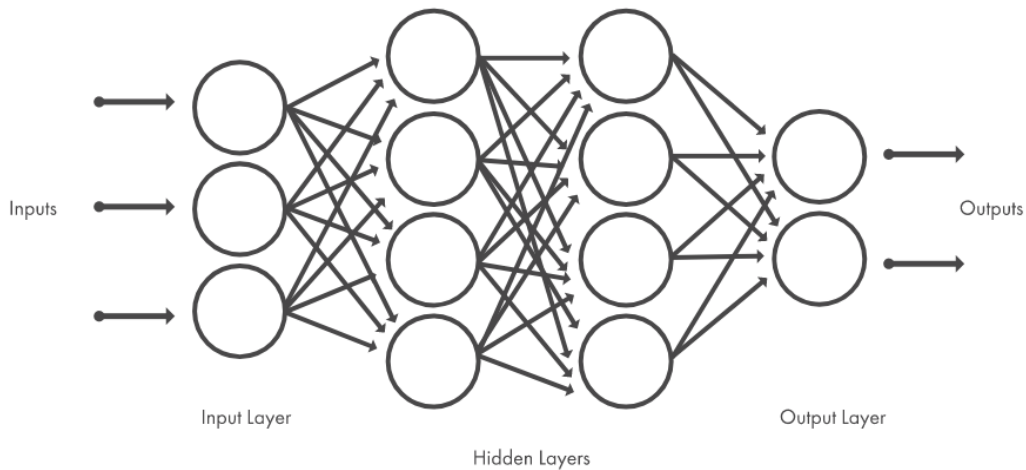


Figure 7.41 - Layers that constitute a neural network, which consist of a set of interconnected nodes [190].

CNNs are essential tools for deep learning and were inspired from the biological structure of a visual cortex, which contains arrangements of simple and complex cells [191]. A CNN convolves learned features with input data, and uses 2D convolutional layers, making this architecture well suited to processing 2D data, such as images [190], [192]. This type of deep neural network eliminates the need for manual feature extraction, which is the big difference between machine learning and deep learning, so it is not necessary to identify features to classify images. In turn, features are extracted directly from images. The relevant features are not pre-trained. They are learned while the network trains on a collection of images instead [190], [192]. Thus, deep learning models can be highly accurate.

In this work, deep learning (CNN) was chosen over machine learning because CNN provides automatic feature extraction and a high-performance GPU is available for training process [190]. The number of types of data (3 labels – Normal gait, PF, and F) is quite small, and the number of collected motion periods is of the order of a thousand, more specifically, 1368.

Since CNN is a classifier by nature, it is not necessary to use all metrics from all previously constructed sets of ASMs. This time, only the 41 relevant metrics obtained from the PCA procedure that used Global's data will be used in the CNN, because this particular PCA procedure is the most valid one. In fact, it is the only PCA procedure done that the number of observations is greater than the number of variables. Thus, each motion period will be represented as a matrix with 100 rows (samples) and 41 columns (metrics).

As CNN it was used an online available Matlab® toolbox *hagaygarty/mdCNN* supporting 1D, 2D and 3D kernels [193]. Once each motion period is represented by a matrix, each one will be regarded as an image (2D). The default size of each input image is 28x28 [193], so each motion

period will be first resampled and then resized, as depicted in Fig. 7.42. As in the first stage, the same training data will be used to train the CNN, and the same test data will be used to get the accuracy of the classifier. Finally, two neural networks were trained and tested. One considered PF's data as normal gait (Case 1), and the other considerer PF's data as different from the other locomotion modes (Case 2). Results of the accuracy were obtained for both situations.

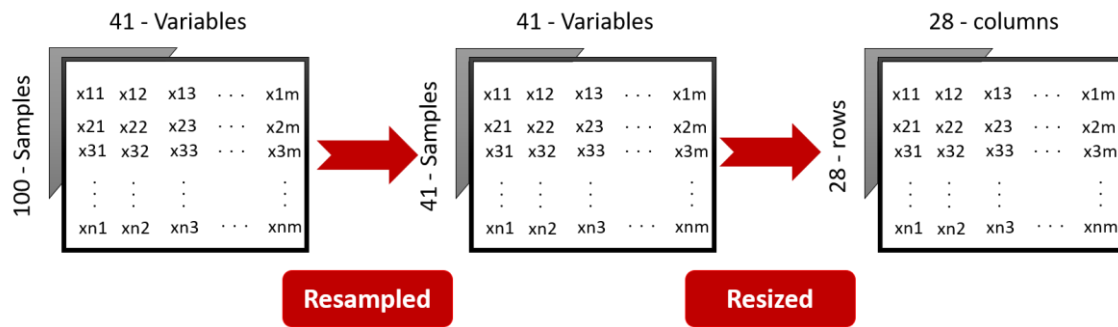


Figure 7.42 – Processes of resampling and resizing to use data as input in the CNN.

7.3.2. Results

For the first case, the trained CNN was able to achieve 100% of accuracy with the test data, exemplarily distinguishing the normal gait from F's situations. In the second case, the results were less good, having the trained CNN reached an accuracy of 81.92%. From 275 normal gait cycles, 230 were identified as normal gait, and the rest 44 were classified as PF's situation and 1 as F's situation. The total of 34 F's motion periods were identified correctly. Finally, from 34 PF's motion periods, only 17 were correctly identified, and the rest was included in the group of normal gait. The following table contains the results of the second case. Overall, the accuracy in both cases were better when compared to the results of the last stage.

Table 7.19 – Results of the Case 2 of the stage 3 (Input image: 28x28)

Locomotion mode	Normal Gait	F	PF	Total	Success rate (%)
WF & Global	230	1	44	275	83.64%
F	0	34	0	34	100%
PF	17	0	17	34	50%

Since the input image's default size 28x28 represents loss of information, the size of the input image was changed to 100x41. The exact same size of the matrix that contains the relevant information of each motion period. This last attempt to get better results was only performed when

PF's data were considered as different from other types of data, because in the other situation the accuracy was 100% and it can't be improved. With this change, the accuracy improved to 92.71%, which is a great result. All F's motion periods were all classified correctly. In a total of 34 PF's motion period, 30 were well identified and 4 were considered as normal gait. 254 normal gait cycles were well classified, and only 21 were considered as PF's motion period. The results are available in Table 7.20.

Table 7.20 – Results of the Case 2 of the stage 3 (Input image: 100x41)

Locomotion mode	Normal Gait	F	PF	Total	Success rate (%)
WF & Global	254	0	21	275	93.26%
F	0	34	0	34	100%
PF	4	0	30	34	88.24%

7.4. Stage 4

In the last stage, a new set of small indoor trials was performed in order to test the implemented classifiers in a different and more complex scenario. Thus, a subject (Male, 23 years old, 1.83m, 65Kg) perform a simple walking trial where at the end he could F on a sofa or stop. A total of 6 trials were performed, where in 3 the subject simulated a F, and in the other 3 he just stopped instead of F. This walking trial consists in walk forward, turn to the right, climb a small step, and stop or F on the sofa in the delineated finish line. Figure 7.43 depicts the top view of the walking trial.

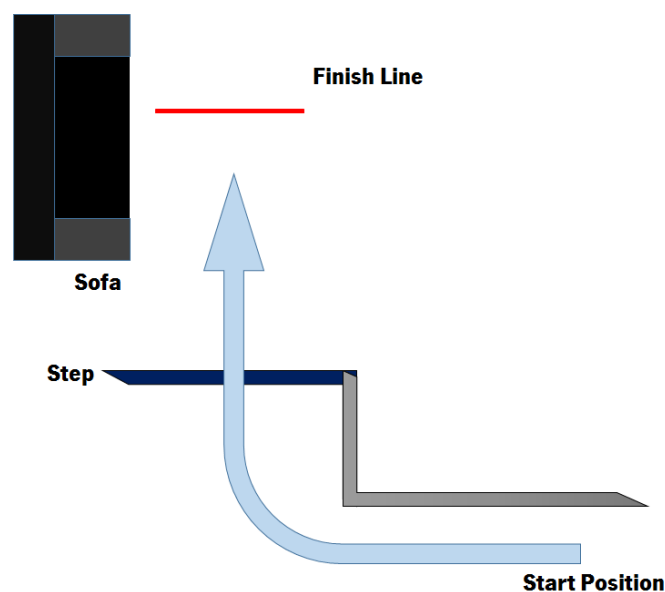


Figure 7.43 – Top view of the walking trial performed in stage 4.

As performed in the last stages, two considerations will be taking into account, namely: i) PF's data will be considered as normal gait (Case 1); and ii) PF's data will be considered as different from the other locomotion modes (Case 2). Results of the accuracy were obtained for both situations and for both classifiers. In the first case, there will only be 2 labels (normal gait - 1; F's situation - 2). In the other case, there will be 3 labels (normal gait - 1; F's situation - 2; PF's situation - 3).

Starting with the ASMs based classifier, the results for the first case are depicted in Table 7.21, where the accuracy of the classifier was 83.33%. On the other hand, Table 7.22 contains the same information as the previous table but for the second case. This time the accuracy was 45.83%.

Table 7.21 – Results of the Case 1 of the stage 4 (ASMs based classifier)

Locomotion mode	Normal Gait	F	PF	Other	Total	Success rate (%)
WF & Global	18	0	0	0	18	100%
F	1	0	1	1	3	0%
PF	2	0	0	1	3	66.67%

Table 7.22 – Results of the Case 2 of the stage 4 (ASMs based classifier)

Locomotion mode	Normal Gait	F	PF	Other	Total	Success rate (%)
WF & Global	11	0	0	7	18	61.11%
F	0	0	0	3	3	0%
PF	1	0	0	2	3	0%

Concerning the CNN classifier, the results for the case 1 are shown in Table 7.23, where the accuracy was 91.67%. In turn, the information about the case 2 is available on Table 7.24. Under these circumstances the accuracy was 75%.

Table 7.23 – Results of the Case 1 of the stage 4 (CNN)

Locomotion mode	Normal Gait	F	Total	Success rate (%)
WF & Global	18	0	18	100%
F	2	1	3	33.33%
PF	3	0	3	100%

Table 7.24 – Results of the Case 2 of the stage 4 (CNN)

Locomotion mode	Normal Gait	F	PF	Total	Success rate (%)
WF & Global	16	0	2	18	88.89%
F	2	1	0	3	33.33%
PF	2	0	1	3	33.33%

7.5. Discussion

The PCA procedure proved to be very important, due to the reduction of the number of metrics from 228 to 61 non-repeatable between types of data. With this reduction, it was expected that not only would the relevant information continue to the next steps, but also the computational weight would be reduced and thus the processing time shortened. Another important fact about these results is the high predominance of the Mag and metrics derived from Mag in the outcomes of the PCA procedures. Obviously, this can be a complicated issue in future works due to the ferromagnetic influences in indoor environments. In these tests, trials were performed in an environment free of these ferromagnetic influences, however results will be totally different if trials are carried out in indoor environments, not only in the PCA procedures but also in the next steps of this failure detection system. Furthermore, only one PCA procedure has more observations than variables. However, the results are close to each other. At least, there are 25 common metrics between all different locomotion modes.

Concerning the results of the ASMs block, it is certain that results show that the PF's data is very close to normal gait data (WF & Global). Every time PF's data was considered similar to WF and Global's data, the results were optimal. On the other hand, when PF's data were considered as different from other types of data the results were greatly reduced. For example, when the PF's set of ASM was constructed, its sensitivity was less than 50%. The study of the number of failures per metric, represented by several histograms, reveals that, generally, data from the x-axis of the Mag of all sensing devices have no leakage record beyond the weighted standard deviation values. There is only one exception when the PF's set of ASMs was constructed and the weighted STD was low. In this particular situation, those metrics have failed greatly. These metrics are measured on a perpendicular axis to the sagittal plane, which means that they are measured on a perpendicular axis to the direction of movement. Still, Mag_Z_3, Acc_Z_13, Mag_Z_13, and WD_Mag_Z_13 were the variables that have been outside the normal range of the respective ASM values more

times. All of them are parallel to the direction of movement. Thus, the results presented for this study were expected.

Finally, the results of the ASMs based classifier and the CNN were very impressive and promising due to the high accuracy presented in both classifiers and also due to the used amount of data. Obviously, it would be expected that the CNN would have better results. In fact, in both scenarios, that was verified. When PF's data were considered as normal gait, the accuracy was 100% for the CNN and 97.38% for the ASMs based classifier. On the other hand, when PF's data were considered as different from other types of data, the accuracy was 81.92% for the CNN and 79.3% for the other classifier. However, the difference is quite small between values, which highlights the ASMs based classifier when compared to a deep learning technique. One fact that highlights the ASMs is the fact that only the ASMs based classifier can indicate the moment of failure, which is truly important to know better the human gait and to direct studies to more specific parts of the human gait. This is the only way to gain a deeper understanding of F prevention.

Concerning the tests with the CNNs, when the size of the input image was changed to use all information of each motion period, the accuracy improved to 92.71% in the second case (PF's data as different from other types of data). This result is very impressive and demonstrates that, in fact, PF's data have differences from normal gait. Perhaps, more data will help ASMs based classifier to achieve better results under these circumstances.

Taken into account the results of the stage 4, it is possible to claim that CNN had a better performance over the ASMs based classifier again. The performed trials had different movements from those recorded previously to construct both classifiers. The inclusion of a step, a curve, and a F on a sofa make classification much more difficult for classifiers. Even, in this situation, the F is not complete, because, in previous trials, the F was complete near the ground, which it is not happening in this particular case.

Chapter 8 – Conclusions

As described throughout this master's thesis, IMUs or sensing devices are devices with a wide range of applications in human gait, where their use can bring about quite interesting advantages when compared to other techniques and approximates the gait monitoring to the AAL environments. Nowadays, this device, whose constitution is easy to understand, presents innumerable variants of its concept through trademarks that constantly try to overcome the disadvantages of this device, making it more perfect. However, research groups have also contributed greatly to this evolution.

Currently, a considerable number of people present abnormal gait patterns as consequence of neurological diseases or muscular weakness. Consequently, the occurrence of Fs in these people is seen as a major risk that can lead people to fatal or non-fatal injuries, which are very costly. Therefore, it is necessary to achieve effective methodologies to assist and rehabilitate the impaired walking. According to the state of the art in Fs, one thing is granted: Fs are a huge problem to the elderly population and any effort to avoid or prevent a F can save many lives. Research groups and commercial brands focused in F detection systems based in sensors that constitute IMUs, however, they realized that only detecting Fs would not be enough to prevent or save lives. So, it is necessary to create F risk assessment models to diagnose patient's risk and give them the proper treatment, although still having the gap of not preventing impact in case of F, being necessary to estimate Fs or detect PFs. Thus, PF detection systems became crucial devices that can actually save lives by detecting a F some time before it happens. Some studies achieved great results, however it really needs to be more accurate, reliable, and practical, and future works will focus on these aspects essentially through support vector machines or other types of classifiers.

Chapter 4 addresses the improvement of a real time monitoring gait system able to provide for an intuitive real time visual interface and real-time data visualization and recording with 3D IMUs. The first and most important conclusion to be drawn from this chapter is that in fact the use of an intuitive interface greatly facilitates the interaction between the user and the presented system. In addition, the interface created has all the proposed requirements obtained from a previous analysis of the system. Consequently, the use of this system is much more practical and interactive. The intervention of a large group of survey participants also greatly helped to

understand the strengths and weaknesses of the interface, and in general the participants considered the Matlab® GUI as "Good", which reaffirms that the objectives initially proposed were achieved. Based on these assessments some changes were delineated and included in the proposed GUI.

Concerning the validation process of the IMUs based system in Chapter 5, it is possible to conclude that this system can be used to collect data from gait's trials and separate and process data correctly. According to the communication protocol's experiment, it is consensual that the presence of other wireless communications affect the good performance of the system. So, in order to overcome this difficulty, it would be advantageous to change the frequency band of the communication protocol depending on the location where the data is collected. Therefore, an unused frequency band or a frequency band in which its signal is weak should be chosen. The distance between sensory modules and the base station can also affect the number of lost frames. The presence of electrically conductive metals such as copper inside the laboratory, can reflect and absorb the radio waves and consequently interfere with their transmission. Thus, this can also be a reason why so many frames were lost in this environment and in the corridor. The number of sensory modules can also affect the loss of frames due to overlapping of message signals or frames. However, the gait speed has almost no influence on the loss of frames.

According to the verification of the sensors' typical signals, it is possible to claim the validity of the system due to the similarities between the typical signals presented in the scientific literature and those measured by the IMUs based system. Concerning the comparisons performed in the foot and in the thigh, IMUs' system had a good behaviour measuring correctly the walk forward event. In the first topic, Mag proved to be the one with least noise, and in the second topic, Gyro proved to be ready to measure normal thigh variations. On the last topic (Lower back), there was no complete similarity due to gait speed. From this experiment it is highly recommended the use of a low-pass filter to reduce the noise presented in the sensors' measures.

The results for knee F-E angles are in accordance with the literature. This error range is within the values found in the gait analysis literature when using IMUs. The implemented knee angle measurement system based on IMUs is able to be used in gait analysis, however in future work the results can be improved with other calibration methods or a post-processing procedure. Further, note that the determination of the angles was out of the scope of this work and the author would have to check if other methods instead of the ones used for orientation estimation would provide for better results.

Taking into account the calibration tests, chapter 6, it is possible to claim that the PM, theoretically, should be the calibration method if the sensors were ideal. However, its results show a small error when compared to other methods. Even Gyro's offsets measured on-body were very close to those measured in a horizontal surface. Once again, and as in the previous validation results, the RMSE values of the several calibration's methods when compared to an optical reference are in accordance with the scientific literature. In general, calibration's procedures make the IMUs' system more accurate in estimating the angles of the sensory modules.

In this thesis, the major concepts of human gait classification were demonstrated offline and detailed comparisons were evaluated due to the implementation of two different methods present in literature, namely: ASMs and CNNs. From these results, it was concluded which is the more adequate procedure to apply in the human classification. In fact, it was concluded that the combination of different types of features (gait parameters or metrics) provides a more robust tool for detection of user's locomotion since each type of feature contributes with distinct information regarding the gait pattern. Additionally, it was concluded that the selection of the most discriminative features contributes either to improve the performance of the locomotion mode recognition, either to reduce the computation cost of this process. In this case, PCA revealed itself as an important procedure in this metrics' reduction. According to the PCA procedure, the results from this part revealed that Mag's sensors or metrics derived from this sensor are relevant. However, this can be dangerous if the IMUs' system is used in indoor environments where the ferromagnetic influence is high.

Concerning the classification phase of the locomotion mode recognition, the CNN classifier was selected for implementation due to its advantages as pointed out in the revised studies. Its results were better than the ASMs based classifier. However, in the way it was implemented, it is not possible to know when a change was detected. On the other hand, the ASMs based classifier provides this information. Indeed, the characteristics of this supervised machine learning approach that supports its better results are: convergence to a global optimal, avoiding the local minima and over-fitting in the training process; ability to minimize both structural and empirical risk leading to a better generalization for new data classification even with a limited training data set, producing stable and reproducible results; capacity of operate with nonlinear and multidimensional data, as parameters of gait.

The work herein presented enables to answer the RQs outlined in Chapter 1.

- **RQ1:** What are the most used sensors to perform gait monitoring? Can the drift be compensated in the IMUs based system? And under what conditions? This RQ is addressed in Chapter 2.

According to the literature, there are several techniques to monitor human gait. However, in the wearable field, the most used sensors are Acc, Gyr and Mag. Based on the surveys accomplished in this thesis, drift cannot be removed entirely from the estimation of angles. However, it can be greatly reduced by the use of a Mag as an input in a sensor fusion's algorithm. Without this sensor, the error is higher. The estimated angles by an IMU when compared to an optical reference would be more different as time goes by, and the RMSE value between signals would increase. Overall, drift occurs more in indoor environments due to the ferromagnetic influence. In this type of environment, the Mag does not give reliable measures, and generally it is not used. Usually, the use of sensor fusion algorithms helps in the reduction of this error.

- **RQ2:** What are the most commonly used sensors in F or PF detection systems? This RQ is addressed in Chapter 3.

The commonly used sensors in the field of Fs are the sensors that constitute sensing devices. They are essentially used in commercial devices that detect F's situations. Through this sensors it is possible to obtain metrics such as e.g.: SVM, SMA, ASMA, or SVd.

- **RQ3:** To what extent does the GUI help to improve the user-system relationship? What is the reliability of the proposed ALSM? This RQ is addressed in Chapter 4.

To overcome the limitations of the IMUs based system of the CMEMS, a Matlab GUI was created to fulfil certain requisites. According to a performed inquiry, users identified the GUI as intuitive and easy to use. In general, the opinions about the Matlab GUI were positive. This interface helps to understand what is happening in real-time. All information of the system is there. Concerning the ALSM, it was used several times with no failures or loss of information.

- **RQ4:** Considering the used wireless IMUs based system, how many IMUs can be connected to the base station without problems? What can be done to increase the number of connected modules? This RQ is addressed in Chapter 5.

At least 3 modules can be connected to the base station without problems in any environment. With this number of modules, the percentage loss of frames is low, and at a short distance from the base station it is near 0%. If the user pretends to use more modules with few losses of frames, he needs to pay attention to the following points: i) Use the modules as close to the base station as possible; ii) Select the freer frequency's channel; iii) Use fully charged batteries; and iv) Do not use the modules too close to each other.

- **RQ5:** Given the sampling frequency of the system, is it possible to get the data of the human gait correctly? This RQ is addressed in Chapter 5.

In this master's thesis, a comparison between sensors' signals measured by the IMUs based system and typical signals from the scientific literature was performed. In there it is possible to see some examples of typical signals and the homologous signal measured by the CMEMS' system, and the similarities are huge. So, by using a 30 Hz as sampling frequency it is possible to acquire data of the human gait correctly. Theoretically, a human stride is given per 1-2s, which represents a range of frequency of 0.5-1 Hz. So, the sampling frequency of 30 Hz respects the Theorem of Nyquist.

- **RQ6:** Is it possible to perform an on-body calibration without major errors? This RQ is addressed in Chapter 6.

In Chapter 6 was proved that the Gyro's offsets measured on-body were very close to those measured in a horizontal surface. Concerning other sensors (Acc and Mag), what should be measured equally by all axes does not happen. In fact, there are no ideal sensors that measure equally in all directions. However, the error's difference to other calibration methods is relevant, although the error in the calculation of the angles is in agreement with the literature.

- **RQ7:** Which are the metrics with greater potential to detect F and PF's situations in the implemented classifiers? This RQ is addressed in Chapter 7.

Mag's sensors or metrics derived from this sensor measured in the anteroposterior direction are the metrics with greater potential do detect these particular situations, according to the results obtained in the Chapter 7. Obviously, it was expected that metrics with components in

the direction of the movement could have more importance or relevance in this area, because they vary much more than those that are measured in a perpendicular direction.

- **RQ8:** Which is the best classifier to be used in the recognition of normal gait, F and PF's modes of locomotion? This RQ is addressed in Chapter 7.

In Chapter 7 was proved that the CNN based classifier presented better results in terms of accuracy. However, it has some disadvantages since this CNN was not constructed by the author or the team. With the CNN based classifier it is not possible to know what metrics failed or when it failed. At the moment, only the ASMs based classifier is able to give that information. Perhaps more gait data will allow better results in both classifiers, and possibly bring the ASMs based classifier closer to the CNN based classifier.

Hereupon, it is concluded that the delineated goals and RQs raised in introduction of this thesis were addressed. Besides, it was verified that the developed work during the master's thesis improved the applicability of the IMUs based system from CMEMS, as well as contributed to knowledge with a general and robust tool for offline detection of F and PF's situations. Consequently, the classification strategies herein proposed and validated become closer to the ideal system that contains a F detection system and a F forecasting system.

8.1. Future work

As future work it is necessary to realize experiments of subjects walking in other different locomotion modes, such as ascending/descending stairs; start/stop walking; sit-to-stand/stand-to-sit; walking with changes in speed; and others. As well as collecting data from different types of F. Basically it is pretended to have a system capable not only to say if a normal gait or a F or PF's situation is happening, but also how it is happening and what the subject is doing. Also more data from more trials will increase greatly the classifier's accuracy. In the case of the CNN, it requires a huge amount of data in order to the results being more reliable.

The implementation of the classifiers was only offline. Nevertheless, an online implementation in the IMUs based system would be a great step to a new and innovative product as long as the results of the classifiers with new and more data were promising. It is also suggested an additional reduction of the metrics so that the computational weight decreases and, therefore, the data processing is faster. Given the results of Chapter 7, it is possible to retain that there are

metrics that never leave the limits of their ASMs. Therefore, a study on the influence of the disappearance of these metrics on the accuracy of the classifier should be done. Another statistical method, which also removes the relevant metrics, must be experienced. The metrics excluded in this study (e.g. stride length, walking velocity or other metrics with one value per gait cycle) should also be included in this study in the future. Moreover, an important study about the time of detection of F and PF's situations will be truly important.

Additionally, in order to overcome the lack of a database of human gait, it would be interesting to build such database with relevant gait parameters acquired from healthy and/or elderly subjects during walking over different conditions of speed and ground, and using an IMUs based system. Obviously, IMUs should be in specific positions of the body according to a specific orientation. This database could be available to be used for diverse tasks relative to the gait analysis, and also it could be used to increase the data of the used CNN and get more accurate results.

The IMUs' system can also be improved in the future with some changes at the hardware level. Firstly, the antennas should be changed to narrow beam adaptive antennas in order to prevent or mitigate the risk of interference. The battery should be also changed to smartphone's batteries with the same voltage due to their high value of milliampere hour (mAh). Sometimes, this value of mAh is ten times superior when compared to the value of the current batteries of the system. Besides, smartphone's batteries are rechargeable and durable. The base station can also be programmed to select automatically the least used frequency channel every time the system is used. Then, the entire system should be tested for different sampling frequencies and distances between IMUs and the base station in different environments. Meanwhile, the team is planning to develop a new IMU-based system.

As a future work, it is also suggested to execute trials with the base station and the sensory modules in different rooms of an indoor environment. A future study that focus on the interference of conductive metals in this system it is highly recommended, which may allow meet new limitations, as well as new resolutions of existing problems. And concerning the validation of the joint angle measurement system, it is proposed that adduction/abduction and internal/external rotation angles should also be performed in the validation process.

Concerning the Matlab® GUI, there are some improvements that should be made in order to get closer to commercial softwares. Add a real-time virtual 3D visualization of the monitored

subject without all the problems that it entails, and information panels about the real-time status of the subject obtained from the constructed online classifier.

References

- [1] J. Rueterbories, E. G. Spaich, B. Larsen, and O. K. Andersen, "Methods for gait event detection and analysis in ambulatory systems," *Med. Eng. Phys.*, vol. 32, no. 6, pp. 545–552, 2010.
- [2] D. J. Fish, "Pathology Forum: Characteristic Gait Patterns in Neuromuscular Pathologies," *J. Prosthetics Orthot.*, vol. 9, no. 2, pp. 163–167, 1997.
- [3] A. Muro-de-la-Herran, B. Garcia-Zapirain, and A. Mendez-Zorrilla, "Gait analysis methods: An overview of wearable and non-wearable systems, highlighting clinical applications," *Sensors (Switzerland)*, vol. 14, no. 2, pp. 3362–3394, 2014.
- [4] S. D. Berry and R. Miller, "Falls: Epidemiology, Pathophysiology, and Relationship to Fracture," *Curr. Osteoporos. Rep.*, vol. 6, no. 4, pp. 149–154, 2008.
- [5] Institute of Medicine, *The Second Fifty Years: Promoting Health and Preventing Disability*. Washington, D. C., 1992.
- [6] S. Heinrich, K. Rapp, U. Rissmann, C. Becker, and H. H. K??nig, "Cost of falls in old age: A systematic review," *Osteoporos. Int.*, vol. 21, no. 6, pp. 891–902, 2010.
- [7] E. R. Burns, J. A. Stevens, and R. Lee, "The direct costs of fatal and non-fatal falls among older adults - United States," *J. Safety Res.*, vol. 58, pp. 99–103, 2016.
- [8] M. A. Hanson, H. C. Powell, A. T. Barth, J. Lach, and B. P. Maité, "Neural network gait classification for on-body inertial sensors," in *Proceedings - 2009 6th International Workshop on Wearable and Implantable Body Sensor Networks, BSN 2009*, 2009, pp. 181–186.
- [9] S. Nadeau, C. Duclos, L. Bouyer, and C. L. Richards, "Guiding task-oriented gait training after stroke or spinal cord injury by means of a biomechanical gait analysis," *Prog. Brain Res.*, vol. 192, pp. 161–180, 2011.
- [10] SENSO 2012, "SENSO Supports," 2012. [Online]. Available: <https://www.senso-connect.com/our-fall>. [Accessed: 29-Mar-2017].
- [11] Tunstall Healthcare, "iVi Intelligent Pendant." [Online]. Available: <http://www.tunstall.co.uk/solutions/ivi>. [Accessed: 29-Mar-2017].
- [12] T. Tamura, T. Yoshimura, M. Sekine, M. Uchida, and O. Tanaka, "A wearable airbag to prevent fall injuries," *IEEE Trans. Inf. Technol. Biomed.*, vol. 13, no. 6, pp. 910–914, 2009.

- [13] P. Macedo, J. A. Afonso, L. A. Rocha, and R. Simoes, "A Telerehabilitation System Based on Wireless Motion Capture Sensors," in *PhyCS - Proceedings of the International Conference on Physiological Computing Systems*, 2014, pp. 55–62.
- [14] W. Tao, T. Liu, R. Zheng, and H. Feng, "Gait analysis using wearable sensors," *Sensors*, vol. 12, no. 2, pp. 2255–2283, 2012.
- [15] S. L. Patterson, M. M. Rodgers, R. F. Macko, and L. W. Forrester, "Effect of treadmill exercise training on spatial and temporal gait parameters in subjects with chronic stroke: A preliminary report," *J. Rehabil. Res. Dev.*, vol. 45, no. 2, pp. 221–228, 2008.
- [16] T. Liu, Y. Inoue, and K. Shibata, "Development of a wearable sensor system for quantitative gait analysis," *Meas. J. Int. Meas. Confed.*, vol. 42, no. 7, pp. 978–988, 2009.
- [17] S. T. Boerema, L. Van Velsen, L. Schaake, T. M. Tonis, and H. J. Hermens, "Optimal Sensor Placement for Measuring Physical Activity with a 3D Accelerometer," *Sensors (Switzerland)*, vol. 14, pp. 3188–3206, 2014.
- [18] E. Campo, S. Bonhomme, M. Chan, and D. Esteve, "Remote tracking patients in retirement home using wireless multisensor system," in *e-Health Networking Applications and Services (Healthcom), 2010 12th IEEE International Conference on*, 2010.
- [19] S. Beynon, J. L. Mcginley, F. Dobson, and R. Baker, "Correlations of the Gait Profile Score and the Movement Analysis Profile relative to clinical judgments," *Gait Posture*, vol. 32, no. 1, pp. 129–132, 2010.
- [20] M. Sekine, T. Tamura, M. Akay, T. Fujimoto, T. Togawa, and Y. Fukui, "Discrimination of Walking Patterns Using Wavelet-Based Fractal Analysis," *IEEE Trans. Neural Syst. Rehabil. Eng.*, vol. 10, no. 3, pp. 188–196, 2002.
- [21] D. A. Winter, "Kinematic and Kinetic Patterns in Human Gait: Variability and Compensating Effects," vol. 3, pp. 51–76, 1984.
- [22] Y.-C. Lin, B.-S. Yang, and Y.-T. Yang, "People Recognition by Kinematics and Kinetics of Gait," pp. 1996–1999, 2009.
- [23] F. Höflinger, J. Müller, R. Zhang, L. M. Reindl, and W. Burgard, "A Wireless Micro Inertial Measurement Unit (IMU)," *IEEE Trans. Instrum. Meas.*, vol. 62, no. 9, pp. 2583–2595, 2013.
- [24] N. Ahmad, R. A. R. Ghazilla, N. M. Khairi, and V. Kasi, "Reviews on Various Inertial Measurement Unit (IMU) Sensor Applications," *Int. J. Signal Proccesing Syst.*, vol. 1, no. 2, pp. 256–262, 2013.

- [25] E. Palermo, S. Rossi, F. Marini, F. Patanè, and P. Cappa, "Experimental evaluation of accuracy and repeatability of a novel body-to-sensor calibration procedure for inertial sensor-based gait analysis," *Meas. J. Int. Meas. Confed.*, vol. 52, no. 1, pp. 145–155, 2014.
- [26] P. Picerno, A. Cereatti, and A. Cappozzo, "Joint kinematics estimate using wearable inertial and magnetic sensing modules," *Gait Posture*, vol. 28, no. 4, pp. 588–595, 2008.
- [27] S. Kobashi, Y. Tsumori, S. Imawaki, S. Yoshiya, and Y. Hata, "Wearable knee kinematics monitoring system of MARG sensor and pressure sensor systems," *2009 IEEE Int. Conf. Syst. Syst. Eng.*, pp. 3–8, 2009.
- [28] S. Qiu, Z. Wang, H. Zhao, and H. Hu, "Using Distributed Wearable Sensors to Measure and Evaluate Human Lower Limb Motions," *IEEE Trans. Instrum. Meas.*, vol. 65, no. 4, pp. 939–950, 2016.
- [29] O. J. Woodman, "An introduction to inertial navigation," Cambridge, 696, 2007.
- [30] "LIS331DLH - MEMS digital output motion sensor ultra low-power high performance 3-axes 'nano' accelerometer," 2009.
- [31] P. A. Hölzl, B. G. Zagar, and S. Member, "Improving the Spatial Resolution of Magneto Resistive Sensors via Deconvolution," *IEEE Sens. J.*, vol. 13, no. 11, pp. 4296–4304, 2013.
- [32] M. D. Djurić-Jovičić, N. S. Jovičić, and D. B. Popović, "Kinematics of Gait: New Method for Angle Estimation Based on Accelerometers," *Sensors (Switzerland)*, no. 11, pp. 10571–10585, 2011.
- [33] A. Sant' Anna, N. Wickström, H. Eklund, R. Zöfner, and R. Tranberg, "Assessment of Gait Symmetry and Gait Normality Using Inertial Sensors: In-Lab and In-Situ Evaluation," in *Communications in Computer and Information Science*, vol. 357 CCIS, J. Gabriel, J. Schier, S. Van Huffel, E. Conchon, C. Correia, A. Fred, and H. Gamboa, Eds. Berlin, Heidelberg: Springer Berlin Heidelberg, 2013, pp. 239–254.
- [34] D. Novak *et al.*, "Automated detection of gait initiation and termination using wearable sensors," *Med. Eng. Phys.*, vol. 35, no. 12, pp. 1713–1720, 2013.
- [35] A. Laudanski, S. Yang, and Q. Li, "A concurrent comparison of inertia sensor-based walking speed estimation methods," *Proc. Annu. Int. Conf. IEEE Eng. Med. Biol. Soc. EMBS*, pp. 3484–3487, 2011.
- [36] A. Valtazanos, D. K. Arvind, and S. Ramamoorthy, "Using wearable inertial sensors for

- posture and position tracking in unconstrained environments through learned translation manifolds,” *Proc. 12th Int. Conf. Inf. Process. Sens. networks - IPSN '13*, p. 241, 2013.
- [37] Q. Li and J. Zhang, “Post-trial anatomical frame alignment procedure for comparison of 3D joint angle measurement from magnetic/inertial measurement units and camera-based systems,” *Physiol. Meas.*, vol. 35, no. 11, pp. 2255–68, 2014.
- [38] Xsens, “IMU Inertial Measurement Unit.” [Online]. Available: <https://www.xsens.com/?gclid=CN-voaCpl9ECFQ2eGwod-e800A>. [Accessed: 09-Nov-2016].
- [39] InterSense, “IMU Inertial Measurement Unit.” [Online]. Available: <http://www.intersense.com/>. [Accessed: 09-Nov-2016].
- [40] Technaid, “Motion Analysis.” [Online]. Available: <http://www.technaid.com/>. [Accessed: 09-Nov-2016].
- [41] I Measure U, “Maximise athletic potential unencumbered by injury.” [Online]. Available: <http://imeasureu.com/>. [Accessed: 09-Nov-2016].
- [42] Noraxon, “Human Movement Metrics - Research and Medical Solutions for EMG, Kinetics and Kinematics.” [Online]. Available: <http://www.noraxon.com/>. [Accessed: 09-Nov-2016].
- [43] SparkFun, “What is SparkFun?” [Online]. Available: <https://www.sparkfun.com/static/about>. [Accessed: 09-Nov-2016].
- [44] M. Benocci, L. Rocchi, E. Farella, L. Chiari, and L. Benini, “A Wireless System for Gait and Posture Analysis Based on Pressure Insoles and Inertial Measurement Units,” in *Pervasive Computing Technologies for Healthcare, 2009. PervasiveHealth 2009. 3rd International Conference on*, 2009.
- [45] J. Barton, A. Gonzalez, J. Buckley, B. O’Flynn, and S. C. O’Mathuna, “Design , Fabrication and Testing of Miniaturised Wireless Inertial Measurement Units (IMU),” in *Electronic Components and Technology Conference, 2007. ECTC '07. Proceedings. 57th*, 2007, pp. 1143–1148.
- [46] Y.-L. Tsai, T.-T. Tu, H. Bae, and P. H. Chou, “EcoIMU : A compact , wireless , gyro-free inertial measurement unit based on two triaxial EcoIMU : A Dual Triaxial-Accelerometer Inertial Measurement Unit for Wearable Applications,” no. January, 2011.
- [47] K. Y. Lim *et al.*, “A Wearable , Self-Calibrating , Wireless Sensor Network for Body Motion Processing,” in *IEEE International Conference on Robotics and Automation, 2008. ICRA*

2008, 2008, pp. 1017–1022.

- [48] L. Ambrozic, M. Gorsic, S. Slajpah, R. Kamnik, and M. Munih, “Wearable sensory system for robotic prosthesis,” in *International Journal of Mechanics and Control*, 2014, vol. 15, no. 1, pp. 53–59.
- [49] S. Tadano, R. Takeda, and H. Miyagawa, “Three Dimensional Gait Analysis Using Wearable Acceleration and Gyro Sensors Based on Quaternion Calculations,” *Sensors (Switzerland)*, vol. 13, pp. 9321–9343, 2013.
- [50] T. Seel, J. Raisch, and T. Schauer, “IMU-Based Joint Angle Measurement for Gait Analysis,” pp. 6891–6909, 2014.
- [51] M. M. Hamdi, M. I. Awad, M. M. Abdelhameed, and F. A. Tolbah, “Lower limb motion tracking using IMU sensor network,” *2014 Cairo Int. Biomed. Eng. Conf.*, pp. 28–33, 2014.
- [52] S. Lambrecht *et al.*, “Inertial sensor error reduction through calibration and sensor fusion,” *Sensors (Switzerland)*, vol. 16, no. 2, pp. 1–16, 2016.
- [53] A. Leardini, G. Lullini, S. Giannini, L. Berti, M. Ortolani, and P. Caravaggi, “Validation of the angular measurements of a new inertial-measurement-unit based rehabilitation system: comparison with state-of-the-art gait analysis,” *J. Neuroeng. Rehabil.*, vol. 11, no. 1, pp. 136–143, 2014.
- [54] F. Feldhege *et al.*, “Accuracy of a custom physical activity and knee angle measurement sensor system for patients with neuromuscular disorders and gait abnormalities,” *Sensors (Switzerland)*, vol. 15, no. 5, pp. 10734–10752, 2015.
- [55] G. Blumrosen and A. Luttwak, “Human Body Parts Tracking and Kinematic Features Assessment Based on RSSI and Inertial Sensor Measurements,” *Sensors (Switzerland)*, vol. 13, pp. 11289–11313, 2013.
- [56] D. Novak, M. Gorsic, J. Podobnik, and M. Munih, “Toward Real-Time Automated Detection of Turns during Gait Using Wearable Inertial Measurement Units,” pp. 18800–18822, 2014.
- [57] A. Ahmadi *et al.*, “3D Human Gait Reconstruction and Monitoring Using Body-Worn Inertial Sensors and Kinematic,” *J. IEEE SENSORS*, pp. 1–9, 2016.
- [58] Z. Fang, T. Yu, L. Chen, S. Chen, and C. Wang, “Optimal Thigh Dip Angle Reduction By Acceleration And Angular Velocity Sensing,” no. 2012, pp. 1158–1163, 2015.
- [59] S. Minto, S. Member, D. Zanotto, E. M. Boggs, and G. Rosati, “Validation of a Footwear-

- Based Gait Analysis System with Action-Related Feedback,” *IEEE Trans. Neural Syst. Rehabil. Eng.*, vol. 24, no. 9, pp. 1–10, 2015.
- [60] V. Joukov, M. Karg, and D. Kulic, “Online tracking of the lower body joint angles using IMUs for gait rehabilitation,” *Conf. Proc. ... Annu. Int. Conf. IEEE Eng. Med. Biol. Soc. IEEE Eng. Med. Biol. Soc. Annu. Conf.*, vol. 2014, pp. 2310–2313, 2014.
- [61] A. Laudanski, B. Brouwer, and Q. Li, “Measurement of Lower Limb Joint Kinematics using Inertial Sensors During Stair Ascent and Descent in Healthy Older Adults and Stroke Survivors,” *J. Healthc. Eng.*, vol. 4, no. 4, pp. 555–576, 2013.
- [62] F. Öhberg, R. Lundström, and H. Grip, “Comparative analysis of different adaptive filters for tracking lower segments of a human body using inertial motion sensors,” *Meas. Sci. Technol. Meas. Sci. Technol*, vol. 24, no. 24, pp. 85703–85703, 2013.
- [63] S. Sessa, M. Zecca, Z. H. Lin, L. Bartolomeo, H. Ishii, and A. Takanishi, “A Methodology for the Performance Evaluation of Inertial Measurement Units,” *J. Intell. Robot. Syst.*, vol. 71, no. 2, pp. 143–157, 2013.
- [64] G. Tao, Z. Huang, Y. Sun, S. Yao, and J. Wu, “Biomechanical model-based multi-sensor motion estimation,” *2013 IEEE Sensors Appl. Symp. SAS 2013 - Proc.*, pp. 156–161, 2013.
- [65] S. J. M. Bamberg, A. Y. Benbasat, D. M. Scarborough, D. E. Krebs, and J. a Paradiso, “Gait analysis using a shoe-integrated wireless sensor system.,” *IEEE Trans. Inf. Technol. Biomed.*, vol. 12, no. 4, pp. 413–23, 2008.
- [66] S. Zihajehzadeh, P. K. Yoon, B. S. Kang, and E. J. Park, “UWB-Aided Inertial Motion Capture for Lower Body 3-D Dynamic Activity and Trajectory Tracking,” *IEEE Trans. Instrum. Meas.*, vol. 64, no. 12, pp. 3577–3587, 2015.
- [67] T. Beravs, P. Reberšek, D. Novak, J. Podobnik, and M. Munih, “Development and validation of a wearable inertial measurement system for use with lower limb exoskeletons,” *11th IEEE-RAS Int. Conf. Humanoid Robot.*, no. October 26-28, pp. 212–217, 2011.
- [68] R. Takeda, S. Tadano, A. Natorigawa, M. Todoh, and S. Yoshinari, “Gait posture estimation by wearable acceleration and gyro sensor,” *IFMBE Proc.*, vol. 25, no. 9, pp. 111–114, 2009.
- [69] Y. Guo, G. Zhao, Q. Liu, Z. Mei, K. Ivanov, and L. Wang, “Balance and knee extensibility evaluation of hemiplegic gait using an inertial body sensor network.,” *Biomed. Eng. Online*, vol. 12, p. 83, 2013.

- [70] Y. Guo, D. Wu, G. Liu, G. Zhao, B. Huang, and L. Wang, "A low-cost body inertial-sensing network for practical gait discrimination of hemiplegia patients.," *Telemed. J. E. Health.*, vol. 18, no. 10, pp. 748–54, 2012.
- [71] K. Kawano, S. Kobashi, M. Yagi, K. Kondo, S. Yoshiya, and Y. Hata, "Analyzing 3D knee kinematics using accelerometers, gyroscopes and magnetometers," *2007 IEEE Int. Conf. Syst. Syst. Eng. SOSE*, 2007.
- [72] G. Ligorio, E. Bergamini, I. Pasciuto, G. Vannozzi, A. Cappozzo, and A. Sabatini, "Assessing the Performance of Sensor Fusion Methods: Application to Magnetic-Inertial-Based Human Body Tracking," *Sensors*, vol. 16, no. 2, pp. 1–14, 2016.
- [73] A. M. Sabatini, G. Ligorio, and A. Mannini, "Fourier-based integration of quasi-periodic gait accelerations for drift-free displacement estimation using inertial sensors," *Biomed. Eng. Online*, vol. 14, no. 1, p. 106, 2015.
- [74] S. Bakhshi, M. H. Mahoor, and B. S. Davidson, "Development of a body joint angle measurement system using IMU sensors," *33rd Annu. Int. Conf. IEEE Eng. Med. Biol. Soc. Conf.*, vol. 2011, pp. 6923–6, 2011.
- [75] N. C. Bejarano, E. Ambrosini, A. Pedrocchi, G. Ferrigno, M. Monticone, and S. Ferrante, "A novel adaptive, real-time algorithm to detect gait events from wearable sensors," *IEEE Trans. Neural Syst. Rehabil. Eng.*, vol. 23, no. 3, pp. 413–422, 2015.
- [76] Y. Chen, W. Hu, Y. Yang, J. Hou, and Z. Wang, "A method to calibrate installation orientation errors of inertial sensors for gait analysis," *2014 IEEE Int. Conf. Inf. Autom. ICIA 2014*, no. 61174027, pp. 598–603, 2014.
- [77] E. Palermo, S. Rossi, F. Patanè, and P. Cappa, "Experimental evaluation of indoor magnetic distortion effects on gait analysis performed with wearable inertial sensors.," *Physiol. Meas.*, vol. 35, no. 3, pp. 399–415, 2014.
- [78] J. Favre, R. Aissaoui, B. M. Jolles, J. A. de Guise, and K. Aminian, "Functional calibration procedure for 3D knee joint angle description using inertial sensors," *J. Biomech.*, vol. 42, no. 14, pp. 2330–2335, 2009.
- [79] Xensor Integration, "Datasheet XEN-1210," 2011.
- [80] M. Kyrarini, X. Wang, and A. Graser, "Comparison of vision-based and sensor-based systems for joint angle gait analysis," *2015 IEEE Int. Symp. Med. Meas. Appl. MeMeA 2015 - Proc.*, pp. 375–379, 2015.

- [81] J. Zhang, A. C. Novak, B. Brouwer, and Q. Li, "Concurrent validation of Xsens MVN measurement of lower limb joint angular kinematics.," *Physiol. Meas.*, vol. 34, no. 8, pp. N63-9, 2013.
- [82] R. Khusainov, D. Azzi, I. E. Achumba, and S. D. Bersch, "Real-time human ambulation, activity, and physiological monitoring: taxonomy of issues, techniques, applications, challenges and limitations," *Sensors (Basel)*, vol. 13, no. 10, pp. 12852–12902, 2013.
- [83] U. Laessoe, H. C. Hoeck, O. Simonsen, T. Sinkjaer, and M. Voigt, "Fall risk in an active elderly population—can it be assessed?," *J Negat Results Biomed*, vol. 6, p. 2, 2007.
- [84] M. Kangas, A. Konttila, I. Winblad, and T. Jämsä, "Determination of simple thresholds for accelerometry-based parameters for fall detection," *Annu. Int. Conf. IEEE Eng. Med. Biol. - Proc.*, pp. 1367–1370, 2007.
- [85] H. Luukinen, M. Herala, K. Koski, R. Honkanen, P. Laippala, and S.-L. Kivelä, "Fracture Risk Associated with a Fall According to Type of Fall Among the Elderly," *Osteoporos. Int.*, vol. 11, no. 7, pp. 631–634, 2000.
- [86] P. Boissy, S. Choquette, M. Hamel, and N. Noury, "User-based motion sensing and fuzzy logic for automated fall detection in older adults.," *Telemed. J. E. Health.*, vol. 13, no. 6, pp. 683–693, 2007.
- [87] J. Huang, P. Di, K. Wakita, T. Fukuda, and K. Sekiyama, "Study of Fall Detection Using Intelligent Cane Based on Sensor Fusion," *Int. Symp. Micro-NanoMechatronics Hum. Sci. MHS 2008. Nagoya, 6-9 Nov.*, pp. 495–500, 2008.
- [88] J. Huang, W. Xu, S. Mohammed, and Z. Shu, "Posture estimation and human support using wearable sensors and walking-aid robot," *Rob. Auton. Syst.*, vol. 73, pp. 24–43, 2015.
- [89] M. Mubashir, L. Shao, and L. Seed, "A survey on fall detection: Principles and approaches," *Neurocomputing*, vol. 100, pp. 144–152, 2013.
- [90] T. Zhang, J. Wang, L. Xu, and P. Liu, "Using Wearable Sensor and NMF Algorithm to Realize Ambulatory Fall Detection," *ICNC 2006 Adv. Nat. Comput.*, vol. 4222, pp. 488–491, 2006.
- [91] M. Kangas, I. Vikman, J. Wiklander, P. Lindgren, L. Nyberg, and T. Jamsa, "Sensitivity and specificity of fall detection in people aged 40 years and over," *Gait posture*, vol. 29, pp. 571–574, 2009.
- [92] M. J. Mathie, A. C. Coster, N. H. Lovell, and B. G. Celler, "Accelerometry : providing an integrated , practical method for long-term , ambulatory monitoring of human movement," *Physiol. Meas.*, vol. 25, no. 2, 2004.

- [93] M. A. Estudillo-Valderrama, L. M. Roa, J. Reina-Tosina, and D. Naranjo-Hernandez, "Design and Implementation of a Distributed Fall Detection System," *IEEE Trans. Inf. Technol. Biomed.*, vol. 13, no. 6, pp. 874–881, 2009.
- [94] R. Igual, C. Medrano, and I. Plaza, "Challenges, issues and trends in fall detection systems.," *Biomed. Eng. Online*, vol. 12, no. 1, p. 66, 2013.
- [95] C. F. Lai, S. Y. Chang, H. C. Chao, and Y. M. Huang, "Detection of cognitive injured body region using multiple triaxial accelerometers for elderly falling," *IEEE Sens. J.*, vol. 11, no. 3, pp. 763–770, 2011.
- [96] J. T. Perry, S. Kellog, S. M. Vaidya, J.-H. Youn, H. Ali, and H. Sharif, "Survey and evaluation of real-time fall detection approaches," *2009 6th Int. Symp. High Capacit. Opt. Networks Enabling Technol.*, pp. 158–164, 2009.
- [97] N. D. Lane, E. Miluzzo, H. Lu, D. Peebles, T. Choudhury, and A. T. Campbell, "A survey of mobile phone sensing," *IEEE Commun. Mag.*, vol. 48, no. 9, pp. 140–150, 2010.
- [98] K. Aminian and B. Najafi, "Capturing human motion using body-fixed sensors: Outdoor measurement and clinical applications," *Comput. Animat. Virtual Worlds*, vol. 15, no. 2, pp. 79–94, 2004.
- [99] R. Gigi *et al.*, "Deviations in gait metrics in patients with chronic ankle instability: a case control study.," *J. Foot Ankle Res.*, vol. 8, no. 1, p. 1, 2015.
- [100] A. Elbaz, A. Mor, G. Segal, R. Debi, N. Shazar, and A. Herman, "Novel classification of knee osteoarthritis severity based on spatiotemporal gait analysis," *Osteoarthr. Cartil.*, vol. 22, no. 3, pp. 457–463, 2014.
- [101] F. Bianchi, S. J. Redmond, M. R. Narayanan, S. Cerutti, and N. H. Lovell, "Barometric pressure and triaxial accelerometry-based falls event detection," *IEEE Trans. Neural Syst. Rehabil. Eng.*, vol. 18, no. 6, pp. 619–627, 2010.
- [102] J. J. Kavanagh and H. B. Menz, "Accelerometry: A technique for quantifying movement patterns during walking," *Gait Posture*, vol. 28, no. 1, pp. 1–15, 2008.
- [103] N. Wang, E. Ambikairajah, N. H. Lovell, and B. G. Celler, "Accelerometry based classification of walking patterns using time-frequency analysis," *Proc. 29th Int. Conf. IEEE EMBS*, vol. 2007, pp. 4899–902, 2007.
- [104] M. Iosa, T. Marro, S. Paolucci, and D. Morelli, "Stability and harmony of gait in children with cerebral palsy," *Res. Dev. Disabil.*, vol. 33, no. 1, pp. 129–135, 2012.

- [105] B. Kaluža and M. Luštrek, “Fall detection and activity recognition methods for the confidence project: a survey,” in *In Proceedings of the 12th International Multiconference Information Society 2008*, 2008, pp. 22–25.
- [106] D. M. Karantonis, M. R. Narayanan, M. Mathie, N. H. Lovell, and B. G. Celler, “Implementation of a real-time human movement classifier using a triaxial accelerometer for ambulatory monitoring,” *IEEE Trans. Inf. Technol. Biomed.*, vol. 10, no. 1, pp. 156–167, 2006.
- [107] J. M. Kang, T. Yoo, and H. C. Kim, “A wrist-worn integrated health monitoring instrument with a tele-reporting device for telemedicine and telecare,” *IEEE Trans. Instrum. Meas.*, vol. 55, no. 5, pp. 1655–1661, 2006.
- [108] Jiangpeng Dai, Xiaole Bai, Zhimin Yang, Zhaohui Shen, and Dong Xuan, “PerFallD: A pervasive fall detection system using mobile phones,” *2010 8th IEEE Int. Conf. Pervasive Comput. Commun. Work. (PERCOM Work.*, pp. 292–297, 2010.
- [109] G. Wu and S. Xue, “Portable preimpact fall detector with inertial sensors,” *IEEE Trans. Neural Syst. Rehabil. Eng.*, vol. 16, no. 2, pp. 178–183, 2008.
- [110] T. Zhang, J. Wang, P. Liu, and J. Hou, “Fall Detection by Embedding an Accelerometer in Cellphone and Using,” *J. Comput. Sci.*, vol. 6, no. 10, pp. 277–284, 2006.
- [111] J. Klucken *et al.*, “Unbiased and Mobile Gait Analysis Detects Motor Impairment in Parkinson’s Disease,” *PLoS One*, vol. 8, no. 2, 2013.
- [112] Skyguard, “MySOS Mandown,” 2014. [Online]. Available: <https://gadgetcommunities.wordpress.com/2014/09/11/>. [Accessed: 29-Mar-2017].
- [113] CareTech, “SensorBand II,” 2017. [Online]. Available: <http://www.caretech.com.au/products-/fall-sensor.html>. [Accessed: 28-Mar-2017].
- [114] Alert-it Care Alarm Technology, “Badge-iT Fall Detector,” 2016. [Online]. Available: <http://alert-it.co.uk/#Badge-iTFall-and-Personal-Alarm-Badge>. [Accessed: 28-Mar-2017].
- [115] Visonic, “Fall detector MCT-241MD PERS,” 2017. [Online]. Available: <http://www.visonic.com/Products/Wireless-Emergency-Response-Systems/Fall-detector-mct-241md-pers-wer>. [Accessed: 29-Mar-2017].
- [116] Vitalbase, “Vitalbase,” 2016. [Online]. Available: <http://www.vitalbase.co.uk/>. [Accessed: 29-Mar-2017].
- [117] Climax Technology Co. Ltd, “Climax Fall Sensor,” 2017. [Online]. Available: <http://climax.manufacturer.globalsources.com/si/6008800221031/pdtl/Fall->

- prevention/1046434163/Fall-Sensor.htm. [Accessed: 29-Mar-2017].
- [118] Tynetec, "Tynetec Fall Detector," 2017. [Online]. Available: <http://www.tynetec.co.uk/telecare-devices/wrist-worn-fall-detector>. [Accessed: 29-Mar-2017].
- [119] Blue Alert Medical Alarm Company, "Blue Alert Fall Detection Sensor." [Online]. Available: <http://www.bluealertalarm.com/index.cfm?page=equipment>. [Accessed: 29-Mar-2017].
- [120] CSEM SA., "CSEM Wrist Fall Detection," 2017. [Online]. Available: <http://www.csem.ch/home>. [Accessed: 29-Mar-2017].
- [121] Tynetec, "Tynetec Wrist Worn Fall Detector," 2017. [Online]. Available: <http://www.tynetec.co.uk/telecare-devices/wrist-worn-fall-detector>. [Accessed: 29-Mar-2017].
- [122] N. Pannurat, S. Thiemjarus, and E. Nantajeewarawat, "Automatic fall monitoring: a review," *Sensors (Basel)*, vol. 14, no. 7, pp. 12900–12936, 2014.
- [123] S. G. Brauer, Y. R. Burns, and P. Galley, "A prospective study of laboratory and clinical measures of postural stability to predict community-dwelling fallers.," *J. Gerontol. A. Biol. Sci. Med. Sci.*, vol. 55, no. 8, pp. M469–M476, 2000.
- [124] K. Berg, "Measuring balance in the elderly: preliminary development of an instrument," *Physiother. Canada*, vol. 41, no. 6, 1989.
- [125] D. PW, W. DK, C. J, and S. S, "Functional reach: a new clinical measure of balance," *J Gerontol*, vol. 45, no. 6, 1990.
- [126] S. Brauer, Y. Burns, and P. Galley, "Lateral reach: a clinical measure of medio-lateral postural stability.," *Physiother. Res. Int.*, vol. 4, no. 2, pp. 81–88, 1999.
- [127] K. D. Hill, J. Bernhardt, A. M. McGann, D. Maltese, and D. Berkovits, "A New Test of Dynamic Standing Balance for Stroke Patients: Reliability, Validity and Comparison with Healthy Elderly," *Physiother. Canada*, vol. 48, no. 4, 1996.
- [128] M. N. Nyan, F. E. H. Tay, and M. Z. E. Mah, "Application of motion analysis system in pre-impact fall detection," *J. Biomech.*, vol. 41, no. 10, pp. 2297–2304, 2008.
- [129] E. A. N. Kim, S. Z. Mordiffi, W. H. Bee, K. Devi, and D. Evans, "Evaluation of three fall-risk assessment tools in an acute care setting," *J. Adv. Nurs.*, vol. 60, no. 4, pp. 427–435, 2007.
- [130] D. Oliver, M. Britton, P. Seed, F. C. Martin, and A. H. Hopper, "Development and evaluation

- of evidence based risk assessment tool (STRATIFY) to predict which elderly inpatients will fall: case-control and cohort studies.," *BMJ*, vol. 315, no. 7115, pp. 1049–53, 1997.
- [131] D. Podsiadlo and S. Richardson, "The Timed 'Up & Go': A Test of Basic Functional Mobility for Frail Elderly Persons," *J. Am. Geriatr. Soc.*, vol. 39, no. 2, pp. 142–148, 1991.
- [132] D. Barthel and F. Mahoney, "Baltimore City Medical Society Functional Evaluation : the Barthel Index," *Md. State Med. J.*, vol. 14, pp. 56–61, 1965.
- [133] S. L. Vaught, "Gait, balance, and fall prevention.," *Ochsner J.*, vol. 3, no. 2, pp. 94–7, 2001.
- [134] D. Van Dyke, B. Singley, K. G. Speroni, and M. G. Daniel, "Evaluation of fall risk assessment tools for psychiatric patient fall prevention: a comparative study," *J. Psychosoc. Nurs. Ment. Heal. Serv.*, vol. 52, no. 12, pp. 30–35, 2014.
- [135] Centers for Disease Control and Prevention, "STEADI - Older Adult Fall Prevention," 2017. [Online]. Available: <https://www.cdc.gov/steady/>. [Accessed: 27-Mar-2017].
- [136] B. Najafi, D. G. Armstrong, and J. Mohler, "Novel Wearable Technology for Assessing Spontaneous Daily Physical Activity and Risk of Falling in Older Adults with Diabetes," *J. Diabetes Sci. Technol.*, vol. 7, no. 5, pp. 1147–1160, 2013.
- [137] A. Leone, G. Rescio, A. Caroppo, and P. Siciliano, "A wearable EMG-based system pre-fall detector," *Procedia Eng.*, vol. 120, pp. 455–458, 2015.
- [138] M. N. Nyan, F. E. H. Tay, and E. Murugasu, "A wearable system for pre-impact fall detection," *J. Biomech.*, vol. 41, no. 16, pp. 3475–3481, 2008.
- [139] A. Lopez-Yunez *et al.*, "A novel approach for high speed wireless pre-fall detection multisensory system," *Midwest Symp. Circuits Syst.*, pp. 857–859, 2014.
- [140] J. Liu, X. Zhang, and T. E. Lockhart, "Fall Risk Assessments Based on Postural and Dynamic Stability Using Inertial Measurement Unit," *Saf. Health Work*, vol. 3, no. 3, p. 192, 2012.
- [141] J. Liu, T. E. Lockhart, M. Jones, and T. Martin, "Local Dynamic Stability Assessment of Motion Impaired Elderly Using Electronic Textile Pants," *IEEE Trans. Autom. Sci. Eng.*, vol. 5, no. 4, pp. 117–122, 2013.
- [142] J. B. Dingwell and J. P. Cusumano, "Nonlinear time series analysis of normal and pathological human walking," *Chaos An Interdiscip. J. Nonlinear Sci.*, vol. 10, no. 4, p. 848, 2000.
- [143] T. E. Te Lockhart and J. Liu, "Differentiating fall-prone and healthy adults using local dynamic stability," *Ergonomics*, vol. 51, no. 12, pp. 1860–1872, 2008.

- [144] V. Lugade, V. Lin, A. Farley, and L. S. Chou, "An artificial neural network estimation of gait balance control in the elderly using clinical evaluations," *PLoS One*, vol. 9, no. 5, pp. 1–8, 2014.
- [145] S. A. England and K. P. Granata, "The influence of gait speed on local dynamic stability of walking," *October*, vol. 25, no. 2, pp. 172–178, 2007.
- [146] T. E. Lockhart, R. Soangra, J. Zhang, and X. Wu, "Wavelet based automated postural event detection and activity classification with single IMU," *Biomed. Sci. Instrum.*, vol. 49, no. Cdc 2010, pp. 224–233, 2013.
- [147] J. Zhang, T. E. Lockhart, and R. Soangra, "Classifying lower extremity muscle fatigue during walking using machine learning and inertial sensors," *Ann. Biomed. Eng.*, vol. 42, no. 3, pp. 600–612, 2014.
- [148] H. B. Menz, S. R. Lord, and R. C. Fitzpatrick, "Acceleration patterns of the head and pelvis when walking on level and irregular surfaces," *Gait Posture*, vol. 18, no. 1, pp. 35–46, 2003.
- [149] J. Baek, G. Lee, W. Park, and B. Yun, "Accelerometer signal processing for user activity detection," *Knowledge-Based Intell. Inf. Eng. Syst.*, vol. Lecture No, pp. 610–617, 2004.
- [150] F. Wu, H. Zhao, Y. Zhao, and H. Zhong, "Development of a wearable-sensor-based fall detection system," *Int. J. Telemed. Appl.*, vol. 2015, 2015.
- [151] Q. T. Huynh, U. D. Nguyen, K. T. Liem, and B. Q. Tran, "Detection of Activities Daily Living and Falls Using Combination Accelerometer and Gyroscope," in *5th International Conference on Biomedical Engineering in Vietnam*, vol. 46, Springer, Cham, 2015, pp. 184–189.
- [152] F. R. Allen, E. Ambikairajah, N. H. Lovell, S. Member, and B. G. Celler, "An Adapted Gaussian Mixture Model Approach to Accelerometry- Based Movement Classification Using Time-Domain Features," *New York*, pp. 3600–3603, 2006.
- [153] C. J. Chen and L. S. Chou, "Center of mass position relative to the ankle during walking: A clinically feasible detection method for gait imbalance," *Gait Posture*, vol. 31, no. 3, pp. 391–393, 2010.
- [154] H. G. Kang and J. B. Dingwell, "Intra-session reliability of local dynamic stability of walking," *Gait Posture*, vol. 24, no. 3, pp. 386–390, 2006.
- [155] D. Lafond, H. Corriveau, R. Hébert, and F. Prince, "Intrasession reliability of center of

- pressure measures of postural steadiness in healthy elderly people,” *Arch. Phys. Med. Rehabil.*, vol. 85, no. 6, pp. 896–901, 2004.
- [156] M. Benoussaad, B. Sijobert, K. Mombaur, and C. A. Coste, “Robust foot clearance estimation based on the integration of foot-mounted IMU acceleration data,” *Sensors (Switzerland)*, vol. 16, no. 1, pp. 1–13, 2015.
- [157] D. Trojaniello, A. Cereatti, N. Valeri, A. Ravaschio, and U. Della Croce, “Foot clearance estimation during overground walking and obstacle passing using shank-worn MIMU in healthy elderly and Parkinson’s disease subjects,” *Gait Posture*, vol. 42, no. December, p. S25, 2015.
- [158] InvenSense, “MPU-6000 and MPU-6050 Product Specification,” 2013.
- [159] Honeywell, “3-Axis Digital Compass IC,” 2011.
- [160] J. A. Afonso, H. D. Silva, P. Macedo, and L. A. Rocha, “An enhanced reservation-based MAC protocol for IEEE 802.15.4 networks,” *Sensors*, vol. 11, no. 4, pp. 3852–3873, 2011.
- [161] M. Kochlán, J. Micek, and P. Ševčík, “2.4 GHz ISM Band Radio Frequency Signal Indoor Propagation,” in *Federated Conference on Computer Science and Information Systems*, 2014, vol. 2, pp. 1027–1034.
- [162] M. Fitzmaurice, “USE OF 2.4 GHZ FREQUENCY BAND FOR COMMUNICATIONS BASED TRAIN CONTROL DATA COMMUNICATIONS SYSTEMS,” in *Joint Rail Conference*, 2006, pp. 263–267.
- [163] A. R. Jiménez, F. Seco, C. Prieto, and J. Guevara, “A comparison of pedestrian dead-reckoning algorithms using a low-cost MEMS IMU,” *WISP 2009 - 6th IEEE Int. Symp. Intell. Signal Process. - Proc.*, no. April 2009, pp. 37–42, 2009.
- [164] M. Susi, V. Renaudin, and G. Lachapelle, “Motion mode recognition and step detection algorithms for mobile phone users,” *Sensors (Switzerland)*, vol. 13, no. 2, pp. 1539–1562, 2013.
- [165] N. P. Fey, A. M. Simon, A. J. Young, and L. J. Hargrove, “Controlling Knee Swing Initiation and Ankle Plantarflexion With an Active Prosthesis on Level and Inclined Surfaces at Variable Walking Speeds,” *IEEE J. Transl. Eng. Heal. Med.*, vol. 2, no. August, 2014.
- [166] RoMeLa (Robotics & Mechanisms Lab), “DARwIn OP: Open Platform Humanoid Robot for Research and Education.” [Online]. Available: <http://www.romela.org/darwin-op-open-platform-humanoid-robot-for-research-and-education/>. [Accessed: 25-Jan-2017].
- [167] Trossen Robotics, “Darwin-OP Humanoid Research Robot - Deluxe Edition.” [Online].

- Available: <http://www.trossenrobotics.com/p/darwin-OP-Deluxe-humanoid-robot.aspx>.
[Accessed: 26-Jan-2017].
- [168] T. Pham *et al.*, "DARwIn OP Fabrication Manual," 2011.
- [169] F. Dunn, I. Parberry, and A. . Fallis, *3D Math Primer for Graphics and Game Development, 2nd Edition*, 2nd ed., vol. 53, no. 9. A K Peters/CRC Press 2011, 2011.
- [170] S. Bonnet, C. Bassompierre, C. Godin, S. Leseq, and A. Barraud, "Calibration methods for inertial and magnetic sensors," *Sensors Actuators, A Phys.*, vol. 156, no. 2, pp. 302–311, 2009.
- [171] D. Jurman, M. Jankovec, R. Kamnik, and M. Topič, "Calibration and data fusion solution for the miniature attitude and heading reference system," *Sensors Actuators, A Phys.*, vol. 138, no. 2, pp. 411–420, 2007.
- [172] ST-Microelectronics, "Application note Using LSM303DLH for a tilt compensated electronic compass," 2010.
- [173] L. Cucu, "Applying Kalman Filtering on a Quadruped Robot," 2012.
- [174] Open Source Physics - OSP, "Tracker Video Analysis and Modeling Tool," 2017. [Online]. Available: <http://physlets.org/tracker/>. [Accessed: 03-Mar-2017].
- [175] R. Mahony, S. Member, T. Hamel, and J. Pflimlin, "Nonlinear Complementary Filters on the Special Orthogonal Group," *IEEE Trans. Automat. Contr.*, vol. 53, no. 5, pp. 1203–1218, 2008.
- [176] S. O. H. Madgwick, "An efficient orientation filter for inertial and inertial/magnetic sensor arrays," 2010.
- [177] I. T. Jolliffe, *Principal Component Analysis*, Second Edi. Springer, 2002.
- [178] A. Singh, "PCA in Remote sensing," pp. 1680–1682.
- [179] W. Liu, "Variants of Principal Components Analysis," pp. 1083–1086, 2007.
- [180] C. Plagemann, C. Stachniss, and W. Burgard, "Efficient failure detection for mobile robots using mixed-abstraction particle filters," *Springer Tracts Adv. Robot.*, vol. 22, pp. 93–107, 2006.
- [181] M. Dev Anand, T. Selvaraj, and S. Kumanan, "Fault detection and fault tolerance methods for industrial robot manipulators based on hybrid intelligent approach," *Adv. Prod. Eng. Manag.*, vol. 7, no. 4, pp. 225–236, 2012.
- [182] A. L. Christensen, *Fault Detection in Autonomous Robots*. 2008.

- [183] P. Pastor, M. Kalakrishnan, L. Righetti, and S. Schaal, "Towards associative skill memories," in *IEEE-RAS International Conference on Humanoid Robots*, 2012, pp. 309–315.
- [184] P. Pastor *et al.*, "From dynamic movement primitives to associative skill memories," *Rob. Auton. Syst.*, vol. 61, no. 4, pp. 351–361, 2013.
- [185] P. Pastor, M. Kalakrishnan, S. Chitta, E. Theodorou, and S. Schaal, "Skill Learning and Task Outcome Prediction for Manipulation," *IEEE Int. Conf. Robot. Autom.*, pp. 3828–3834, 2011.
- [186] D. Kappler, P. Pastor, M. Kalakrishnan, W. Manue, and S. Schaal, "Data-Driven Online Decision Making for Autonomous Manipulation," in *rss*, 2015.
- [187] H. Asadi, R. Dowling, B. Yan, and P. Mitchell, "Machine learning for outcome prediction of acute ischemic stroke post intra-arterial therapy," *PLoS One*, vol. 9, no. 2, pp. 14–19, 2014.
- [188] A. M. S. Muniz *et al.*, "Comparison among probabilistic neural network, support vector machine and logistic regression for evaluating the effect of subthalamic stimulation in Parkinson disease on ground reaction force during gait," *J. Biomech.*, vol. 43, no. 4, pp. 720–726, 2010.
- [189] J. André, C. Santos, and L. Costa, "Skill Memory in Biped Locomotion: Using Perceptual Information to Predict Task Outcome," *J. Intell. Robot. Syst. Theory Appl.*, vol. 82, no. 3–4, pp. 379–397, 2016.
- [190] MathWorks, "Deep Learning: 3 things you need to know," 2017. [Online]. Available: <https://www.mathworks.com/discovery/deep-learning.html>. [Accessed: 07-Jul-2017].
- [191] H. Hubel and T. N. Wiesel, "Receptive fields of single neurones in the cat's striate cortex," *J. Physiol.*, vol. 148, pp. 574–591, 1959.
- [192] K. P. Murphy, *Machine Learning: A Probabilistic Perspective*. Cambridge, Massachusetts: The MIT Press, 2012.
- [193] H. Garty, "hagaygarty/mdCNN," 2017. [Online]. Available: <https://www.mathworks.com/matlabcentral/fileexchange/58447-hagaygarty-mdcnn>. [Accessed: 07-Jul-2017].
- [194] VBOX Automotive, "VBOX Inertial Measurement Unit - Overview." [Online]. Available: <https://www.vboxautomotive.co.uk/index.php/en/products/modules/inertial-measurement-unit>. [Accessed: 30-Dec-2016].

- [195] M. J. Thompson, M. Li, and D. A. Horsley, "Low power 3-axis lorentz force navigation magnetometer," *Proc. IEEE Int. Conf. Micro Electro Mech. Syst.*, no. 3, pp. 593–596, 2011.

Appendices

Appendix 1

The main characteristics of the sensors that constitute the sensing devices are available in the following tables for Acc, Mag, Gyro, and temperature sensor, respectively.

Table I - Acc's main characteristics

Parameter	Description	Units
Supply Voltage	2.375-3.46	V
Full-Scale Range	± 2 ; ± 4 ; ± 8 ; ± 16	g
Sensitivity Scale Factor	16.384; 8.192; 4.096; 2.048	LSB/g
Sensitivity Change vs. Temperature	± 0.02	%/ $^{\circ}$ C
Power Spectral Density	400	μ g/ \sqrt Hz
Normal Operating Current (only)	500	μ A

Table II – Mag's main characteristics

Parameter	Description	Units
Supply Voltage	2.16-3.6	V
Full-Scale Range	± 8	Gauss
Resolution	5	Mili-Gauss
Linearity	0.1	\pm %FS
Hysteresis	± 25	ppm
Cross-Axis Sensitivity	$\pm 0.2\%$	\pm %FS/Gauss
Average Current Draw	100	μ A

Table III – Gyro's main characteristics

Parameter	Description	Units
Supply Voltage	2.375-3.46	V
Full-Scale Range	± 250 ; ± 500 ; ± 1000 ; ± 2000	$^{\circ}$ /s
Sensitivity Scale Factor	131; 65.5; 32.8; 16.4	LSB/($^{\circ}$ /s)
Power Spectral Density	0.005	$^{\circ}$ /s/ \sqrt Hz
Normal Operating Current (only)	500	μ A

Table IV – Temperature sensor's main characteristics

Parameter	Description	Units
Supply Voltage	2.375-3.46	V
Range	-40 to +85	°C
Sensitivity	340	LSB/°C
Temperature Offset	-521	LSB
Linearity	±1	°C